Steady-state and Emergency Dendritic Cell Development at a Clonal Level

Dawn Shuiping Lin

ORCID ID: orcid.org/0000-0002-7872-6931

A thesis submitted in total fulfilment of the degree of Doctor of Philosophy

June, 2019

The Walter and Eliza Hall Institute of Medical Research
Department of Medical Biology
Faculty of Medicine, Dentistry and Health Science
The University of Melbourne
Australia

Abstract

Recent clonal fate and single cell RNA-sequencing studies demonstrate that significant lineage imprinting is already in place within individual haematopoietic stem and progenitor cells (HSPCs). Dendritic cells (DCs) represent one such branch of haematopoiesis and are responsible for pathogen-sensing and activation of the adaptive immune response. At the population level, all three major DC subtypes including type 1 conventional DCs (cDC1s), type 2 conventional DCs (cDC2s) and plasmacytoid DCs (pDCs), can be generated from a restricted common DC progenitor (CDP) population downstream of HSPCs. However, recent clonal evidence has suggested earlier subtype-specific imprinting within the CDP and even early HSPC populations. Therefore, the current hierarchical model of haematopoiesis is insufficient to explain the complexity and dynamics of DC development. The aim of this thesis was to investigate the development of DCs at the single cell level.

One caveat of most prior single cell lineage tracing studies was that clonal fate was only measured at a single time point. Therefore, questions remain as to whether the fate bias observed at a snapshot in time is consistent with earlier or later times. Here, using cellular barcoding, I develop an experimental and computational framework to allow robust periodical examination of lineage outputs of thousands of transient clones during DC development *in vitro*. I reveal that single HSPC clones are largely programmed regarding the types of DCs to make (fate), the number of DCs to produce (size), and when DC generation occurs (timing). Together, I define these unique properties as a clone's cellular trajectory. Importantly, I demonstrate that a large proportion of early HSPCs are already committed towards either cDC or pDC generation, even when clonal output is measured over time. This finding is consistent with and further complements the most recent evidence of DC subtype imprinting during early haematopoiesis.

Exogenous administration of Flt3 ligand (FL) is known to preferentially induce 'emergency' DC development, and is shown to provide promising therapeutic benefits in various conditions such as infection and cancer. However, how FL signals regulate cell proliferation and differentiation during early DC development is largely unknown. In this thesis, I investigate the clonal aetiology of this process. Using cellular barcoding, I demonstrate that emergency DC generation is predominantly driven by increased

expansion of pre-existing HSPC clones that are already primed with DC potential. Consistently, enhanced cell cycle activity is found to be prominent within most early HSPCs after short exposure to FL. In particular, using a single cell multi-omics profiling approach, I identify key cellular and molecular events within a unique group of early HSPCs that are most responsive to FL stimulation, which include increased cell division, maintenance of hyper-proliferative potential and establishment of a DC lineage program.

Collectively, the findings presented in this thesis provide new insights into the control and regulation of DC fate within individual HSPCs during steady-state and emergency haematopoiesis, with important implications regarding the maintenance or manipulation of DC generation in health and disease.

Declaration

This is to certify that:

I. This thesis comprises only my original work towards the degree of Doctor of Philosophy except where indicated in the Preface.
II. Due acknowledgement has been made in the text to all other material used.
III. The thesis is fewer than 100,000 words in length, exclusive of tables, figures and bibliographies.

Dawn Shuiping Lin
June, 2019

Preface

Chapter 3

My contribution to this chapter was 70%. I planned and performed all experiments described in this chapter. Barcoding data pre-processing and analysis was performed by Dr Andrey Kan and myself. The PieMaker visualization algorithm was initially developed by Dr Jerry Gao and subsequently optimized by Dr Andrey Kan. Contribution of all co-authors has been acknowledged in the manuscript. I wrote the majority of the manuscript (Introduction: 70%; Methods: 70%; Results: 95%; Discussion: 80%), with contribution from all co-authors.

Chapter 4

My contribution to this chapter was 95%. I planned and performed most experiments described in this chapter. Single cell RNA sequencing experiment was conducted in collaboration with SCORE at WEHI. For this experiment, all sample preparation and isolation were completed by myself and RNA library generation was performed by Ms Tracey Baldwin at SCORE. Pre-processing and analysis of all barcoding data was performed by myself independently. Pre-processing and analysis of single cell RNA sequencing data was performed by myself in collaboration with Mr Luyi Tian. Contribution of all co-authors has been acknowledged in the manuscript. I wrote the majority of the manuscript (Introduction: 95%; Methods: 95%; Results: 95%; Discussion: 95%), with contribution from all co-authors.

Therefore, my total contribution to the work presented in this thesis was approximately 85%.

The publication status of all chapters is as follows:

Chapter 3: Published by Cell Reports on March 6, 2018
Chapter 4: Submitted for publication to Nature Immunology on June 28, 2019

I acknowledge the following sources of funding:

The University of Melbourne
Walter and Eliza Hall Institute of Medical Research

Acknowledgements

It is impossible to do a PhD and write a thesis without the support and love from many wonderful people along the way. I am super grateful for all my mentors, colleagues, friends and families and the words below cannot justify my gratitude, but I will try.

First of all, I would like to thank my primary supervisor, Shalin Naik, for offering me such amazing and exciting projects and the continuous guidance and support along the way. I could not ask for a better mentor at the beginning of my scientific career, who is always generous with his time and generous in offering plenty of encouragement, opportunities and sometimes challenges.

I would also like to thank my supervisor and mentor, Phil Hodgkin, who is a truly inspiring scientist and I feel absolutely honoured to work with him. I am thankful to my PhD advisor committee, Samir Taoudi, Stephen Nutt and Gabrielle Belz, for their continuous support, guidance, encouragement and insightful discussion.

I am super grateful to all the past and present members of the Naik lab, who make my past five years truly wonderful and enjoyable. In particular, I would like to thank Jaring Schreuder for the endless support in the lab for almost my entire Honours and PhD years. I would like to thank Jerry Gao, Tom Weber and Luyi Tian for helping and training me in analysing the barcoding and scRNA-seq data. I would like to thank Daniela Zalcenstein, Jessica Tran, and Daniel Brown for all the helps regarding scRNAseq. I would like to thank Denise Miles, Imma Creus, Jordan Michael, Katie Fennel, Sara Tomei for being awesome lab mates and coffee buddies.

It has been fantastic to work alongside amazing people at WEHI for the past five years. Although Molecular Medicine Division is no longer existing, I would like to thank Sonja Gustin and Fiona McGrath for their help with all the administrative works, particular in their assistance in planning my postdoc tour. I am thankful for Matt Ritchie, Tracey Baldwin and Kristen Fairfax for their help in computational analysis, experimental work and insightful discussion.

I would also like to thank colleagues and friends from the Immunology Division, for making me feel like a part of this wonderful division. I am particular grateful to Andrey Kan, who is a very close collaborator on the work presented here in Chapter 3, for those endless meetings and discussions before our paper submission. I would like to thank Su Heinzel, Julia Marchingo, Kim Pham, Miles Horton, Kim McIntosh, Michael Chopin, Ken Shortman, Angela D'Amico, Rebecca Delconte, Joanna Groom and many others for their insightful discussion and share of protocols and reagents.

WEHI is a fantastic place to do science, but it wouldn't be the case without the wonderful people from Bioservices, FACS lab, Media kitchen and many more. Specially thanks to Simon Monard, Melanie Le Page, Tim McCulloch, Casey Anttila, Stacey Woodrow, Chayanica Nasa, Keti Florides, Merle Dayton, Liana Mackiewicz, Carolina Alvarado and Jessica Martin. I would also like to thank other WEHI colleagues including Ashley Ng, Stephen Wilcox, Jian-Guo Zhang, Diana Hansen and Lisa Ioannidis for discussions, reagents and collaboration.

To my awesome friends, in no particular order; Iromi Wanigasuriya, Janidu Wanigasuriya, Andres Tapia del Fierro, Lucille Wagner, Sam Adler, Maggie Potts, Kathy Potts, Olivia Stonehouse, Jordan Michael, Imma Creus, Sara Tomei, Isabella Kong, Amania Sheikh, Stephanie Trazise, Angela Huang, Caleb Dawson, Suad Abdirahman and many more. Thank you for all the laughter during coffee, lunch, drinks, board games and road trips. You are truly wonderful!

Finally, a special thanks to my partner, Francois Wong, as well as my parents, mum, dad, and my siblings Niki, Ben and Feifei. Thank you for putting up with me for all these years. I know none of you understand science and what I am doing every day, but thank you for trying to understand it by asking a lot of questions. Thank you for being proud of me, that really means a lot.

Table of Content

List of Tables

List of Figures

Chapter 1. Introduction

Introduction to dendritic cells (DCs)

Dendritic cells (DCs) are an important component of the immune system, and act as messengers between the innate and adaptive arms by recognizing circulating danger signals and presenting them in the form of antigens to T lymphocytes to mount the adaptive immune responses (Banchereau and Steinman, 1998; Merad et al., 2013; Murphy et al., 2015). Since the discovery of DCs by Ralph Steinman and Zanvil Cohn in the 1970s (Steinman and Cohn, 1973; 1974; Steinman et al., 1975; 1974), many studies have examined the development, diversity and functional properties of DCs. It is now well established that DCs represent a distinct haematopoietic branch, and consist of different subsets including conventional DC (cDC) type 1 (cDC1), cDC type 2 (cDC2) and plasmacytoid DCs (pDCs) (Guilliams et al., 2014; Perié and Naik, 2015). These subsets differ in their surface marker expression, transcriptional networks and functions in the immune system (Merad et al., 2013).

Phenotypic definition of DCs

cDCs

cDCs are the classical DCs first identified in mice by Steinman and Cohn, which were named due to their large stellate morphology with dendrite extensions (Steinman and Cohn, 1973). Both mature cDC1s and cDC2s express high levels of integrin CD11c and major histocompatibility complex class II (MHCII) (Merad et al., 2013; Shortman and Naik, 2007). Both surface markers are often included in common gating strategies to identify cDCs. In addition, at steady-state, both cDC subsets express low levels of co-stimulatory molecules including CD40, CD80 and CD86, which can be up-regulated upon maturation to enable efficient activation of T cells (Dress et al., 2018).

Historically, murine cDC1s and cDC2s were mainly segregated by the respective presence vs absence of CD8α expression on the cell surface (Shortman and Heath, 2010). However, it was later shown that CD8α is only expressed by resident cDC1s from lymphoid organs such as the spleen but not those from non-lymphoid tissues, *in vitro* cultures or other species such as human, macaque and sheep (Crozat et al., 2011; Merad et al., 2013). This precluded thorough cross-species comparison of DC diversity for a long time until other markers were identified that could segregate the two cDC subsets in different tissues and species. Similar to CD8α, expression of several markers was found to be heterogeneous across tissues. For example, lymphoid tissue $CD8\alpha^+$ cDCs and $CD103^+$ $CD11b^-$ cDCs in various non-lymphoid tissues were shown to be developmentally and functionally equivalent populations, thus both represent cDC1s (del Rio et al., 2010; Edelson et al., 2010; Ginhoux et al., 2009; Helft et al., 2010). However, CD103 is highly expressed by most non-lymphoid tissue cDC1s, but only a fraction of cDC1s that reside in lymphoid organs (Annacker et al., 2005). Therefore, CD103 is commonly used to define non-lymphoid tissue cDC1s, but not splenic cDC1s.

There are a few conserved markers that allow segregation of cDC1s from cDC2s across different tissues and species. One of these is the XC chemokine receptor 1 (XCR1), which was initially found to be expressed by both resident and migratory cDC1s across mouse, human and sheep (Crozat et al., 2011; 2010). A recent proteomic profiling study on DCs using multi-parametric flow cytometry and mass cytometry further supported the use of XCR1 as a part of a conserved gating strategy to robustly isolate cDC1s across tissues

(spleen, liver, lung, kidney, skin, small and large intestine) and species (mouse, human and macaque) (Guilliams et al., 2016). Another conserved marker is the C-type lectin receptor Clec9A, also known as DNGR-1. High level of Clec9A was found on both murine and human cDC1s in lymphoid and non-lymphoid tissues (Caminschi et al., 2008; Poulin et al., 2010; Sancho et al., 2008). Of note, low levels of Clec9A were also found on murine pDCs and progenitors with cDC potential, and thus can be used as a genetic lineage tracing model for fate mapping of cDCs (Schraml et al., 2013). Another C-type lectin receptor CD205 (DEC-205) is sometimes used to segregate the two cDC subsets as higher expression was found on cDC1s. However, caution must be taken to exclude other CD205 expressing cells including Langerhans cells (LCs) and thymic epithelial cells (Jiang et al., 1995). Lastly, differential expression of CD24 can also be used to distinguish cDC1s and cDC2s, as well as cDC precursors with cDC1 or cDC2 bias, as higher expression was observed on the cDC1 branch (Naik et al., 2006).

cDC2s are commonly defined by the absence or low expression of the aforementioned cDC1 markers, as well as the positive expression of CD11b or CD172α (Sirpα), which are not expressed by cDC1s (Gurka et al., 2015; Lahoud et al., 2006). Of note, despite low expression of CD11b during steady-state *in vivo*, cDC1s can up-regulate its expression spontaneously in culture (Vremec et al., 1997). Therefore, the use of CD11b should be avoided *in vitro*. In addition, a subset of migratory $CD11b^{-}$ $CD172\alpha^{+}$ cDC2s has been described in the skin draining LNs, which exhibits cDC2 characteristics including dependency on the key cDC2 transcription factor interferon regulatory factor 4 (Irf4) and strong migratory cDC2 gene signatures (Tussiwand et al., 2015). Thus, the use of CD11b in defining cDC2s is further restricted and CD172α has been demonstrated as a more conserved marker across tissues and species (Guilliams et al., 2016). Importantly, commonly defined cDC2 gating strategies using the combination of CD11c, MHCII and cDC1/cDC2 markers was not sufficient to isolate a homogeneous population, which lead to incomplete understanding of the exact role of cDC2s in the immune system to date. This is due to two major limitations: 1) potential contamination of other cell types such as macrophages; and 2) potential existence of multiple sub-populations with distinct biological properties within the common cDC2 gate.

Although F4/80 (a macrophage marker) is commonly included in DC isolation strategies, when used alone it is not sufficient for robust segregation of macrophages and cDC2s in

most tissues. This is because cDC2s also express low level of F4/80 (Gurka et al., 2015). Co-expression of F4/80 and CD64 (another macrophage marker), however, results in robust identification of macrophages, as demonstrated by a recent large-scale single cell profiling study (Guilliams et al., 2016). This study further suggested a robust gating strategy to exclude Langerhans cells (LCs) from cDC2s in the mouse skin and cutaneous LNs. This strategy includes 1) pre-exclusion of macrophages based on CD64 and F4/80 co-expression; 2) identification of cDC1s as $XCR1^{+}$ $CD172\alpha^{-}$; 3) segregation of LCs ($CD24^{hi}$) from bona fide cDC2s ($CD24^{lo}$) in the $XCR1^{-}$ $CD172\alpha^{+}$ gate.

Importantly, significant heterogeneity has been observed in cDC2s isolated using common strategies. For example, differential expression of the Endothelial cell-selective adhesion molecule (ESAM) on splenic cDC2s has been reported (Lewis et al., 2011). The development of the $ESAM^{+}$ subset is dependent on Notch signalling, as Notch2 receptor deletion lead to specific ablation of these cells. In contrast to $ESAM^{-}$ cells, a higher proportion of $ESAM^{+}$ $CD11b^{+}$ DCs also expressed CD4 and DCIR2, the initial markers used to define cDC2s in early studies (Shortman and Heath, 2010). In addition, differential ESAM expression seems to separate $CD11b^{+}$ cDC2s into cells that are more monocyte-like ($ESAM^{-}$) and more cDC2-like ($ESAM^{+}$), as revealed by gene expression profiling using microarrays (Lewis et al., 2011). Other surface markers such as DCAL2 and DCIR2 (Kasahara and Clark, 2011) and transcriptional factors such as Klf4 (Tussiwand et al., 2015) have been reported to allow fractionation of cDC2s into functional distinct subsets. However, the relationship between these reported cDC2 subsets has not been established. Therefore, systematic characterization of the commonly defined cDC2 compartment is required to fully understand the extend of heterogeneity, which could potentially be facilitated by large-scale single cell profiling technologies.

pDCs

pDCs were characterized as a distinct branch of DCs two decades after the discovery of cDCs (Reizis, 2019; Shortman et al., 2013; Swiecki and Colonna, 2015). As an interesting fact, the original description of pDCs was published in a scientific report examining cell composition in the human lymph nodes, which was written in German in the late 1950s, prior to the realization of DCs as a distinct immune cell type (LENNERT and REMMELE, 1958; Swiecki and Colonna, 2015). Unlike cDCs, pDCs were first

discovered in human (LENNERT and REMMELE, 1958; Siegal et al., 1999) and later characterized in mice (Asselin-Paturel et al., 2001; Björck, 2001; Nakano et al., 2001) as the major interferon (IFN)-secreting cells in the immune system in response to viral infection. Consistent with its superior capacity to produce and secrete type I IFNs, pDCs have a plasma cell-like morphology but not the classical large stellate feature of DCs in the steady-state (Shortman et al., 2013). Upon activation, some pDCs can become cDC-like by acquiring a dendritic morphology and acquisition of cDC-like functions such as antigen presentation and T cell priming (Shortman et al., 2013). However, such attributed features of pDCs were questioned by a few recent studies, which highlighted significant heterogeneity within the commonly defined pDC compartment and suggested potential contamination of DC precursors that can generate both mature cDCs and pDCs (see below). Thus, further investigation is required to establish whether *bona fide* pDCs can be activated to perform cDC-like functions.

Regardless of the controversy, pDCs are commonly defined by the markers discussed below. In the steady-state, murine pDCs are low in CD11c and MHCII, which distinguishes them from cDC1s and cDC2s that both express high level of these markers. pDCs can be further identified as CD45R (B220), CD137 (Bst2) or Siglec-H positive (Murphy et al., 2015; Swiecki and Colonna, 2015). Of note, none of the aforementioned markers are uniquely expressed by pDCs. For example, CD45R is also highly expressed on B cells (Coffman and Weissman, 1981). Thus, careful pre-exclusion of B cells by positive expression of markers such as CD19 is required. In addition, while Bst2 was shown to be a rather specific pDC marker in naïve mice under steady-state, promiscuous expression was found across most immune cells after stimulation with IFN (Blasius et al., 2006). Thus, caution must be taken in using Bst2 to define pDCs in any non-steady-state conditions. Lastly, the commonly used pDC marker, Siglec-H, was shown to be expressed in subsets of macrophages in the spleen and LNs, as well as in some DC progenitors with cDC and pDC potential (Swiecki et al., 2014; Zhang et al., 2006). In fact, several recently described DC precursor populations are defined by positive expression of Siglec-H (Rodrigues et al., 2018; Schlitzer et al., 2015). Together, these results further suggested that pDCs defined in many early studies may have contained contaminating cells and many properties attributed to pDCs may require re-evaluation.

Multiple markers have been reported to segregate pDCs into different subsets with different functional properties. First, differential CD4 expression has been described in pDCs across multiple mouse organs including the LNs, spleen, liver, thymus, BM and lung (Yang et al., 2005). $CD4^-$ pDCs were shown to express higher level of CCR7 and CD62L in the steady-stage, as well as higher level of co-stimulatory molecules after CpG-B stimulation (Yang et al., 2005). In addition, compared to the $CD4^+$ pDCs, these cells can produce higher level of cytokines including IFNα, Interleukin (IL) -12 (IL-12), IL-6 and TNFα after stimulation (Yang et al., 2005).Another differentially expressed marker is recombination activating gene 1 (RAG1) (Pelayo et al., 2005). $RAG1^+$ pDCs were less potent in stimulating T cells and producing cytokines such as IFNα and TNFα than the $RAG1^-$ fraction (Pelayo et al., 2005; Sathe et al., 2013). However, while Rag1 was initially thought to segregate pDCs from the myeloid and lymphoid pathways, later study rejected this hypothesis and showed that pDCs from either origin can express RAG1 (Shigematsu et al., 2004). Thus, it is still unclear the origin and biological relevance of RAG1 expression on pDCs.

Some markers seem to segregate the commonly defined pDCs into subsets that are at different developmental stages, rather than bona fide subsets with distinct functions. One of these markers is Ly49Q. $Ly49Q^-$ pDCs are present in the mouse BM but not in the periphery tissues including the spleen, LNs or PB (Kamogawa-Schifter et al., 2005). Upon culturing of these cells with Fms like tyrosine kinase (Flt3) ligand (FL), which recapitulates splenic DC development in vitro, up-regulation of Ly49Q was observed. This suggested the direct precursor-progeny relationship between the two subsets. Another marker is Sca1. $Sca1^-$ pDCs are predominantly found in the BM and represent a smaller proportion of commonly defined pDCs in secondary lymphoid organs such as the spleen and LNs (Niederquell et al., 2013). These cells have a more proliferative phenotype and can give rise to $Sca1^+$ pDCs with or without activation by TLR ligands, in both *in vitro* and *in vivo* assays (Niederquell et al., 2013). Thus, $Sca1^-$ pDCs appear to be an immediate precursor of $Sca1^+$ pDCs.

Lastly, CCR9 represents a crucial marker to define *bona fide* pDCs and allows exclusion of contaminating DC precursors from the commonly used gating strategies (Lin et al., 2018; Schlitzer et al., 2012; 2011). Multiple studies have confirmed that $CCR9^-$ cells within the commonly defined pDC compartment ($B220^+$, $Bst2^+$ or Siglec-H^+) are DC

precursors that can give rise to both cDCs and pDCs, whereas CCR9^{+} pDCs are mostly post-mitotic and incapable of further differentiation (Lin et al., 2018; Schlitzer et al., 2011; 2012; Segura et al., 2009). Importantly, a continuous live cell imaging study demonstrated that most CCR9^{+} pDCs transited through a Siglec-H^{+} CCR9$^{–}$ stage (Dursun et al., 2016). However, it remains to be determined whether cDCs also transit through a similar phenotypic stage. Importantly, the relationships between the aforementioned contaminating DC precursors (Ly49Q$^{–}$, Sca1$^{–}$ and CCR9$^{–}$) has not been established, which can be investigated using single cell profiling techniques such as multi-parametric flowcytometry and scRNAseq. Nevertheless, due to the significant heterogeneity within the commonly defined pDC compartment, any future studies should include CCR9 in defining *bona fide* murine pDCs.

Recently, significant heterogeneity within the human pDC compartment has also been reported. Human pDCs are commonly defined by the absence of CD11c expression and the positive expression of CD123 or CD303. An early study identified two functionally distinct pDC subsets in human peripheral blood mononuclear cells (PBMCs), separated by differential expression of surface marker CD2 (Matsui et al., 2009). CD2^{+} pDCs represent the minor subset (~15%) that display cDC-like properties, including the capacity to potently induce T cell proliferation and produce IL-12 upon activation (Matsui et al., 2009). Another study also reported the segregation of human pDCs based on CD2 expression and demonstrated that CD2^{+} pDCs were better at surviving due to the higher expression of pro-survival protein BCL2 (Bryant et al., 2016). Importantly, a CD2^{hi}CD5^{+}CD81^{+} subset can be found within the commonly defined pDC compartment in human blood, BM and tonsil, which are functionally more related to cDCs than traditional pDCs (Zhang et al., 2017). These cells express low level of Irf7 (a pDC transcription factor) and produce little to no type I IFNs upon CpG stimulation. In contrast, they express higher levels of co-stimulatory molecules including CD40, CD80 and CD86 and capable of activating B and T lymphocytes. Importantly, these CD2^{hi}CD5^{+}CD81^{+} cells can also be found within commonly defined murine pDC population (Zhang 2017).

In accordance with the notion that commonly defined pDCs might contain cDC precursors, three recent single cell profiling studies on human PBMCs independently identified a small subset of phenotypic ‘pDCs’ that were capable of further DC

development. This subset was characterized by the expression of Axl and Siglec-6 and was termed AS cells in the study conducted by Villani et al. (Villani et al., 2017). Compare to 'pure' pDCs, AS cells were potent stimulators for T cell proliferation (Villani et al., 2017). Importantly, at the population level, AS cells developed into mostly cDC2s and to a less extent, pDCs but not cDC1s (Villani et al., 2017). See et al. also described a small subset of $CD123^+$ cells (a common human pDC gate) that express Axl and Siglec-6 (See et al., 2017). However, as opposed to AS cells in the other study (Villani et al., 2017), these cells did not generate any pDCs when probed by CD303 expression *in vitro* (See et al., 2017). Lastly, a distinct cluster of cells that shared similar characteristics to the newly identified AS cells (Villani et al., 2017) was identified in human blood, tonsil and spleen using mass cytometric analysis (Alcántara-Hernández et al., 2017). Importantly, the study showed that the pDC-like AXL^+ cells also expressed CD2, CD5 and CD81, characteristics of the contaminating cell population discussed above (Zhang et al., 2017).

Together, these recent findings highlight the heterogeneity within the commonly defined pDC population and urge the necessity to include additional markers in routine isolation of *bona fide* pDCs, both in mouse and human. While inclusion of CCR9 is sufficient to allow accurate identification of murine pDCs, a conserved human pDC gating strategy is yet to be determined. In addition, whether the 'novel' pDC-like populations described in these different studies represent the same or different cell types remains to be determined. Furthermore, it was unclear whether there was any fate heterogeneity within these populations as clonal tracking assays were not performed in any of the aforementioned studies. Further studies are required to answer these fundamental questions regarding pDC biology.

Table 1.1 Expression of surface markers on murine DC subsets

	cDC1	cDC2	pDC
CD11c	+++	+++	+
MHCII	++	++	+
CD40	+/–	+/–	+/–
CD80	+/–	+/–	+/–
CD86	+/–	+/–	+/–
CD8α	subset	–	subset
CD4	–	+/–	+/–
CD103	subset	–	–
Clec9A (DNGR-1)	++	–	+
CD205 (Dec-205)	+	–	–
XCR1	+	–	–
CD24	++	+	ND
CD11b	–	+	–
CD172α (Sirpα)	–	++	+
CD45RA (B220)	–	–	+
Siglec-H	ND	ND	+
CD137 (Bst2)	–	–	+
CCR9	ND	ND	+
F4/80	–	+/–	–
CD64	–	–	–
ESAM	+/–	+/–	ND
DCIR2	–	+/–	–
DCAL2	–	+/–	–

Transcription factors (TFs)

In addition to surface markers that help demarcate the DC subsets, many TFs are differentially expressed by the distinct DC subsets. These TFs can play important roles in fate determination, subtype maturation, regulation of specialized immune functions or other cell type specific biological properties such as migration (Miller et al., 2012). Regardless of their exact role, targeted depletion of selected TF-expressing cells using diphtheria toxin (DT) or DT receptor (DTR), as well as depletion using the Cre-loxP system, leads to selective ablation of DC subtypes of interest, which allow subsequent characterization of their specialized biological properties (Durai and Murphy, 2016).

Table 1.2 Key transcription factors involved in DC development or function

cDC1	cDC2	pDC
Irf8	Irf4	Irf8
Zbtb46	Zbtb46	E2-2 (Tcf4)
Id2	RelB	SpiB
Nfil3	Notch2	Irf7
Batf3	Klf4	
Cbfb		
Runx1		

cDC1s

The development of cDC1s is coordinated by a network of TFs including Zbtb46 (BTBD4), Irf8 (ICSBP), DNA binding protein 2 (Id2), Nfil3 and Batf3 (Murphy et al., 2015). For example, Zbtb46 is selectively expressed by both cDC subsets and their committed precursors, but not pDCs, monocytes and macrophages (Meredith et al., 2012; Satpathy et al., 2012). DT treatment in Zbtb46-DTR mice leads to elimination of cDC1s and severe reduction of cDC2s (Meredith et al., 2012). In addition, Zbtb46-GFP reporter mice is available and allow robust identification of cells along the cDC trajectory (Satpathy et al., 2012).

Irf8 is a crucial TF implicated in both early and late stages of DC development (Murphy et al., 2015). Irf8 is selectively expressed by both cDC1s and pDCs within the mature DC compartment and deletion of this TF resulted in total loss of both subsets (Aliberti et al., 2003; Schiavoni et al., 2002). Importantly, expression of Irf8 in early progenitor populations is critical to exclude granulocyte potential and guide commitment towards the DC lineage (Becker et al., 2012; Kurotaki et al., 2014). Irf8 is also crucial in terminal maturation of cDC1s in various tissues such as the lung and spleen (Bajaña et al., 2016). Due to the importance of Irf8 in regulating cDC1 development, Irf8 dependency within the cDC compartment is used to define *bona fide* cDC1s based on the current nomenclature (Guilliams et al., 2014).

Irf8 interacts with multiple TFs to orchestrate DC development. The interaction between two TFs from the Runx family, namely the core-binding factor subunit beta (Cbfb) and Runx1, controls the expression of Irf8 and therefore is implicated in guiding DC commitment in early progenitors (Satpathy et al., 2014). Other TFs have been demonstrated to act downstream of Irf8 to regulate DC development, which include Id2 and Batf3. Id2 is a member of the Helix-loop-helix (HLH) family and is expressed on both cDC subsets with higher expression on cDC1s (Hacker et al., 2003; Jackson et al., 2011). Interestingly, Id2 has been demonstrated to promote cDC1 development via the suppression of pDC development, but it does not appear to play a role in cDC2 commitment (Jackson et al., 2011).

Similarly, Batf3, a TF further downstream in DC development, is specifically involved in cDC1 generation. Mice with genetic deletion of Batf3 lack cDC1s in both lymphoid and non-lymphoid tissues and represent a powerful tool for the characterization of the specialized roles of cDC1s (Edelson et al., 2010; Hildner et al., 2008; Mashayekhi et al., 2011). Initially, Batf3 was proposed to play a role in maintaining the survival of mature cDC1s, but not in the proliferation or differentiation of this subset (Jackson et al., 2011). However, a recent study suggested an essential role of Batf3 in maintaining autoactivation of Irf8 (Grajales-Reyes et al., 2015). Thus, it appears that cDC1 development is regulated by a tightly controlled feedback loop involving multiple TFs, which include Irf8 and Batf3. Interestingly, Batf3 expression is also controlled by another TF called Nfil3. Nfil3$^{-/-}$ mice have reduced Batf3 expression and absence of cDC1s, but not cDC2s or pDCs

(Kashiwada et al., 2011). However, whether Nfil3 is involved in the Irf8-Batf3 axis in regulating cDC1 development has not been established.

cDC2s

Multiple TFs have been implicated in regulating cDC2 development and/or function, which include Zbtb46, RelB, Irf4, Notch2 and Klf4. As discussed above, Zbtb46 is a marker of cDC commitment and is highly expressed along both the cDC1 and cDC2 trajectories. RelB is the first TF described that play a selective role in DC development. RebB null mice have reduced number of cDC2s, whereas cDC1 generation is unaffected (Wu et al., 1998).

While Irf8 dependency is used to define *bona fide* cDC1s, cDC2s are commonly identified based on positive Irf4 expression (and lack of Irf8 expression) within the cDC compartment (Guilliams et al., 2014). However, whether the development of cDC2s is dependent on Irf4 is debatable. The confusion might arise from the lack of consensus in defining *bona fide* cDC2s and the significant heterogeneity within the commonly defined cDC2 population in most studies. The initial study characterizing the $Irf4^{-/-}$ mouse model reported a severe reduction of cDC2s ($CD11b^{hi}$ $CD4^{+}$ $CD8^{-}$) in the spleen (Suzuki et al., 2004). However, it is now clear that not all splenic cDC2s express CD4 on the cell surface. $CD4^{+}$ cDC2s only represent a subset of cells that are $ESAM^{+}$ and are dependent on Notch signalling (Lewis et al., 2011). Another study suggested a role of Irf4 in regulating the migration, but not development of a subset of cDC2s (Bajaña et al., 2012). This conclusion was based on the observation that normal numbers of cDC2s were found in the skin upon Irf4 deletion, which lacked chemokine receptor CCR7 and failed to migrate to the cutaneous LNs (Bajaña et al., 2012). This in turn leaded to a reduction in cDC2 numbers in the cutaneous LNs (Bajaña et al., 2012). Other studies suggested multiple roles of Irf4 in cDC2 biology, including the regulation of survival (Persson et al., 2013), MHCII antigen presentation (Vander Lugt et al., 2014) and terminal differentiation of cDC2 subsets (Bajaña et al., 2016).

The commonly defined cDC2 population is highly heterogenous and distinct subsets can be distinguished based on the dependency of different transcriptional networks. At least two transcriptional and functional distinct subsets have been described so far, which

include the Notch2-dependent and Klf4-dependent cDC2s. The Notch2-dependent cDCs can be identified by the positive expression of surface marker ESAM (Lewis et al., 2011; Satpathy et al., 2013). Importantly, ESAM expression is not restricted to cDC2s, but can be found on a subset of cDC1s, defined as $CD24^+$ $DEC\text{-}205^+$ (Satpathy et al., 2013). In addition, the generation of these $ESAM^+$ cDC1s was dependent on Notch signalling, but to a less extent compared to $ESAM^+$ cDC2s (Satpathy et al., 2013). Therefore, caution must be taken in attributing specialized functions to the subset of cDC2s using the Notch2 deletion model. Conversely, Klf4 appears to regulate the development of another distinct cDC2 subset. Conditional deletion of Klf4 in the DC compartment leaded to approximately 50% reduction of $CD11b^+$ cDCs across multiple tissues (Tussiwand et al., 2015). Notably, a complete absence of a distinct migratory DC population was observed in the skin draining LNs. Interestingly, these cDCs are $CD11b^-$ $CD24^-$, but express Sirpα and Irf4 (Tussiwand et al., 2015), thus represent a subset of cDC2s based on the current definition (Irf4 expressing) (Guilliams et al., 2014).

pDCs

The development and function of pDCs are orchestrated by a number of TFs including E2-2 (Tcf4), SpiB, Irf7 and Irf8. In particular, E2-2 is thought to be the master regulator of pDC development, which acts in a mutually antagonizing manner with Id2 to control cDC1 vs pDC differentiation at the common DC progenitor (CDP) level, respectively (Cisse et al., 2008; Ghosh et al., 2010; Hacker et al., 2003; Jackson et al., 2011). E2-2 promotes pDC development by supporting pDC-specific genes including SpiB and Irf7 and repressing Id2 hence cDC1-specific genes, and vice versa. Thus, competition between E2-2 and Id2 is thought to be the basis of divergence between pDCs and cDC1s, downstream of Irf8 that controls the development of both subsets.

The ETS transcription factor SpiB is highly expressed on pDCs, but not cDCs (Schotte et al., 2004). SpiB is thought to synergize with E2-2 in promoting pDC development (Nagasawa et al., 2008). This is because reduced SpiB level impairs E2-2 induced pDC development and co-exprssion of SpiB and E2-2 further promotes the generation of pDCs (Nagasawa et al., 2008). Importantly, unlike E2-2, overexpression of SpiB alone cannot overcome the block of pDC development induced by Id2 overexpression (Nagasawa et al., 2008). Conversely, Irf7 is not involved in pDC development but plays a crucial role

in regulating the major function of pDCs. Upon Irf7 deletion, severe impairment of IFN production by pDCs was observed (Honda et al., 2005).

Major functions of DCs

Since their discovery, DCs have been recognized by their remarkable ability in antigen presentation to stimulate T lymphocytes and activate specific adaptive immunity (Banchereau and Steinman, 1998). However, there is accumulating evidence suggesting that DCs are critically involved in multiple aspects of both the innate and adaptive immunity, in addition to their characteristic role in antigen presentation and T cell activation (Merad et al., 2013; Murphy et al., 2015). Furthermore, distinct DC subtypes are found to exhibit overlapping yet specialized immune functions (**Figure 1.1**).

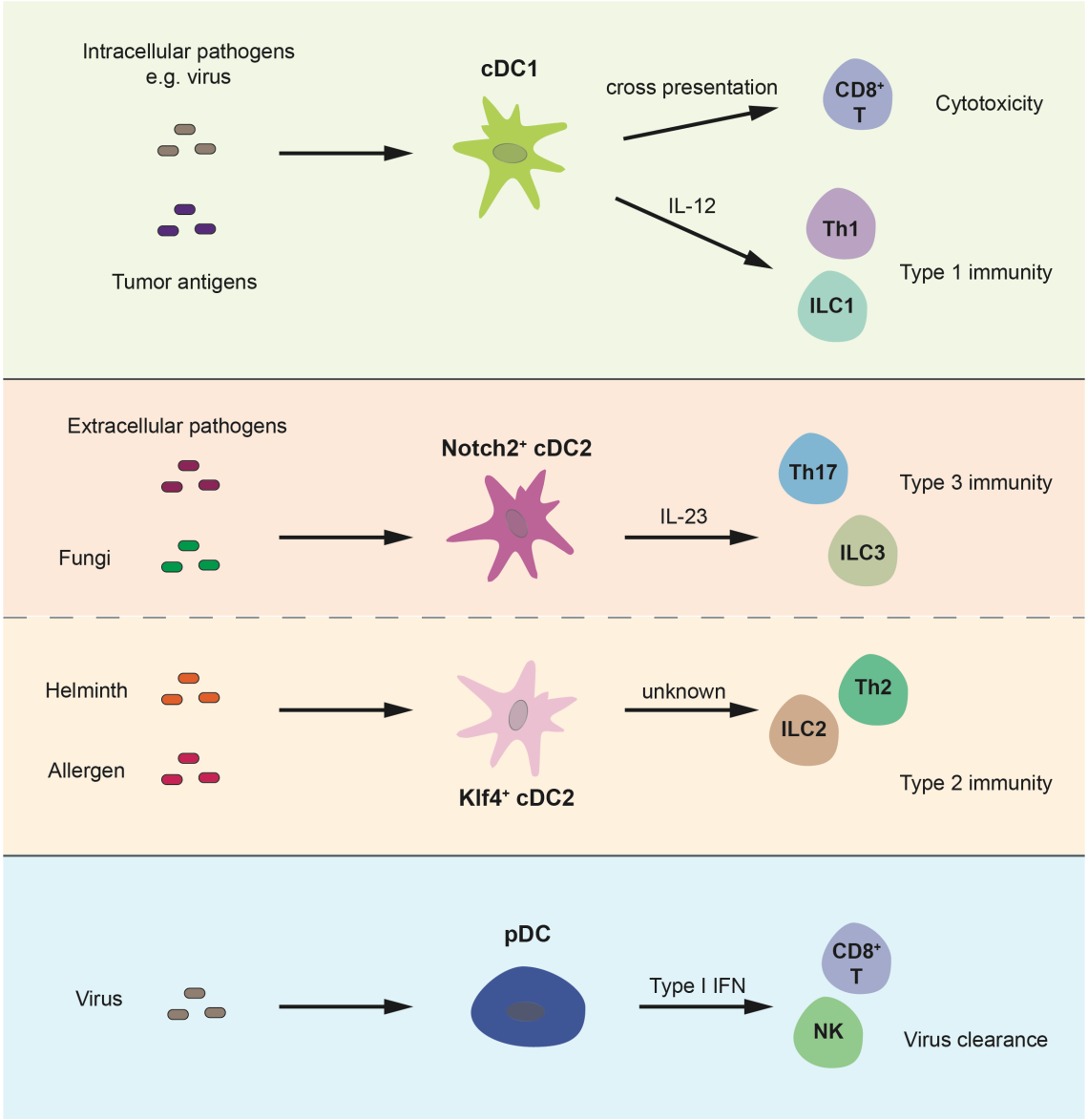

Figure 1.1 Summary of major immune functions of each DC subsets.

The three DC subtypes play distinct roles in the immune system. cDC1s are mainly specialized in recognizing and cross presenting intracellular pathogens and tumor antigens to activate $CD8^+$ T cells, as well as producing IL-12 to prime type 1 immunity. cDC2s are heterogenous and comprise subtypes that might involve in recognizing extracellular pathogens, fungi, helminths or allergens to induce type 2 or type 3 immunity. pDCs are mainly involved in the clearance of viruses by producing large amounts of type I IFN.

cDC1s

cDC1s are critical in the recognition and clearance of intracellular pathogens including a variety of viruses, intracellular bacteria and protozoans (Murphy et al., 2015). Some examples include *Plasmodium berghei* (Lundie et al., 2008), *Toxoplasma gondii* (Mashayekhi et al., 2011; Sousa et al., 1997), *Listeria monocytogenes* (Alexandre et al., 2016; Belz et al., 2005; Edelson et al., 2011; Yamamoto et al., 2013), Herpes simplex virus type 1 (HSV1) (Jirmo et al., 2009; Nopora et al., 2012; Zelenay et al., 2012), mouse Cytomegalovirus (MCMV) (Torti et al., 2011) and Rotavirus (RV) (Sun et al., 2017). The control of intracellular infection by cDC1s is due to their unique and nonredundant roles in antigen cross presentation (discussed below) to activate $CD8^+$ cytotoxic T cells, as well as their ability to rapidly and efficiently produce IL-12 to mediate type I immunity. In addition, recent studies have demonstrated a role of cDC1s in neutrophil recruitment during fungal (Del Fresno et al., 2018) or cutaneous bacterial infections (Janela et al., 2019).

Classical antigen presentation can be classified into two categories: the MHCII-restricted pathway and the MHCI-restricted pathway (Cresswell, 2005). The MHCII pathway involves the acquisition of exogenous antigens and subsequent presentation to $CD4^+$ helper T cells. In contrast, endogenous (intracellularly-derived) antigens are mainly presented via the MHCI restricted pathway to activate $CD8^+$ cytotoxic T cells. The latter often requires initial infection of the presenting cells such as the DCs by intracellular parasites (Heath et al., 2004). However, intracellular pathogens, particularly many viruses, have developed various immune evasion mechanisms by either 1) avoid infecting immune cells such as DCs and thus being able to escape classical MHCI antigen presentation, or 2) down-regulation of MHCI surface expression after infection of host cells (Ploegh, 1998).

Contrary to the classic antigen presentation via the MHCI pathway to activate $CD8^+$ cytotoxic T cells, cDC1s have evolved another mechanism called antigen cross presentation (or cross priming) to overcome immune evasion by these intracellular pathogens (Bevan, 1976; 1987). Antigen cross presentation involves the acquisition of exogenous antigens from another source and subsequent presentation via the MHCI (not MHCII) pathway, thus allowing activation of $CD8^+$ cytotoxic T lymphocytes (Heath et

al., 2004). This unique ability allows cDC1s to present antigens derived from intracellular pathogens without being infected themselves, thus keeping their immune functions intact to counteract the aforementioned immune evasion mechanisms. cDC1s, but not cDC2s, were shown to be the major cell type to cross present (Bedoui et al., 2009; Belz et al., 2005; Haan et al., 2000; Hildner et al., 2008; Schnorrer et al., 2006). Antigens amenable to cross presentation include soluble proteins (Pooley et al., 2001) and cell-associated antigens such as apoptotic or necrotic cells (Desch et al., 2011; Zelenay et al., 2012), virus-infected cells (Sigal 1999; Ramirez 2002), tumor antigens (Huang et al., 1994) and peptide-loaded cells (Haan et al., 2000). Thus, cDC1s not only play crucial roles in the induction of immunity against intracellular pathogens, but also in antitumor immunity.

cDC1s are not only critical in inducing antigen specific $CD8^+$ cytotoxicity via cross presentation, but also play essential roles in directing type I immune response, which is required for the clearance of intracellular pathogens (Murphy et al., 2015). cDC1s are shown to be the nonredundant source of IL-12 (Hochrein et al., 2001; Mashayekhi et al., 2011; Schulz et al., 2000; Sousa et al., 1997), which is required to induce early release of IFN-γ from nature killer (NK) cells and type 1 innate lymphoid cells (ILC1s) to control intracellular infections in a nonspecific manner (Sonnenberg and Artis, 2015). This process is known as the early stage of the type I immune response. During the late stage of type I immunity, activated type 1 T helper cells (Th1) and $CD8^+$ T cells become the major source of IFN-γ (Annunziato et al., 2015). Importantly, cDC1s are also critical during this late stage due to their ability to induce polarization of Th1 cells and priming of $CD8^+$ T cells (Durai and Murphy, 2016). Therefore, cDC1s play critical roles in mediating type I immunity during both the early and late phases.

Due to the superior ability of cDC1s in antigen cross presentation of cellular antigens including tumor antigens (Heath et al., 2004; Hildner et al., 2008; Shortman and Heath, 2010), this cell type has been demonstrated to play critical roles in mediating anti-tumor immunity. Firstly, the abundance of cDC1s in the tumor microenvironment (TME) correlates with higher tumor regression and better patient survival and outcome (Barry et al., 2018; Böttcher et al., 2018; Broz et al., 2014; Roberts et al., 2016). Conversely, a lack of cDC1s leads to failure in $CD8^+$ cytotoxic T cell responses and resistance to checkpoint immunotherapy (Sánchez-Paulete et al., 2016; Spranger et al., 2015; 2017). In addition,

vaccination strategy targeting cDC1s leads to potent cytotoxic T cell response and help control tumor growth (Hartung et al., 2015).

In the past decades, immunotherapy has emerged as one of the most effective therapies against multiple cancer types and revolutionized the field of immunology and cancer research (Pardoll, 2012). Cancer immunotherapy was selected as breakthrough of the year by the journal Science in 2013 and the 2018 Nobel Prize in Physiology or Medicine was awarded to two pioneering researchers in cancer immunotherapy; Dr James P. Allison and Dr Tasuku Honjo. One of the most common and effective immunotherapy approaches is via inhibition of immune checkpoints on T cells such as cytotoxic T-lymphocyte-associated antigen 4 (CTLA-4), programmed death 1 (PD-1) and its ligand PD-L1 (Sharma and Allison, 2015). CTLA-4 and PD-1 are both immune checkpoints on $CD8^+$ cytotoxic T lymphocytes and found to be overactivated in the TME, leading to inhibition of cytotoxicity against cancer cells. Thus, the major focus of immunotherapy research to date has been on understanding cytotoxic T cell immunity against cancer.

Despite the remarkable potential of immunotherapy, responses are variable in their effectiveness to different cancers, and between patients. Furthermore, resistance can arise even after an initial successful response. There are multiple requirements for a successful cytotoxic T cell response: 1) uptake of tumor antigens by APCs in the TME; 2) trafficking of antigen-loaded APCs to the spleen and/or tumor-draining LNs (TdLNs); 3) cross-presentation of tumor antigens to prime the $CD8^+$ cytotoxic T cells; 4) trafficking of tumor-specific effector cytotoxic T cells to TME; 5) overcoming the immunosuppressive TME and killing of cancer cells by cytotoxic T cells. When one or more of these requirements are not met, it could lead to unresponsiveness and/or resistance to checkpoint blockade therapies. Importantly, a few recent studies have highlighted the crucial roles of cDC1s at almost all key steps of a cytotoxic T cell response, even beyond its well-established role in antigen cross presentation and $CD8^+$ T cell priming (**Figure 1.2**).

First, despite being a minor population compared to other APCs such as macrophages in the TME, cDC1s are the major, if not the only cell type that can carry intact tumor antigens to the TdLNs (Roberts et al., 2016; Salmon et al., 2016). Once they reach the TdLNs, cDC1s can either directly prime cytotoxic T cells via antigen cross presentation,

or transfer antigens to resident APCs for further priming (Roberts et al., 2016). Second, cDC1s are the major cell type that cross present tumor antigens to $CD8^+$ cytotoxic T cells, and disruption of this process leads to impaired antitumor response during anti-PD-1 treatment (Alloatti et al., 2017). In addition, intra-tumoral cDC1s have been shown to be the major source of the chemokines CXCL9/10, which are required in the recruitment of both endogenous and adoptively transferred effector $CD8^+$ cytotoxic T lymphocytes to the TME (Spranger et al., 2017). More importantly, cDC1s can be directly involved in facilitating the anti-PD-1 response inside TME via cytokine interaction with $CD8^+$ T cells. The recent work by Garris et al., has proposed a 'licensing' model of cytotoxic T cell response and highlighted the importance of the crosstalk between $CD8^+$ T cells and cDC1s within the TME (Garris et al., 2018). Upon binding to anti-PD-1 antibodies, cytotoxic T cells release IFN-γ, which triggers IL-12 production from intra-tumural cDC1s, but not any other cell types in the TME. In turn, cDC1-derived IL-12 activates tumor-infiltrating cytotoxic T cells and elicit effective anti-tumor immunity. Together, these findings demonstrated essential roles of cDC1s in mediating anti-tumor immune responses.

Despite the critical roles of cDC1s in promoting cytotoxic T cell responses, this cell type is usually extremely sparse within the TME (Salmon et al., 2016). Moreover, in tumors that are resistant to T cell therapies, cDC1s are largely absent in the TME (Spranger et al., 2015; 2017). This unresponsiveness can be rescued by administration of culture-derived DCs activated with TLR3 agonist poly I:C in the resistant tumors (Spranger et al., 2015). Therefore, it is important to understand the mechanisms of how DC numbers are maintained in the TME. Two recent studies have highlighted the role of NK cells in recruiting and accumulating cDC1s within the TME, via the production of chemokines CCL5 and XCL1 (Böttcher et al., 2018) and the DC-promoting cytokine FL (Barry et al., 2018). This NK-cDC1 axis is correlated with better clinical outcomes. In addition, endogenous type I IFN signalling is shown to facilitate the accumulation of cDC1s within the TME, as deletion of IFN receptor 1 (IFNAR) in DCs leads to absence of CD8 T cell responses and failure in tumor rejection (Diamond et al., 2011; Fuertes et al., 2011). Together, these studies have highlighted the complex networks in controlling DC number within the TME.

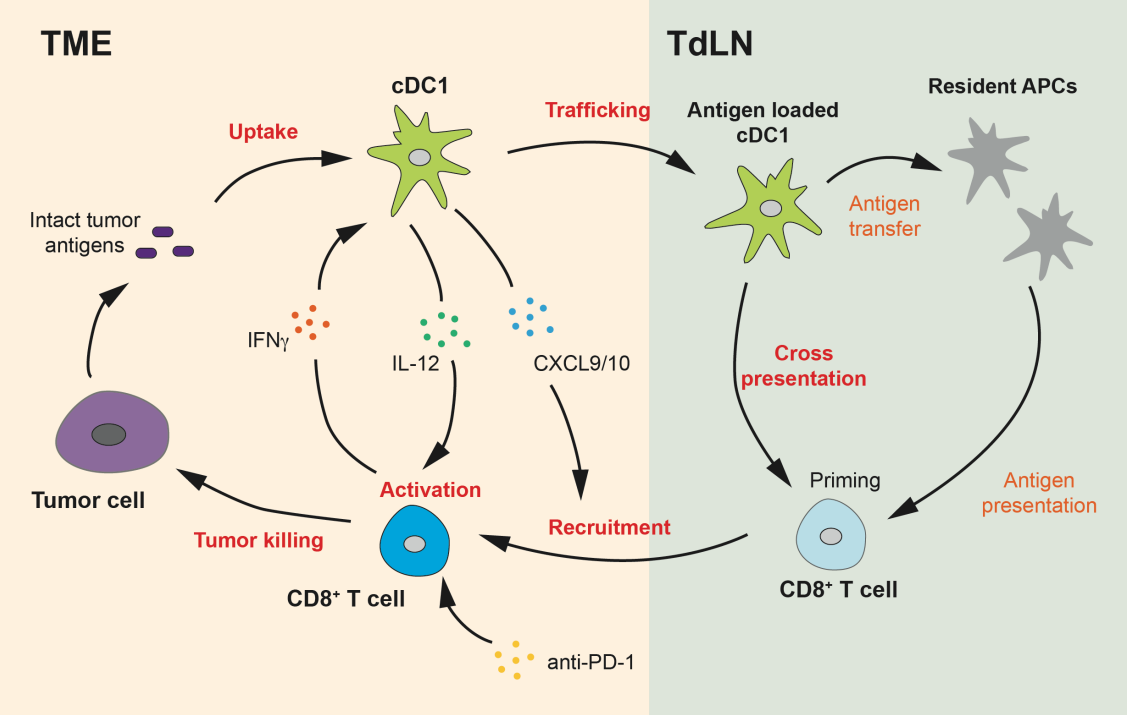

Figure 1.2 The critical roles of cDC1s in inducing and maintaining potent antitumor immunity.

cDC1s are essential in the induction and maintenance of antitumor cytotoxic responses. First, intratumoral cDC1s involve in the uptake of intact tumor antigens in the TME and the subsequent trafficking to the TdLN, where antigens are cross presented to prime naïve $CD8^+$ T cells. Alternatively, tumor antigens can be transferred to resident APCs in the TdLN to allow $CD8^+$ T cell priming. After that, primed $CD8^+$ T cells are recruited into the TME, and this process is dependent on chemokines CXCL9/10 that are released by cDC1s. Once primed $CD8^+$ T cells enter the TME, further activation by IL-12 is required to enable efficient killing of tumor cells. The production of IL-12 from cDC1s is facilitated by IFNγ signals from $CD8^+$ T cells upon binding with checkpoint inhibitors such as anti-PD-1.

cDC2s

Unlike cDC1s, the specialized function of cDC2s in the immune system is poorly understood due to the significant heterogeneity within the commonly defined cDC2 population and the lack of tools to specifically delete cDC2s. While both cDCs are capable of classic antigen presentation via the MHCII pathway to activate $CD4^+$ T cells, cDC2s are more efficient in this process (Dudziak et al., 2007; Pooley et al., 2001; Schnorrer et al., 2006; Vander Lugt et al., 2014). On the other hand, cDC2s do not appear to cross present exogenous antigens via the MHCI pathway and therefore, play a minimal role in inducing $CD8^+$ cytotoxic immunity (Vander Lugt et al., 2014). In contrast to cDC1s, cDC2s do not seem to facilitate type 1 immunity to control intracellular infections, but are involved in the induction of type 2 and type 3 immune responses upon recognition of extracellular pathogens or fungus (Dress et al., 2018; Schlitzer et al., 2013; Williams et al., 2013). Furthermore, cDC2s are critical in activating $CD4^+$ conventional T cells to facilitate $CD4^+$ antitumor responses (Binnewies et al., 2019).

Importantly, different subpopulations of cDC2s appear to mediate the distinct immune responses. Klf4-dependent cDC2s are shown to be responsible for the induction of type 2 immunity (Tussiwand et al., 2015), which is involved in controlling helminth infection and induction of airway allergic reactions (Annunziato et al., 2015; Mesnil et al., 2012; Murphy et al., 2015). This is possibly due to the regulation of IL-10 and IL-33 expression by this subset of cDC2s, which is essential for Th2 cell differentiation (Williams et al., 2013). On the other hand, the Notch2-dependent cDC2s appear to be responsible for the induction of type 3 immunity (Lewis et al., 2011; Satpathy et al., 2013). Notch2-dependent cDC2s are shown to be the critical source of IL-23 (Satpathy et al., 2013), which leads to production of IL-22 and IL-17 by ILC3s and Th17 cells to promote type 3 immune response (Kinnebrew et al., 2012; Lewis et al., 2011; Persson et al., 2013; Schlitzer et al., 2013).

pDCs

The most pronounced and well characterized role of pDCs in the immune system is their superior capacity to rapidly produce and release large amounts of type I IFNs in response to viral infection (Cervantes-Barragan et al., 2012; Shigematsu et al., 2004; Swiecki et

al., 2010). Recognition of most viruses is mediated via the engagement of TLR7 and TLR9, which are abundantly expressed in the endosomal compartments of pDCs. RNA viruses and endogenous RNAs are recognized by TLR7, whereas TLR9 senses CpG-containing DNA viruses and endogenous DNAs (Swiecki and Colonna, 2015). pDCs express high level of Irf7, which regulates the production of type I IFNs (Honda et al., 2005). After engagement of TLR7 or TLR9, pDCs activate the myeloid differentiation primary response protein 88 (MYD88)-IRF7 pathway, which leads to the production of large amount of type I IFNs (Swiecki and Colonna, 2015).

pDCs have been implicated in the pathogenesis of multiple autoimmune diseases with a type I IFN signature, most notably systemic lupus erythematosus (SLE) (Ganguly et al., 2013). Immune complexes containing autoantibodies attached to endogenous nucleic acids are found in the serum of SLE patients. These immune complexes can activate pDCs via TLR7, TLR9 or CD32 (FcyRIIa), which lead to continuous production of type I IFNs and ultimately contribute to disease progression (Barrat et al., 2005; Båve et al., 2003; Means et al., 2005). In addition to SLE, pDCs have been implicated in the initiation and progression of other autoimmune diseases such as Type I diabetes and psoriasis (Ganguly et al., 2013). Thus, pDCs represent an attractive therapeutic target in preventing or treating autoimmune diseases such as SLE.

Historically, pDCs were thought to be an immature form of classical DCs that could acquire cDC-like phenotypes such as the stellate morphology, and functions such as antigen presentation upon maturation (Nakano 2001; Sapoznikov 2007; Shortman 2013). However, such attributed properties of pDCs are highly controversial, as remarkable heterogeneity within the commonly defined pDC compartment has been demonstrated. In particular, precursors with the potential for further development into cDCs have been found in the phenotypically defined pDC population, in both mouse and human (as discussed aboved). Thus, it is possible that previous observations of phenotypic and functional changes of pDCs merely reflects differentiation of cDCs from contaminating DC precursors.

Distinct properties between pDCs and cDCs regarding cancer progression have been observed. In contrast to cDC1s, which have a demonstrated role in inducing antitumor immunity, the abundance of intra-tumoral pDCs usually correlates with poor prognosis

in cancer (Sisirak et al., 2012). This is because pDCs in the tumor microenvironment tend to be immunosuppressive rather than immunostimulatory, by inducing regulatory T cell (Treg) activation and expansion, and suppression of cytotoxic T cell responses (Fallarino et al., 2004; Sisirak et al., 2012). Another major difference between cDCs and pDCs in the context of cancer research is that pDCs have been identified as the cell of origin in a form of leukaemia called the blastic plasmacytoid dendritic cell neoplasm (BPDCN), but either cDC1- or cDC2-transforming cancer has been observed (Chaperot et al., 2001). BPDCN represents a rare and aggressive form of leukaemia and it is largely incurable (Ceribelli et al., 2016).

DC development

Mature DCs typically live for 3-5 days in circulation and in most lymphoid and nonlymphoid organs (Kamath et al., 2000; Yifan Zhan 2016). Thus, to maintain stable numbers of DCs from the different subtypes in the body at any given time, constant replenishment from the haematopoietic system is required. DCs, like most other haematopoietic cells, develop from haematopoietic stem cells (HSCs) via a process called haematopoiesis. Thus, maintaining DC homeostasis requires proper control and regulation of this process. The current understanding of DC development in the context of the classical and revised models of haematopoiesis will be discussed here.

DC development in the context of a classical model of haematopoiesis

The classical model of haematopoiesis is usually represented as a hierarchical, step wise lineage commitment model (Ema et al., 2014; Haas et al., 2018). In this model, the most primitive HSCs reside at the top of the hierarchy, which have self-renewal capacity and are multipotent. This endows them with the capacity to repopulate the entire blood system over long periods of time. Following the HSC stage, a multipotent progenitor (MPP) population emerges. These MPPs can no longer self-renew but maintain the capacity to differentiate into all blood lineages. While there are many versions of such hierarchical trees, one of the most commonly used models describes the first branching event to occur downstream of MPPs into common lymphoid progenitors (CLPs) (Kondo 1997) and common myeloid progenitors (CMPs) (Akashi 2000), which are restricted towards lymphoid or myeloid lineages, respectively. Downstream of CLPs and CMPs, further branching events occur, which result in step by step lineage restriction through oligo-, bi- and eventually uni-potent progenitor populations to reconstitute the entire blood system. Interestingly, despite the early separation of myeloid and lymphoid development described in most models, all three subtypes of DC can derive from both developmental pathways to form a unique haematopoietic lineage (**Figure 1.3**).

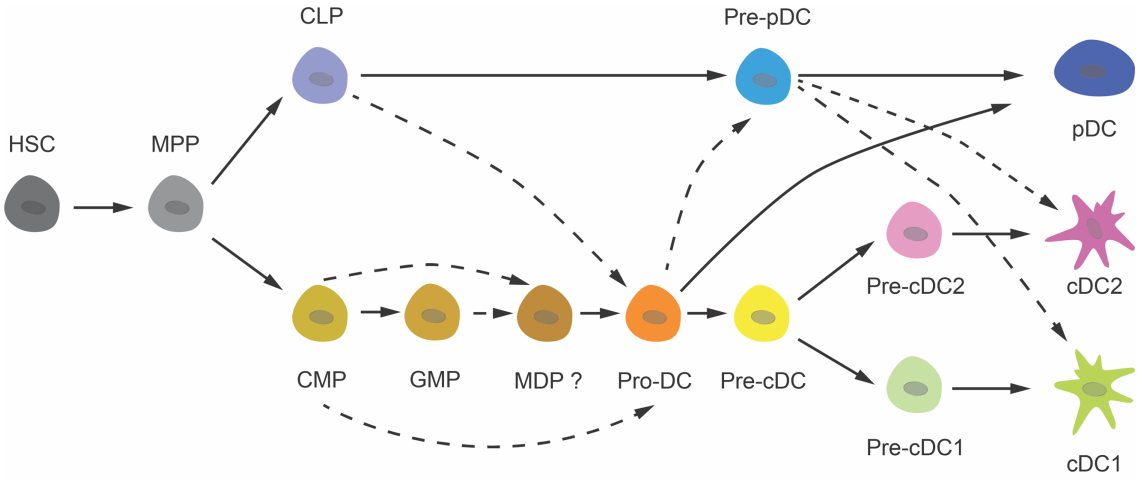

Figure 1.3 Schematic of DC development from different progenitor populations.

The traditional hierarchical model of DC development considers a step by step lineage restriction, leading to DC commitment and differentiation. The model starts with a pool of self-renewal HSCs giving rise to downstream MPPs, both have the ability to regenerate all haematopoietic lineages. In most models, the haematopoietic system then branches into the myeloid and lymphoid developmental pathways. One unique feature of DC development is the potential to developed from both pathways. The myeloid pathway of DC development is relatively well characterized with multiple intermediated progenitor populations being identified. The lymphoid pathway of DC development is less understood. Solid arrows indicate well established populations and pathways. Dotted arrows depict uncharacterized or controversial populations and pathways.

Early progenitors with DC potential

DCs were initially thought to have a myeloid origin as they could develop alongside granulocytes and macrophages in a granulocyte-macrophage colony-stimulating factor (GM-CSF) supplemented-culture system (Inaba et al., 1993). Furthermore, DCs and macrophages can have a similar morphology and share some overlapping functions. Subsequently, an early thymic precursor population was identified that could generate both lymphocytes and cDC1s, which led to the theory that cDC1s were of lymphoid origin and cDC2s developed from a myeloid pathway (Ardavin et al., 1993; Wu et al., 1995). However, this was soon questioned with the discovery of CMPs (Akashi et al., 2000) and CLPs (Kondo et al., 1997), and the characterization of their DC potential. A series of studies confirmed that all DC subtypes could be generated from both CMPs and CLPs

(Chicha et al., 2004; D'Amico and Wu, 2003; Manz et al., 2001; Sathe et al., 2013; Traver et al., 2000; Wu et al., 2001). A recent study further suggested the co-existence of myeloid and lymphoid developmental pathways for DC generation in human (Salvermoser et al., 2018).

To discriminate DC development originated from the myeloid vs lymphoid pathways, two features of lymphoid origin were examined extensively in mature DC subsets. These included expression of RAG1 and DJ rearrangement of immunoglobulin heavy chain (IgH) gene (Pelayo et al., 2005). One study showed that a proportion of both thymic and splenic pDCs and cDC1s from thymus, but not spleen, displayed IgH gene rearrangement (Corcoran et al., 2003). As thymus is the site of T lymphocyte maturation, this supported the hypothesis that DJ rearrangement reflected a lymphoid origin of DCs in the thymus compare to other organs. However, another study using a RAG1-GFP reporter line demonstrated that only a proportion of pDCs were RAG1-GFP$^+$ with pre-T cell receptor gene expression, but that these could be generated from both CMPs and CLPs, thus arguing the direct link between RAG1 expression and lymphoid developmental history (Shigematsu et al., 2004). However, despite having the potential to general all myeloid lineages, CMPs were also shown to retain some lymphoid potential, so this result may not be as surprising (Akashi et al., 2000). Therefore, one could argue that those CMP-derived pDCs with DJ rearrangement and RAG1 expression may have originated from this small subset of CMPs with residual lymphoid potential (Harman et al., 2006). Indeed the lymphoid and pDC potential of CMPs was restricted to those that were Flt3$^+$ (D'Amico and Wu, 2003; Karsunky et al., 2003). Importantly, regardless of the myeloid or lymphoid origins, DC development seemed to be regulated via similar transcriptional controls involving the transcription factor Irf8 (Becker et al., 2012). Together, the convergence of DC development from myeloid and lymphoid pathways remains poorly understood.

Macrophage and DC progenitors (MDPs)

Historically, DCs and macrophages were both thought to be monocyte-derived and that these three cell types constituted the mononuclear phagocyte system that were closely related in development and shared similar immune functions (Guilliams et al., 2014). However, as oppose to classical steady-state DCs, monocyte-derived DCs are GM-CSF-dependent, but not FL-dependent and display an inflammatory phenotype (Shortman and

Naik, 2007). Hence, these monocyte-derived cells represent a distinct lineage. Next, a progenitor population was described to give rise to monocytes, macrophages and steady-state cDCs and was termed monocyte-macrophage DC progenitor (MDP) (Fogg et al., 2006). These MDPs were defined as Lin^{-} $cKit^{+}$ $Sca1^{-}$ $CX3CR1^{+}$ $IL7R\alpha^{-}$ $CD34^{+}$ $CD16/32^{+}$ (Fogg et al., 2006). Later studies had included M-CSFR (CSF1R or CD115) as an additional positive marker for MDPs and showed that MDPs could give rise to pDCs (Auffray et al., 2009; Waskow et al., 2008).

However, the MDPs used in these studies were shown to have overlapping phenotypes with other progenitors (Auffray et al., 2009; Fogg et al., 2006; Waskow et al., 2008), hence it was unclear whether their lineage potential was indeed restricted to DCs and macrophages at a single cell level. Furthermore, the culture assays used in these studies were dependent on M-CSF or GM-CSF, rather than FL, which did not reflect steady-state DC development. Another contradiction was the lack of DC potential in the granulocyte-monocyte progenitor (GMP) population (D'Amico and Wu, 2003), which was thought to be upstream of the reported MDPs.

The existence of MDPs was further questioned by a recent study (Sathe et al., 2014), which conducted a systematic evaluation of the reported MDPs and other potential progenitors using adoptive transfer, agar colony assays and clonal liquid assays including FL culture. This study confirmed that previous reported 'MDP populations' were not restricted to DC and macrophage generation and failed to find such population within the $Lin^{-}MCSFR^{+}$ BM fraction (Sathe et al., 2014). Therefore, whether DCs and macrophages share a common restricted developmental stage is highly debatable.

Common DC progenitors (CDPs)

The observation of DC development from both the myeloid and lymphoid arms raised the question of whether a restricted DC progenitor population existed that could generate all DC subtypes but not any other lineages. In 2007, two independent groups discovered such a population from the bone marrow (BM) that could generate both cDCs and pDCs in FL cultures and in the spleen upon transfer *in vivo* (Naik et al., 2007; Onai et al., 2007). These common DC progenitors (CDPs) or pro-DCs were defined as lin^{-} $ckit^{int}$ $Flt3^{+}$ $M\text{-}CSFR^{+}$ in mouse (Naik et al., 2007; Onai et al., 2007). In addition, pro-DCs were shown to

produce different DC subtypes in non-lymphoid tissues such as intestine and kidney (Bogunovic et al., 2009; Ginhoux et al., 2009; Varol et al., 2009). Pro-DCs were shown to proceed immediately downstream of the previous reported MDPs, which were in turn downstream of CMPs, indicating pro-DCs are the first dedicated DC progenitor population in the haematopoietic tree (Liu et al., 2009). In contrast to myeloid progenitors, $Flt3^+$ lymphoid progenitors do not generate detectable amount of pro-DCs upon transplantation (Onai et al., 2007). Thus, how DC commitment arises from the lymphoid pathway and what intermediate progenitors involve remain largely unknown.

cDC precursors

Downstream of pro-DCs, a pre-cDC population was identified from the spleen as $CD11c^{int}$ $MHCII^-$ $CD45RA^{lo}$ $CD43^{int}$ $Sirpa^{int}$ $CD4^-$ $CD8^-$ that could generate both cDC1s and cDC2s but not pDCs and other lineages (Naik et al., 2006). Furthermore, expression of CD24 was shown to separate pre-cDCs that were biased towards cDC1s ($CD24^{hi}$ pre-cDC) or cDC2s ($CD24^{lo}$ pre-cDC) (Naik et al., 2006). Later, pre-cDCs were shown to also reside in the BM, LN and blood (Liu et al., 2009), suggesting terminal differentiation of cDC1s and cDC2s might occur after pre-cDCs migration from the BM and in the final organ of residence. However, recent examination of pre-cDC heterogeneity using single cell transcriptional profiling identified Siglec-H and Ly6C as markers that could segregate restricted cDC1 and cDC2 precursors, which were both found in BM, blood and spleen (Schlitzer et al., 2015). Another independent group also identified restricted pre-cDC1s and pre-cDC2s in the BM using transcription factor Zbtb46 and surface marker M-CSFR (Grajales-Reyes et al., 2015).

Collectively, pre-cDC1s could be defined as $CD24^{hi}$ Siglec-H^- $Ly6C^-$ $cKit^{int}$ $MHCII^{int}$ $Zbtb46^+$ and pre-cDC2s as $CD24^{lo}$ Siglec-H^- $Ly6C^+$ $cKit^-$ $MHCII^-$ $MCSFR^+$ (Grajales-Reyes et al., 2015; Naik et al., 2006; Schlitzer et al., 2015). However, these independently identified cDC-restricted precursors have not been compared and will require further investigation to confirm whether they represent the same or different populations. Nonetheless, these findings indicate that cDC1 and cDC2 commitment likely occurs in the BM before entering the periphery. This notion was further supported by intravital imaging of peripheral tissues from the Clec9A-confetti mice, which revealed that the majority DC clones found in the peripheral tissues such as the spleen consisted of a single

DC subtype (Cabeza-Cabrerizo et al., 2019). This finding further suggested that DC progenitors in peripheral tissues were predominantly those with DC subtype committed fate at the clonal level.

pDC precursors

In contrast to the in-depth characterization of cDC development, the steps in pDC development are less well understood. Several pDC precursor populations have been described. One study suggested that the Ly49Q$^-$ fraction within the phenotypically defined pDC population (CD11c$^+$ B220$^+$) was the immediate pDC precursor (Omatsu et al., 2005). However, since these cells up-regulate Ly49Q and acquire typical pDC features without further division, one could argue that they are only an immature form of pDCs that had already acquired such fate. Another possible pre-pDC candidate is CCR9$^-$ MHCII$^{-/lo}$ cells within the phenotypically defined pDC population (CD11c$^+$ Bst$^+$ Siglec-H$^+$). However, although CCR9$^-$ pDCs could give rise to CCR9$^+$ cells, they were also able to differentiate into cDC-like cells under stimulation such as GM-CSF or in certain tissues after *in vivo* transfer (Schlitzer et al., 2011; 2012). In addition, our recent work confirmed that CCR9$^-$ cells were precursors of both cDCs and pDCs (Lin et al., 2018). Thus, CCR9$^-$ pDC-like cells do not represent a pDC-committed precursor population. Recently, a population defined as lin$^-$ ckit^{int} Flt3$^+$ M-CSFR$^-$ was shown to preferentially (but not exclusively) generate pDCs (Onai et al., 2013). Interestingly, it appeared that the prominent pDC progenitors could be generated directly from either pro-DCs or lymphoid-primed multipotent progenitors (LMPPs) (Onai et al., 2013), suggesting possible early priming of pDC before specification of DC branching.

A recent study identified a lymphoid precursor population with almost exclusive pDC output and suggested a predominant contribution to pDC generation from the lymphoid developmental pathway, rather than the myeloid pathway as commonly believed (Rodrigues et al., 2018). These 'pre-pDCs' were identified by the co-expression of Siglec-H and Ly6D and were found within the Lin$^-$ cKit$^{int/lo}$ Flt3$^+$ IL7R$^+$ compartment, as opposed to most other DC progenitors including the CDPs (Naik et al., 2007; Onai et al., 2007) and the previously described pDC-biased M-CSFR$^-$ precursors (Onai et al., 2013), which are both IL7R$^-$. The production of pDCs from these 'pre-pDCs' peaked between three to five days in FL culture, suggesting a relatively late stage precursor identity of

these cells. Despite the positive expression of IL7R, the Siglec-H^+ $Ly6D^+$ 'pre-pDCs' did not generate any B cells *in vitro*, but could produce a small number of cells with cDC phenotypes (~5%). Thus, these cells represent a pDC precursor population with the most restricted pDC fate described in the literature so far.

However, there were a few potential caveats in interpreting the findings from this study (Rodrigues et al., 2018). First, the mature pDCs was defined by the co-expression of CD317 and CD45RA, but did not consider CCR9 expression. Thus, these 'mature pDCs' might still contain contaminating DC precursors and this could lead to over-estimation of pDC commitment by the 'pre-pDC' population described in the study. Second, there was no real indication that these cells were of lymphoid origin. As discussed earlier, myeloid-derived pDCs can displayed lymphoid characteristics such as RAG1 expression and DJ rearrangement (Shigematsu et al., 2004). Similarly, positive IL7R might not be indicative of a lymphoid identity. A further contradicting observation was that the development of these 'pre-pDCs' and mature pDCs were dependent on the DC development factor FL, but not the lymphoid cytokine IL-7 (Rodrigues et al., 2018). Hence, one could argue that the observed lymphoid-like signatures of pDCs and the newly described 'pre-pDCs' might be due to other aspects of pDC biology such as their function in type I IFN production and secretion, which might require a similar machinery to antibody secretion in B cells. Together, whether pDCs are predominantly generated via a lymphoid developmental pathway is still largely debatable.

DC development in the context of a revised model of haematopoiesis

Despite intense research over the past few decades on identifying the step by step commitment of DC development and diversification, recent work, particularly those taking single cell approaches, have highlighted striking molecular and functional heterogeneity within a variety of progenitor populations. There is now accumulated evidence indicating that single HSPCs, which were previously believed to have multilineage potential, are indeed mostly lineage-biased or even lineage-restricted at this early stage. These findings led to the proposition that current hierarchical models of haematopoiesis were not sufficient to explain or account for most of the controversies discussed above, and revised models of haematopoiesis have recently been proposed (Giladi et al., 2018; Karamitros et al., 2018; Laurenti and Göttgens, 2018; Velten et al., 2017a).

One of the most popular revised models has been termed the continuous model of haematopoiesis (Laurenti and Göttgens, 2018; Velten et al., 2017a). In this model, phenotypically defined HSPC populations are described as clouds of cells. Each cell within a defined cloud shares previously attributed properties such as expression of key surface markers and gene signatures, but already exhibits different degree of lineage priming towards different lineages. In addition, as opposed to a step by step commitment process as described in the classical models, this model considers a more gradual and continuous differentiation process along developmental trajectories of individual clones. The evidence leading to the proposal of such a model will be discussed below.

Functional heterogeneity of HSCs

According to the classical model, HSCs are postulated to reside at the apex of the hierarchical tree. However, significant heterogeneity in lineage output and repopulation dynamics has already been observed in the most primitive HSC population. Early attempts to resolve such heterogeneity and remodel the hierarchical tree has led to further fractionation of the HSC compartment (Schroeder, 2010). Classification based on differential capacity to repopulate the blood system divides HSCs into three categories: the long-term repopulating HSCs (LT-HSCs), the intermediate-term HSCs (IT-HSCs) and the short-term HSCs (ST-HSCs) (Ema et al., 2014). Despite the lack of any empirical evidence, such nomenclature system and the intention to fit these cell types into a

hierarchical model has leaded to the impression that LT-HSCs give rise to ST-HSCs via the IT-HSC intermediate state.

Another common classification of the HSC compartment considers distinct fate biases observed in transplantation studies, which results in three classes including the myeloid-biased, lymphoid-biased and balanced HSCs (Muller-Sieburg et al., 2004; 2012). Because the classical model considers the most primitive HSCs to be both self-renewing (hence leads to long-term repopulation) and multipotent, one would expect the balanced HSCs to represent the LT-HSCs discussed above. Surprisingly, this was not the case. In fact, LT-HSCs were found to have the greatest overlap with HSCs that were biased towards myeloid generation and most balanced HSCs displayed repopulating kinetics similar to the IT-HSCs (Dykstra et al., 2007; Ema et al., 2014). The lymphoid-biased HSCs were shown to have the least repopulating capacity and hence were most similar to ST-HSCs (Dykstra et al., 2007; Ema et al., 2014). Together, these observations further challenged the notion that these HSC subtypes represent discrete developmental stages in a hierarchical model.

In fact, none of the aforementioned classifications could explain the complexity and heterogeneity observed in the repopulating dynamics of HSCs using single cell fate analysis including *in vitro* single cell cultures and *in vivo* single cell transplantation (Benz et al., 2012; Dykstra et al., 2007; Morita et al., 2010; Muller-Sieburg et al., 2004; 2002; Notta et al., 2016a; Sieburg et al., 2006; Yamamoto et al., 2013). In addition, clonal lineage bias was also observed in the fetal liver HSC compartment, both in mouse and human, which represents a more primitive population than the adult HSCs in the BM (Benz et al., 2012; Notta et al., 2016a). More importantly, fate bias within single HSCs was demonstrated to sustain over serial transplantation, thus represents an inheritable property of individual HSCs (Dykstra et al., 2007; Muller-Sieburg et al., 2002; 2004; Yamamoto et al., 2013). Together, the complexity revealed by single cell fate tracking studies further challenged the practicality of the hierarchical model of haematopoiesis.

Importantly, lineage-restricted HSCs have recently been described. Several research groups independently discovered the existence of a subset of cells with restricted fate towards the megakaryocyte (Mk) lineage within the phenotypically defined HSC compartment (Carrelha et al., 2018; Haas et al., 2015; Rodriguez-Fraticelli et al., 2018;

Sanjuan-Pla et al., 2013). These Mk-committed cells displayed HSC-like characteristics with respect to their long-term repopulating patterns and hence demonstrating their ability to self-renew (Carrelha et al., 2018; Rodriguez-Fraticelli et al., 2018; Sanjuan-Pla et al., 2013). One study suggested these Mk-committed HSCs were relatively quiescent and contributed little to Mk production in the steady-state, but served as an emergency reservoir upon stimulation (Haas et al., 2015). In contrast, other studies demonstrated steady contribution from the Mk-restricted clones in steady-state un-perturbed haematopoiesis (Carrelha et al., 2018; Rodriguez-Fraticelli et al., 2018). More recently, a subset of myeloid/lymphoid-restricted HSCs, which lost the potential to generate erythrocytes was described in the human HSC compartment (Belluschi et al., 2018). Together, these findings highlighted the need for revaluation of HSC definition, as the two fundamental properties (self-renewal and multipotency) according to the classical model do not always co-exist within single phenotypically defined HSCs.

Functional heterogeneity of progenitors

While lineage restriction amongst HSCs is relatively rare (Carrelha et al., 2018), downstream multipotent and oligo-potent progenitor populations such as MPPs and CMPs have been demonstrated to be largely lineage-imprinted (Naik et al., 2013; Perié et al., 2015; Velten et al., 2017a). In particular, early priming of DC fate has been described by several studies.

One of the earliest lines of functional evidence regarding progenitor heterogeneity was from a study using cellular barcoding to track the development of single mouse lymphoid-primed multipotent progenitors (LMPPs) (Naik et al., 2013). At the population level, LMPPs were demonstrated to maintain the potential towards myeloid, lymphoid and DC lineages, but not erythrocytes and megakaryocytes (Adolfsson et al., 2005). Strikingly, at the single cell level, the majority of LMPPs were biased towards one or two lineages, whereas only 3% of LMPPs were multi-outcome. Interestingly, approximately 50% of the LMPPs had a DC-restricted output in the spleen (Naik et al., 2013), which could indicate profound DC lineage specification within the early LMPP population. Importantly, the observed fate heterogeneity seemed to be an intrinsic property of progenitors as siblings derived from single cells had similar fate when transferred in

separate mice (Naik et al., 2013). This implied that the lineage fate of most LMPPs might be restricted or even imprinted at stages earlier than in branching of CMPs and CLPs.

A similar finding was recently demonstrated in the human early lymphoid primed multipotent lymphoid progenitor (MLP) population, which represent the human counterpart of murine LMPPs (Helft et al., 2017). This study utilized an *in vitro* culture system that allowed the formation of both cDCs and myeloid cells and found that over one third of single human MLPs generated only cDCs, suggesting early imprinting of DC fate in the MLP population (Helft et al., 2017). Similarly, another study conducted a systematic evaluation of single cell fate to multiple lineages from distinct HSPC populations *in vitro* and *in vivo,* and demonstrated that human DC lineage specification occurred in parallel with myeloid and lymphoid specification at early HSPC stage (Lee et al., 2017).

Importantly, early fate specification of DC subtypes was also observed. As introduced earlier, pro-DCs as a population could generate all three types of DCs. However, clonal FL culture assays showed that only approximately 15% were truly multi-potent (generated all DC subtypes) while the others were biased towards one or two subsets, suggesting possible pre-commitment in some cells within the population (Naik et al., 2007; Onai et al., 2007; 2013). Importantly, when pooling the outputs of all single cells together, the profile was similar to that of the population controls in the same experiment (Naik et al., 2007). Hence, tracking cell fate at single cell level demonstrates heterogeneity that adds up to the population-level outcome of defined populations, a feature that is often neglected.

Most of the aforementioned single cell tracking studies only assessed clonal output at a single time point, which might not reveal the true lineage potential of single clones. A recent study in our lab conducted longitudinal tracking of DC fate of single LSKs and confirmed significant functional heterogeneity within these early HSPCs (Lin et al., 2018) (**Chapter 3**). Amongst the DC-generating LSKs, the majority of clones had a restricted output towards either cDCs or pDCs, indicating early DC subtype specification at early stages of development.

Together, these findings based on single cell fate tracking challenged the notion that DC developed alongside other myeloid and lymphoid cells through discrete stages in the classical hierarchical model and highlighted early imprinting of DC fate at the single cell level. Importantly, a recent study showed that Irf8 expression in LMPPs increase accessibility of enhancers near DC lineage genes, indicating a potential molecular determinant of early DC priming (Kurotaki et al., 2019a)

Molecular heterogeneity of HSPCs

Consistent with the notion that most single HSPCs display lineage bias or lineage restriction at the functional level, single cell expression profiling using multiplexed PCR (Guo et al., 2013; Pina et al., 2012; 2015; Wilson et al., 2015) and more recently scRNAseq (Giladi et al., 2018; Grover et al., 2016; Karamitros et al., 2018; Nestorowa et al., 2016; Paul et al., 2015; Tusi et al., 2018; Velten et al., 2017a) have highlighted molecular heterogeneity within multiple phenotypically defined HSPC populations. Considering fate decisions are executed at a single cell level, the observed heterogeneity at the transcriptional level might reflect the priming states responsible for the ultimate lineage bias measured at the functional level. In fact, early HSPCs were shown to form a continuum of lowly-primed undifferentiated cells, where they gradually acquire lineage programs towards different directions without passing discrete developmental stages, as oppose to the classical model of haematopoiesis (Giladi et al., 2018; Karamitros et al., 2018; Laurenti and Göttgens, 2018; Velten et al., 2017a). These observations lead to proposal of the continuous model of haematopoiesis.

Importantly, definitive evidence demonstrating a direct causation relationship between transcriptional priming and functional bias is lacking. This is because a single cell cannot simultaneously be tested for both gene expression and lineage output. Recent studies have utilized a multi-omics single cell profiling approach to correlate the two features, where single cells were index sorted to record surface marker expression, followed by either gene expression analysis or lineage tracking assays (Karamitros et al., 2018; Velten et al., 2017a). Subsequently, comparison between the gene signatures and fate biases of cells with similar phenotypic profiles allowed inference of the transcriptional network correlated with specific lineage output. However, one confounding factor of such an

approach was the assumption that a set of surface markers can define a relatively homogenous population.

Recently, another novel method called SIS-seq has been developed in our lab to allow correlation of gene signatures with lineage output of single cells (Tian et al., 2018). This method is based on the observation that sisters derived from the same founder clones are largely conserved in lineage output and kinetics (Lin et al., 2018; Naik et al., 2013). Therefore, individual clones can be pre-expanded *in vitro* to generate a pool of sisters, which can then be split to undergo either gene expression analysis using scRNAseq or fate tracking assays. This study has led to the identification of potential novel regulators of DC development (Tian et al., 2018).

Flt3 and Flt3 ligand (FL)

While many factors such as transcription factors and cytokines are demonstrated to be critical in DC development and subtype diversification, most of them also have overlapping roles in other haematopoietic developmental pathways. However, the cytokine FL appears to play a unique and indispensable role in DC development. The receptor for FL, Flt3, is shown to expressed in a variety of haematopoietic cells. Here, the role of Flt3 and FL will be discussed in the context of early haematopoiesis and DC development.

FL in early haematopoiesis

The receptor Flt3 was first identified in 1991 by two independent groups and found to be highly expressed in cells within the early HSPC compartment, but largely absent in mature haematopoietic cells (Matthews et al., 1991; Rosnet et al., 1991). This suggested a putative role of Flt3 in regulating early haematopoiesis. Flt3 is structurally similar to other members of the receptor tyrosine kinase III family, including cKit, an important early HSPC marker and receptor for stem cell factor (SCF), and cFms, receptor for colony stimulating factor-1 (CSF1 or M-CSF) (McKenna, 2000). Two years after the identification of Flt3 receptor, its ligand Flt3 ligand (FL) was successfully cloned and purified (Hannum et al., 1994; Lyman et al., 1994; 1993). This led to an explosion of interest in investigating the role of FL on early haematopoiesis.

In the late 1990s, a large number of studies utilized *in vitro* colony forming assays to assess the growth and differentiation of haematopoietic progenitors in response to FL alone, or in combination with various other haematopoietic cytokines such as stem cell factor (SCF), G-CSF, GM-CSF, IL-6 and IL-7. Interestingly, when used alone, FL had minimal effect to sustain the survival and/or promote the growth of haematopoietic cells (Hirayama et al., 1995; Jacobsen et al., 1995; Veiby et al., 1996) (Brashem-Stein et al., 1996; Broxmeyer et al., 1995). However, when used in combination with other haematopoietic cytokines, remarkable synergistic effect was observed in promoting cell proliferation and/or differentiation to generate both myeloid and lymphoid cells, but not erythrocytes or megakaryocytes (Banu et al., 1999; Brashem-Stein et al., 1996; Broxmeyer et al., 1995; Hirayama et al., 1995; Hudak et al., 1995; Jacobsen et al., 1995;

Namikawa et al., 1996; Ray et al., 1996). Despite the limitations regarding the lack of markers to purify distinct HSPC populations, the exclusive use of *in vitro* colony assays to determine cell properties and the lack of proper evaluation of the interplay between survival, proliferation and differentiation effects of FL in these early studies, these findings clearly demonstrated important roles of FL in regulating early haematopoiesis.

In vivo studies further revealed important roles of FL during early haematopoiesis. *In vivo* administration of FL seemed to induce mobilization of early HSPCs from the BM into the periphery. This was supported by the observation of increased colony formation *in vitro* and enhanced lineage reconstitution *in vivo* using cells from the peripheral blood (PB) or organs such as the spleen after FL injection, particularly in combination with other blood mobilizers such as G-CSF (Brasel et al., 1997; 1996; de Kruijf et al., 2010; Molineux et al., 1997; Neipp et al., 1998; Papayannopoulou et al., 1997; Sudo et al., 1997). One of the demonstrated mechanisms regulating FL-induced mobilization of early haematopoietic progenitors was via the interaction between chemokine CXCL12 and chemokine receptor CXCR4 (Fukuda et al., 2005). A recent study also reported superior outcomes using FL and Plerixafor (a stem cell mobilizer) than the combination of G-CSF and Plerixafor in inducing mobilization of mouse LSKs (He et al., 2014). Thus, FL could potentially be used in combination with other blood mobilizers to boost the number of early HSPCs in the blood for stem cell transplantation.

Consistent with the notion suggested by the *in vitro* studies that FL promotes selective proliferation and/or differentiation of haematopoietic cells, FL administration or overexpression *in vivo* also resulted in enhanced production of mature cells within both the myeloid and lymphoid compartments, but not megakaryocytes or erythrocytes (Brasel et al., 1996; Tsapogas et al., 2014). However, mice with genetic disruption of Flt3 had few defects in the generation of mature myeloid and lymphoid populations, despite a reduction in the early B cell progenitors in the BM (Mackarehtschian et al., 1995). This was suggestive of a potential role of Flt3 in regulating early lymphopoiesis, but not during the later stage of B cell development or myelopoiesis. On the other hand, FL-deficient mice displayed a more severe haematological defect with reduced cellularity in the PB and multiple organs (McKenna et al., 2000). In agreement with the Flt3 mutant mice, a more severe defect was observed in the lymphoid compartment compared to the myeloid populations (McKenna et al., 2000; Sitnicka et al., 2003). Importantly, reduction in cell

numbers was again more apparent in the early lymphoid progenitors such as the CLPs and pro-B cells than in the more differentiated lymphoid populations such as pre-B cells and mature B cells (McKenna et al., 2000; Sitnicka et al., 2003). Therefore, this could indicate downstream rescue mechanisms in myeloid and lymphoid development to compensate for the early defect caused by the absence of FL signalling. Overall, FL appears to regulate early, but not late stages of lymphoid development.

Flt3 expression in early haematopoietic progenitors

With the identification of multiple markers to better delineate developmental stages of the early HSPC compartment and the use of *in vivo* transplantation studies to determine lineage output, restricted expression patterns of Flt3 associated with distinct progenitor cell behaviour were identified. In 2001, two independent studies demonstrated that positive Flt3 expression within the early HSPC compartment (defined as LSKs in these studies) correlated with the loss of self-renewal capacity, hence indicated the lack of Flt3 expression within the most primitive, long-term repopulating HSC population (Adolfsson et al., 2001; Christensen and Weissman, 2001). Consistent with this notion, little disruption was observed in the HSC compartment upon genetic knockout of FL (Sitnicka et al., 2003).

Later, the top 25% Flt3 expressing cells within the LSK compartment were shown to have significantly reduced lineage potential towards megakaryocytes and erythrocytes (Mk/E) while retaining both lymphoid and myeloid potential (Adolfsson et al., 2005). The identification of these $Flt3^{+}$ lymphoid-biased multipotent progenitors (LMPPs) challenged the classical hierarchical model at the time, which implied the segregation of myeloid and lymphoid pathways as the earliest lineage commitment event during haematopoiesis (Akashi et al., 2000; Kondo et al., 1997). This model also concurred with early evidence presented earlier, which suggested that FL did not seem to play a role in Mk/E development, either *in vitro* or *in vivo*. Furthermore, recent evidence showing the lack of co-expression of Flt3 and EpoR mRNAs at the single cell level within the HSPC compartment (Mooney et al., 2017) and the identification of primitive Mk-biased long-term repopulating cells (Carrelha et al., 2018; Haas et al., 2015; Rodriguez-Fraticelli et al., 2018; Sanjuan-Pla et al., 2013) further supported the early Mk/E divergence model.

However, this model was challenged by another study in 2006, which demonstrated notable reconstitution of platelets and erythrocyte precursors by the LMPPs upon transplantation (Forsberg et al., 2006). Thus, it remains controversial whether Flt3 downregulation within the LSK compartment marks the loss of Mk/E lineage potentials. Despite controversial findings between the two groups (Adolfsson et al., 2005; Forsberg et al., 2006), both agreed that all haematopoietic lineages (Mye/Lym/Mk/E assessed in these studies) developed through a $Flt3^+$ stage using a Flt3-cre lineage tracing model that allowed fluorescent tagging of cells with Flt3 expressing history (Boyer et al., 2011; Buza-Vidas et al., 2011).

Flt3 expression remains on some haematopoietic cells after the MPP stage. Positive expression of Flt3 is maintained in the majority of CLPs and a small fraction of CMPs (D'Amico and Wu, 2003; Karsunky et al., 2003) (Mooney et al., 2017). The discrepancy in Flt3 expression between CLPs and CMPs likely explains the more severe defect on early lymphoid development than myelopoiesis upon disruption of Flt3 signalling. Importantly, Flt3 expression is gradually lost in cells with increase commitment towards most haematopoietic lineages including myeloid, lymphoid and Mk/E, but is maintained in cells with DC potential and mature DCs (D'Amico and Wu, 2003; Karsunky et al., 2003). Thus, the action of FL on myeloid and lymphoid development is likely to be restricted to $Flt3^+$ early multipotent HSPCs and lymphoid progenitors, but not downstream committed progenitors that do not express Flt3 receptor.

DC development is dependent on FL

Unlike other haematopoietic lineages, continuous Flt3 expression is observed along the entire DC developmental trajectory, from the early multipotent MPPs to the non-lineage restricted CMPs and CLPs, the oligo-potent MDPs and DC-committed precursors such as the CDPs and pre-cDCs. Within the mature haematopoietic cell compartment, Flt3 expression is maintained in DCs including cDC1s, cDC2s and pDCs, but not any other cells. Importantly, within the non-DC committed progenitor populations such as CMPs, DC precursor activity is restricted to only the Flt3 expressing cells (D'Amico and Wu, 2003). Thus, due to the continuous expression of Flt3 on progenitors along the DC trajectory, FL could theoretically regulate all stages of DC development. In fact, FL

dependency is often used as a main criterion to establish the DC identity (Schraml and Reis e Sousa, 2015).

While normal numbers of mature myeloid and lymphoid cells upon Flt3 KO were reported in an initial study (Mackarehtschian et al., 1995), significant defects in the generation of mature cDCs and pDCs were later confirmed (Waskow et al., 2008), suggestive of a unique role of Flt3 in DC development compared to other haematopoietic lineages. Consistent with this notion, a profound reduction in the number of DCs and DC progenitors was observed in mice with FL deficiency, with milder defects in myeloid and lymphoid development (Kingston et al., 2009; McKenna et al., 2000). Disruption to DC development can also be induced using Flt3 inhibitors (Tussiwand et al., 2005). Interestingly, a more profound defect in DC development was observed in mice with FL deficiency than those with Flt3 disruption (Ginhoux et al., 2009; Waskow et al., 2008). Importantly, differential dependency of Flt3 and FL was also observed between cDC subsets within multiple nonlymphoid tissues, where much more profound defect in cDC1 development was reported (Ginhoux et al., 2009). This is partly because progenitors with Flt3 disruption become more sensitive to other cytokines such as M-CSF and SCF that can compensate for the lack of Flt3/FL signalling and enhance DC development (Durai et al., 2018).

Importantly, enforced expression of STAT3 or PU.1, downstream signal transducers of FL, on non-DC committed progenitors such as Mk/E-restricted progenitors (MEPs) could rescue DC differentiation potential (Onai et al., 2006). This finding highlighted the essential role of FL in establishing DC fate. In addition, FL as a single factor was able to promote the development of the three DC subtypes *in vitro* (Angelov et al., 2005; Brasel et al., 2000; Brawand et al., 2002; Naik et al., 2005). This FL culture system has been extensively characterized and is now regularly used in studying DC development *in vitro*. This again highlighted the indispensable role of FL in DC development. Conversely, reduced number of DCs in a variety of experimental models, either via Flt3 inhibition or DT/DTR mediated depletion, resulted in an increase in FL serum levels (Birnberg et al., 2008; Meredith et al., 2012; Tussiwand et al., 2005). This suggested the potential existence of a tightly controlled feedback loop in regulating FL level to compensate for the reduction of DCs.

FL induces emergency DC development

While a lack of FL signalling leads to defects in DC generation, supra-physiological amounts of FL induces emergency DC development (i.e. high number of DCs), particularly of the cDC1 subset (O'Keeffe et al., 2002). Emergency haematopoiesis is also known as demand-adapted or inflammatory haematopoiesis, where the production of certain cell types is up-regulated in response to external challenges such as infection (Manz and Boettcher, 2014; Takizawa et al., 2012). For example, *Plasmodium chabaudi* infection was shown to increase FL serum levels, which led to an increase in the number of early progenitors in the BM and preferential expansion of cDC1s in the spleen (Guermonprez et al., 2013). Emergency generated cDC1s helped to control the infection via activation of $CD8^+$ T cells. Importantly, upon deletion of Flt3 or FL, the emergency expansion of early HSPCs (LSKs), intermediate DC progenitors (MDPs and CDPs) as well as cDC1s was compromised, suggesting the critical role of FL along the entire DC developmental trajectory (Guermonprez et al., 2013). FL-induced cDC1 expansion was also shown to be critical for the resistance to intracellular pathogen *Toxoplasma gondii*, where FL KO mice become highly susceptible to acute *T.gondii* infection (Dupont et al., 2015). In addition, emergency cDC1 development can be induced by exogenous injection of FL, which was demonstrated to increase resistance to a variety of pathogens including *Listeria monocytogenes* (Gregory et al., 2001) and Simian immunodeficiency viruses (SIV) (Reeves et al., 2009). In addition, potential clinical benefits have been demonstrated when incorporating FL injection into multiple vaccination strategies (i.e. use FL as a vaccine adjuvant) against SIV in macaques (Kwissa et al., 2007), as well as human immunodeficiency virus (HIV) and lymphocytic choriomeningitis virus (LCMV) in human (Nayak et al., 2006; Sumida et al., 2004).

FL-mediated emergency cDC1 generation facilitates antitumor immunity

Exogeneous injection of FL is not only beneficial in controlling a variety of pathogenic infections, but could potentially also be used as an antitumor agent. Because of the essential role of cDC1s in cross presenting tumor antigens to generate specific $CD8^+$ cytotoxic T cell responses (see earlier **1.4.1**), harnessing this cell type in the context of cancer immunotherapy has been actively explored. However, due to the extremely sparse nature of this cell type in most lymphoid tissues and TME and the requirement of

continuous priming and activation of $CD8^+$ T cells to generate potent antitumor responses, a strategy to boost the number of cDC1s *in vivo* might be superior to a cell-based DC immunization strategy. One simple strategy to enhance DC numbers *in vivo* is via exogeneous FL administration as this cytokine was shown to selectively expand cDC1s (O'Keeffe et al., 2002). Thus, to date, many studies have evaluated the therapeutic benefits of FL administration *in vivo*, either as a single agent or in combination with other therapeutic substances.

Many early studies have demonstrated promising therapeutic benefits of FL treatment as a monotherapy in mice, where delayed tumor growth and/or regression in a diverse range of cancer models was observed. These cancer models included fibrosarcoma (Lynch et al., 1997), melanoma (Esche et al., 1998), lymphoma (Esche et al., 1998), lung carcinoma (Chakravarty et al., 1999), ovarian (Silver et al., 2000), prostate (Ciavarra et al., 2000), colon (Favre-Felix et al., 2000) and breast (Braun et al., 1999; Chen et al., 1997) cancers. However, the antitumor effect of FL injection alone appeared to be transient and termination of treatment led to tumor relapse in a prostate cancer model (Ciavarra et al., 2000). In addition, despite significant tumor regression in some studies, complete tumor rejection was never observed and FL injection alone did not seem to induce a memory T cell response, hence not likely to provide protection against secondary challenges (Chakravarty et al., 1999; Dong et al., 2002).

Due to the limited therapeutic effects of using FL as a single agent, many studies have explored the use of FL in combination with other strategies. First, combination of FL administration with radiotherapy resulted in increased survival of mice bearing Lewis lung carcinoma (Chakravarty et al., 1999). In addition, the use of FL as an adjuvant in multiple tumor immunization protocols including peptide-based (Marroquin et al., 2002; Merad et al., 2002), cell-based (Fong et al., 2001), DNA-based (Parajuli et al., 2001) or RNA-based (Kreiter et al., 2011) vaccination, with or without other agents such as cytokines or immune-stimulatory substances, significantly augmented the antitumor response in both mouse and human. Co-injection of FL with other cytokines has also been examined, such as GM-CSF in a sarcomas model (Berhanu et al., 2006), and G-CSF or GM-CSF in breast cancer patients (Gasparetto et al., 2002). However, minimal therapeutic benefits were observed in the Sarcoma model after FL and GM-CSF

administration, despite the increase in the number of DCs in the periphery and TME (Berhanu et al., 2006).

More recently, the efficacy of FL treatment in combination of BRAF inhibition or checkpoint inhibition therapies has been demonstrated. Importantly, combination of anti-CTLA-4 antibody with FL significantly enhanced antitumor immunity than anti-CTLA-4 alone or in combination with GM-CSF in a B16 melanoma model (Curran and Allison, 2009). In addition, two independent studies have demonstrated that expansion and activation of cDC1s after FL and poly I:C co-injection helped reduce tumor size in melanoma models (Salmon et al., 2016; Sánchez-Paulete et al., 2016). This combination therapy also synergized with checkpoint blockade therapies such as anti-PD-1and anti-CD317 antibodies, which further promote tumor regression (Salmon et al., 2016; Sánchez-Paulete et al., 2016). Importantly, a population of cDC1 precursors that were $CD11c^{+}$ $MHCII^{+}$ $CD103^{-}$ $CD11b^{-}$ and were largely $IRF8^{+}$ $IRF4^{-}$ was found to be dramatically expanded after FL injection, indicating exogeneous FL was likely to induce emergency cDC1 development from the BM (Salmon et al., 2016).

While animal studies have demonstrated promising efficacy of FL treatment in enhancing antitumor immunity, several clinical studies have also been conducted, which showed that this treatment was safe and well tolerated in most healthy volunteers and patients (Anandasabapathy et al., 2015; Disis et al., 2002; Evans et al., 2002; Fong et al., 2001; Higano et al., 2004; Morse et al., 2000). In addition to safety, significant tumor regression was observed in two of 12 patients with advanced cancer when receiving immunization with a carcinoembryonic antigen peptide and FL, demonstrating positive clinical outcome (Fong et al., 2001). Together, these results demonstrated high potential of using FL in the context of cancer immunotherapy against multiple cancer types.

Aims and objectives

The main focus of this thesis is to investigate the development of DCs at the single cell level, both during the steady-state and emergency conditions.

The first aim is to systematically characterize the clonal dynamics and to define clonal cellular trajectories during steady-state DC development. To address this aim, cellular barcoding will be used to label single HSPCs and to track DC development *in vitro* over time in a FL-supplemented DC culture system.

The second aim is to understand the clonal aetiology of FL-mediated emergency DC generation in vivo. To address this aim, three key questions will be investigated. First, whether early HSPCs actively respond to supra-physiological levels of FL stimulation and predominantly contribute to emergency DC development will be established. Second, cellular barcoding will be used to examine the dynamic changes in lineage output of single HSPCs during FL-mediated emergency DC development. Lastly, a single cell multi-omics profiling approach will be utilized to interrogate the cellular and molecular events during the early phase of FL-mediated emergency DC development.

The first aim will be addressed in **Chapter 3**. The second aim will be addressed in **Chapter 4**.

Chapter 2. Materials and Methods

Summary

This chapter includes additional details on materials and methods that are not thoroughly described in **Chapter 3** and **Chapter 4**. These include 1) common materials used; 2) additional details in tissue preparation and isolation; 3) additional details in materials and methods involving flow cytometry; 4) a detailed protocol of cellular barcoding; and 5) a detailed protocol of single cell RNA-sequencing using CEL-Seq2.

Buffers and media

FACS buffer

FACS buffer was prepared by adding 2mM Ethylenediamine tetra acetic acid (EDTA) and 0.5% Fetal calf serum (FCS; Hyclone) to Phosphate-buffered saline (PBS; Life Technologies).

Red cell removal buffer (RCRB)

RCRB was prepared by the WEHI media kitchen, which comprises of 12 mM Sodium Bicarbonate ($NaHCO_3$), 156 mM Ammonium chloride (NH_4Cl) and 0.1 mM EDTA dissolved in Type I water.

DC standard medium

DC standard medium was prepared by adding 10% FCS to RPMI 1640 media (WEHI media kitchen). RPMI 1640 medium was prepared by dissolving RPMI 1640 powder (Life Technologies) in Type I water with the following supplements: 20.6mM Sodium Bicarbonate ($NaHCO_3$), 0.87mM Sodium Pyruvate ($C_3H_3NaO_3$), 29mM Hepes Buffer 1.68M, 0.087mM 2-Mercaptoethanol (2ME) and 1 × Penicillin-Streptomycin.

DC conditioned medium

To prepare DC conditioned medium, freshly isolated mouse BM cells was first cultured with DC standard medium supplemented with 800 ng/mL of Flt3 ligand (FL; BioXcell) for three days. The cells were then harvested and supernatant was collected via centrifugation and filtered through a 0.22 μM filter. The filtered supernatant was aliquoted and stored at – 80 ºC as DC conditioned medium for future experiments.

Tissue preparation and single cell suspension

Bone marrow

Bone marrow cells from hip, tibia and femur were collected by flushing with FACS buffer using a 1 ml syringe through a 21-gauge or 22-gauge needle. The cell suspension was filter using a 70 μm cell strainer followed by centrifugation (1100g, 5 minutes, 4 ^{o}C). Supernatant was removed using vacuum suction and cell pellet was resuspended in 1-2 ml of RCRB and incubated at 4 ^{o}C for two minutes, followed by a wash in a large volume of FACS buffer.

Spleen

Spleens were meshed with a large volume of FACS buffer through 70 μm cell strainers with 3 ml syringe plungers. Cell suspension was centrifuged and supernatant was removed. Removal of red blood cells was performed by resuspending cell pellet in 1-2 mL of RCRB and incubated at 4 ^{o}C for two minutes, followed by a wash in a large volume of FACS buffer.

Bleed

Eye or mandible bleeds were performed by animal technicians at WEHI, according to institutional guidelines. Typically, 50 to 100 μL of blood was obtained from one mouse at each time point. Red blood cell lysis was performed using 5 ml of RCRB for five to ten minutes, followed by a wash in a large volume of FACS buffer.

Flow Cytometry

Antibody staining

Single cell suspensions were prepared as indicated above. Cells were resuspended to a concentration of no more than 1×10^8 cells/ml in FACS buffer containing antibodies of interest at 4 °C for at least 30 minutes. Cells were then washed with a large volume of FACS buffer to remove unbound antibodies. Secondary antibody staining or Magnetic-Activated Cell Sorting (MACS) enrichment was performed if required. Propidium iodide (PI) was added to a final concentration of 1 μg/mL to exclude dead cells prior to flow cytometry analysis or sorting. All antibodies used in this thesis is listed in **Table 2.1**.

Table 2.1 Antibodies used for flow cytometry

Name	Alternative names	Clone	Conjugate	Source
CD3	T3	17A2	Pacific Blue	In house
CD4	Leu-3, T4	GK1.5	FITC	In house
CD8α	T8, Ly-2	53-6.7	A700	In house
CD8α	T8, Ly-2	53-6.7	FITC	In house
CD8α	T8, Ly-2	53-6.7	PE/Cy7	BioLegend
CD11b	Mac1	M1/70	A700	In house
CD11b	Mac1	M1/70	Biotin	In house
CD11b	Mac1	M1/70	BV785	BD Biosciences
CD11b	Mac1	M1/70	PE	In house
CD11c	Integrin-αx	N418	APC	In house
CD16/32	Fcγ R III/II, Ly-17	2.4G2	BV605	BD Biosciences
CD19	B4	ID3	FITC	In house
CD19	B4	ID3	PE/Cy7	BD Biosciences
CD24	HSA	ML5	BV711	BD Biosciences
CD24	HSA	M1/69	PE/Cy7	BioLegend
CD34	Mucosialin	RAM34	FITC	BD Biosciences
CD45.1	Ly5.1	A20	BV650	BD Biosciences
CD45.2	Ly5.2	104	PE	BioLegend
CD48	BLAST-1, SLAMF2	HM48-1	PE	eBioscience

CD117	cKit	ACK-4	APC	In house
CD117	cKit	2B8	PerCP/e710	eBioscience
CD127	IL7Rα	A7R34 2.2	Biotin	In house
CD135	Flt3	A2F10	Biotin	eBioscience
CD135	Flt3	A2F10.1	BV421	BD Biosciences
CD135	Flt3	A2F10	PE	eBioscience
CD150	SLAM	TC15-12F12.2	PE/Cy7	BioLegend
CD172α	Sirpα	P84	PE/Dazzle 594	BioLegend
CD199	CCR9	eBioCW1.2	PE/Cy7	eBioscience
CD317	Bst2, PDCA-1	120G8	Pacific Blue	In house
F4/80	Ly-71, EMR1	BM8	A700	In house
F4/80	Ly-71, EMR1	BM8	APC-e780	Invitrogen
Gr1	Ly6C/G	RB68C5	A594	In house
Gr1	Ly6C/G	RB68C5	A700	In house
Ly6C		AL-21	BV605	BD Biosciences
Ly6G		1A8	PE/Cy7	BioLegend
MHCII	I-A/I-E	M5/114.15.2	APC-e780	eBioscience
MHCII	I-A/I-E	M5/114.15.2	BV650	BD Biosciences
MHCII	I-A/I-E	M5/114.15.2	eFlour 450	eBioscience
Sca1	Ly6A/E	E13-161.7	A594	In house
Siglec-F		E50-2440	BV421	BD Biosciences
Siglec-H		eBio440c	eFlour 450	eBioscience
Siglec-H		eBio440c	PE	eBioscience
Streptavidin			APC/Cy7	BD Biosciences
Streptavidin			BV421	BioLegend
Streptavidin			BV650	BD Biosciences
XCR1	GPR5, CCXCR1	REA707	APC-Vio770	Miltenyi Biotec

MACS enrichment or depletion

Cells were resuspended to a concentration of no more than 1×10^8 cells per ml of FACS buffer with microbeads of interest added at a ratio of 1:5. The list of microbeads used in this thesis is shown in **Table 2.2**. The mixture was incubated at 4 ^oC for at least 15 minutes. Cells were then washed with large volume of FACS buffer and resuspended in FACS buffer at 5×10^7 cells/ml. Depending on total cell number of the sample, either a MS (up to 1×10^7 bound cells) or LS (up to 1×10^8 bound cells) column was fitted onto the MACS separator and primed with FACS buffer. Prior to sample loading, a 27-gauge needle and syringe were used to break down cell clumps to prevent clotting within the column. The negative fraction containing depleted (not labelled with beads) cells was collected while the positive fraction containing enriched (labelled with beads) cells was bound to the column due to magnetic force. After sample loading and washing, the column was removed from the MACS separator and the positive fraction was eluted into a clean tube using a plunger.

Table 2.2 MACS beads used

Name	Source	Catalogue number
Anti-APC	Miltenyi Biotec	130-090-855
Anti-Biotin	Miltenyi Biotec	130-090-485
Anti-PE	Miltenyi Biotec	130-048-801
CD117	Miltenyi Biotec	130-091-224
CD11c	Miltenyi Biotec	120-000-322

Instruments and software

Flow cytometry analysis was performed on either a BD LSRFortessa or LSRII cytometers (Beckton Dickinson). Cell sorting was performed by staff at the WEHI FACS facility or myself on a BD Influx, BD Fusion or BD FACSAria-II/III sorter (Beckton Dickinson). When sorting cells in bulk, a 70 μm nozzle was usually used and cells were collected into 1.5 ml Eppendorf tubes primed with FCS to allow cells slide down to the bottom and minimize cell death. When sorting single cells for scRNAseq experiments, a 100 μm nozzle was used and cells were collected into a 384-well plate containing pre-aliquoted CEL-Seq2 reagent mix (Plates prepared by SCORE; see below). Index sorting mode was

used to record flow cytometric output of individual sorted cell and the corresponding well ID. Data analysis was performed using Flowjo (Treestar), PieMaker (developed in house by Jerry Gao and improved by Andrey Kan) (Lin et al., 2018)and R.

Cellular barcoding

Overview

Cellular barcoding involves the tagging of individual cells with unique and inheritable barcodes (Gerrits et al., 2010; Lu et al., 2011; Naik et al., 2013; 2014). The barcode library used in this thesis consists of 2608 random stretches of DNA that can be delivered into cells using lentiviruses. This library was developed and generated by my supervisor Dr Shalin Naik and colleagues at the NKI (Naik et al., 2013).

All barcoding experiments presented in this thesis were performed in accordance with the published method. Briefly, freshly isolated HSPCs were transduced with the barcode library as described below. The barcode transduced HSPCs were then either seeded in FL culture (**Chapter 3**) or transplanted into recipient mice (**Chapter 4**) to allow cell division and differentiation over time. Progeny populations were then isolated at the indicated time point and DNA barcodes within each population were amplified and sequenced as described below. Barcode data processing and analysis were performed as described in **Chapter 3** and **Chapter 4**.

Barcode transduction

Freshly isolated HSPCs were resuspended in StemSpan medium (Stem Cell Technologies) supplemented with 50 ng/mL SCF (generated in-house by Dr Jian-Guo Zhang) and transferred to a 96-well round bottom plate at less than 1×10^5 cells/well. Lentivirus was added and the plate was centrifuged at 900 g for 90 minutes at 22 °C prior to incubation at 37 °C and 5% CO_2 for 4.5 or 14.5 hours. The amount of lentivirus used was pre-determined in titration experiments to give 10-20% transduction efficiency. After incubation, cells were washed using a large volume of PBS or RPMI containing 10-20 % FCS to remove residual virus. Cells were then suspended in either culture medium for *in vitro* FL culture (**Chapter 3**) or PBS for transplantation (**Chapter 4**).

Barcode amplification and sequencing

Viagen lysis

Freshly isolated progeny populations were transferred to a 96-well PCR plate at a density of less than 5 $\times 10^5$ cells/well. Cells were centrifuged and resuspended in 40 µL of Viagen lysis buffer (Viagen) containing 0.5 mg/mL Proteinase K (Invitrogen). The plates were then sealed with PCR rubber mat and run on PCR machines at 55 °C for two hours, followed by 85 °C for 30 minutes and 95 °C for 5 minutes. Samples then proceeded to next step or were stored at –20 °C. Caution was taken at all steps to avoid barcode contamination between samples. This step was performed at the 'semi-clean' pre-PCR common laboratory area.

First round barcode PCR

The first round PCR amplifies barcode DNA using common primers including the TopLiB 5' – TGC TGC CGT CAA CTA GAA CA – 3' and BotLiB 5' – GAT CTC GAATCA GGC GCT TA – 3'. Master mix of reagents (**Table 2.3**) was prepared in the 'barcode-free' room to avoid contamination of reagents. Next, in the 'semi-clean' common laboratory area, 110 µL of the prepared PCR master mix was added to each sample, which contained 40 µL of cell lysate from the previous step. The sample was mixed then split into two wells of 75 µL each for technical replicates. The plates were sealed with fresh PCR rubber mat and run on PCR machines using the setting indicated in **Table 2.4**. Caution was taken at all steps to avoid barcode contamination between samples.

Table 2.3 Reagents used in first round barcode PCR

	Reagents per sample (μL)
Water	78.1
NEB buffer (10 ×)	15
NEB $MgCl_2$ (25 mM)	12
dNTP (10 mM each)	3
TopLiB (100 μM)	0.75
BotLiB (100 μM)	0.75
Taq DNA polymerase	0.4
Total	110

Table 2.4 Program for first round barcode PCR

Temperature	Duration	Number of cycles
95 °C	5 minutes	1
95 °C	15 seconds	30
57.2 °C	15 seconds	
72 °C	15 seconds	
72 °C	10 minutes	1
4 °C	Infinity	

Second round barcode PCR

The second round PCR introduces an 82-bp well-specific 5' end forward index primer (384 in total) and an 86-bp plate-specific 3' reverse index primer (8 in total). In the 'barcode-free' room, the master mix of reagents was prepared (**Table 2.5**) and transferred into a new PCR plate at 27 μL per well. A different forward index primer (6 μM, 2.5 μL) was added to each well and the primer identity was recorded. Caution was taken to avoid cross contamination of index primers. Next, in the 'barcode-concentrated' post-PCR room, 0.5 μL of first round PCR product was added to each well and the well ID was recorded (to allow correspondence of index primer identity). The plates were sealed with

fresh PCR rubber mat and run on PCR machines using the setting indicated in **Table 2.6**. Caution was taken to avoid barcode contamination between samples. Products from this round of PCR were run on a 2% agarose gel to confirm a PCR product was generated. Once confirmed, individual samples were pooled and proceeded to next step or stored at –20 °C.

Table 2.5 Reagents used in second round barcode PCR

	Reagents per sample (μL)
Water	21
NEB buffer (10 ×)	3
NEB $MgCl_2$ (25 mM)	2.4
dNTP (10 mM each)	0.6
Illumina Reverse primer	0.15
Taq DNA polymerase	0.075
Total	27

Table 2.6 Program for second round barcode PCR

Temperature	Duration	Number of cycles
95 °C	5 minutes	1
95 °C	5 seconds	30
57.2 °C	5 seconds	
72 °C	5 seconds	
72 °C	10 minutes	1
4 °C	Infinity	

Bead clean-up of PRC products and sequencing

Room temperature NucleoMag NGS Clean-up and Size select magnetic beads (Macherey-Nagel) were vortexed until well dispersed. 75 μL of beads were added to 50 μL of pooled PCR products (1.5 × bead to sample ratio) in a 1.5 mL LoBind Eppendorf tube (Sigma Aldrich) and mixed thoroughly, followed by five minutes incubation at room temperature. The tube was then placed on a magnetic stand for five minutes, or until liquid

appeared clear. The supernatant was removed gently to avoid disturbance of pellet, which contained beads and desired DNAs. Next, 200 µL of freshly prepared 80% EtOH was added to the tube and incubate for 30 seconds before removal of supernatant. This washing step was then repeated and the tube was kept on the stand with lid open for 8-15 minutes to allow air drying of pellet. Once the pellet was completely dry, the tube was removed from magnetic stand and the pellet was resuspended in 15 µL of 10 mM Trizma (pH 7.5). Tthe mixture was incubated at room temperature for two minutes and placed the tube on the magnetic stand for five minutes, or until liquid appeared clear. 14.5 µL of supernatant (post clean up PCR product) was carefully transferred to a new 1.5 mL LoBind Eppendorf tube. Next, the concentration and quality of PCR products was checked using a using a D1000 DNA screen tape (Agilent Technologies) on the Tapestation (Agilent Technologies) following the manufacturer's instructions. Deep sequencing was then performed on the Illumina NextSeq platform at WEHI by Dr. Stephen Wilcox.

Single cell RNA-sequencing

CEL-Seq2 plate preparation

384-well plates (Greiner, 785290) containing CEL-Seq2 reagents were prepared by staff from Single Cell Open Research Endeavour (SCORE) at WEHI. Each well contained 1.2 µL of mixture including 20 nM indexed polydT primer (custom design, IDT), 1:6.000.000 dilution of ERCC RNA spike-in mix (Ambion), 1 mM dNTPs (NEB), 1.2 units SUPERaseIN Rnase Inhibitor (Thermo Fisher), 0.2 % v/v Triton X-100 solution (Sigma Aldrich) in DEPC water (Thermo Fisher).

CEL-Seq2 library generation

Library generation was performed by Ms Tracey Baldwin from SCORE, using an modified CEL-Seq2 protocol (Hashimshony et al., 2016) that was optimized by SCORE. The procedure is described below.

First strand cDNA generation

Sorted plates were thawed and briefly spun down by centrifugation (1000 g, 1 minute) and incubated at 65 ºC for five minutes, followed by immediate chilling on ice for two minutes. This step allowed cell lysis and RNA to anneal with the mRNA capture well-specific primers. To enable first strand cDNA generation, reverse transcription (RT) reaction mix containing 0.4 µL First Strand buffer (Invitrogen), 0.2 µL DTT (0.1M; Invitrogen), 0.1 µL RNaseOUT (Invitrogen), 0.1 µL SuperScript II (Invitrogen) was added to each well and the plate was incubated at 42 ºC for 60 minutes, followed by heat inactivation at 70 ºC for 10 minutes and chilling to 4 ºC on ice. Next, barcoded cDNAs from individual wells per plate were pooled into a 1.5 mL LoBind tube for the next steps.

Exonuclease I treatment

Exo I (NEB) was added to the pooled sample at a final concentration of 1 U/µL and the tube was incubated at 37 ºC for 30 minutes, followed by enzyme inactivation at 80 ºC for 10 minutes and chilling to room temperature on ice. Bead clean-up was performed at 1.2 × bead to sample ratio (1.1x SPRI buffer, 0.1x NucleoMag NGS Clean-up beads) following the manufacture's instruction, similar to the description above. The cDNAs were then eluted in 17 µL DEPC water and transferred to a fresh 0.2 ml PCR tube.

2nd strand DNA synthesis and clean up

To enable second strand DNA generation, 2 µL of 10X second strand buffer (NEB) and 1 µL second strand enzyme (NEB) were added to the 17 µL purified sample from the previous step, followed by incubation at 16 °C for two hours. Next, bead clean-up was performed at 1.2 × bead to sample ratio as described previously. At the final step, the mixture containing both cDNA and beads was resuspended in 6.4 µL DEPC water.

In Vitro transcription (IVT)

To generate amplified RNA (aRNA) via IVT, reaction mix containing 6.4 µL rNTPs (A/G/C/U), 1.6 µL 10X T7 buffer and 1.6 µL T7 Megascript (all from MEGAscript T7 Transcription Kit) was added to the 6.4 µL sample from the previous step. The mixture was incubated at 37 °C for 14 hours, followed by storage at 4 °C. To remove leftover primers, 6 µL of EXO-SAP-IT (Affymetrix) was added, followed by incubation at 37 °C for 15 minutes. The aRNA was then chilled and kept on ice until the next step.

RNA fragmentation

On ice, 5.5 µL of 10X Fragmentation buffer (Ambion) was added to the aRNA sample from the previous step, followed by incubation at 94 °C for 2.5 minutes. To avoid over-fragmentation, the mixture was immediately transferred to ice with addition of 2.75 µL Fragmentation Stop buffer (Ambion). The fragmented aRNA was purified using RNAClean XP beads (Beckman Coulter) at 1.8 × bead to sample ratio according to the manufacturers' instructions, eluted in 5 µL DEPC water and transferred to a fresh 0.2 mL PCR tube.

Reverse transcription (RT)

RT was performed to transcribed aRNA into cDNA. Briefly, 1 µL 5'- tagged random hexamer RT primer 9 (GCCTTGGCACCCGAGAATTCCANNNNNN) and 0.5 µL dNTPs (NEB) was added to the 5 µL fragmented aRNA sample. The mixture was incubated at 65 °C for 5 minutes and chilled on ice for 2 minutes. Next, reagent mix containing 2 µL First Strand buffer (Invitrogen), 1 µL DTT (0.1M; Invitrogen), 0.5 µL RNaseOUT (Invitrogen), 0.5 µL SuperScript II (Invitrogen) was added. The mixture was

incubated at 25 ºC for 10 minutes followed by 42 ºC for 60 minutes. Half of the sample was store at -80 ºC and the other half was kept at 4 ºC before proceeding to the next step.

Library amplification and sequencing

Reagent mix containing 12.5 µL 1X KAPA HiFi HotStart ReadyMix (KapaBiosystems), 1 µL RNA PCR RP1 Primer (Illumina), 1 µL Indexed RPIX primer (Illumina) and 5.5 µL water was added to half of the sample (5 µL) from the previous step. PCR was performed using the following program: 1) 98 ºC for two minutes; 2) two cycles of 98 ºC for 20 seconds followed by 55 ºC for 30 seconds and 72 ºC for 60 seconds; 3) nine cycles of 98 ºC for 20 seconds followed by 65 ºC for 30 seconds and 72 ºC for 60 seconds; 4) 72 ºC for 10 minutes; 5) hold at 4 ºC. After PCR, two consecutive bead clean-ups were performed as previously described. The first used 0.8 × bead to sample ratio and the second used 0.9 X bead to sample ratio. After both clean-up steps, the amount and quality of the library was checked on Tapestation (Agilent Technologies) using a high sensitivity D5000 tape (Agilent Technologies) before submitting to sequencing on the Illumina NextSeq platform by Dr Stephen Wilcox at WEHI. The sequencing configuration was RD1 / RD2 / index; 14bp / 72bp / 6bp. An average of 50,000 – 200,000 reads per cell were sequenced.

Chapter 3. Multiple Trajectories of Steady-state DC Development

Summary

In this chapter, I used cellular barcoding to track the development of DC subtypes from single early HSPC clones. In collaboration with colleagues, I developed computational tools to visualize and characterize this dynamic process. This work revealed key clonal features during DC development, which include the types of DCs a clone will make (fate), the number of DCs it will produce (size), and when DC generation occurs within this clone (timing). Collectively, these clonal properties were defined as cellular trajectories. Systematic characterization of cellular trajectories of thousands of HSPC clones revealed early separation of cDC and pDC fate in the majority of HSPCs. Furthermore, cellular trajectories were demonstrated to be largely intrinsically programmed in single HSPCs during early stages of DC development. These findings provide important insights into the complexity of clonal DC development.

This chapter has been published by Cell Reports on Vol 22, Page 2557-2566. The full paper including main and supplementary information is attached here.

Main

Report

Cell Reports

DiSNE Movie Visualization and Assessment of Clonal Kinetics Reveal Multiple Trajectories of Dendritic Cell Development

Graphical Abstract

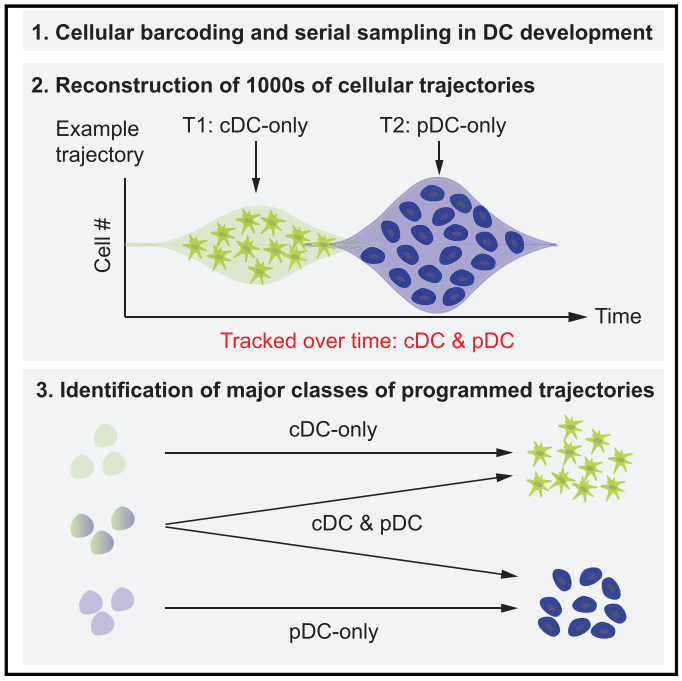

Authors

Dawn S. Lin, Andrey Kan, Jerry Gao, Edmund J. Crampin, Philip D. Hodgkin, Shalin H. Naik

Correspondence

naik.s@wehi.edu.au

In Brief

Lin et al. develop a framework to longitudinally track and visualize clonal cellular trajectories during dendritic cell development. The authors demonstrate that properties including fate bias and the timing and size of clonal bursts are heterogeneous within populations yet largely imprinted in single progenitors at early developmental stages.

Highlights

- A cellular trajectory is defined by a clone's fate and cell production over time
- DiSNE movies allow dynamic visualization of clonal cellular trajectories
- Single HSPCs follow different cellular trajectories in DC development
- Cellular trajectories of individual clones are intrinsically programmed

Lin et al., 2018, Cell Reports 22, 2557–2566
March 6, 2018
https://doi.org/10.1016/j.celrep.2018.02.046

CellPress

Cell Reports
Report

DiSNE Movie Visualization and Assessment of Clonal Kinetics Reveal Multiple Trajectories of Dendritic Cell Development

Dawn S. Lin,[1,2,3,7] Andrey Kan,[2,3,7] Jerry Gao,[1] Edmund J. Crampin,[4,5,6] Philip D. Hodgkin,[2,3] and Shalin H. Naik[1,2,3,8,*]
[1]Molecular Medicine Division, Walter and Eliza Hall Institute, Parkville, VIC 3052, Australia
[2]Immunology Division, Walter and Eliza Hall Institute, Parkville, VIC 3052, Australia
[3]Faculty of Medicine, Dentistry & Health Sciences, University of Melbourne, Parkville, VIC 3010, Australia
[4]Systems Biology Laboratory, University of Melbourne, Parkville, VIC 3010, Australia
[5]Centre for Systems Genomics, University of Melbourne, Parkville, VIC 3010, Australia
[6]ARC Centre of Excellence in Convergent Bio-Nano Science and Technology, Melbourne School of Engineering, University of Melbourne, Parkville, VIC 3010, Australia
[7]These authors contributed equally
[8]Lead Contact
*Correspondence: naik.s@wehi.edu.au
https://doi.org/10.1016/j.celrep.2018.02.046

SUMMARY

A thorough understanding of cellular development is incumbent on assessing the complexities of fate and kinetics of individual clones within a population. Here, we develop a system for robust periodical assessment of lineage outputs of thousands of transient clones and establishment of bona fide cellular trajectories. We appraise the development of dendritic cells (DCs) in *fms*-like tyrosine kinase 3 ligand culture from barcode-labeled hematopoietic stem and progenitor cells (HSPCs) by serially measuring barcode signatures and visualize these multidimensional data using developmental interpolated t-distributed stochastic neighborhood embedding (DiSNE) time-lapse movies. We identify multiple cellular trajectories of DC development that are characterized by distinct fate bias and expansion kinetics and determine that these are intrinsically programmed. We demonstrate that conventional DC and plasmacytoid DC trajectories are largely separated already at the HSPC stage. This framework allows systematic evaluation of clonal dynamics and can be applied to other steady-state or perturbed developmental systems.

INTRODUCTION

Dendritic cells (DCs) represent a distinct branch of hematopoiesis and are responsible for pathogen sensing and activation of the adaptive immune response (Merad et al., 2013). There are three major subtypes, including plasmacytoid DCs (pDCs), type 1 conventional DCs (cDC1s), and type 2 cDCs (cDC2s) (Guilliams et al., 2014). DC development is relatively well established at the population level and can be recapitulated in *fms*-like tyrosine kinase 3 ligand (FL) cultures (Naik et al., 2005). According to the current hierarchical model of hematopoiesis (Guo et al., 2013; Månsson et al., 2007), all DC subtypes can be generated from a restricted common DC progenitor (CDP) population downstream of hematopoietic stem and progenitor cells (HSPCs) (Naik et al., 2007, 2013; Onai et al., 2007) via discrete subtype-committed precursor stages (Grajales-Reyes et al., 2015; Naik et al., 2006; Onai et al., 2013; Schlitzer et al., 2015). However, clonal evidence has suggested earlier lineage imprinting (Ema et al., 2014; Lee et al., 2017; Naik et al., 2013; Notta et al., 2016; Sanjuan-Pla et al., 2013; Yamamoto et al., 2013) or even DC subtype imprinting (Helft et al., 2017; Lee et al., 2017; Naik et al., 2007; Onai et al., 2007) within individual HSPCs. Importantly, most lineage tracing studies measured clonal fate at only a single time point. Therefore, questions remain as to whether the fate bias observed at one snapshot in time is consistent over time.

Some studies have assessed clonal contribution longitudinally (e.g., by serially sampling progeny derived from HSPCs in the blood) and have been instrumental in highlighting clonal properties, including repopulation kinetics and lineage bias (Dykstra et al., 2007; Kim et al., 2014; Naik et al., 2013; Sun et al., 2014; Verovskaya et al., 2013; Wu et al., 2014; Yamamoto et al., 2013). However, these approaches are not feasible in tracking DC development, as DCs are rare, and most are residential in lymphoid tissues such that serial sampling *in vivo* is not possible (Shortman and Naik, 2007). Long-term imaging can allow accurate reconstruction of pedigrees from transient progenitors that produce rare progeny such as DCs *in vitro*. However, because of technical demands it generally only allows assessment of 10–100 s clones for a short period of days to weeks, which might not be sufficient to allow full differentiation (Dursun et al., 2016; Skylaki et al., 2016). Recent "pedigree" tools that measure evolving barcodes in progeny can infer developmental history (Frieda et al., 2017; Kalhor et al., 2017; McKenna et al., 2016) but are limited in their assessment of clonal kinetics.

Another method that aims to recapitulate the dynamic aspects of development and differentiation is "pseudo-time" analyses,

which infer developmental trajectories by assuming that single cells within a population represent different ''snapshots'' along archetypal paths and align cells on the basis of their proteomic or transcriptomic profiles (Wagner et al., 2016). These models can be of great benefit in understanding the order of gene and protein expression in developmental pseudo-time. A confounding factor, however, is the inability to assess individual clones, as data are derived from a snapshot assessment or with no lineage connection when assessed between time points. Therefore, such archetypal trajectories may mask heterogeneity at the clonal level, including features such as kinetics, lineage bias, and division destiny (Marchingo et al., 2014).

Cellular barcoding allows tracking of clonal fate by differential tagging of individual progenitors with unique and heritable DNA barcodes (Bystrykh et al., 2012; Naik et al., 2014). Quantification and barcode comparison between progeny cell types allows inference of lineage relationships (i.e., barcodes shared between cell types implies common ancestors, whereas differing barcodes implies separate ancestors). Here we combine cellular barcoding and DC development in FL cultures to facilitate longitudinal assessment of clonal kinetics in a robust, controlled, and high-throughput manner by serially sampling progeny from the same wells at multiple time points. Our results highlight that there are several distinct classes of cellular trajectories in DC development: each consists of clones with a similar pattern of DC subtypes produced over time but with varying properties including the timing, duration, and magnitude of clonal waves. Importantly, using clone-splitting experiments, we demonstrate that many of these cellular trajectories are ''programmed'' within individual HSPCs. Furthermore, we demonstrate that pDC and cDC development has already largely diverged at the HSPC stage, not downstream in the CDPs, as is currently assumed. Our results offer a powerful analytical and visualization framework that reveals the diversity of clonal kinetics and cellular trajectories.

RESULTS

Longitudinal Tracking of Clonal DC Development Reveals Time-Varying Patterns

To track clonal DC development longitudinally, we barcode-labeled mouse Sca1^{+} cKit^{hi} cells that contained early HSPCs and cultured them with FL to allow DC generation (Figures 1A and S1A). The cultures were serially split in two at various times such that half of the cells were sorted for the DC subtypes using flow cytometry for subsequent barcode analysis, and half were kept in culture with a compensating amount of fresh media (Figure 1A). To accurately define the DC subtypes, we used CD11c, major histocompatibility complex class II (MHCII), Siglec-H, C-C chemokine receptor type 9 (CCR9), Sirpα, and CD24 (Figure 1B). In addition, we sorted cells that were outside these DC gates collectively as ''non-DCs'' to allow estimation of the recovery of barcodes in the culture at any given time points and track clones that still contained DC progenitors. CCR9 inclusion was critical to define bona fide pDCs as Siglec-H^{+}CCR9^{-} cells generated cDCs upon re-culture (Figure S2) (Schlitzer et al., 2011). Importantly, individual samples were separated into technical replicates after sorting and cell lysis to allow assessment of technical variation of barcode recovery (Figure 1A). Furthermore, control experiments (Figure S1B) were performed and demonstrated that serial sampling of barcoded progeny at the indicated time intervals was a robust approach to measure DC clonal kinetics (Figures S1C and S1D).

Our method assessed DC developmental dynamics and revealed time-varying patterns. The percentages of barcodes detected at each time point over total seeded barcoded cells varied and were consistently lower than the percentages of detected barcodes across time (Table S1). Stacked histograms of the number of cells produced by each detected clone over time (Figures 1C and 1D) showed a temporal shift of DC contribution by a spectrum of large and small clones, and this pattern was apparent for all DC subtypes. This indicated that DC generation was not sustained by a set of ''stable'' clones within the tracking period, and the contribution by different clones was not equal. We also generated a heatmap showing the barcode contribution to the number of DCs (biomass) from all cell types at all time points to capture the entirety of the data (Figure 1E). Again, the shift of clonal contribution to cell types over time was apparent, as was their bias.

Next, we reasoned that the asynchronous waves of clonal contribution could affect classification of clone output. For example, if a multipotent clone generated pDCs at an early time point and cDCs later, it would be classified as having a pDC-only or cDC-only fate depending on which time point was assessed. To test this, we first categorized clones into four classes (no DCs, pDC only, cDC only, and pDC/cDC) and determined that only ~30%–40% of clones generated DCs when considered at any given single time point (Figures 2A and S1E). However, when we compared the ''across time'' fate, taking into account a clone's capacity to produce DCs at multiple time points, that proportion of DC-generating clones increased to nearly 90%. In addition, ~20% of clones were re-classified from unipotent (pDC or cDC only) when measured at single time points to multipotent (pDC/cDC) when all time points were considered (Figure 2A). The asynchronous contribution to different DC subtypes over time was indeed apparent in the majority of clones using violin plots (Figure 2C). Therefore, fate should be considered in the context of time for a full appreciation of a clone's potential. We further quantified the contribution to the number of DC subtypes by different classes of clones on the basis of the definition ''across time'' and observed lower contribution by multipotent (~40%) than unipotent (~60%) clones to both pDCs and cDCs (Figure 2B). These results highlight the importance of tracking development longitudinally to accurately and thoroughly interpret cellular output. Furthermore, our results indicate that cDCs and pDCs are largely generated by progenitors that have already branched.

DiSNE Movies Allow Visualization of Clonal Dynamics

To facilitate interpretation of the kinetics of clonal contribution, we developed a dynamic visualization tool termed developmental interpolated t-distributed stochastic neighborhood embedding (t-SNE) (DiSNE) time-lapse movies (Movies S1, S2, and S3). First, t-SNE (Van der Maaten and Hinton, 2008) was applied to reduce the dimensionality of the dataset to a two-dimensional (2D) map in which the properties of clones in terms of subtypes and number of cells produced at different times

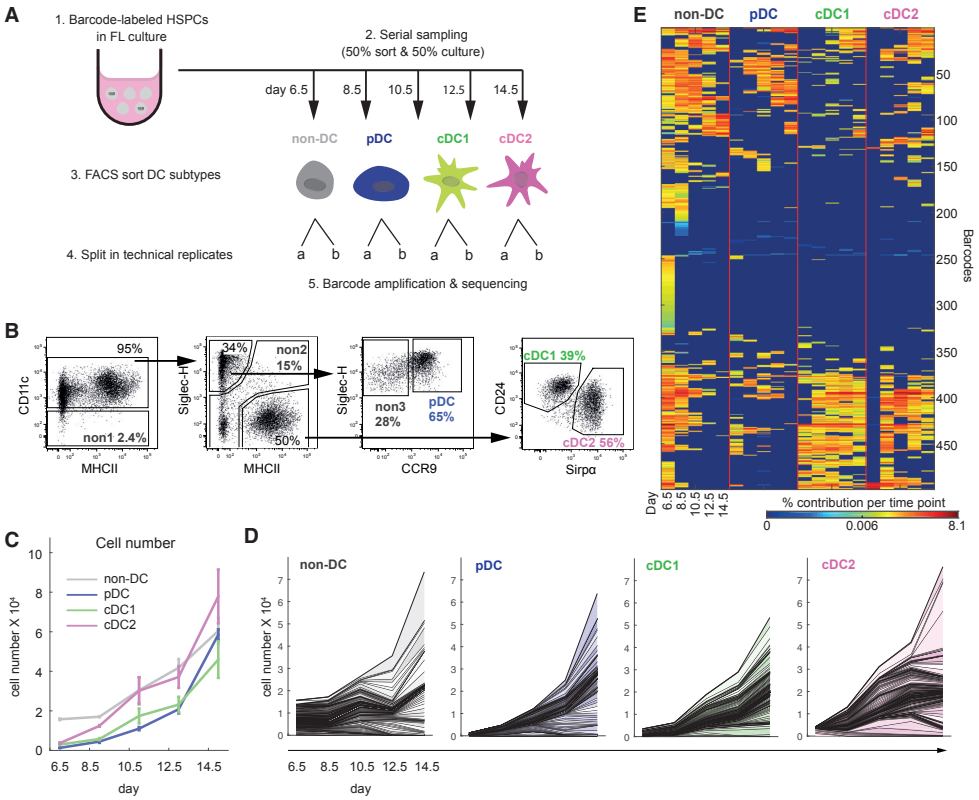

Figure 1. Longitudinal Tracking Reveals Asynchronous Waves of DC Generation

(A) Experimental setup. HSPCs (cKit$^+$Sca1$^+$) from mouse bone marrow (BM) were transduced with lentivirus containing DNA barcodes and cultured in FL-supplemented DC conditioned medium. At each time point, cells were equally split for either DC subtype isolation or further development in culture. Non-DCs (non1 + non2 + non3), pDCs, cDC1s, and cDC2s were sorted as in (B) at each time point. Samples were then lysed and split into technical replicates, and barcodes were amplified and sequenced.

(B) Gating strategy to isolate pDCs, cDC1s, cDC2s, and non-DCs using CD11c, MHCII, Siglec-H, CCR9, Sirpα, and CD24. Numbers represent percentages of cells from parent gate.

(C) Number of DC subtype generation over time at the population level.

(D) Stacked histogram showing clonal contribution (i.e., per barcode) to each DC subtype number over time. Clones are shown in the same order for each subtype. It is apparent that clones differ in size and also in timing of expansion.

(E) Heatmap representation of clonal output to DC subtypes from individual time points.

Data in (C) are average ± SEM of three independent cultures from one experiment, representative of three independent experiments. (D) and (E) show all clones from one representative culture.

dictated the position of each barcoded HSPC. To visualize clonal fate and DC biomass, we created "t-SNE pie maps" by generating a pie chart representing the proportional output to different DC subtypes and altering point size, respectively (Figure 3). Finally, changes in pie size and composition were interpolated between flanking data points during DC development for dynamic visualization.

We performed DiSNE visualization on data pooled from three independent wells, incorporating all time points available (Figure 3; Movie S1). Similar to the heatmap representation, heterogeneity was observed, but patterns were more easily distinguishable considering that the bias was incorporated into one pie, rather than four elements, and that clone size was better represented through dot size rather than color. These DiSNE movies (Movies S1, S2, and S3) portrayed the dynamic process of DC development encompassing the complexities of qualitative, quantitative, and now temporal characteristics of each clone underlying development. Therefore, DiSNE movies are an effective and powerful tool for visualization of clonal dynamics, and this technique has been packaged into a standalone software package PieMaker (https://data.mendeley.com/datasets/9mkz5n9jtf/1).

Multiple Trajectories of DC Development

To further characterize the clonal dynamics of DC development, we compared several clustering methods and observed similar

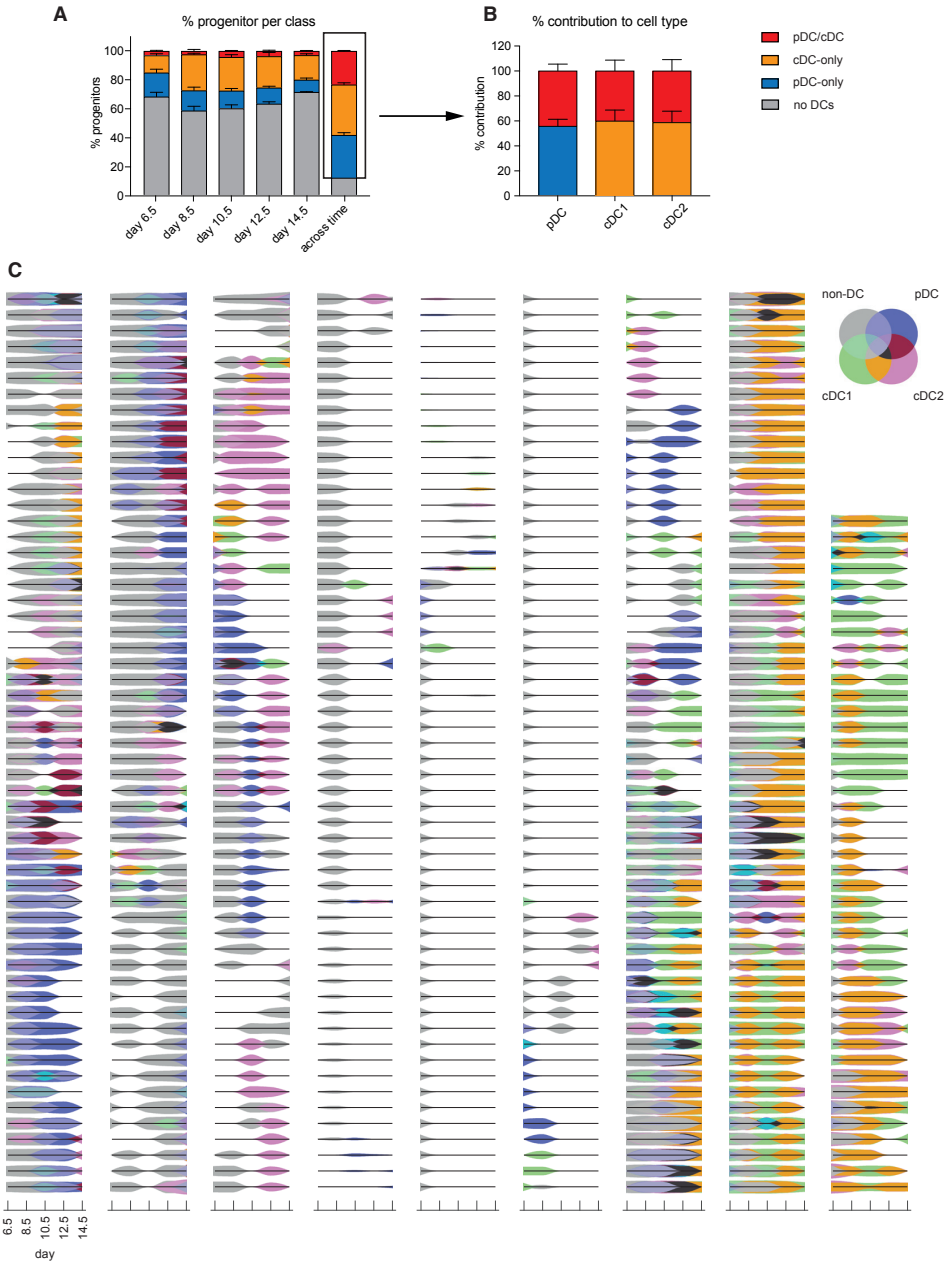

Figure 2. Longitudinal Tracking Allows Accurate Interpretation of Clonal Fate

(A) Categorization of clones into four classes, including no DCs, pDC only, cDC only, and pDC/cDC, on the basis of subtype output at a single time point or across time.

(B) Percentage contribution to cell types from three classes of clones on the basis of across-time definition.

(C) Violin plots showing clonal output of individual barcodes over time. The width of the violin is proportional to the contribution of the clone to the corresponding cell type at that time point.

Data in (A) and (B) are average + SEM of three independent cultures from one experiment, representative of three independent experiments. (C) shows the same clones as in Figures 1D and 1E, from one representative culture.

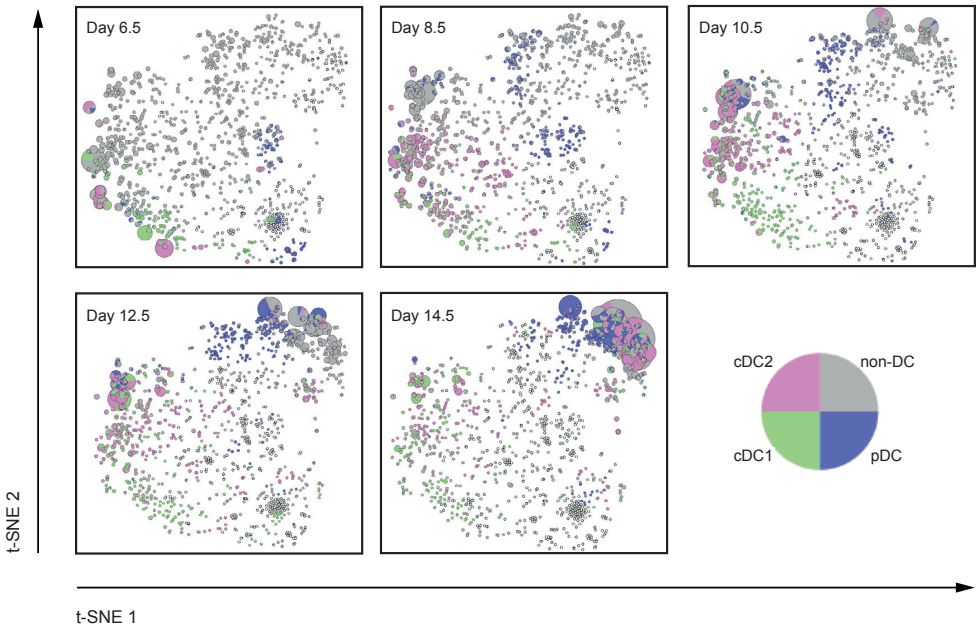

Figure 3. Visualizing Diversity of DC Cellular Trajectories Using DiSNE

Static t-SNE pie map at each time point (see Movie S1 for a dynamic visualization). Each circle represents a barcode-labeled progenitor and the size scaled to the number of cells produced by that clone per time point. Each sector in the pie chart represents the proportion of each cell type produced. Data are pooled from three independent cultures (368 data points each [out of 368, 410, and 384] for equivalence) from one experiment, representative of three independent experiments. Movies S2 and S3 show results from the other two experiments.

results (Figure S3). We then applied density-based spatial clustering of applications with noise (DBSCAN) (Ester et al., 1996), which best cohered with our DiSNE visualization and identified 16 clusters (Figure 4A). Visualization using spindle plots for each cluster showed that clusters were mainly separated by distinct fate bias or timing of contribution with similar fate output (Figure 4B). Interestingly, t-SNE mostly positioned clusters with a similar fate but asynchronous waves of contribution across a band in the plot (see manually annotated circles in Figure 4A) to form four major groups of trajectories, including cDC biased, pDC biased, multipotent, and a group of very small clones with mixed output (Figures 4B and 4F). There was large variation in the number of clones and DC biomass produced by each cluster (Figure 4C). The most prominent trajectory was cDC biased, which comprised ~43% of clones that contributed ~60% of cDC generation (Figures 4D and 4E). Similarly, ~33% of clones followed a pDC-biased trajectory, which generated more than half of pDCs (Figures 4D and 4E). Only 12% of clones were identified in the multipotent clusters, which contributed to 36% of pDCs, 31% of cDC1s, and 39% of cDC2s (Figures 4D and 4E). In addition, cluster 2 was in a region containing very small clones that were mostly unipotent. These represented 12% of total clones and fewer than 1% of the total number of DCs generated (Figures 4D and 4E). Importantly, independent wells within the same experiment were reproducible by comparing the occurrence of barcodes in each cluster (Figure 4G) and between experiments using Jensen-Shannon (JS) divergence (Amir et al., 2013) to holistically assess similarity between datasets (Figure 4H). Thus, we have identified multiple major trajectories of DC development and demonstrated the majority of clones within the HSPC fraction, but not all, follow cDC- or pDC-biased trajectories that contribute to the majority of their biomass.

Cellular Trajectories Are Intrinsically Programmed

Next, we asked whether the cellular trajectories of siblings derived from a single clone are highly correlated. To this end, we applied clone splitting by first pre-expanding barcoded progenitors for 4.5 days and then equally split the wells into two parallel FL cultures (Figure 5A). We then performed serial sampling and barcode analysis on both arms of the experiment as described. We compared the fate and clone size of shared barcodes (58% in experiment 1 and 73% in experiment 2) in parallel cultures across all time points (Figures 5B–5D and S4). Fate conservation was defined using JS divergence or cosine similarity, in which both measured similarity in clonal kinetics (types of progeny produced and the order) and produced similar results (Figure S4B). Size conservation was measured as the base two logarithm of the ratio of biomass between the shared barcodes, which essentially measured the discrepancy in division number between splits. Interestingly, we found that many sisters were concordant in their cellular trajectories, implying that descendant cells carried a "memory" of what DCs to make, when to

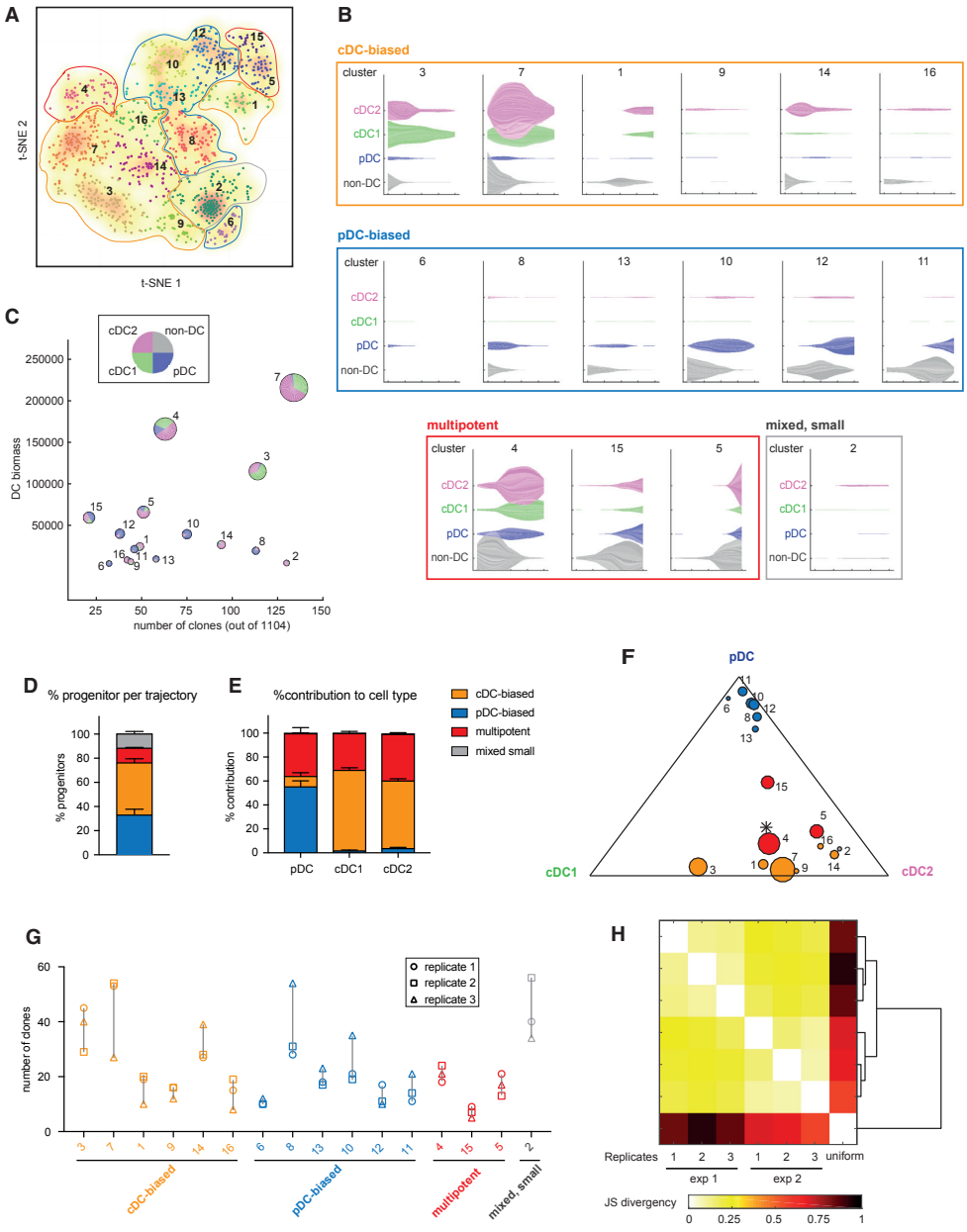

Figure 4. Identification of Major Classes of DC Cellular Trajectories

(A) DBSCAN-based algorithm identifies 16 clusters on the t-SNE map (as in Figure 3). Most clusters correlate well with the overlaid barcode density heatmap. The clusters are manually annotated into four major classes of trajectories on the basis of distinct fate output.

(B) Spindle plots showing contribution to each subtype over time by clones from individual clusters. The width of the spindle is proportional to the contribution of the cluster to the corresponding cell type at that time point, and each partition of the spindle (varying color shades) represents individual clones within the cluster.

(C) Each cluster is quantified in terms of both the number of clones (out of a total of 1,104, pool of three independent cultures) it includes (x axis) and DC biomass (the number of DCs it contributes) (y axis, pie radius). Pie charts show cluster compositions in terms of DC subtypes.

(D) Percentage progenitors from each trajectory class as defined in (A) and (B).

(E) Percentage contribution to cell types by each trajectory class. In (D) and (E), average + SEM of three independent cultures is shown.

(legend continued on next page)

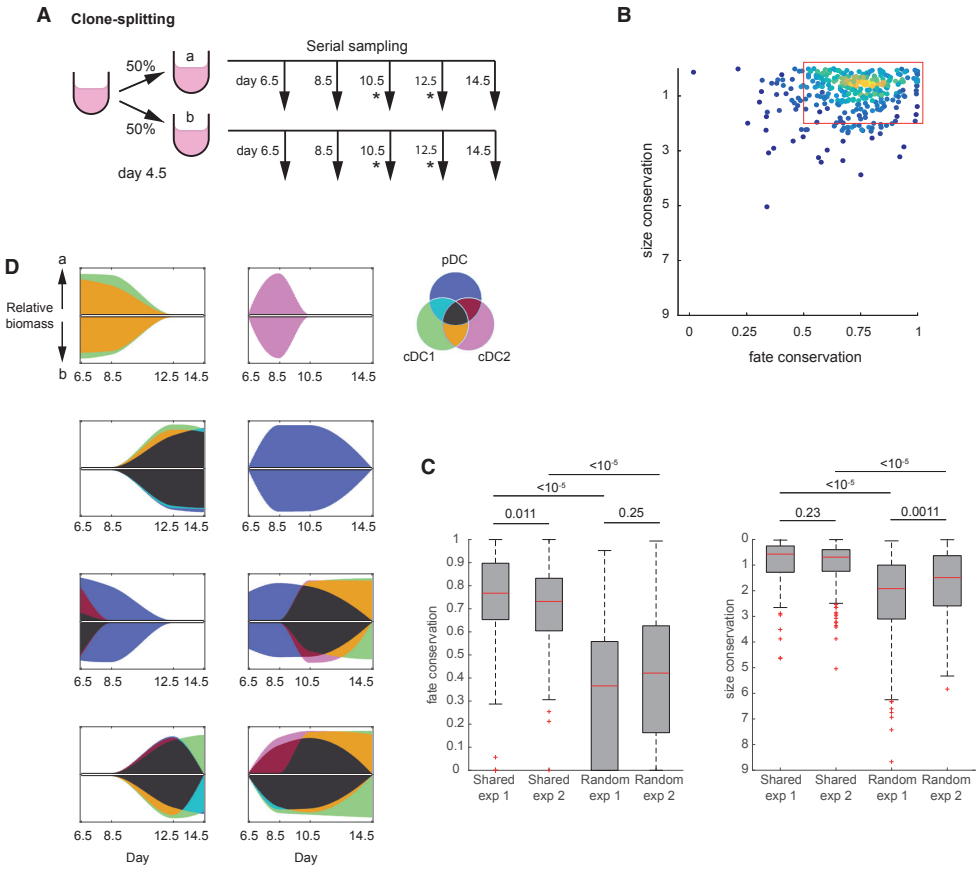

Figure 5. Clonal Cellular Trajectories Are Largely Programmed

(A) Schematic of clone-splitting experiment. Barcoded progenitors were pre-expanded in FL culture for 4.5 days and split into two parallel cultures (a and b). Serial sampling was then performed from both arms as described in Figure 1A. Asterisk, data from day 10.5 are lacking in experiment 1, and data from day 12.5 are lacking in experiment 2 because of technical issues.

(B) Conservation of shared barcodes across all time points. Each point represents a barcode with reads detected in both halves of the split culture. For each barcode, size conservation is defined as the base 2 logarithm of ratio of total read counts, and fate conservation is defined as JS divergence. Clones inside the gate represent 80% of total shared barcodes, which contributes to 80% of total biomass. Data are a pool of two sets of parallel cultures from experiment 1, representative of two independent experiments.

(C) Summary of fate and clone conservation value comparing split barcodes with randomly paired unrelated barcodes. Boxplots span interquartile range: The central line indicates the median; the bottom and top edges of the box indicate the 25th and 75th percentiles, respectively; the whiskers extend to the most extreme data points not considered outlier; an outlier is a point further than 1.5 interquartile ranges from the box in either direction. Pooled data from both independent experiments are shown. Statistical significance is measured using Mann-Whitney U test.

(D) Paired violin plots comparing cellular trajectories from two arms of split culture (a versus b). Eight examples of clones with high conservation values are shown. Full list of clones from experiment 1 is shown in Figure S4.

make them, and how many cells to produce (Figures 5 and S4A). These results are consistent with fate being a heterogeneous, yet intrinsic and heritable property of individual founder cells when measured in similar environments.

DISCUSSION

The framework developed here provides a statistically robust, quantitative, visually intuitive approach for high-throughput

(F) Ternary plot showing subtype bias of each cluster. Circle size is proportional to DC biomass of the cluster. Asterisk denotes the population average.

(G) Barcode representation from the three independent cultures (replicates) in each cluster.

(H) JS divergence measuring the similarity between independent cultures within the same experiment (very low value, highly similar pattern), between two independent experiments (low value, reproducible pattern), and between uniformly distributed pattern on the defined t-SNE region (high value, dissimilar pattern).

tracking of clonal kinetics. It allows systematic examination of lineage trajectories of any developmental system, whereby cells can be cultured *ex vivo* and subsampled at desired time intervals. Our results indicate that assessment of bona fide clonal cellular trajectories is crucial to accurately determine clonal fate, as opposed to measuring fate at a fixed time point. In addition, by incorporating clone splitting, we demonstrate that clonal fate and waves of contribution to DCs is heterogeneous yet largely programmed early in the developing clone. This provides the rationale to combine our method with other approaches such as single-cell RNA sequencing in parallel to not only measure cellular trajectories but the underlying molecular trajectories that guide these properties or to test the effect of biological variation or perturbation such as drug treatment and genetic manipulation on one arm of the clone-splitting experiment.

Importantly, we demonstrate that the majority of HSPCs already have a cDC- or pDC-biased fate by measuring clonal output across multiple time points in FL cultures of DC development. Our results do not support the current model, which implies a common origin of cDCs and pDCs from CDPs (Guilliams et al., 2014). This could be partly explained in that many prior studies do not incorporate CCR9 to define pDCs, leading to possible misallocation of cDC precursors as pDCs. Similarly, two recent studies (See et al., 2017; Villani et al., 2017) using single-cell profiling of the human DC compartment independently identified contaminating DC precursors within the phenotypically defined pDCs. Future studies should determine whether those populations and murine Siglec-H^{+}CCR9^{-} cells represent the same precursor population. Our observation of early cDC and pDC bifurcation is also partly supported by the identification of cDC-, cDC1-, and cDC2-committed progenitors in various fractions of HSPCs and downstream progenitors (Grajales-Reyes et al., 2015; Schlitzer et al., 2015; Schraml et al., 2013). Importantly, our results indicate that a pDC-committed progenitor population likely exists within HSPC fraction, indicative of early branching, similar to a recent study (Lee et al., 2017).

Our results highlight a remarkable degree of heterogeneity within early HSPC population. Longer term efforts should appraise not only progenitors but also their progeny at a single-cell level to determine how origin dictates functional heterogeneity. This information, combined with the molecular drivers that underlie true cellular trajectories, and within an *in vivo* context, are necessary for a full understanding of development.

EXPERIMENTAL PROCEDURES

Mice

All mice were bred and maintained under specific pathogen-free conditions at the Walter and Eliza Hall Institute (WEHI), according to institutional guidelines. Either C57BL/6 (CD45.2) or C57BL/6 Pep^{3b} (CD45.1) male mice aged 8–16 weeks were used.

Cellular Barcoding

Barcode transduction, amplification, and data processing were performed largely as described previously (Naik et al., 2013). See the Supplemental Information for detailed procedures.

FL Culture and Serial Sampling

Labeled cells (5 × 10^{3}) were cultured with 200 μL DC conditioned medium supplemented with hFL (BioXcell, 800 ng/mL) per well in a 96-well round-bottom plate. After 6.5 days of culture, cells were gently mixed a few times with a pipette, half were removed for subtype isolation by flow cytometry, and another half were kept in culture with medium topped up to 200 μL. The same procedure was repeated every 2 days. At the last time point, all cells from each well were harvested and sorted.

Clone-splitting experiments were performed to assess conservation of fate between shared barcodes over time. Briefly, wells were split into two at day 4.5 and both cultured until day 6.5. After that, serial sampling was performed on both splits every 2 days, and analysis was performed from each split well as the other samples.

Barcode Categorization

Each barcode was categorized into four classes: "no DCs" (produced no mature DCs), "pDC only" (produced pDCs but no cDC1s or cDC2s), "cDC only" (produced cDC1 and/or cDC2 cells but no pDCs), and "pDC/cDC" (produced pDCs and either one or both cDC types). Barcode categorization was done on the basis of minimal read count and minimal proportion. In Figure 2A, minimal read count was set to 750, and minimal proportion was set to 5%. For example, if barcode A had 1,000 reads in pDC, 600 reads in cDC1, and 90,000 reads in cDC2, the cDC1 reads was first set to zero, as it did not pass the minimal read count threshold. As this barcode produced 1% pDCs (< 5%) and 99% cDC2s, it was classified as a cDC-only clone. Categorization was performed on the basis of data at each time point independently or on the basis of data across time. For categorization across time, a barcode was considered to produce a certain subtype X if it produced subtype X at any of the time points. Categorization was repeated using varying value combination of the two thresholds to verify that small changes in the values of these parameters qualitatively resulted in similar outcomes (Figure S1E).

Visualization Using t-SNE, Static Pie Maps, and DiSNE Movies

First, t-SNE was performed with default parameters to reduce the dimensions of the dataset to 2D (Van der Maaten and Hinton, 2008). Hyperbolic arcsine-transformed biomass counts from all time points were pooled from three independent cultures as input for the t-SNE algorithm. Barcodes that did not produce any DCs were excluded. The output of t-SNE was used for downstream visualization and clustering. To visualize clonal output and size on the t-SNE map, each barcode was represented as a pie chart (t-SNE pie maps). The segments of the chart depict the proportion of each subtype at a particular time point. The radius of the pie chart reflects the total biomass of the given barcode at the given time point. For the purpose of visualizing individual cellular trajectories (developmental changes over time) and clusters (see below), a cubic spline-based interpolation for time values between experimental time points was applied. Depending on the settings for DiSNE movie generation, linearly interpolated frames can be added between frames that correspond to experimental time points (see manual for PieMaker software at: https://data.mendeley.com/datasets/9mkz5n9jtf/1).

Clustering

To identify major patterns, several clustering methods were applied, including DBSCAN (Ester et al., 1996), Gaussian-mixture clustering, and the affinity propagation algorithm (Frey and Dueck, 2007). These methods were applied on both raw data and using scatterplots derived from t-SNE as input. These methods were capable of producing similar results. For example, raw data-based clustering resulted in clusters that were spatially consistent when projected onto t-SNE plots (Figure S3A) and produced trajectories with similar patterns (data not shown).

A barcode density plot using kernel density estimation via diffusion (Botev et al., 2010) was generated to assess the feasibility of each particular clustering method by first running each of the three algorithms on grids of parameter values and visually inspecting how well the resulting clustering aligned with the barcode density plot. DBSCAN-based clustering was found to align with the density plot best. Therefore, DBSCAN was used to identify cluster centroids, and each unassigned point was assigned to the cluster with the nearest centroids. The resulting clusters were manually categorized a "cDC biased," "pDC biased," "multipotent," or "mixed, small" on the basis of visual inspection of the corresponding DiSNE movie, visualization of subtype output per cluster using spindle plots (Figure 3B), and visualization of fate bias per

cluster using ternary plots (Figure 3F). The spindle plots are stacks of biomasses of barcodes included in the corresponding cluster. Individual barcodes can be distinguished by varying color shades. The ternary plot was generated using proportions of pDC, cDC1, and cDC2 biomasses (non-DCs excluded) to define coordinates for each cluster in the equilateral triangles.

Conservation between Shared Barcodes in Split Cultures

Given a split culture, barcodes without any DC biomass in each of the split parts (non-DCs only) and barcodes that were present only in one of the splits were excluded, and the rest were identified as shared barcodes. Fate conservation was computed to measure similarity between kinetics of DC subtype production (e.g., whether split parts of the same clone produced same types of DCs and in the same order). First, biomass values were hyperbolic arcsine-transformed, and JS divergence and cosine similarity were computed. Both methods produced very similar results (Figure S4B), and hence JS divergence was used to estimate fate conservation in Figure 5. Size conservation was computed to measure similarity in clonal expansion between the split parts of the same clone. First, total biomass per barcode was calculated (sum of biomass from all subtypes from all time points) for each split part. Next, the ratio of the smaller total biomass to the larger was calculated, and the base 2 logarithm of this ratio was computed as a measure of size conservation. For example, a difference of 1 could be interpreted that one part of the clone made on average one more division round. Note that biomass of non-DCs was excluded during computation of both fate and size conservation. Random controls were generated by randomly paired unrelated barcodes in the same culture to assess whether the observed conservation was due to chance.

Statistical Analysis

The Mann-Whitney U test was performed to measure the significance of the observed difference between groups. All data are presented in boxplots that span the interquartile range.

DATA AND SOFTWARE AVAILABILITY

The data reported in this study have been deposited to Mendeley Data at 10.17632/9mkz5n9jtf/1.

SUPPLEMENTAL INFORMATION

Supplemental Information includes Supplemental Experimental Procedures, four figures, one table, and three movies and can be found with this article online at https://doi.org/10.1016/j.celrep.2018.02.046.

ACKNOWLEDGMENTS

We thank the Walter and Eliza Hall fluorescence-activated cell sorting (FACS) laboratory, Dr. Stephen Wilcox, and Dr. Tom Weber for technical support. We thank Dr. Samir Taoudi, Prof. Gabrielle Belz, and Prof. Stephen Nutt for insightful discussions. This work was supported by grants from the National Health & Medical Research Council, Australia, GNT1062820, GNT1100033, and GNT1145184, and the Australia Research Council's special initiative Stem Cells Australia.

AUTHOR CONTRIBUTIONS

Conceptualization, D.S.L., A.K., J.G., and S.H.N.; Methodology, D.S.L., A.K., J.G., and S.H.N.; Software, A.K. and J.G.; Formal Analysis, A.K.; Investigation, D.S.L.; Visualization, D.S.L. and A.K.; Writing – Original Draft, D.S.L., A.K., and S.H.N.; Writing – Review & Editing, D.S.L., A.K., J.G., E.J.C., P.D.H., and S.H.N.; Supervision, S.H.N., E.C., and P.D.H.

DECLARATION OF INTERESTS

The authors declare no competing interests.

Received: August 20, 2017
Revised: November 21, 2017
Accepted: February 9, 2018
Published: March 6, 2018

REFERENCES

Amir, el-A.D., Davis, K.L., Tadmor, M.D., Simonds, E.F., Levine, J.H., Bendall, S.C., Shenfeld, D.K., Krishnaswamy, S., Nolan, G.P., and Pe'er, D. (2013). viSNE enables visualization of high dimensional single-cell data and reveals phenotypic heterogeneity of leukemia. Nat. Biotechnol. *31*, 545–552.

Botev, Z.I., Grotowski, J.F., and Kroese, D.P. (2010). Kernel density estimation via diffusion. Ann. Stat. *38*, 2916–2957.

Bystrykh, L.V., Verovskaya, E., Zwart, E., Broekhuis, M., and de Haan, G. (2012). Counting stem cells: methodological constraints. Nat. Methods *9*, 567–574.

Dursun, E., Endele, M., Musumeci, A., Failmezger, H., Wang, S.-H., Tresch, A., Schroeder, T., and Krug, A.B. (2016). Continuous single cell imaging reveals sequential steps of plasmacytoid dendritic cell development from common dendritic cell progenitors. Sci. Rep. *6*, 37462.

Dykstra, B., Kent, D., Bowie, M., McCaffrey, L., Hamilton, M., Lyons, K., Lee, S.-J., Brinkman, R., and Eaves, C. (2007). Long-term propagation of distinct hematopoietic differentiation programs in vivo. Cell Stem Cell *1*, 218–229.

Ema, H., Morita, Y., and Suda, T. (2014). Heterogeneity and hierarchy of hematopoietic stem cells. Exp. Hematol. *42*, 74–82.e2.

Ester, M., Kriegel, H.P., Sander, J., and Xu, X. (1996). A density-based algorithm for discovering clusters in large spatial databases with noise. In Proceedings of the Second International Conference on Knowledge Discovery and Data Mining, pp. 226–231.

Frey, B.J., and Dueck, D. (2007). Clustering by passing messages between data points. Science *315*, 972–976.

Frieda, K.L., Linton, J.M., Hormoz, S., Choi, J., Chow, K.K., Singer, Z.S., Budde, M.W., Elowitz, M.B., and Cai, L. (2017). Synthetic recording and in situ readout of lineage information in single cells. Nature *541*, 107–111.

Grajales-Reyes, G.E., Iwata, A., Albring, J., Wu, X., Tussiwand, R., Kc, W., Kretzer, N.M., Briseño, C.G., Durai, V., Bagadia, P., et al. (2015). Batf3 maintains autoactivation of Irf8 for commitment of a CD8α(+) conventional DC clonogenic progenitor. Nat. Immunol. *16*, 708–717.

Guilliams, M., Ginhoux, F., Jakubzick, C., Naik, S.H., Onai, N., Schraml, B.U., Segura, E., Tussiwand, R., and Yona, S. (2014). Dendritic cells, monocytes and macrophages: a unified nomenclature based on ontogeny. Nat. Rev. Immunol. *14*, 571–578.

Guo, G., Luc, S., Marco, E., Lin, T.-W., Peng, C., Kerenyi, M.A., Beyaz, S., Kim, W., Xu, J., Das, P.P., et al. (2013). Mapping cellular hierarchy by single-cell analysis of the cell surface repertoire. Cell Stem Cell *13*, 492–505.

Helft, J., Anjos-Afonso, F., van der Veen, A.G., Chakravarty, P., Bonnet, D., and Reis E Sousa, C. (2017). Dendritic cell lineage potential in human early hematopoietic progenitors. Cell Rep. *20*, 529–537.

Kalhor, R., Mali, P., and Church, G.M. (2017). Rapidly evolving homing CRISPR barcodes. Nat. Methods *14*, 195–200.

Kim, S., Kim, N., Presson, A.P., Metzger, M.E., Bonifacino, A.C., Sehl, M., Chow, S.A., Crooks, G.M., Dunbar, C.E., An, D.S., et al. (2014). Dynamics of HSPC repopulation in nonhuman primates revealed by a decade-long clonal-tracking study. Cell Stem Cell *14*, 473–485.

Lee, J., Zhou, Y.J., Ma, W., Zhang, W., Aljoufi, A., Luh, T., Lucero, K., Liang, D., Thomsen, M., Bhagat, G., et al. (2017). Lineage specification of human dendritic cells is marked by IRF8 expression in hematopoietic stem cells and multipotent progenitors. Nat. Immunol. *15*, 3221.

Månsson, R., Hultquist, A., Luc, S., Yang, L., Anderson, K., Kharazi, S., Al-Hashmi, S., Liuba, K., Thorén, L., Adolfsson, J., et al. (2007). Molecular evidence for hierarchical transcriptional lineage priming in fetal and adult stem cells and multipotent progenitors. Immunity *26*, 407–419.

Marchingo, J.M., Kan, A., Sutherland, R.M., Duffy, K.R., Wellard, C.J., Belz, G.T., Lew, A.M., Dowling, M.R., Heinzel, S., and Hodgkin, P.D. (2014). T cell signaling. Antigen affinity, costimulation, and cytokine inputs sum linearly to amplify T cell expansion. Science *346*, 1123–1127.

McKenna, A., Findlay, G.M., Gagnon, J.A., Horwitz, M.S., Schier, A.F., and Shendure, J. (2016). Whole-organism lineage tracing by combinatorial and cumulative genome editing. Science *353*, aaf7907.

Merad, M., Sathe, P., Helft, J., Miller, J., and Mortha, A. (2013). The dendritic cell lineage: ontogeny and function of dendritic cells and their subsets in the steady state and the inflamed setting. Annu. Rev. Immunol. *31*, 563–604.

Naik, S.H., Proietto, A.I., Wilson, N.S., Dakic, A., Schnorrer, P., Fuchsberger, M., Lahoud, M.H., O'Keeffe, M., Shao, Q.X., Chen, W.F., et al. (2005). Cutting edge: generation of splenic CD8+ and CD8- dendritic cell equivalents in Fms-like tyrosine kinase 3 ligand bone marrow cultures. J. Immunol. *174*, 6592–6597.

Naik, S.H., Metcalf, D., van Nieuwenhuijze, A., Wicks, I., Wu, L., O'Keeffe, M., and Shortman, K. (2006). Intrasplenic steady-state dendritic cell precursors that are distinct from monocytes. Nat. Immunol. *7*, 663–671.

Naik, S.H., Sathe, P., Park, H.Y., Metcalf, D., Proietto, A.I., Dakic, A., Carotta, S., O'Keeffe, M., Bahlo, M., Papenfuss, A., et al. (2007). Development of plasmacytoid and conventional dendritic cell subtypes from single precursor cells derived in vitro and in vivo. Nat. Immunol. *8*, 1217–1226.

Naik, S.H., Perié, L., Swart, E., Gerlach, C., van Rooij, N., de Boer, R.J., and Schumacher, T.N. (2013). Diverse and heritable lineage imprinting of early haematopoietic progenitors. Nature *496*, 229–232.

Naik, S.H., Schumacher, T.N., and Perié, L. (2014). Cellular barcoding: a technical appraisal. Exp. Hematol. *42*, 598–608.

Notta, F., Zandi, S., Takayama, N., Dobson, S., Gan, O.I., Wilson, G., Kaufmann, K.B., McLeod, J., Laurenti, E., Dunant, C.F., et al. (2016). Distinct routes of lineage development reshape the human blood hierarchy across ontogeny. Science *351*, aab2116.

Onai, N., Obata-Onai, A., Schmid, M.A., Ohteki, T., Jarrossay, D., and Manz, M.G. (2007). Identification of clonogenic common Flt3+M-CSFR+ plasmacytoid and conventional dendritic cell progenitors in mouse bone marrow. Nat. Immunol. *8*, 1207–1216.

Onai, N., Kurabayashi, K., Hosoi-Amaike, M., Toyama-Sorimachi, N., Matsushima, K., Inaba, K., and Ohteki, T. (2013). A clonogenic progenitor with prominent plasmacytoid dendritic cell developmental potential. Immunity *38*, 943–957.

Sanjuan-Pla, A., Macaulay, I.C., Jensen, C.T., Woll, P.S., Luis, T.C., Mead, A., Moore, S., Carella, C., Matsuoka, S., Bouriez Jones, T., et al. (2013). Platelet-biased stem cells reside at the apex of the haematopoietic stem-cell hierarchy. Nature *502*, 232–236.

Schlitzer, A., Loschko, J., Mair, K., Vogelmann, R., Henkel, L., Einwächter, H., Schiemann, M., Niess, J.-H., Reindl, W., and Krug, A. (2011). Identification of CCR9- murine plasmacytoid DC precursors with plasticity to differentiate into conventional DCs. Blood *117*, 6562–6570.

Schlitzer, A., Sivakamasundari, V., Chen, J., Sumatoh, H.R.B., Schreuder, J., Lum, J., Malleret, B., Zhang, S., Larbi, A., Zolezzi, F., et al. (2015). Identification of cDC1- and cDC2-committed DC progenitors reveals early lineage priming at the common DC progenitor stage in the bone marrow. Nat. Immunol. *16*, 718–728.

Schraml, B.U., van Blijswijk, J., Zelenay, S., Whitney, P.G., Filby, A., Acton, S.E., Rogers, N.C., Moncaut, N., Carvajal, J.J., and Reis e Sousa, C. (2013). Genetic tracing via DNGR-1 expression history defines dendritic cells as a hematopoietic lineage. Cell *154*, 843–858.

See, P., Dutertre, C.-A., Chen, J., Günther, P., McGovern, N., Irac, S.E., Gunawan, M., Beyer, M., Händler, K., Duan, K., et al. (2017). Mapping the human DC lineage through the integration of high-dimensional techniques. Science *356*, eaag3009.

Shortman, K., and Naik, S.H. (2007). Steady-state and inflammatory dendritic-cell development. Nat. Rev. Immunol. *7*, 19–30.

Skylaki, S., Hilsenbeck, O., and Schroeder, T. (2016). Challenges in long-term imaging and quantification of single-cell dynamics. Nat. Biotechnol. *34*, 1137–1144.

Sun, J., Ramos, A., Chapman, B., Johnnidis, J.B., Le, L., Ho, Y.-J., Klein, A., Hofmann, O., and Camargo, F.D. (2014). Clonal dynamics of native haematopoiesis. Nature *514*, 322–327.

Van der Maaten, L., and Hinton, G. (2008). Visualizing data using t-SNE. J. Mach. Learn. Res. *9*, 2579–2605.

Verovskaya, E., Broekhuis, M.J.C., Zwart, E., Ritsema, M., van Os, R., de Haan, G., and Bystrykh, L.V. (2013). Heterogeneity of young and aged murine hematopoietic stem cells revealed by quantitative clonal analysis using cellular barcoding. Blood *122*, 523–532.

Villani, A.-C., Satija, R., Reynolds, G., Sarkizova, S., Shekhar, K., Fletcher, J., Griesbeck, M., Butler, A., Zheng, S., Lazo, S., et al. (2017). Single-cell RNA-seq reveals new types of human blood dendritic cells, monocytes, and progenitors. Science *356*, eaah4573.

Wagner, A., Regev, A., and Yosef, N. (2016). Revealing the vectors of cellular identity with single-cell genomics. Nat. Biotechnol *34*, 1145–1160.

Wu, C., Li, B., Lu, R., Koelle, S.J., Yang, Y., Jares, A., Krouse, A.E., Metzger, M., Liang, F., Loré, K., et al. (2014). Clonal tracking of rhesus macaque hematopoiesis highlights a distinct lineage origin for natural killer cells. Cell Stem Cell *14*, 486–499.

Yamamoto, R., Morita, Y., Ooehara, J., Hamanaka, S., Onodera, M., Rudolph, K.L., Ema, H., and Nakauchi, H. (2013). Clonal analysis unveils self-renewing lineage-restricted progenitors generated directly from hematopoietic stem cells. Cell *154*, 1112–1126.

Supplementary Figures

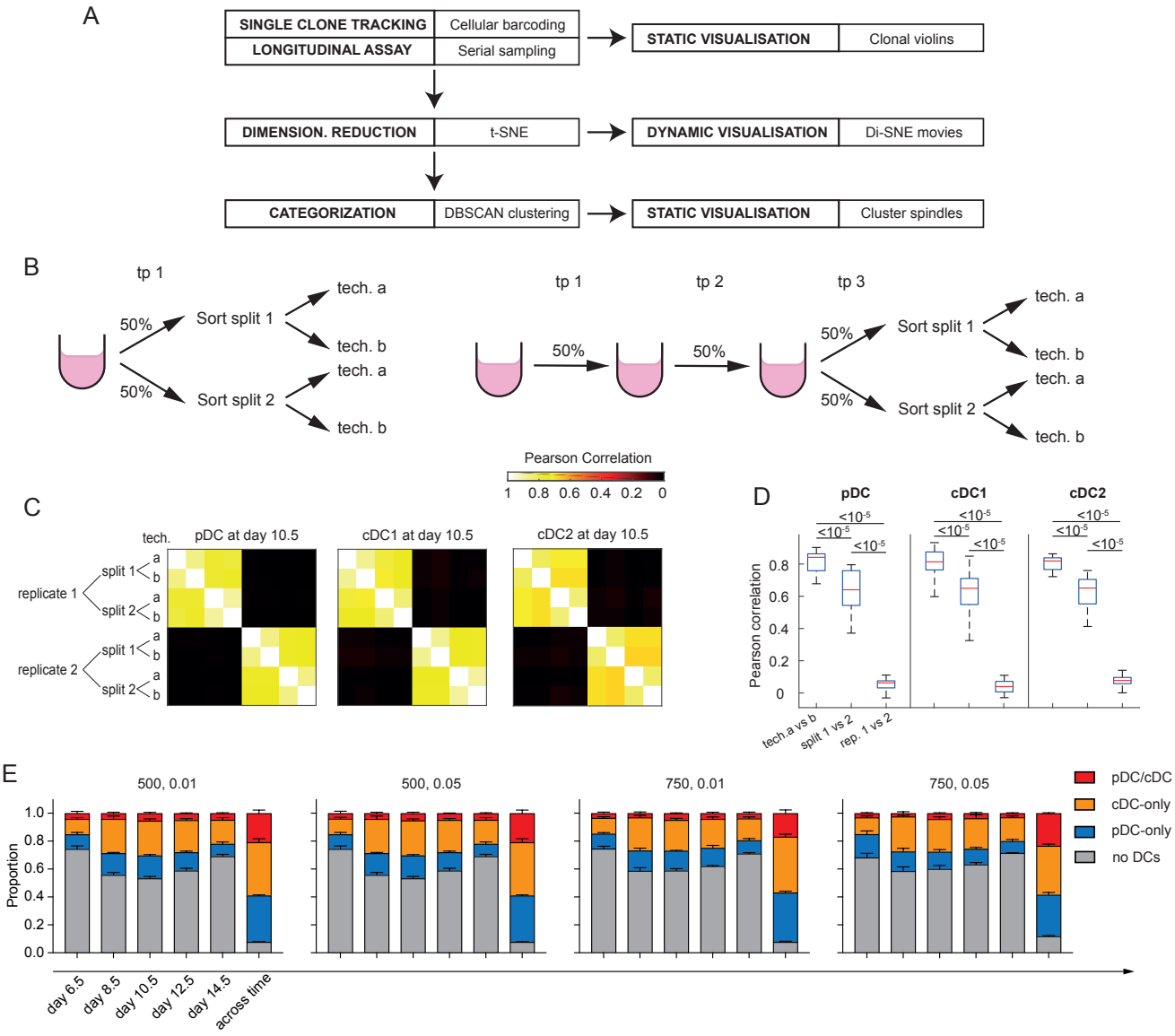

Figure S1. Optimization and validation of experimental set up. Related to Figure 1 & 2.
(A) Workflow used in this framework to study clonal dynamics. Left boxes: general methods; Right boxes: specific methods used in the study.
(B) Schematic of sampling controls. Same sampling procedure was performed as described in Figure 1A until the corresponding time point when each split was sorted separately and barcode signatures were compared.
(C) Correlation heatmaps comparing Pearson Correlation between technical replicates (tech a vs b, split after sorting), sampling controls (split 1 vs 2) and unrelated samples (replicate 1 vs 2). Examples from day 10.5 are shown. Pearson correlation was calculated using hyperbolic arcsine-transformed values of read counts before pre-precessing.
(D) Summary of Pearson correlation of all samples at all time points from one experiment. Boxplots show interquartile range; middle bar depicts median. One experiment was performed, with two replicates per time point. Mann-Whitney U test was performed.
(E) Barcode categorization using different thresholds (minimal read counts, minimal proportion) as described in Experimental Procedures. Data shown are average + SEM of 3 independent cultures from one experiment, representative of 3 independent experiments

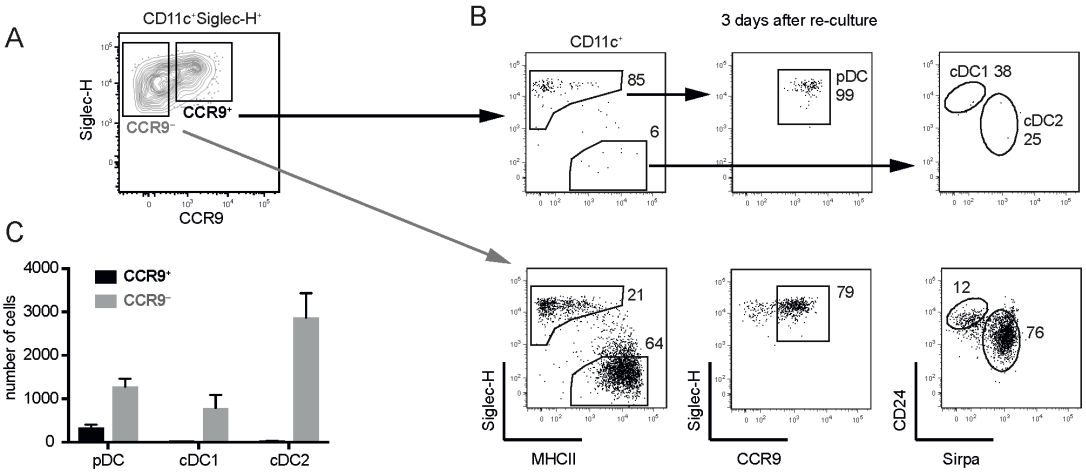

Figure S2. Siglec-H^{+}CCR9^{-} cells are DC precursors. Related to Figure 1B.
(A) CCR9^{+} and CCR9^{-} cells from the CD11c^{+}Siglec-H^{+} fraction of cultured DCs were sorted.
(B) Cells were re-cultured and analyzed by FACS at day 3. CCR9^{-} cells generated both cDCs (Siglec-H^{-}MHCII^{hi}) and pDCs (Siglec-H^{+}CCR9^{+}) upon re-culture, while viable CCR9^{+} cells maintained the original phenotype (Siglec-H^{+}CCR9^{+}). Numbers in example FACS plot depict percentage of parent gate.
(C) Summary of number of cells generated at day 3 from Siglec-H^{+}CCR9^{+} and Siglec-H^{+}CCR9^{-} cells. Data shown are average + SEM of 3 replicates, representative of 3 independent experiments.

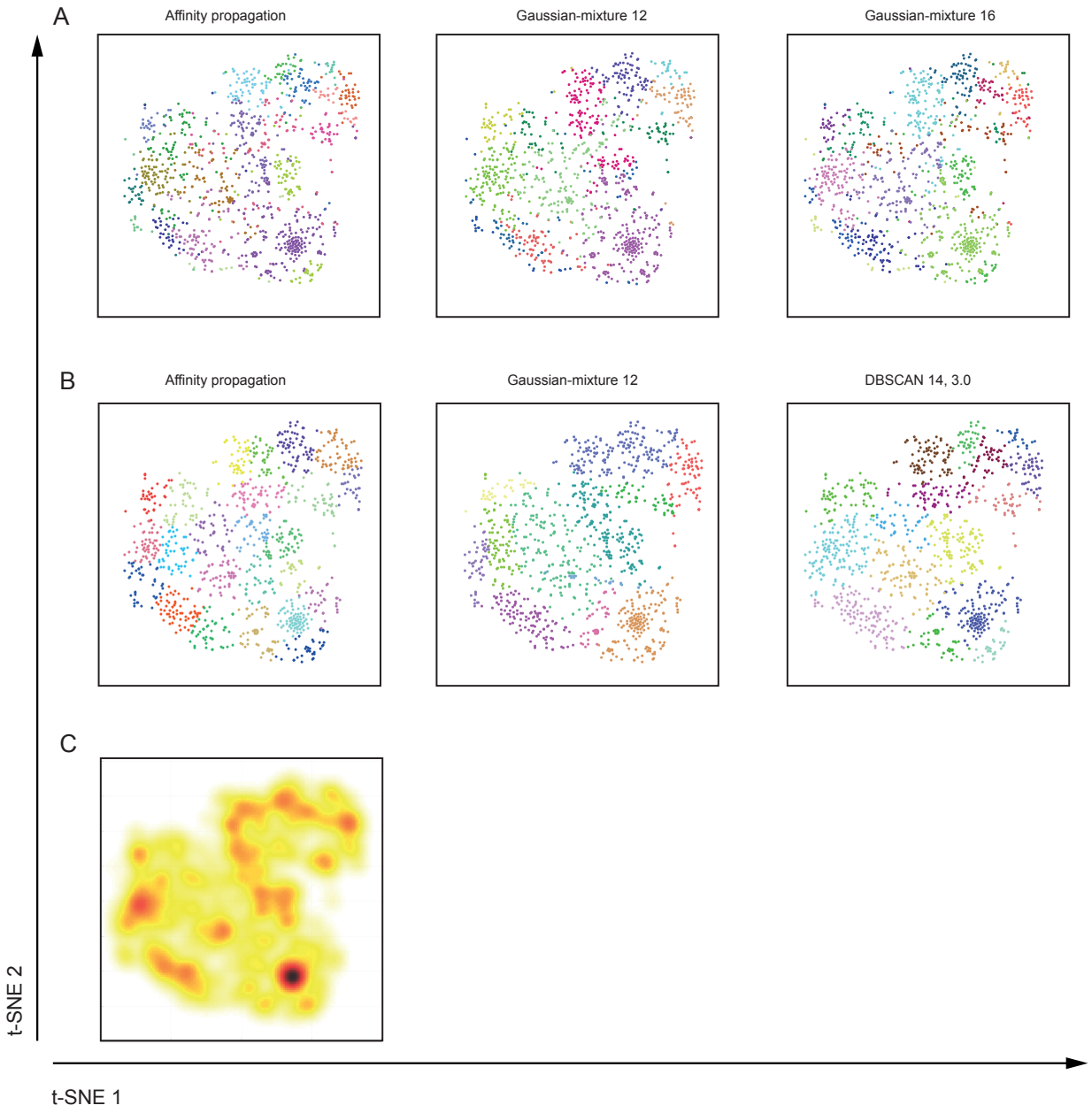

Figure S3. Comparison of different clustering methods. Related to Figure 4.
(A) Clustering using raw data as input. Clusters produced by affinity propagation and Gaussian-mixture clustering (12 or 16 components) are projected onto t-SNE plots. Most clusters produced are spatially consistent with t-SNE.
(B) Clustering using t-SNE as input. Clusters produced by affinity propagation, Gaussian-mixture clustering (12 components) and DBSCAN (same as Figure 4A) are shown. Note that DBSCAN produces clusters that correlate best with the dense regions of barcodes in (C).
(C) t-SNE density heatmap.

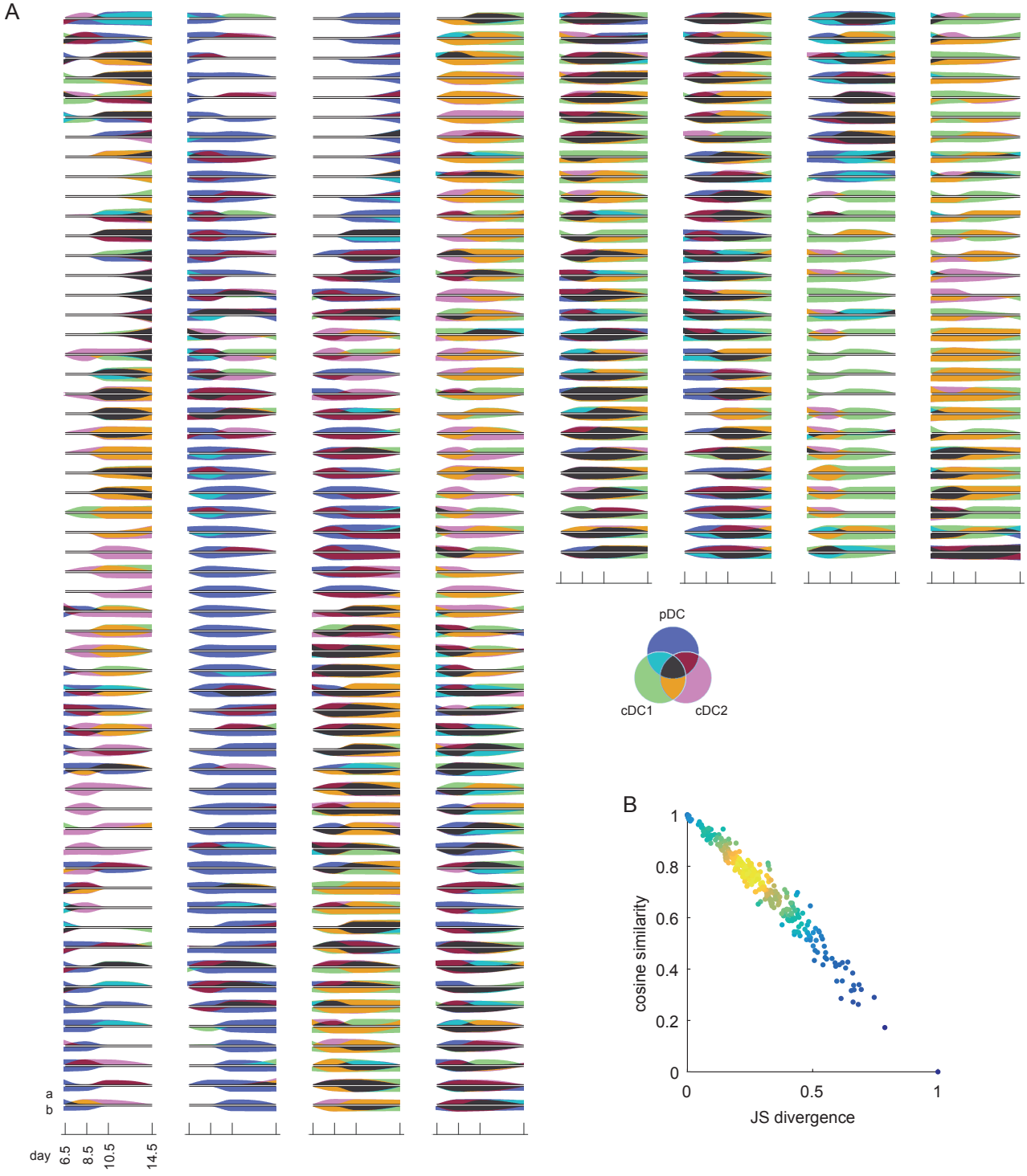

Figure S4. Comparison of cellular trajectories in clone-split cultures. Related to Figure 5.
(A) Full list of paired violin plots comparing trajectories of shared barcodes (a vs b) as in Figure 5D.
(B) Linear correlation between JS divergence and cosine similarity to measure fate conservation of shared barcodes. Cosine similarity of 1 or JS divergence of 0 indicates identical output. Each dot represents one shared barcode. Color depicts density of barcodes.
Data are pooled from 2 sets of parallel cultures from experiment 1, representative of 2 independent experiments.

Supplementary Table

Table S1. Percentage of detected barcoded cells over the seeded barcoded cells in each well.
Related to Experimental Procedures.

	Across time	Day 6.5	Day 8.5	Day 10.5	Day 12.5	Day 14.5
Well 1	46.0	15.3	25.3	33.9	32.7	28.5
Well 2	50.4	9.6	29.9	38.8	37.0	29.1
Well 3	46.7	14.3	36.5	24.8	27.4	24.8

Supplementary Materials and Methods

SUPPLEMENTAL EXPERIMENTAL PROCEDURES

Isolation of bone marrow progenitors

Bone marrow cells from hip, tibia and femur were stained with anti-CD117 allophycocyanin (APC) at 4 °C for at least 30 minutes. CD117 enrichment was then performed using MACS after incubation with anti-APC magnetic beads according to manufacturer's protocol (Miltenyl Biotec). CD117-enriched cells were stained with anti-Sca1 antibody. Finally, cells were resuspended in FACS buffer (PBS with 0.5% FBS and 2 mM EDTA) containing propidium iodide (1 µg/ml) before sorting $cKit^+Sca1^+$ (SK) cells using a BD Influx, BD Fusion or BD FACSAria-II/III (Beckton Dickinson).

Isolation of DC subtypes

Cells removed from culture were stained with antibodies against CD11c, MHCII, Siglec-H, CCR9, Sirpα and CD24. pDCs were gated as $CD11c^+MHCII^{-/low}Siglec\text{-}H^+CCR9^+$. cDC1s were gated as $CD11c^+MHCII^+Sirp\alpha^-CD24^{hi}$. cDC2s were gated as $CD11c^+MHCII^+Sirp\alpha^+CD24^+$. Fractions other than these three DC subtypes were sorted together as non-DCs (non1 + non2 + non3).

Sampling controls

Sampling controls were included to test whether there was an equal chance of capturing the same barcodes in two fractions (Figure S1B). To control for the first time point, wells were split and each half was analyzed by sorting DC subtypes and recovering barcodes. To control for the second time point, half of the culture was discarded at day 6.5 and the other half was kept in wells and then each half was analyzed at day 8.5. Similarly, to control for later time points, half of the culture was discarded and the other half kept in wells at each time point prior to analysis.

Barcode transduction

Progenitors were transferred into a 96-well round bottom plate at $< 1 \times 10^5$ cells/well in 100 µl StemSpan medium (Stem Cell Technologies) with 50 ng/ml stem cell factor (generated in-house) and small amount of lentivirus containing the barcode library and GFP reporter (Naik et al., 2013). The amount of lentivirus was pre-determined in control experiments to give approximately 10% transduction efficiency. The plate was centrifuged at 900 *g* for 90 minutes at 22 °C prior to incubation at 37 °C and 5% CO_2-in-air for 4.5 hours. After transduction, cells were washed using a large volume of RPMI containing 10% FBS and resuspended in FL-supplemented DC conditioned medium (Naik et al., 2005).

Barcode amplification

Sorted cell populations were lysed in 40 µl Viagen lysis buffer containing 0.5 mg/ml Proteinase K (Invitrogen) and split into technical replicates. Barcodes in cell lysate were then amplified following two rounds of PCRs. The first PCR amplified barcode DNA using TopLib 5'-TGCTGCCGTCAACTAGAACA-3' and BotLib primers 5'-GATCTCGAATCAGGCGCTTA-3'. In the second round PCR, each sample received an 82-bp well-specific index primer (384 in total) and an 86-bp plate-specific index primer (8 in total). The use of two index primers per sample allowed multiplexing of more than 3000 samples per sequencing run. Index primer sequences are available on request. Caution was taken at all steps to avoid barcode contamination between samples. Products from second round PCR with index primers were run on a 2% agarose gel to confirm a PCR product was generated, prior to being cleaned with size selected beads (NucleoMag NGS) according to the manufacturer's protocol. The cleaned PCR products were pooled and deep sequencing was performed on the Illumina NextSeq platform.

Barcode data processing

First, number of reads per barcode in each technical replicate from each sorted sample was calculated using processAmplicons function from edgeR package (Robinson et al., 2010). The quality of the samples was assessed by comparing technical replicates. The majority of samples used across all experiments (253 out of 264) met the following criteria: (1) average total read number across the two replicates was $\geq 10^4$; (2) ratio between the smaller and the larger number of total reads was ≥ 0.2 (i.e. less than one order of magnitude); and (3) Pearson correlation coefficient between barcode read counts in two replicates was ≥ 0.6.

Read counts between technical replicates from the samples were averaged, except for barcodes that had reads in one technical replicate but not the other due to technical reasons, which were set to zero read count. Total read counts of each sample was then normalized to 10^5.

The total number of barcoded cells seeded was estimated by multiplying the total number of cells seeded (5000) and the average %GFP detected (indicative of transduction efficiency) in each culture. Percentage of barcodes detected

was then calculated as number of barcodes present after quality control over number of barcoded cells seeded (Table S1).

Heatmaps

Heatmaps were generated to visualize clonal output to DC subtypes at different time points using barcode biomass multiplied by a factor of 100 and hyperbolic arcsine transformed. Such a transformation resembles log-transformation with pre-selected logarithm base. The advantage of using hyperbolic arcsine is that this function is defined at zero. The order of barcodes in both visualization methods was produced using an algorithm for optimal leaf ordering for hierarchical clustering (Bar-Joseph et al., 2001), as implemented in optimalleaforder function from MATLAB R2015b (MathWorks). In brief, such an ordering maximizes sum of similarities between adjacent barcodes, e.g., adjacent rows in the heatmap.

Biomass computation

Since every sample (e.g., "pDC at day 6.5" or "cDC1 at day 10.5") is normalized to 10^5 reads, barcode read counts only reflect the contribution of the barcode to a particular subtype but not to the entire culture. Therefore, barcode biomass per time point was computed using normalized barcode read counts (as described above) and subtype proportion (number of cells per subtype / sum of all subtypes) as inputs, so that the sum of all barcode biomass at any time point represented 100% of the culture.

SUPPLEMENTAL REFERENCES

Bar-Joseph, Z., Gifford, D.K., and Jaakkola, T.S. (2001). Fast optimal leaf ordering for hierarchical clustering. Bioinformatics (Oxford, England) *17 Suppl 1*, S22–S29.

Naik, S.H., Proietto, A.I., Wilson, N.S., Dakic, A., Schnorrer, P., Fuchsberger, M., Lahoud, M.H., O'Keeffe, M., Shao, Q.X., Chen, W.F., et al. (2005). Cutting edge: generation of splenic CD8+ and CD8- dendritic cell equivalents in Fms-like tyrosine kinase 3 ligand bone marrow cultures. Journal of Immunology *174*, 6592–6597.

Naik, S.H., Perié, L., Swart, E., Gerlach, C., van Rooij, N., de Boer, R.J., and Schumacher, T.N. (2013). Diverse and heritable lineage imprinting of early haematopoietic progenitors. Nature *496*, 229–232.

Robinson, M.D., McCarthy, D.J., and Smyth, G.K. (2010). edgeR: a Bioconductor package for differential expression analysis of digital gene expression data. Bioinformatics (Oxford, England) *26*, 139–140.

Chapter 4. Clonal Aetiology of Emergency DC Development

Summary

In **Chapter 3**, I characterized steady-state clonal DC development and demonstrated early imprinting of single HSPCs with regards to their cellular trajectories, including their distinct fate bias. In this chapter, I aimed to understand whether heterogeneous lineage priming in single HSPC clones was already stably established. To this end, I investigated the molecular and cellular events within single HSPC clones during FL-mediated emergency DC development. I observed minimal contribution to DC generation via emergency recruitment of non-DC-primed HSPC clones, thus demonstrated a lack of 'fate plasticity' in these clones upon exogenous FL stimulation. Instead, I determined that FL exposure selectively amplified the expansion of DCs from pre-existing HSPC clones that were already DC-primed, particularly those with multi-lineage potentials. Importantly, during early stages of FL stimulation, there was already an emergence of a unique subset of progenitors that exhibited both hyper-proliferative and DC fate potentials. These findings have important implications for the understanding of the regulation of DC fate during emergency haematopoiesis.

This chapter has been submitted for publication to Nature Immunology on June 28th, 2019. The full manuscript including main and supplementary information is attached here.

Main

Emergency Dendritic Cell Development is Driven by Selective Clonal Expansion of Early Haematopoietic Progenitors

Dawn S. Lin[1,2], Luyi Tian[1,2,4], Tom S. Weber[1,3], Jaring Schreuder[1], Daniela Amann-Zalcenstein[1,3,4], Tracey M. Baldwin[5,6], Samir Taoudi[1,3,4], Matthew E. Ritchie[1,3,4], Philip D. Hodgkin[1,3], Shalin H. Naik [1,3,5*]

1. Immunology Division, Walter and Eliza Hall Institute, Parkville, VIC 3052, Australia
2. Faculty of Medicine, Dentistry & Health Sciences, University of Melbourne, Parkville, VIC 3010, Australia
3. Department of Medical Biology, University of Melbourne, Parkville, VIC 3010, Australia
4. Epigenetic and Development Division, Walter and Eliza Hall Institute, Parkville, VIC 3052, Australia
5. Single Cell Open Research Endeavour (SCORE), Walter and Eliza Hall Institute, Parkville, VIC 3052, Australia
6. Blood Cells and Blood Cancer Division, Walter and Eliza Hall Institute, Parkville, VIC 3052, Australia

*Correspondence: naik.s@wehi.edu.au

Abstract

Exposure to Flt3 ligand (FL) preferentially induces emergency dendritic cell (DC) generation, leading to enhanced targeted immunity against infection or cancer. Here, we employ cellular barcoding to understand how FL affects single haematopoietic stem and progenitor cell (HSPC) fate decisions. We observe little evidence of dormant HSPC recruitment or lineage diversion of HSPCs away from alternative fates. Instead, pre-existing multi-/oligo-potent clones retain their multi-lineage potency, but selectively expand a DC-generating sub-branch, leading to preferential production of DCs. Using a single cell multi-omics profiling approach, we identify key early cellular and molecular events including increased cell division, maintenance of hyper-proliferative potential and establishment of DC fate in HSPCs that are responsive to FL stimulation. Collectively, our results suggest that heterogenous lineage programs within single HSPCs are established and stable, and that selective clonal expansion of a DC-generating branch, rather than FL-instructed fate 'plasticity' drives emergency DC development.

Introduction

Dendritic cells (DCs) are a critical immune cell type that can be categorized into three functionally specialized subsets: conventional DC (cDC) type 1 (cDC1), cDC type 2 (cDC2) and plasmacytoid DC (pDC) [1]. These DC subtypes are ontogenically and functionally distinct from monocyte-derived cells or macrophages [1]. In particular, cDC1s have the unique ability to recognize and cross-present antigens from intracellular pathogens including viruses, bacteria and protozoans to activate $CD8^+$ cytotoxic T lymphocytes (CTLs) [2,3]. In addition, cDC1s play an essential role in initiating and maintaining potent CTL responses in the context of antitumor immunity, due to their crucial involvement in the uptake and trafficking of tumor antigens [4,5], as well as CTL recruitment and activation [6-8]. Indeed, a lack of intra-tumoral cDC1s leads to a failure in anti-tumor CTL generation and is associated with resistance to T cell checkpoint immunotherapies including anti-CTLA4 and anti-PD-L1 blockade [7,9]. Remarkably, given these essential functions, cDC1s are a rare immune cell type and are especially sparse within the tumor microenvironment [5]. Therefore, strategies that may increase their abundance have been keenly sought for the treatment of human diseases.

One such strategy is administration of a cytokine called *fms*-like tyrosine kinase 3 (Flt3) ligand (FL) [5,10-13], which is essential for steady-state DC development [14,15]. Importantly, supra-physiological levels of FL can promote 'emergency' DC generation (*i.e.* higher numbers of DCs), particularly cDC1s [16,17] that can enhance immunity against cancers [5,13,18] and infections [19-22]. However, the cellular origins for emergency DC generation in response to FL remain largely undefined. The receptor for FL (Flt3) is expressed along the entire DC developmental trajectory from early multipotent HSPCs, committed common DC progenitors (CDPs) to mature DC subsets [23-26], which might imply a critical role of FL in regulating DC development from the earliest haematopoietic developmental stages. However, it was shown that Flt3/FL axis is essential in the regulation of late stage DC development in the periphery [27], but dispensable for the generation and maintenance of early HSPC numbers [27-29]. In contrast, FL-transgenic mice exhibit substantial HSPC amplification [30]. However, this is complicated by the possible compensation from other cytokines for DC development [31]. Therefore, the role of FL, and its cellular target of action in emergency DC development remains to be determined.

Recent single cell transcriptional profiling and lineage tracing studies have highlighted substantial lineage bias or even lineage restriction within individual HSPCs that were previously presumed to be multi- or oligo-potent [32-39]. These findings have revolutionized our understanding regarding the generation of cellular diversity during steady-state haematopoiesis [40,41]. However, there is little insight into whether lineage priming programs are already stably established within HPSCs or can be easily diverted via extrinsic cytokine regulation (i.e. fate plasticity). Currently, there is a paucity of clonal-level information of what accounts for skewing of lineage production during emergency haematopoiesis (e.g. a selective increase in DC numbers after FL stimulation). Several non-mutually exclusive clonal-level explanations regarding selective lineage expansion during emergency haematopoiesis are: 1) emergency stimuli preferentially expand HSPCs already primed to a particular lineage (i.e. enhanced clonal expansion), 2) stimuli recruit otherwise dormant progenitors for expansion towards this particular lineage (i.e. recruitment from dormant progenitors), and/or 3) stimuli divert 'plastic' progenitors away from an alternative fate (i.e. recruitment through lineage divergence). To dissect the contribution from each of the aforementioned scenarios, systematic analysis of changes in lineage fate of HSPCs at the single cell level is required.

In this study, we determine that the majority of early HSPCs actively respond to FL exposure both *in vitro* and *in vivo* by becoming highly proliferative. Surprisingly, when using cellular barcoding to interrogate changes in clonal fate, we do not observe rerouting of HSPCs normally primed to non-DC fate. Instead, we discover that selective increases in clonal expansion of pre-existing HSPCs with DC potential is the major driver of emergency DC generation. Consistent with this model, we demonstrate that HSPCs are heterogeneous in their early response to FL stimulation. In particular, we identify a unique group of hyper-proliferative cells that co-expresses gene signatures of both 'early progenitors' and 'DC progenitors'. We therefore identify the earliest molecular and cellular events in HSPCs after FL exposure, leading to preferential DC production. Our findings provide new insights into the control and regulation of DC fate during emergency haematopoiesis, with significant implications for the understanding of immune response to FL that may underpin optimisation of FL therapy for anti-microbial treatment and immunotherapy.

Results

High levels of FL promote DC generation *in vitro*

Given the controversial role of FL during early haematopoiesis [27-30], we sought to first establish the effect of FL on the promotion of DC proliferation and differentiation from early HSPCs. To this end, we cultured $CD11b^{-}cKit^{+}Sca1^{+}$ progenitors in wells containing either high (2 μg/mL) or low (2 ng/mL) FL concentrations *in vitro* and serially examined wells for the divisional kinetics of cells using Cell Trace Violet (CTV) over time. We observed increased cell division in the presence of high levels of FL as early as day 2, as demonstrated by a clear shift in CTV profiles and gradual enrichment of cells in later divisions (Fig. 1a, b). Importantly, in cultures with high levels of FL, a large proportion of cells remained undifferentiated ($CD11c^{low}$ or $MHCII^{low}$ cells) and progressed through multiple cell divisions (Fig. 1c). This led to highly efficient DC generation in cultures with a high versus low FL concentration (Fig. 1d). These results suggested that high levels of FL play an active role in inducing cell division of early HSPCs to promote expansion of DC *in vitro*.

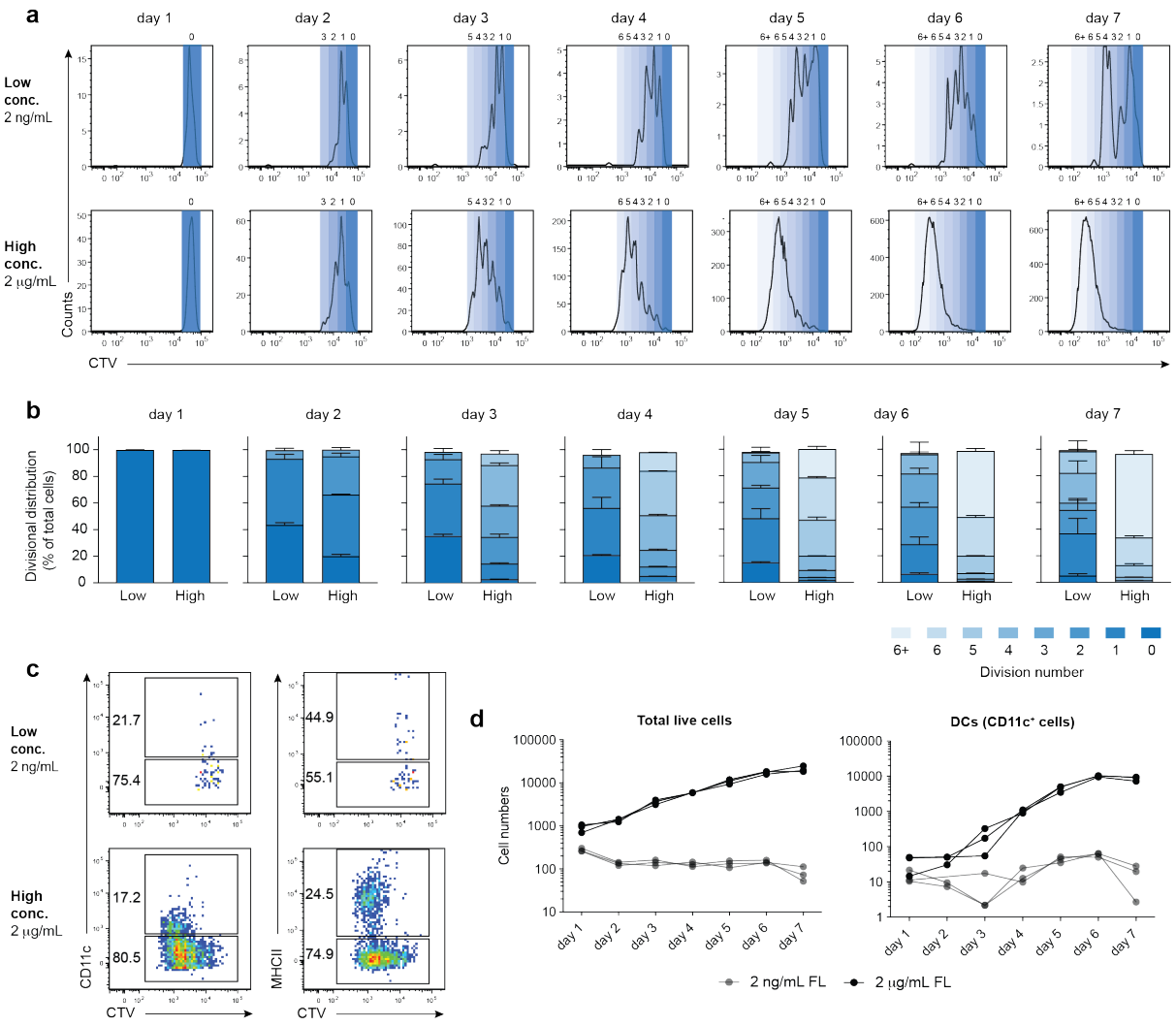

Figure 1. High levels of FL promote enhanced cell division and DC generation *in vitro*.

a-d, CD11b^{-}cKit^{+}Sca1^{+} HSPCs were labelled with CTV and were cultured (~ 1 × 10^3 cells per well) with RPMI supplemented with either high (2 µg/ml) or low (2 ng/ml) concentrations of FL *in vitro.* Cells were serially sampled at each time point from each well (50% of contents) and analysed by flow cytometry daily from days 1-7. **a.** Changes in CTV intensity of total live cells over time. **b.** Stacked histogram showing percentage of cells in each division peak from **a**. **c.** Flow cytometry plots comparing up-regulation of CD11c or MHCII to CTV profiles on day 4. Numbers depict % of cells within the parent gate. **d.** Total inferred number of live cells (left) or DCs (right) in both conditions over time. FACS plots in (**a, c**) show representative plots of one well per condition. Histograms (**b**) show mean ± SEM. Scatter plot (**d**) show individual replicates where lines connect output from the same well serially sampled over time and numbers extrapolated

from the number of prior sampling events; n=3 wells per condition. Data shown are from one representative experiment of two independent experiments.

FL treatment induces emergency DC development from early HSPCs *in vivo*

Next, to examine whether supra-physiological levels of FL can induce emergency DC generation from early HSPCs *in vivo*, $CD11b^{-}cKit^{+}Sca1^{+}$ cells were transplanted into recipient mice receiving daily subcutaneous (s.c.) PBS or FL treatment for 10-12 days, followed by analysis of splenic lineage output two weeks post transplantation. Prior to this study, we optimized our irradiation regimen and determined that use of low dose irradiation (500 RAD) with a 3-day recovery period prior to transplantation allowed sufficient engraftment of donor cells, while minimizing an irradiation-associated cytokine release that can ordinarily mask the effect of exogenous FL. Consistent with prior knowledge[16,17], but now in a transplantation setting, we observed a substantial increase in the number of donor-derived DCs, particularly in the cDC1 subset (~27-fold) (Fig. 2a-d). Conversely, only marginal increases in the number of myeloid (~1.6-fold) and lymphoid (~2-fold) cells were observed (Fig. 2d; Supplementary Fig. 1), indicating that preferential expansion of DCs occurs upon exogenous FL stimulation compared to myeloid and lymphoid lineages.

Next, to determine when FL exerted its greatest influence in increased DC generation during the 12 days administration period, FL was injected daily in different windows of time (days 1-4; 5-8 or 9-12), and DC output was compared to control mice receiving PBS or FL from days 1-12 (Fig. 2e). Importantly, mice receiving FL from days 1-4 had slightly lower but comparable number of DCs (particularly cDC1s) to the positive controls (FL days 1-12), while notably smaller increases in DC generation were observed for mice receiving FL from days 5-8 or days 9-12 (Fig. 2e). These results were consistent with the possibility that FL exposure to a progenitor early in the trajectory of DC development, rather than later, was a major contributor to emergency DC generation.

Taken together, our *in vitro* and *in vivo* findings support a model in which FL stimulation of early HSPCs promotes proliferation and preferential DC lineage formation. This suggests that in addition to the current paradigm of a 'late' effect of FL in DC development [27], FL is also likely to be inducing a response earlier in the hierarchy.

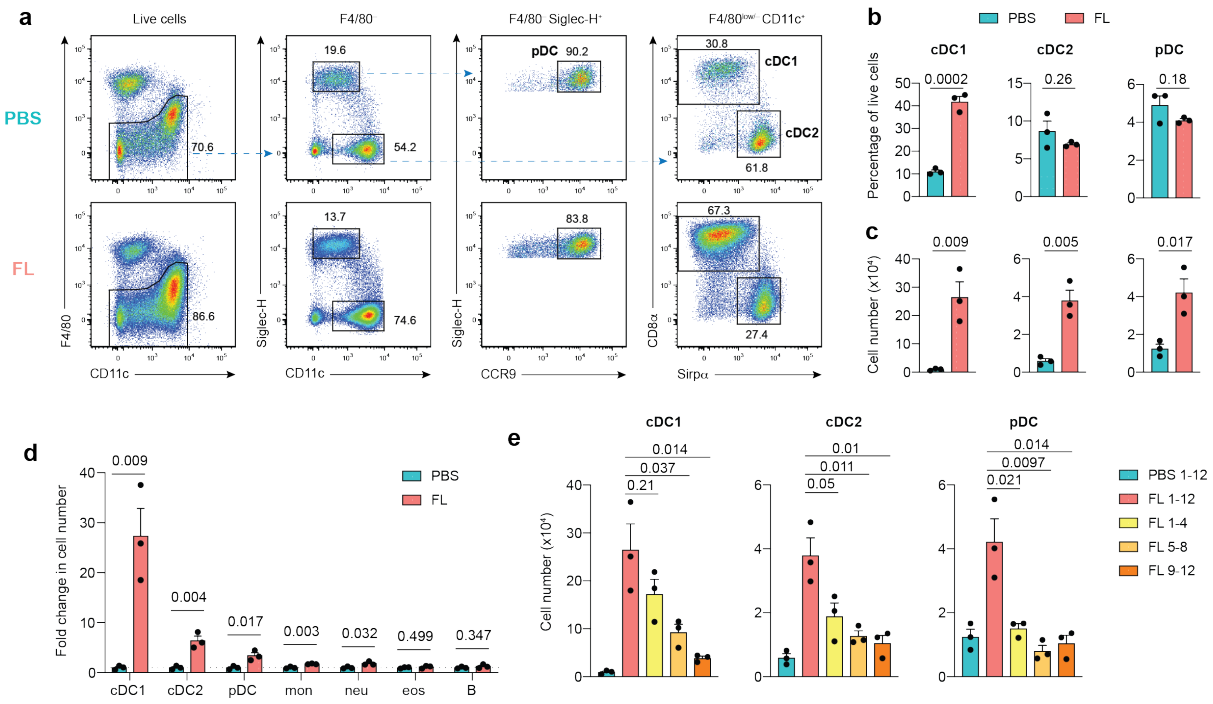

Figure 2. Exogenous FL treatment selectively induces emergency DC development *in vivo*.

a-d, Analysis of splenocytes that received CD11b^{-}cKit^{+}Sca1^{+} HSPCs, followed by daily s.c. injection of PBS or FL for 10-12 days. **a**, Flow-cytometric analysis of DC populations within the CD11c-enriched fraction, with calculation of **b** percentage and **c** numbers of donor-derived DCs. **d,** Fold change in the number of donor-derived cells compared to the average of PBS-treated mice. **e,** Number of donor-derived splenic DC populations from mice receiving daily s.c. injection of PBS from day 1-12 or FL from days 1-12, 1-4, 5-8 or 9-12 two weeks post transplantation of CD11b^{-}cKit^{+}Sca1^{+} HSPCs. All data shown are from one independent experiment, representative of 9 (**a-d**) or 4 (**e**) experimental repeats. Bar graphs (**b-e**) show mean ± SEM. Each point (**b-e**) represents individual biological triplicates. P-values were calculated by an unpaired t test. See Supplementary Fig. 1 for gating strategy for all splenic populations.

Cellular barcoding allows clonal fate tracking during emergency DC development

Having established a model to track emergency DC generation from early HSPCs in a transplantation setting, we next sought to understand the aetiology of this process at a clonal-level. We used cellular barcoding to distinguish the aforementioned clonal scenarios that could explain preferential DC generation, which included 1) enhanced clonal expansion of pre-existing HSPCs; 2) recruitment of dormant HSPCs; and 3) lineage divergence of HSPCs with alternative fates (Fig. 3a). To this end, we tagged individual $CD11b^{-}cKit^{+}Sca1^{+}$ HSPCs with unique and heritable DNA barcodes and transplanted into partially irradiated recipients (500 Rad; day 3 post irradiation), followed by daily s.c. PBS or FL injections for 10 days (Fig. 3b). Two weeks post transplantation, splenic progeny populations were sorted and barcode composition within each population was analysed after barcode PCR amplification and sequencing (Fig. 3b). Comparison of both cell number and barcode number in each population allowed an initial assessment of the proposed clonal scenarios (Fig. 3a): 1) a similar number of DC-generating barcodes (clones) could be indicative of a predominant contribution via enhanced clonal expansion; 2) an increased number of DC-generating barcodes could indicate recruitment of HSPCs; and 3) a corresponding decrease of barcode numbers in another population could indicate lineage divergence of other HSPCs.

Similar to previous results with non-barcoded HSPCs (Fig. 2), emergency DC generation from barcoded HSPCs was observed upon exogenous FL treatment in barcoding experiments (Fig. 3c; Supplementary Fig. 2). When comparing the total number of barcodes detected, we observed little discrepancy between mice receiving PBS or FL treatment (Fig. 3d). This suggested minimal recruitment of HSPCs when exposed to exogenous FL, as we would have anticipated an increase in the number of detectable barcodes in that scenario. Consistently, when comparing the number of barcodes present in each progeny population, we found no significant differences in most populations (Fig. 3e; Supplementary Fig. 2). One exception was a 2-fold increase in the number of barcodes in cDC1s from one independent experiment (Fig. 3e). However, such increase in cDC1-generating clones was less apparent, and not statistically significant in the experimental repeat (Supplementary Fig. 2).

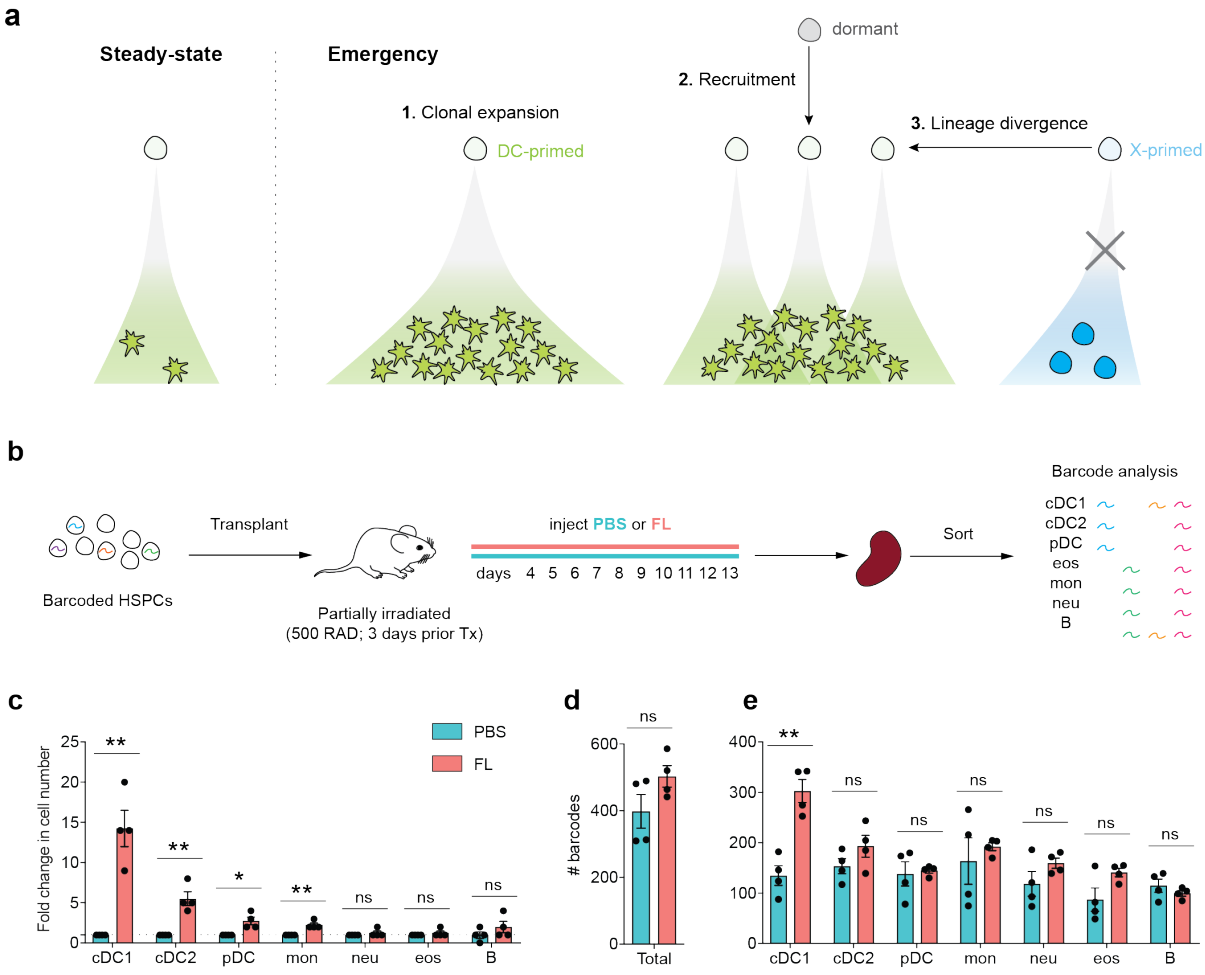

Figure 3. Cellular barcoding for appraisal of emergency DC development at a clonal level.

a. Possible explanations for emergency DC generation at a clonal level: a) enhanced clonal expansion of pre-existing HSPCs; b) recruitment of dormant HSPCs; c) recruitment through lineage divergence of HSPCs primed for other fates. **b.** Experimental set up of cellular barcoding. Barcoded CD45.1^{+}CD11b^{-}cKit^{+}Sca1^{+} HSPCs (5×10^{3}) were transplanted 3 d after sublethal irradiation (500 RAD) of CD45.2 recipient mice, followed by daily PBS or FL administration s.c. from days 4-13. Splenic populations were isolated by FACS on day 14, lysed, and barcodes amplified by PCR, sequenced and analysed. **c.** Fold change in cell numbers of each cell type compared to the average of PBS-treated mice. **d.** Total number of barcodes detected per recipient. **e.** Number of barcodes present in each progeny splenic population. Data shown in (**c-e**) are from one of two independent barcoding experiments. See Supplementary Fig. 2 for data from a repeat experiment. Bar graphs (**c-e**) show mean ± SEM. Each point (**c-e**) represents individual biological

replicate; n=4 mice per condition are shown. P-values are calculated by unpaired t test. ns: no significant differences *P < 0.01, **P < 0.001.

Classification of clones based on distinct lineage output

We next endeavoured to systematically characterize changes in clonal fate, size and distribution of barcode HSPCs between PBS and FL treatments. To achieve this, we first classified barcoded clones based on lineage output as measured by proportional output to different cell types per barcode using a similar approach described previously [39]. We performed t-Distributed Stochastic Neighborhood Embedding (t-SNE)[42] on all barcodes (1595 and 2013 barcodes from PBS and FL, respectively; n = 4 mice per condition) detected from an independent experiment (Fig. 4a). This allowed separation of clones into clusters based on their distinct output to different cell types (Supplementary Fig. 3). To facilitate unbiased classification, we performed DBSCAN clustering[43] on the t-SNE map to identify 20 clusters (Fig. 4a). We generated individual heatmaps showing lineage bias of all barcodes within individual clusters. This analysis demonstrated robust categorization of highly similar clones (Fig. 4b). We then summarized this information by averaging the relative contribution to each cell type from all clones in each cluster and presented the results as a simplified heatmap (Fig. 4c). Consistent with the notion of fate heterogeneity within HSPCs[32-39], we identified large numbers of uni- (clusters 2-5 & 14), bi- (clusters 6-8, 13, 15, 17, 18 & 20) and oligo-potent (clusters 9-12, 16 & 19) clones, indicative of lineage bias within the majority of single HSPCs (Fig. 4b&c). There was also a proportion of multi-potent clones that produced all assessed cell types (cluster 1), which consisted of approximately 5% of total barcodes (Fig. 4b&c).

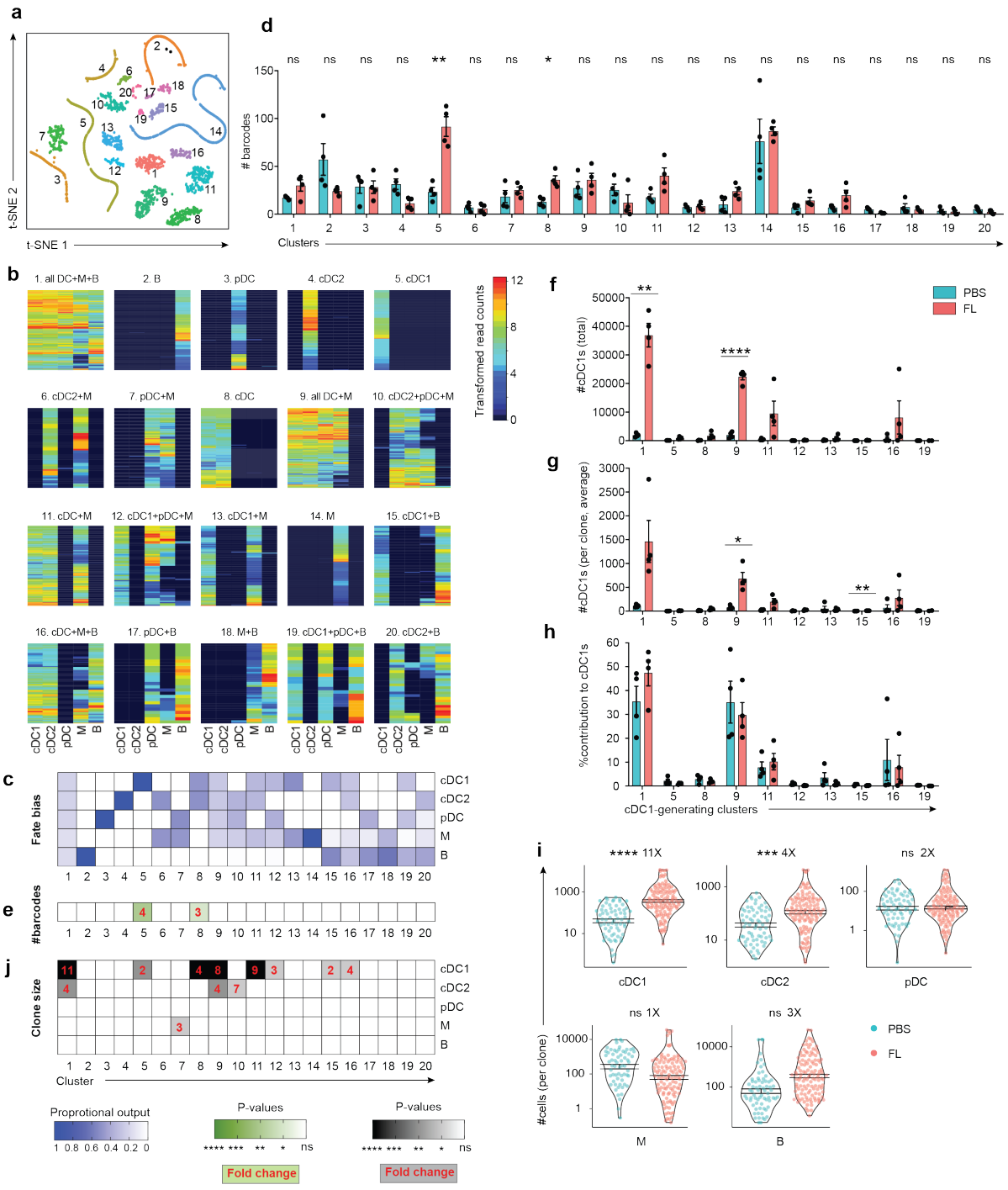

Figure 4. Enhanced clonal expansion drives emergency cDC1 generation.

a. t-SNE plot showing 1595 PBS-treated and 2013 FL-treated barcoded clones. Each point represents one barcoded clone. Color depicts cluster ID identified by DBSCAN clustering. See Supplementary Fig. 3 for related t-SNE plots. **b.** Heatmap representation showing contribution to cell types by individual barcodes within each cluster. **c.** Summary heatmap of data from **b**, showing average proportional output to each cell type by all barcodes within each cluster. **d.** Number of barcodes present in each cluster. **e.** Summary

heatmap showing the comparison of barcode numbers between treatment from each cluster as shown in **d**). Number in each box depicts the fold increase (FL vs average of PBS), and color shading reflects p-value. **f-h.** comparison of PBS- and FL-treated barcoded clones within each cDC1-generating cluster. **f**. Total number of cDC1s. **g.** Average number of cDC1s per clone. **h.** Percentage contribution to cDC1s. **i.** Violin plots showing each clone from Cluster 1, and its numerical contribution to the indicated cell types. Other clusters shown in Supplementary Fig. 4. **j.** Summary heatmap showing of **i** and Supplementary Fig. 4. Number in each box depicts the fold increase (FL vs average of PBS), and color shading reflects p-value. Data shown are the same as in Fig. 3 (i,e, one representative experiment; data from second experiment are shown in Supplementary Fig. 2) for. P-values are calculated by unpaired t test. ns: no significant differences *P < 0.01, **P < 0.001, ***P < 0.0001, ****P < 0.00001.

Minimal contribution to cDC1 generation via emergency recruitment

To quantify any differences in barcode distribution, we compared the number of barcodes present within each cluster from either PBS or FL mice (Fig. 4d & e). We found few differences in most clusters except cluster 5 (cDC1-only) and 8 (cDC1 & cDC2) (Fig 4b-e). Both clusters contained clones that were cDC-restricted, which largely accounted for the increase in the number of cDC1-generating clones from FL-treated mice observed in Fig. 3e. Importantly, we observed no significant reduction in the number of barcodes present in any clusters contributing to myeloid and lymphoid generation (Fig. 4d&e). This suggested the increase in the number of barcodes detected in cDC1s in this experiment (Fig. 3e) was not a result of Flt3-expressing HSPCs being diverted from alternative fates towards cDC1s at high concentrations of FL. Thus, we found no evidence of lineage divergence of HSPCs from alternative fates in response to FL.

To understand whether the bulk of emergency cDC1 generation was derived from these putative 'recruited' cDC-restricted clones, or from HSPCs with other fate potentials, we examined the numerical cDC1 output from all cDC1-generating HSPC clusters (Fig. 4f-h). Surprisingly, the number of cDC1s generated from 'recruited' DC-restricted clusters (5 & 8) was extremely small, and together only contributed to approximately 5% and 3% of cDC1s in PBS and FL conditions, respectively (Fig. 4f-h). Instead, the majority of cDC1 output was derived from the few multi-/oligo-potent clusters (1, 9, 11 & 16) in both PBS (~90% of cDC1s) and FL (~95% of cDC1s) conditions. Together, these results demonstrated minimal contribution to emergency cDC1 development from recruitment of HSPCs upon FL treatment, and maximal contribution from multi-/oligo-potent HSPCs.

Enhanced clonal expansion drives emergency cDC1 generation

Next, we systematically interrogated the changes in clone size within each cluster of HSPCs and their contribution to each lineage, in addition to cDC1 output. The results are presented as an array of violin plots showing individual clones within each cluster (Fig. 4i; Supplementary Fig. 4). Statistical tests (unpaired t-test) and fold changes were computed on clone size per cell type between PBS and FL treatment and presented on each violin plots (Fig. 4i; Supplementary Fig. 4), and this information was also summarized as a simplified heatmap (Fig. 4j; Supplementary Fig. 4).

Importantly, we observed increases in the number of cDC1s produced per clone from all cDC1-generating clusters (8 out of 10 clusters displayed statistically significant differences), indicative of globally enhanced clonal cDC1 production from barcoded HSPCs (Fig. 4j; Supplementary Fig. 4). The average fold increase in clonal cDC1 size was greater in the major cDC1-contributing clusters (e.g. 11-fold increase in cluster 1 containing multi-potent clones) compared to the smaller contributors (e.g. 2-fold increase in cluster 5 containing cDC1-restricted clones) (Fig. 4j). Interestingly, within the multi-/oligo-potent clusters, the generation of other cell types (non-cDC1s) did not increase to the same extent as cDC1s (Fig. 4j). This suggested exogenous FL stimulation can promote enhanced DC generation from all HSPC clones that have potential to make DCs, in particular from the cDC1-producing sub-branch of multi-/oligo-potent clones. This is despite all HSPCs for the lineages tested in this study either expressing surface Flt3 at the time of barcoding and transplantation, or upregulating it upon differentiation from an $Flt3^-$ stage [44,45].

Together, cellular barcoding allowed systematic characterization of clonal fate and size and revealed enhanced clonal expansion of pre-existing cDC1-producing clones as the major contributor to FL-mediated emergency cDC1 development. This was consistent with our *in vitro* results, where we demonstrated increased cell division and proliferation in early HPSCs in response to high concentrations of FL, leading to more efficient generation of DCs (Fig. 1).

Multi-omics profiling of early cellular and molecular events in single HSPCs

One common limitation of our *in vivo* and *in vitro* studies was the inability to assay steady-state controls, given *in vitro* controls were exposed to low concentrations of FL and *in vivo* PBS treated controls were exposed to low dose irradiation (required for engraftment and expansion of barcoded HSPCs). Therefore, to extend our findings in a more physiologically relevant context, and to directly interrogate the earliest cellular and molecular events within individual HSPCs during FL-mediated emergency haematopoiesis, we developed a single cell multi-omics profiling approach using non-irradiated recipients to assess clonal fate dynamics *in vivo* with and without FL treatment.

Briefly, $CD11b^{-}cKit^{+}Sca1^{+}$ early HSPCs were CTV-labelled and transplanted into recipients (non-irradiated) followed by daily s.c. PBS or FL injection for three days (Fig. 5a). At this time, bone marrow (BM) cells was harvested and stained for various surface markers, and single donor-derived cells (Supplementary Fig. 5) were index sorted into wells of 384-well plates containing pre-aliquoted CEL-Seq2 primer mix for later processing (Fig. 5a). Although a very low number of donor-derived cells was expected at this early time point after transplantation into non-irradiated recipients, we were able to sort 376 cells from each condition (from 2 mice per group), and profiled 248 PBS-treated and 276 FL-treated cells that passed additional FACS pre-gating (Supplementary Fig. 5) and quality control (Methods). This single cell multi-omics approach allowed simultaneous detection of surface marker phenotype, division history and the transcriptome of single rare HSPCs treated with PBS or FL following transfer into non-irradiated recipients.

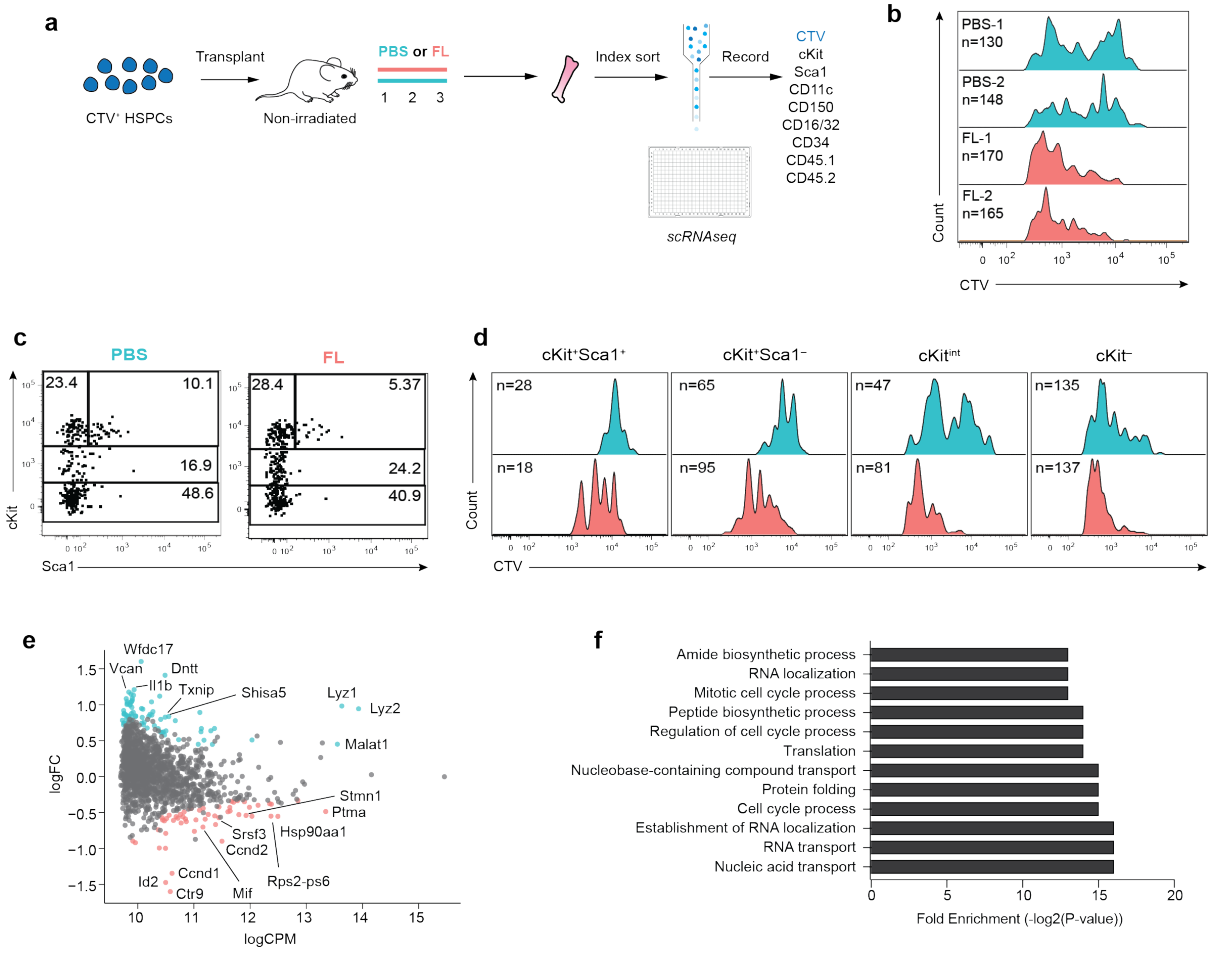

Figure 5. Exogenous FL treatment promotes cell division of early HSPCs.

a. Schematic of the single cell multi-omics profiling experiment set up. CD45.1^{+}CD11b^{-} cKit^{+}Sca1^{+} HSPCs were CTV-labelled and transplanted into non-irradiated CD45.2 recipient mice, followed by daily PBS or FL administration s.c. from days 1-3. BM was harvested on day 4, and stained for the indicated antibodies. Donor-derived cells were indexed sorted (See Supplementary Fig. 5 for gating strategy) for scRNAseq. **b.** CTV profiles of donor-derived cells from individual mice receiving PBS (2 mice) or FL (2 mice); n: number of cells. **c.** Comparison of cKit and Sca1 expression; numbers inside box depict % cells. **d.** CTV profiles of cells from PBS and FL condition within each gate based on cKit and Sca1 expression; n: number of cells. **e.** MD plot comparing differential gene expression between cells derived from PBS vs FL treatment; top DE genes (FDR<0.01) are color either blue (up in PBS) or red (up in FL); the top 10 DE genes are labelled. Supplementary file 1 contains interactive plot of all 1479 genes that passed QC (Methods). **f.** Top 12 enriched GO term biological processes in FL condition.

FL treatment promotes hyper-proliferation of early progenitors

Consistent with the *in vitro* division tracking results (Fig. 1), a clear shift in CTV profiles was observed in cells treated with FL *in vivo* for three days, indicating enhanced cell division of most HSPCs (Fig. 5b). Importantly, increased cell proliferation was not only present in downstream DC progenitors, but was also evident in all FL-treated HSPCs ranging from early to late stages of development, as defined by differential cKit and Sca1 expression (Fig. 5c, d). Thus, these results directly demonstrated an active response to FL stimulation from cells residing in the earliest phenotypic HSPC compartment ($cKit^+Sca1^+$) during FL-induced emergency haematopoiesis.

Similarly, enhanced cell cycle activities were evident at the transcriptomic level (Fig. 5e, f). Differential gene expression (DGE) analysis between PBS- and FL-treated cells revealed up-regulation of large numbers of cell cycle genes, including RNA polymerase-associated protein homologs (e.g. *Ctr9*) and regulators of cyclin-dependent kinases (e.g. *Ccnd1* & *Ccnd2*) (Fig. 5e; Supplementary File. 1 for full list of genes). Interestingly, several of these cell cycle genes were identified to be uniquely expressed in DCs compared to other haematopoietic lineages (e.g. *Ccnd1)*. In addition, upregulation of genes regulating cDC1 fate (e.g. *Id2*), and downregulation of genes characteristic of lymphoid and myeloid fate (e.g. *Dntt, Lyz1, Lyz2*) were identified in FL exposed donor HSPCs. Consistent with this, gene ontology (GO) term analysis highlighted enrichment of cell cycle related biological processes in FL condition (Fig. 5f). Together, these *in vivo* CTV and single cell transcriptomic results demonstrated a distinct early gene expression program change in early HSPCs that were directly responding to exogenous FL stimulation, leading to enhanced cell division and proliferation as well as upregulation of genes associated with cDC1 fate. These observations were consistent with our observation in *in vitro* division tracking (Fig. 1) and barcoded HSPC transplantation assays (Fig. 4).

Selective pattern in progenitor responses to FL stimulation

While we observed a clear global enrichment of cell cycle genes in FL-treated HSPCs, it remained unclear whether hyper-proliferation occurred equally in all cells. To investigate whether FL preferentially stimulated subsets of HSPCs, we first annotated cells into clusters using SC3 clustering[46] based on single cell transcriptomes from all cells in the

experiment (Fig. 6a). We then overlayed and examined other available meta-data for each cell including experimental treatment, CTV intensity, and surface marker expression. This permitted a comprehensive assessment of cellular and molecular properties and heterogeneity across the treatment groups (Fig. 6a, b).

To date, despite many studies investigating HSPC heterogeneity by scRNA-seq, no ground truth reference exists for cell type annotation. Therefore, to assist in cell type identification to a best approximation, we computed similarity scores for single cells by comparing their RNA profiles to gene signatures of bulk RNA-seq of known populations using SingleR[47]. We first compared our single cell data set to all lineages (Supplementary Fig. 6) and sub-selected populations with the closest relationship to clusters in our data (Fig. 6a, c). Using this approach, we were able to clearly distinguish clusters 1-6 from clusters 7-10 with regard to their differentiation potential (Fig. 6a-c). Clusters 7-10 consistently expressed higher levels of HSPC markers, particularly cKit and CD34 (Fig. 6b), and were transcriptionally similar to multipotent progenitors (MPPs) (Fig. 6c). Therefore, these cells likely represented progenitors at early developmental stages. In contrast, clusters 1-6 exhibited few progenitor characteristics and higher degrees of lineage commitment. For example, clusters 1 and 5 expressed high levels of CD16/32 and were transcriptionally similar monocytes and neutrophils, respectively.

Importantly, when comparing division histories of PBS- and FL-treated cells within each cluster, some but not all clusters exhibited significant differences in CTV profiles (Fig. 6d). In particular, cells along the DC developmental trajectory underwent more divisions with FL stimulation. This included cells that were transcriptionally similar to mature DCs (clusters 2-4), CDPs (clusters 3, 6, 8 & 9) or MPPs (clusters 7-10) (Fig. 6c&d). Conversely, cells that exhibited little to no DC or progenitor signatures at this time point, including those with strong monocyte (cluster 1) or neutrophil priming (cluster 5), appeared to divide at a similar rate under both conditions (Fig. 6c&d). Thus, these results demonstrated a selective pattern in how single HSPCs respond to exogenous FL stimulation that reflected DC lineage specification.

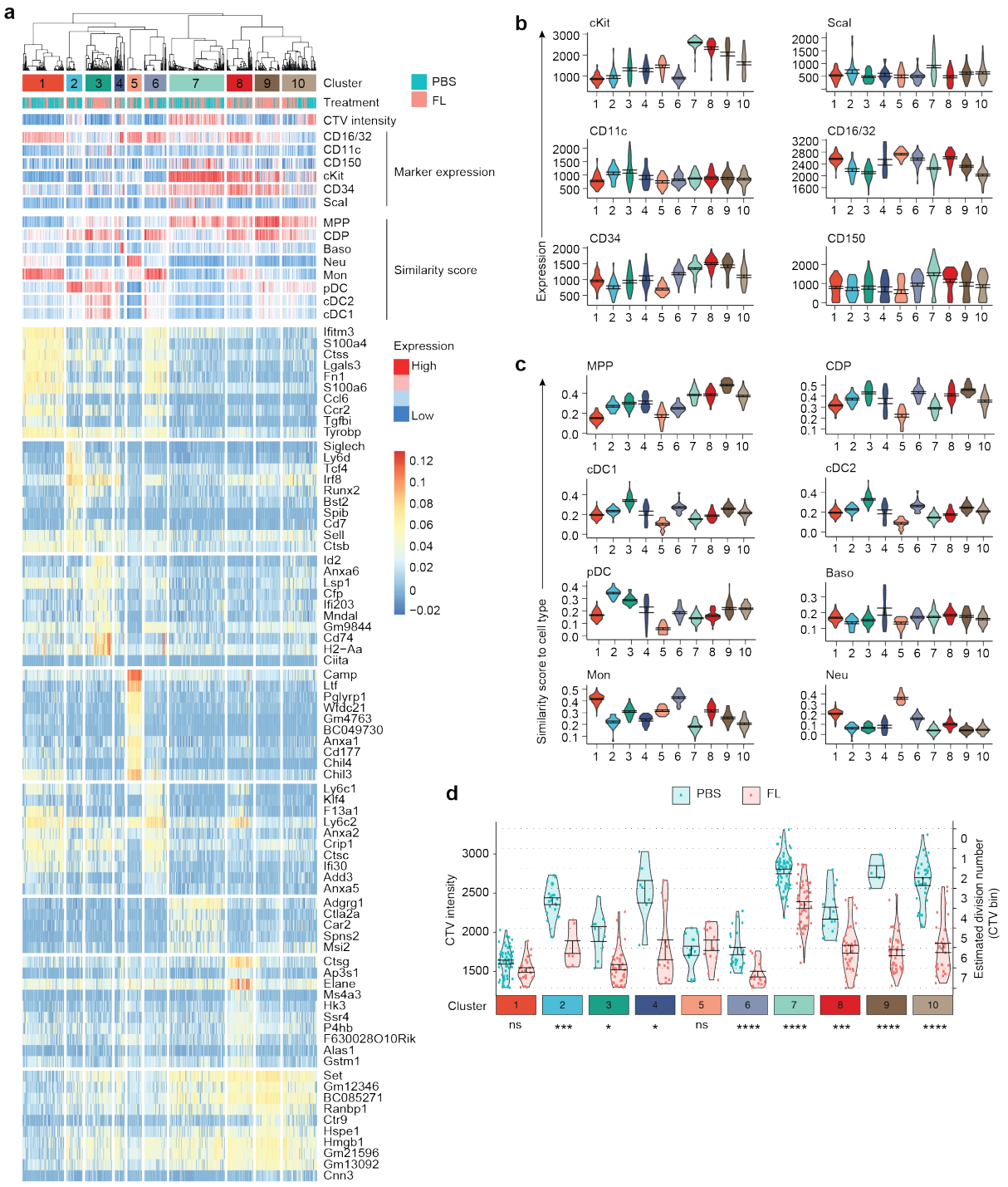

Figure 6. Cell type classification and annotation.

a. Heatmap representation of 524 single cells (in columns) after QC (Methods). Each cells are annotated with the following information: 1) cluster ID identified by SC3 clustering; 2) treatment; 3) CTV intensity; 4) surface marker expression; 5) similarity score to a selection of known cell types (computed using SingleR, see Supplementary Fig. 6 for a list of 120 cell types); and 6) highly expressed genes in each SC3 cluster. Violin plots are

generated for each cluster showing expression levels of surface markers by FACS in **b**, SingleR similarity scores to each cell type in **c**, and division number of cells (dots) estimated by CTV intensity, separated by treatment group in **d**. Bars indicate mean ± SEM in violin plots. Significance in **d** is calculated by the unpaired t test. ns: no significant differences, *P < 0.01, **P < 0.001, ***P < 0.0001, ****P < 0.00001.

Early emergence of DC-primed progenitors

Interestingly, we observed substantial over-representation of FL-treated cells in cluster 3 (83%) and cluster 9 (89%) (Fig. 7a), both appeared to correspond to progenitors along the DC trajectory. Cluster 3 likely represented a mid- to late-stage cDC progenitor population based on several observations. First, a proportion of cells had already up-regulated surface expression of CD11c, indicative of DC differentiation (Fig. 7b). Second, most cells expressed high levels of classical cDC genes such as *H2-Aa*, *Cd74* and *Id2*, and relatively low level of pDC genes such as *Tcf4* (Fig. 7c). In addition, cells were transcriptionally similar to CDPs and cDCs (Fig. 6c). Importantly, FL-treated cells within cluster 3 were found to have divided more than those with PBS treatment (Fig. 6d), suggesting the early emergence of these late-stage cDC precursors was partly driven by the increased proliferation from parental HSPCs upon FL stimulation.

Cells in cluster 9 also seemed to exhibit apparent DC lineage priming as indicated by their transcriptional similarity to CDPs (Fig. 6c), and relatively high levels of known DC lineage priming genes including *Irf8*, *Nfkbia* and *Tcf4* (Fig. 7c). However, in contrast to cluster 3, cells in cluster 9 appeared to be more 'stem'-like and hyper-proliferative, as evidenced by their higher expression of HSPC markers including cKit and CD34 (Fig. 7b), their transcriptional similarity to MPPs (Fig. 6c), and their high levels of genes associated with proliferation including *Set*, *Tuba1b* and *Stmn1*, even when compared to progenitors in clusters 7, 8 & 10 (Fig. 7d; Supplementary File. 2). Additionally, FL-treated cells in cluster 9 had the most dramatic change in cell division history compared to their PBS-treated counterparts (Fig. 6d; average 5-6 divisions in FL compared to 2 divisions in PBS). Therefore, cluster 9 likely represented a unique group of hyper-proliferative early progenitors that were also primed for DC fate, which emerge only in response to supra-physiological amounts of FL stimulation.

Next, we interrogated the relationship between divisional histories of cells and their MPP or CDP signatures (Fig. 7e-g). Whereas most PBS-treated cells rapidly down-regulated an MPP signature with cell division, large numbers of FL-treated cells were able to maintain an MPP-like state (Fig. 7e), likely reflecting their capacity for enhanced proliferation and self-renewal. Similarly, up-regulation of a CDP signature in FL-treated cells appeared to associate with greater numbers of cell divisions (Fig. 7f). Interestingly,

when cells from cluster 3 or 9 were superimposed, we observed co-localization of these cells in the FL-enriched regions (Fig. 7e&f; $MPP^{-}CTV^{-}$ or $CDP^{+}CTV^{-}$). In particular, cluster 9 represented a small but unique group of cells that were highly similar to both CDPs and MPPs (Fig. 7g). These results suggested that FL stimulation induced a unique molecular state featuring hyper-proliferation, maintenance of an MPP-like state, and DC-priming in subsets of HSPCs during the early phase of emergency DC development.

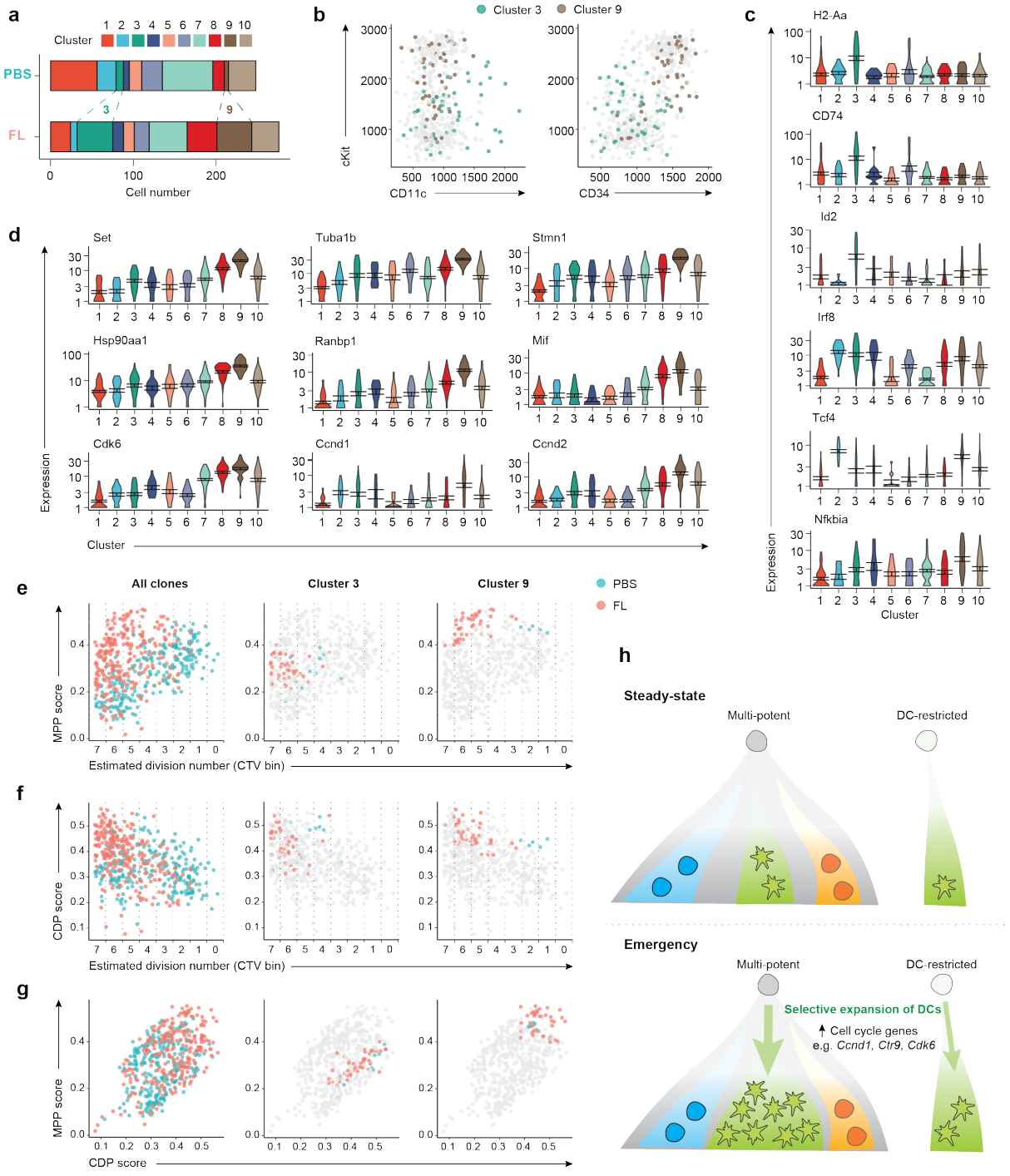

Figure 7. Selective hyper-proliferation of DC-primed progenitors.

a. Number of cells in each cluster from PBS or FL condition. Lines highlight enrichment of FL-treated cells in clusters 3 and 9. **b.** Flow cytometric plots showing cells from clusters 3, 9 or all other cells (grey), comparing cKit vs CD11c expression (left) or cKit vs CD34 expression (right). Violin plots showing expression levels of signature DC genes in **c** and cell cycle genes in **d** in each cluster (see Supplementary file 2 for interactive plots of all genes per cluster). Scatter plots showing all single cells comparing division

number (CTV intensity, x-axis) with SingleR similarity scores (y-axis) for MPPs in **e** and CDPs in **f**. **g.** Scatter plot of cells according to their SingleR similarity score for CDPs vs MPPs. Each dot represents a single cell, and color depicts treatment. **h.** Summary schematic showing selective clonal expansion of DCs as the major driver of FL-mediated emergency DC generation.

Discussion

In this study, we interrogate the clonal aetiology of FL-mediated emergency DC development at a multi-omics level. We profile changes during the early phase of this response and demonstrate a profound yet selective effect in HSPC proliferation. Our results reveal three key events occur within selective subsets of HSPCs in response to FL stimulation. These include 1) increased cell division and proliferation; 2) maintenance of a progenitor-like gene signature across multiple divisions; and 3) establishment of DC lineage program in early HSPCs. These findings are highly consistent with our clonal fate tracking results using cellular barcoding, where selective clonal expansion of HSPCs with pre-existing DC potential are demonstrated to be the major driver of FL-mediated emergency DC development (Fig. 7h).

Our findings provide important insights into the regulation of clonal fate via extrinsic cytokine signals, which has been a central debate in haematopoiesis, where two non-mutually exclusive models have been proposed [48]. In a 'permissive' model, cytokines mainly act as survival and/or proliferation factors that allow selective expansion of HSPCs that are already lineage committed. Conversely, an 'instructive' model implies an active role of cytokines in dictating lineage choices within single multi-potential HSPCs by inducing lineage-specific transcriptional programs with/without inhibition of alternative fate programs. The latter is demonstrated by several landmark studies using continuous live cell imaging to track the output of individual HSPCs with exposure to different stimuli [49-51]. While these studies clearly show that cytokines can instruct lineage choice in single HSPCs, whether cytokine instruction represents the major source of fate determination in other models remains to be determined.

In our model, exogenous FL does not seem to instruct DC development from HSPCs that are not DC-primed, but only affects those that already have pre-established DC potential. Our findings fit with a model where FL stimulation predominantly plays a 'permissive', but not an 'instructive' role in guiding emergency DC generation at a clonal level. However, it is important to note that the majority of DCs are produced by HSPCs that have multi-lineage potential, rather than those with DC-restricted output. Furthermore, although FL stimulation fails to switch HSPCs with alternative fates towards a DC fate, it can preferentially guide enhanced DC generation from multipotent HSPCs, without

inhibiting the development of myeloid or lymphoid lineages from the same clones (Fig. 7h). Therefore, one could argue that FL stimulation does not 'instruct' the establishment of DC fate, but can 'tune' preferential DC production from multipotent HSPC clones through a unique gene program that interleaves DC lineage priming with enhanced cell division. Together, these results suggest that once HSPCs establish a lineage program, it is relatively stable and cannot be easily switched by exogenous FL stimulation.

Whether FL is actively involved in the regulation of early DC development is controversial [27,29,30], where the major action of FL is presumed to be at the late stages of DC development. Here, we provide evidence of an active and possibly predominant contribution from early HSPCs to emergency DC generation in response to supra-physiological levels of FL. Our findings are in agreement with the prior observation that FL overexpression drastically increases HSPC numbers [30], but do not exclude the previously described role for FL in expanding committed DC progenitors and mature DCs [27]. In particular, HSPCs that respond to FL will eventually differentiate into CDPs, pre-DCs and DCs, where FL may certainly additionally contribute to the overall clonal expansion observed from barcoded HSPCs. Collectively, these findings significantly enhance our understanding of the clonal level control of HSPC fate, with implications for the maintenance or manipulation of DC numbers in health and disease.

Methods

Mice

All mice were bred and maintained under specific pathogen-free conditions at WEHI, according to institutional guidelines. CD45.2 (C57BL/6) and CD45.1 (C57BL/6 Pep^{3b}) male mice aged between 8-16 weeks were used. In most transplantation experiments, CD45.1 mice were used as donor and CD45.2 mice were used as recipients. In a few other experiments, CD45.2 mice were used as donor and CD45.1mice were used as recipients.

Transplantation

Recipient mice were either not irradiated or sub-lethally irradiated (500RAD) three days prior to transplantation. Transplantation was performed by intravenously injection of cells resuspended in PBS (FBS free).

Cytokine Injection

PBS or FL (BioXcell) was injected subcutaneous daily for 3-12 days as indicated. FL was resuspended in PBS and injection was performed at 10 μg/mouse per day.

Tissue Preparation and Flow cytometry

Bone marrow cells from hip, tibia and femur were collected by flushing with FACS buffer (PBS containing 0.5% FBS and 2 mM EDTA) through a 22-gauge needle. Spleens were mashed with FACS buffer through 70 μm cell strainers with 3 ml syringe plungers. Red blood cells were lysed by incubating with Red Cell Removal Buffer (RCRB, generated in-house) for 1– 2 minutes, followed by washing and resuspension with FACS buffer. Cells were stained with antibodies of interest at 4 ºC for at least 30 minutes. Secondary antibody staining and/or Magnetic-Activated Cell Sorting (MACS) enrichment was performed as indicated, according to manufacturer's protocol (Miltenyl Biotec). Propidium iodide (PI) was added to exclude dead cells prior to flow cytometry analysis or sorting. Flow cytometry analysis was performed on a BD Fortessa X20 (BD Biosciences). Cell sorting was performed on a BD Influx, BD Fusion or BD FACSAria-II/III (BD Biosciences). Cell numbers were quantified by adding a known number of counting beads (BD Biosciences) and gated based on low forward scatter and side scatter using flow cytometry. The percentage of beads recorded was then used to estimate the

percentage of cells recorded over the total number of cells. Data analysis was performed using FlowJo 9.9.6 (Treestar) or R with data exported using FlowJo 9.9.6.

For the identification of progenitor cells, BM cells were first stained with cKit-APC antibodies and MACS enriched for cKit$^+$ cells using anti-APC magnetic beads. The cKit-enriched fraction was then stained with Sca1 and CD11b antibodies. HSPCs were defined as CD11b$^-$cKit$^+$Sca1$^+$ cells.

For the identification of mature splenic DC, myeloid and lymphoid cell types, splenocytes were first stained with CD11c-APC and/or Siglec-H-PE, followed by MACS enrichment using anti-APC and/or anti-PE beads (CD11c$^+$ and/or Siglec-H$^+$ as the DC-enriched fraction; flow through as myeloid/lymphoid (M/L) -enriched fraction). Populations were defined as the following: cDC1s (F4/80$^{low/-}$Siglec-H$^-$CD11c$^+$CD8α$^+$Sirpα$^-$), cDC2s (F4/80$^{low/-}$Siglec-H$^-$CD11c$^+$ CD8α$^-$Sirpα$^+$) and pDCs (F4/80$^{low/-}$Siglec-H$^+$CCR9$^+$CD11c^{int}) from the DC-enriched fraction. B cells (CD11c$^-$Siglec-H$^-$CD11b$^-$ CD4/8α$^-$CD19$^+$), T cells (CD11c$^-$Siglec-H$^-$CD11b$^-$CD4/8α$^+$CD19$^-$), eosinophils (eos, CD11c$^-$Siglec-H$^-$CD11b$^+$Siglec-F$^+$SSA^{hi}), monocytes (mon, CD11c$^-$Siglec-H$^-$ CD11b$^+$Siglec-F$^-$Gr-1^{int}F4/80^{int}) and neutrophils (neu, CD11c$^-$Siglec-H$^-$CD11b$^+$Siglec-F$^-$Gr-1$^+$F4/80$^-$) from the M/L-enriched fraction. CD45.1 and CD45.2 antibodies were used to distinguish donor-derived vs host-derived cells within each population. The gating strategy of splenic populations is shown in Supplementary Fig. 1.

For index sorting of donor-derived cells in the multi-omics experiment, BM cells were stained with antibodies against cKit, Sca1, Flt3, CD150, CD16/32, CD34, CD11c, CD45.1 and CD45.2. Viable CTV$^+$ cells were index sorted into wells of 384-well plates containing pre-aliquoted Cel-Seq2 reagents. After sorting, potential dead or contaminating endogenous cells were excluded *in silico* using FlowJo 9.9.6 (Treestar) based on stringent FCS, SSC, PI and CD45.1 (donor marker) profile for downstream analysis. 613 out of 748 cells were kept and exported for downstream analysis. See Supplementary Fig. 5 for gating strategy.

CTV Labelling

CTV labelling of cells was performed using the CellTrace Violet Cell Proliferation Kit (ThermoFisher) according to the manufacturer's instructions, with minor adaptation. First, 5 mM CTV stock solution was freshly prepared by dissolving the CTV powder in a single supplied tube with 20 μL of DMSO. To minimize toxicity and cell death, the stock CTV solution was diluted 1 in 10 using PBS. Cells were washed in PBS to remove any residual FBS from previous preparation and resuspended in 500 μL of PBS. Next, 5 μL of diluted CTV solution (500μM) was added to the cell suspension and vortexed immediately. The cell suspension was wrapped in foil to avoid contact with light and incubated at 37 ºC for 20 minutes. A large volume of cold FBS-containing buffer (10% FBS in PBS) was added to the cells and the cell suspension was incubated on ice for 5 minutes before centrifugation. Cells were washed and resuspended in PBS for transplantation, or in medium for DC culture.

Cell culture

Purified HSPCs ($CD11b^{-}cKit^{+}Sca1^{+}$ cells) were labelled with CTV and cultured in RPMI 1640 media (Life Technologies) with freshly added FL (BioXcell) at a final concentration of either 2 μg/mL or 2 ng/mL. Cells were harvested and analysed by flow cytometry at the time points as indicated.

Barcode transduction

Barcode transduction was performed as described [34]. Freshly isolated HSPCs were resuspended in StemSpan medium (Stem Cell Technologies) supplemented with 50 ng/mL stem cell factor (SCF; generated in-house by Dr Jian-Guo Zhang) and transferred to a 96-well round bottom plate at less than 1×10^5 cells/well. Small amount of lentivirus containing the barcode library (pre-determined to give 10-20% transduction efficiency) was added and the plate was centrifuged at 900 g for 90 minutes at 22 °C prior to incubation at 37 °C and 5% CO_2 for 4.5 or 14.5 hours. After incubation, cells were extensively washed using a large volume of FBS-containing buffer (10% FBS in PBS or RPMI) to remove residual viruses. Cells were then washed once using PBS to remove FBS. Cells were resuspended in PBS and transplanted into recipient mice via intravenous injection.

Barcode amplification and sequencing

PCR and sequencing were performed as described previously [34]. Briefly, sorted populations were lysed in 40 μl lysis buffer (Viagen) containing 0.5 mg/ml Proteinase K (Invitrogen) and split into technical replicates. Barcodes in cell lysate were then amplified following two rounds of PCRs. The first PCR amplified barcode DNA using common primers including the TopLiB (5' – TGC TGC CGT CAA CTA GAA CA – 3') and BotLiB (5' – GAT CTC GAATCA GGC GCT TA – 3'). The second PCR introduced an 82-bp well-specific 5' end forward index primer (384 in total) and an 86-bp plate-specific 3' reverse index primer (8 in total) to each sample for later de-multiplexing *in silico*. The sequences of these index primers are available upon request. Products from second round PCR with index primers were run on a 2% agarose gel to confirm a PCR product was generated, prior to being cleaned with size selected beads (NucleoMag NGS) according to the manufacturer's protocol. The cleaned PCR products were pooled and deep sequencing was performed on the Illumina MiSeq or NextSeq platform.

Barcode data processing and quality control (QC)

Processing of barcode data was performed as previously described [34,39], which involved the following steps: 1) number of reads per barcode from individual samples was mapped to the reference barcode library (available upon request) and counted using the *processAmplicons* function from edgeR package [52,53]; 2) samples with total barcode read counts of less than 10^4 was removed; 3) Pearson correlation between technical replicates from the same population was calculated and samples with coefficient of less than 0.6 were removed; 4) read counts were set to zero for barcodes with reads in one but not the other technical replicates; 5) read counts of each barcodes from technical replicates were averaged; 6) total read counts per sample was normalized to 10^6; 7) read counts per sample was transformed using hyperbolic arsine transformation.

Barcode data analysis

Barcodes from all biological replicates (regardless of PBS or FL treatment) within a single independent experiment were pool and analysed. Two independent experiments that passed all technical control criteria, including sufficient donor cell engraftment and optimal barcode transduction rate (5-20%), were presented. Detailed results from the first experiment were presented in Fig. 3&4 and Supplementary Fig. 3&4. Summary results from the second experiment were presented in Supplementary Fig. 2.

After QC, t-SNE[42] was performed using the resulting normalized and transformed barcode read counts (i.e. proportional output to cell type per barcode) to visualize lineage bias of individual barcodes at two-dimension. Next, DBSCAN clustering [43] was performed using the resulting tSNE coordinates to classify barcodes. Heatmaps were generated to visualize lineage output of barcodes identified in each cluster. Barcode numbers present in each biological replicate within each cluster were counted and compared between PBS and FL treatment. Clone size (number of cells generated per cell type per barcode) was calculated based on estimated cell numbers at the population level (based on % recovery of counted beads) and proportional output to cell type per barcode (normalized and transformed barcode read counts).

scRNA-seq using CEL-Seq2

scRNA-seq library was generated using an adapted CEL-Seq2 protocol [54]. Briefly, cells were lysed in 0.2% Triton-X and first strand cDNA were generated. All samples were then pooled and treated with Exonuclease 1, followed by second strand DNA synthesis (NEB), *In vitro* transcription, RNA fragmentation, reverse transcription and library amplification. Library was then size selected using 0.8x followed by 0.9x ratio of sample to beads (NucleoMag NGS) according to the manufacturer's protocol. The amount and quality of the library was checked on Tapestation (Agilent Technologies) using a high sensitivity D5000 tape (Agilent Technologies) before sequencing on the Illumina NextSeq high output (14bp read 1, 72 bp read 2 and 6bp index read).

scRNA-seq data processing and QC

First, reads from individual sorted plate were mapped to the GRCm38 mouse genome using the Subread aligner [55] and assigned to genes using the scPipe package [56] with ENSEMBL v86 annotation. Next, QC was performed using the *detect_outlier* function in scPipe to remove low quality cells. Genes with rare representation were removed next, which included those with average read count less than one and those detected in less than three cells. The top 3000 most variable genes were then selected from each plate of single cells. After these filtering steps, the gene count matrix was combined with indexed sorted information, followed by pooling of data from different sorted plates. 1596 common genes were found between the two plates and were kept for downstream analysis. Mutual nearest neighbors correction (*mnnCorrect* function) from the scran

package [57] was applied to correct for batch effects between plates. Together, these QC steps resulted in the generation of a final single cell dataset of 524 cells (248 from PBS and 276 from FL condition), which contained expression values of CTV, six surface markers and 1596 genes.

scRNA-seq data analysis

Differential gene expression (DGE) analysis was performed using edgeR (*estimateDisp*, *glmFit*, *glmLRT* and use FDR to adjust P-value) [58]. Mean-Difference (MD) plot was generated using the Glimma package [59] for exploration and visualization (See Supplementary file 1 and 2). GO term pathway analysis was performed using the topGO package [60]. SC3 clustering [46] of scRNA-seq data was performed to identify major groups of cells. To facilitate cell type annotation, SingleR was performed using scRNA-seq to compared similarity of each single cell to referenced population-based RNA-seq data [47]. CTV intensity and surface marker expression values were overlayed on the corresponding single cells for cross comparison. CTV bins were calculated by equally fractionate CTV values into eight bins to estimate division numbers of cells (division 0 to 6+).

Statistical analysis

Statistical analysis was performed in Prism (GraphPad) or R. Unpaired Student's t test was performed as indicated in text. Mean ± Standard Error of Mean (SEM) is shown. P-values are reported as the following; ns: P-value >0.01; *: P-value < 0.01; **: P-value < 0.001; ***: P-value < 0.0001; ****: P-value < 0.00001.

Data and code availability

The scRNA-seq data, barcoding data and codes used in all analysis shown in this study are available upon request.

Acknowledgements

We thank the Walter and Eliza Hall Bioservices, FACS laboratory, Dr. Stephen Wilcox and Dr. Susanne Heinzel for technical support. We thank Prof. Stephen Nutt and Dr Ashley Ng for insightful discussions and critical feedback on the paper. This work was supported by grants from the National Health & Medical Research Council, Australia, GNT1062820, GNT1100033, GNT1101378, GNT1124812, GNT1145184, and the Australia Research Council's special initiative Stem Cells Australia.

Author contributions

D.S.L. designed and performed most experiments and analysis, and wrote the manuscript. J.S. assisted with barcoding experiments, D.A-Z. and T.M.B. assisted with scRNA-seq experiments, L.T. and T.S.W. assisted with data analysis, S.T., M.E.R., P.D.H. provided critical input into experimental design and analysis. S.H.N conceptualized and supervised the study, and wrote the manuscript.

Competing interests

The authors declare no competing interests.

References

1. Guilliams, M. *et al.* Dendritic cells, monocytes and macrophages: a unified nomenclature based on ontogeny. *Nature reviews. Immunology* **14,** 571–578 (2014).
2. Murphy, T. L. *et al.* Transcriptional Control of Dendritic Cell Development. *Annual review of immunology* **34,** 93–119 (2015).
3. Hildner, K. *et al.* Batf3 deficiency reveals a critical role for CD8alpha+ dendritic cells in cytotoxic T cell immunity. *Science* **322,** 1097–1100 (2008).
4. Roberts, E. W. *et al.* Critical Role for CD103(+)/CD141(+) Dendritic Cells Bearing CCR7 for Tumor Antigen Trafficking and Priming of T Cell Immunity in Melanoma. *Cancer Cell* **30,** 324–336 (2016).
5. Salmon, H. *et al.* Expansion and Activation of CD103+ Dendritic Cell Progenitors at the Tumor Site Enhances Tumor Responses to Therapeutic PD-L1 and BRAF Inhibition. *Immunity* **44,** 924–938 (2016).
6. Alloatti, A. *et al.* Critical role for Sec22b-dependent antigen cross-presentation in antitumor immunity. *The Journal of experimental medicine* **214,** 2231–2241 (2017).
7. Spranger, S., Dai, D., Horton, B. & Gajewski, T. F. Tumor-Residing Batf3 Dendritic Cells Are Required for Effector T Cell Trafficking and Adoptive T Cell Therapy. *Cancer Cell* **31,** 711–723.e4 (2017).
8. Garris, C. S. *et al.* Successful Anti-PD-1 Cancer Immunotherapy Requires T Cell-Dendritic Cell Crosstalk Involving the Cytokines IFN-γ and IL-12. *Immunity* **49,** 1148–1161.e7 (2018).
9. Spranger, S., Bao, R. & Gajewski, T. F. Melanoma-intrinsic β-catenin signalling prevents anti-tumour immunity. *Nature* **523,** 231–235 (2015).
10. Morse, M. A. *et al.* Preoperative mobilization of circulating dendritic cells by Flt3 ligand administration to patients with metastatic colon cancer. *J. Clin. Oncol.* **18,** 3883–3893 (2000).
11. Fong, L. *et al.* Altered peptide ligand vaccination with Flt3 ligand expanded dendritic cells for tumor immunotherapy. *Proceedings of the National Academy of Sciences* **98,** 8809–8814 (2001).
12. Anandasabapathy, N. *et al.* Efficacy and safety of CDX-301, recombinant human Flt3L, at expanding dendritic cells and hematopoietic stem cells in healthy human volunteers. *Bone Marrow Transplantation 2015 50:7* **50,** 924–930 (2015).
13. Sánchez-Paulete, A. R. *et al.* Cancer Immunotherapy with Immunomodulatory Anti-CD137 and Anti-PD-1 Monoclonal Antibodies Requires BATF3-Dependent Dendritic Cells. *Cancer Discov* **6,** 71–79 (2016).
14. McKenna, H. J. *et al.* Mice lacking flt3 ligand have deficient hematopoiesis affecting hematopoietic progenitor cells, dendritic cells, and natural killer cells. *Blood* **95,** 3489–3497 (2000).
15. Ginhoux, F. *et al.* The origin and development of nonlymphoid tissue CD103+ DCs. *The Journal of experimental medicine* **206,** 3115–3130 (2009).
16. Maraskovsky, E. Dramatic increase in the numbers of functionally mature dendritic cells in Flt3 ligand-treated mice: multiple dendritic cell subpopulations identified. *The Journal of experimental medicine* **184,** 1953–1962 (1996).
17. O'Keeffe, M. *et al.* Effects of administration of progenipoietin 1, Flt-3 ligand, granulocyte colony-stimulating factor, and pegylated granulocyte-macrophage

colony-stimulating factor on dendritic cell subsets in mice. *Blood* **99,** 2122–2130 (2002).
18. Curran, M. A. & Allison, J. P. Tumor vaccines expressing flt3 ligand synergize with ctla-4 blockade to reject preimplanted tumors. *Cancer Res.* **69,** 7747–7755 (2009).
19. Guermonprez, P. *et al.* Inflammatory Flt3l is essential to mobilize dendritic cells and for T cell responses during Plasmodium infection. *Nature Medicine* **19,** 730–738 (2013).
20. Dupont, C. D. *et al.* Flt3 Ligand Is Essential for Survival and Protective Immune Responses during Toxoplasmosis. *Journal of immunology* (2015). doi:10.4049/jimmunol.1500690
21. Gregory, S. H., Sagnimeni, A. J., Zurowski, N. B. & Thomson, A. W. Flt3 ligand pretreatment promotes protective immunity to Listeria monocytogenes. *Cytokine* **13,** 202–208 (2001).
22. Reeves, R. K., Wei, Q., Stallworth, J. & Fultz, P. N. Systemic dendritic cell mobilization associated with administration of FLT3 ligand to SIV- and SHIV-infected macaques. *AIDS Res. Hum. Retroviruses* **25,** 1313–1328 (2009).
23. D'Amico, A. & Wu, L. The early progenitors of mouse dendritic cells and plasmacytoid predendritic cells are within the bone marrow hemopoietic precursors expressing Flt3. *The Journal of experimental medicine* **198,** 293–303 (2003).
24. Karsunky, H., Merad, M., Cozzio, A., Weissman, I. L. & Manz, M. G. Flt3 ligand regulates dendritic cell development from Flt3+ lymphoid and myeloid-committed progenitors to Flt3+ dendritic cells in vivo. *The Journal of experimental medicine* **198,** 305–313 (2003).
25. Naik, S. H. *et al.* Development of plasmacytoid and conventional dendritic cell subtypes from single precursor cells derived in vitro and in vivo. *Nature immunology* **8,** 1217–1226 (2007).
26. Onai, N. *et al.* Identification of clonogenic common Flt3+M-CSFR+ plasmacytoid and conventional dendritic cell progenitors in mouse bone marrow. *Nature immunology* **8,** 1207–1216 (2007).
27. Waskow, C. *et al.* The receptor tyrosine kinase Flt3 is required for dendritic cell development in peripheral lymphoid tissues. *Nature immunology* **9,** 676–683 (2008).
28. Sitnicka, E. *et al.* Key role of flt3 ligand in regulation of the common lymphoid progenitor but not in maintenance of the hematopoietic stem cell pool. *Immunity* **17,** 463–472 (2002).
29. Buza-Vidas, N. *et al.* FLT3 receptor and ligand are dispensable for maintenance and posttransplantation expansion of mouse hematopoietic stem cells. *Blood* **113,** 3453–3460 (2009).
30. Tsapogas, P. *et al.* In vivo evidence for an instructive role of fms-like tyrosine kinase-3 (FLT3) ligand in hematopoietic development. *Haematologica* **99,** 638–646 (2014).
31. Durai, V. *et al.* Altered compensatory cytokine signaling underlies the discrepancy between Flt3(-/-) and Flt3l(-/-) mice. *Journal of Experimental Medicine* **215,** 1417–1435 (2018).
32. Dykstra, B. *et al.* Long-term propagation of distinct hematopoietic differentiation programs in vivo. *Cell stem cell* **1,** 218–229 (2007).

33. Yamamoto, R. *et al.* Clonal analysis unveils self-renewing lineage-restricted progenitors generated directly from hematopoietic stem cells. *Cell* **154,** 1112–1126 (2013).
34. Naik, S. H. *et al.* Diverse and heritable lineage imprinting of early haematopoietic progenitors. *Nature* **496,** 229–232 (2013).
35. Notta, F. *et al.* Distinct routes of lineage development reshape the human blood hierarchy across ontogeny. *Science* **351,** aab2116–aab2116 (2016).
36. Nestorowa, S. *et al.* A single-cell resolution map of mouse hematopoietic stem and progenitor cell differentiation. *Blood* **128,** e20–31 (2016).
37. Velten, L. *et al.* Human haematopoietic stem cell lineage commitment is a continuous process. *Nature cell biology* **19,** 271–281 (2017).
38. Lee, J. *et al.* Lineage specification of human dendritic cells is marked by IRF8 expression in hematopoietic stem cells and multipotent progenitors. *Nature immunology* **15,** 3221 (2017).
39. Lin, D. S. *et al.* DiSNE Movie Visualization and Assessment of Clonal Kinetics Reveal Multiple Trajectories of Dendritic Cell Development. *Cell reports* **22,** 2557–2566 (2018).
40. Velten, L. *et al.* Human haematopoietic stem cell lineage commitment is a continuous process. *Nature cell biology* **19,** 271–281 (2017).
41. Laurenti, E. & Göttgens, B. From haematopoietic stem cells to complex differentiation landscapes. *Nature* **553,** 418–426 (2018).
42. Van der Maaten, L. & Hinton, G. Visualizing data using t-SNE. *Journal of Machine Learning Research* **9,** 2579–2605 (2008).
43. Ester, M., Kriegel, H. P., Sander, J. & Xu, X. A Density-Based Algorithm for Discovering Clusters in Large Spatial Databases with Noise. *Proceedings of the Second International Conference on Knowledge Discovery and Data Mining* 226–231 (1996).
44. Forsberg, E. C., Serwold, T., Kogan, S., Weissman, I. L. & Passegué, E. New evidence supporting megakaryocyte-erythrocyte potential of flk2/flt3+ multipotent hematopoietic progenitors. *Cell* **126,** 415–426 (2006).
45. Boyer, S. W., Schroeder, A. V., Smith-Berdan, S. & Forsberg, E. C. All hematopoietic cells develop from hematopoietic stem cells through Flk2/Flt3-positive progenitor cells. *Cell stem cell* **9,** 64–73 (2011).
46. Kiselev, V. Y. *et al.* SC3: consensus clustering of single-cell RNA-seq data. *Nature methods* **14,** 483–486 (2017).
47. Aran, D. *et al.* Reference-based analysis of lung single-cell sequencing reveals a transitional profibrotic macrophage. *Nature immunology* **20,** 163–172 (2019).
48. Endele, M., Etzrodt, M. & Schroeder, T. Instruction of hematopoietic lineage choice by cytokine signaling. *Experimental cell research* **329,** 207–213 (2014).
49. Rieger, M. A., Hoppe, P. S., Smejkal, B. M., Eitelhuber, A. C. & Schroeder, T. Hematopoietic cytokines can instruct lineage choice. *Science* **325,** 217–218 (2009).
50. Mossadegh-Keller, N. *et al.* M-CSF instructs myeloid lineage fate in single haematopoietic stem cells. *Nature* **497,** 239–243 (2013).
51. Etzrodt, M. *et al.* Inflammatory signals directly instruct PU.1 in HSCs via TNF. *Blood* **133,** 816–819 (2019).
52. Robinson, M. D., McCarthy, D. J. & Smyth, G. K. edgeR: a Bioconductor package for differential expression analysis of digital gene expression data. *Bioinformatics (Oxford, England)* **26,** 139–140 (2010).
53. Dai, Z. *et al.* shRNA-seq data analysis with edgeR. *F1000Research* **3,** 95 (2014).

54. Hashimshony, T. *et al.* CEL-Seq2: sensitive highly-multiplexed single-cell RNA-Seq. *Genome Biology* **17,** 77 (2016).
55. Liao, Y., Smyth, G. K. & Shi, W. The Subread aligner: fast, accurate and scalable read mapping by seed-and-vote. *Nucleic Acids Res* **41,** e108 (2013).
56. Tian, L. *et al.* scPipe: A flexible R/Bioconductor preprocessing pipeline for single-cell RNA-sequencing data. *PLoS Comput Biol* **14,** e1006361 (2018).
57. Haghverdi, L., Lun, A. T. L., Morgan, M. D. & Marioni, J. C. Batch effects in single-cell RNA-sequencing data are corrected by matching mutual nearest neighbors. *Nature biotechnology* **36,** 421–427 (2018).
58. McCarthy, D. J., Chen, Y. & Smyth, G. K. Differential expression analysis of multifactor RNA-Seq experiments with respect to biological variation. *Nucleic Acids Res* **40,** 4288–4297 (2012).
59. Su, S. *et al.* Glimma: interactive graphics for gene expression analysis. *Bioinformatics (Oxford, England)* **33,** 2050–2052 (2017).
60. Alexa, A. & Rahnenfuhrer, J. Gene set enrichment analysis with topGO. *R package* (2014).

Supplementary Figures

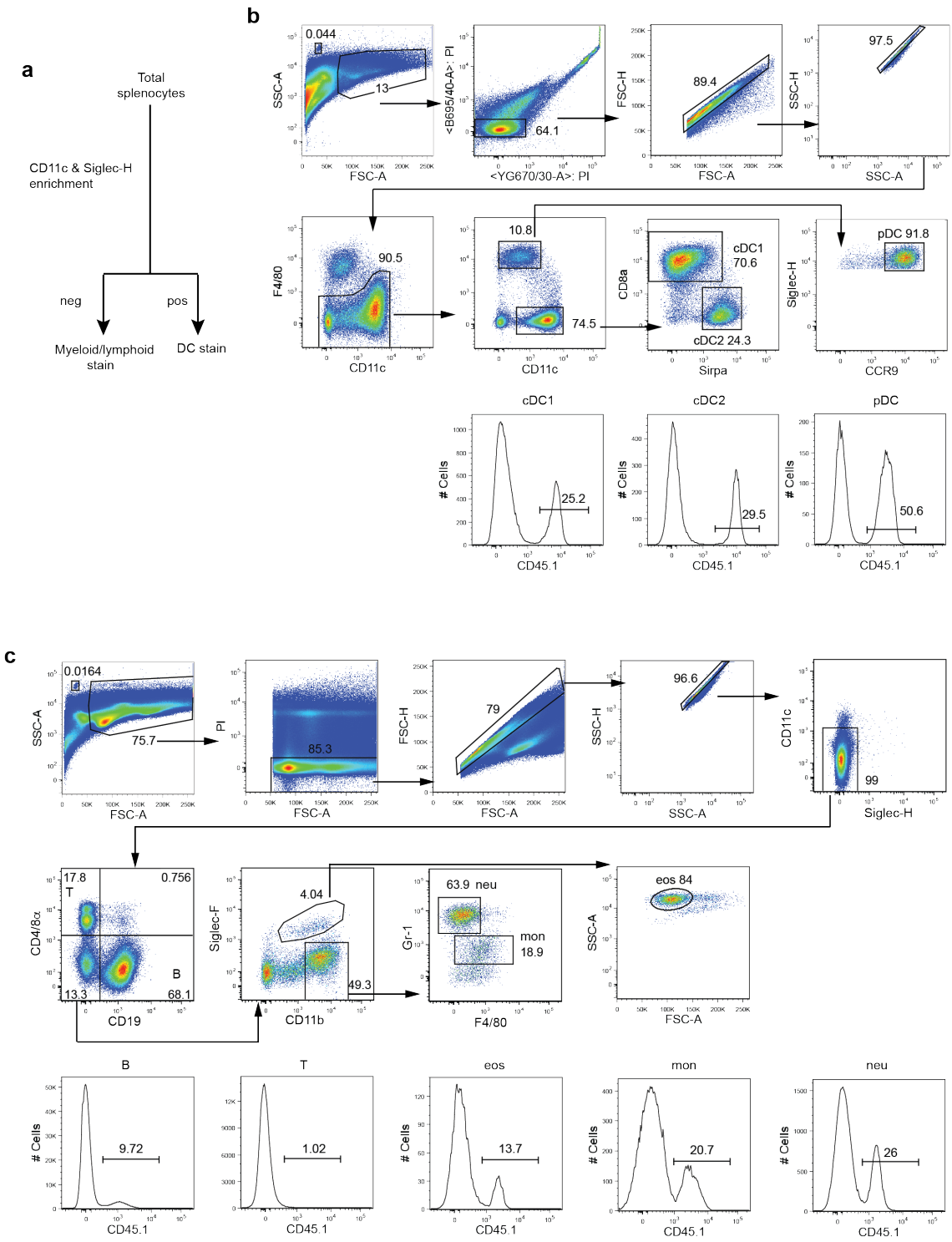

Supplementary Figure 1. Gating strategy to isolate mature progeny populations from spleen.

a. Workflow to fractionate total splenocytes into DC and myeloid/lymphoid fractions. **b.** Gating strategy to isolate cDC1 (F4/80$^-$ Siglec-H$^-$ CD11c$^+$ CD8α$^+$ Sirpα$^-$), cDC2 (F4/80$^-$ Siglec-H$^-$ CD11c$^+$ CD8α$^-$ Sirpα$^+$), pDC (F4/80$^-$ Siglec-H$^+$ CD11c^{int} CCR9$^+$) from the DC-enriched fraction. **c.** Gating strategy to isolate eosinophils (eos) (F4/80$^-$ Siglec-H$^-$ CD11c$^-$ CD11b$^+$ Siglec-F$^+$ SSA^{hi}), monocytes (mon) (F4/80$^-$ Siglec-H$^-$ CD11c$^-$ CD11b$^+$ Siglec-F$^-$ Ly6C$^+$ Ly6G$^-$), neutrophils (neu) (F4/80$^-$ Siglec-H$^-$ CD11c$^-$ CD11b$^+$ Siglec-F$^-$ Ly6C^{int} Ly6G$^+$), B (F4/80$^-$ Siglec-H$^-$ CD11c$^-$ CD11b$^-$ CD19$^+$ CD4/8α$^-$), T (F4/80$^-$ Siglec-H$^-$ CD11c$^-$ CD11b$^-$ CD19$^-$ CD4/8α$^+$) from the myeloid/lymphoid-enriched fraction. Donor-derived cells in each population are identified as CD45.1$^+$. Beads were added to all fractions after enrichment (before final staining) and gated as FSC^{lo}SSC^{hi} to allow estimation of cell numbers. Live cells were gated after exclusion of debris, doublets and PI$^+$ dead cells as indicated. Numbers shown in all FACS plots represent % cells from parent gate.

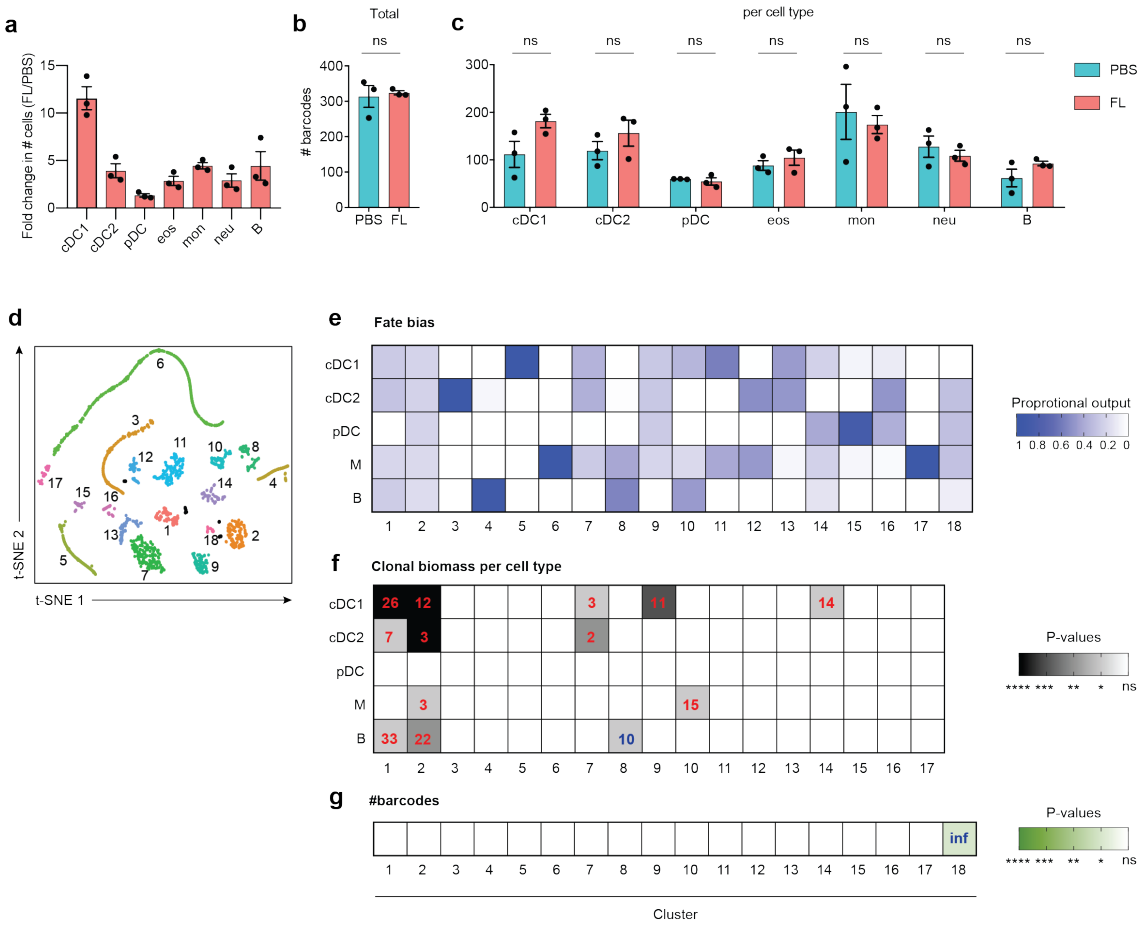

Supplementary Figure 2. Analysis of second barcoding experiment.

Analysis for a second barcoding experiment is shown. **a.** Fold change in cell numbers comparing FL-treated mice (n=3) to the average of PBS-treated mice (n=3). **b.** Total number of barcodes. **c.** Number of barcodes present in each cell type. **d.** t-SNE plot showing the 18 clusters identified by DBSCAN from experiment 2. PBS: 941 barcodes; FL: 972 barcodes. Black dots represent clones that are not classified in any clusters by the algorithm (outliers). **e.** Summary heatmaps showing average proportional output to cell types in **e**; the comparison of clone size in **f**; and the comparison of barcode numbers **g** in each cluster. Number in each box (**f, g**) depicts the fold increase (FL vs average of PBS), and color shading reflects p-value. **a-c,** each dot represents individual recipient mouse; bar graphs show mean ± SEM; P-values in **a-c, f, g** are calculated by unpaired t test. ns: no significant differences, *P < 0.01, **P < 0.001, ***P < 0.0001, ****P < 0.00001.

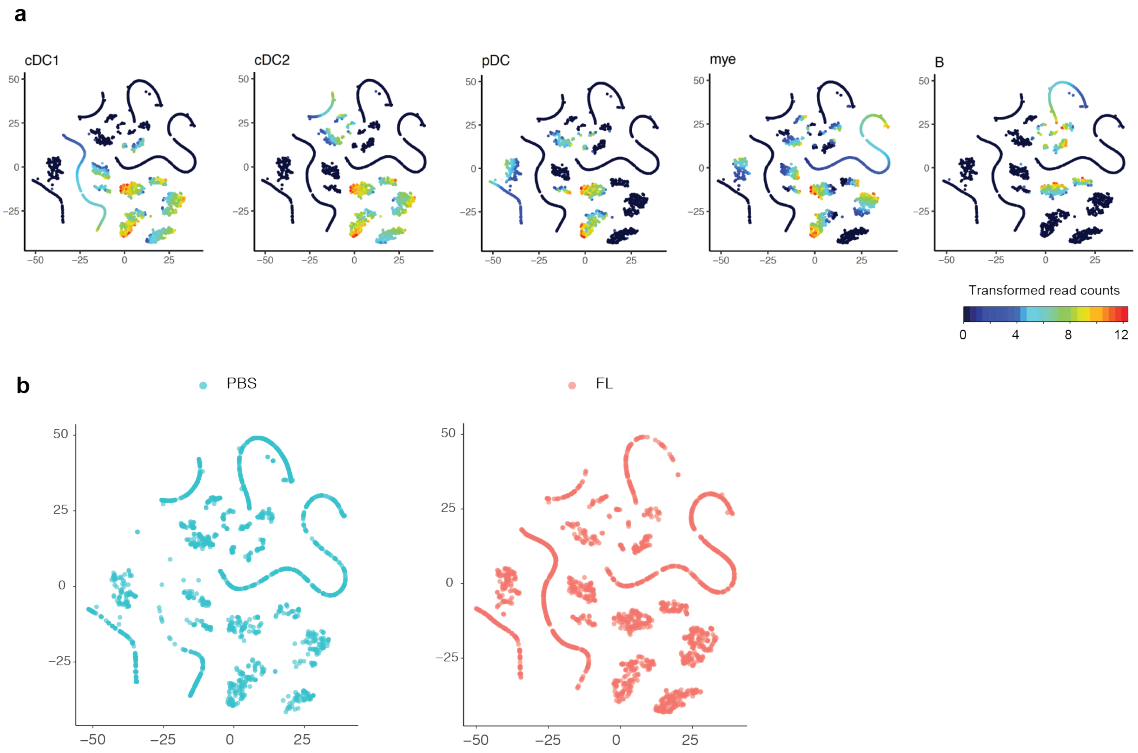

Supplementary Figure 3. t-SNE analysis of barcoding experiment I.

t-SNE plot of 1595 PBS-treated and 2013 FL-treated barcoded clones as shown in **Fig. 4a**. Each point represents one barcoded clone. Color of dots depicts the following: **a)** contribution to cell types by individual barcodes; **b)** PBS or FL treatment received by each clone.

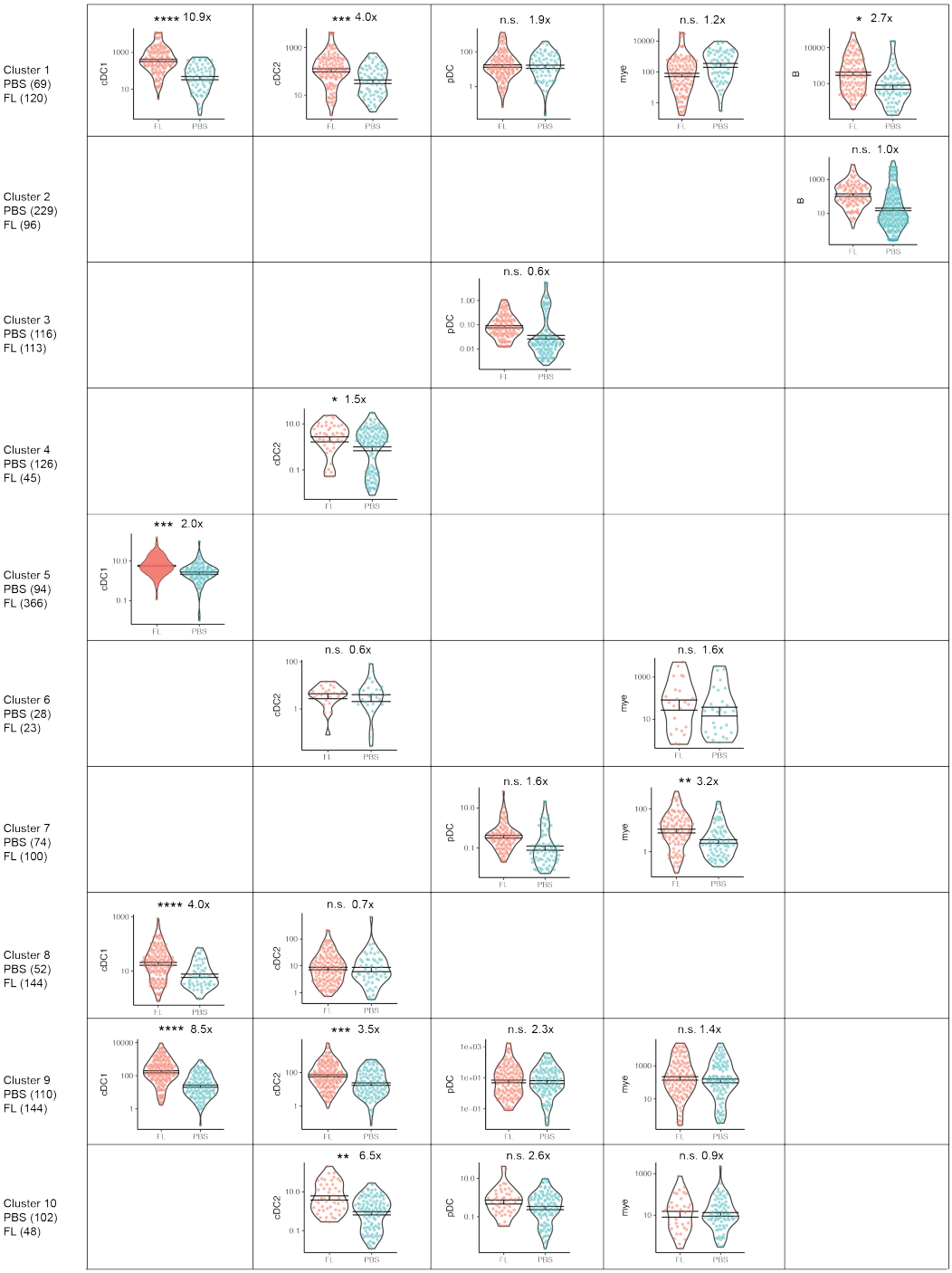
Cluster 1
PBS (69)
FL (120)
**** 10.9x
cDC1
*** 4.0x
cDC2
n.s. 1.9x
pDC
n.s. 1.2x
mye
* 2.7x
B
Cluster 2
PBS (229)
FL (96)
n.s. 1.0x
B
Cluster 3
PBS (116)
FL (113)
n.s. 0.6x
pDC
Cluster 4
PBS (126)
FL (45)
* 1.5x
cDC2
Cluster 5
PBS (94)
FL (366)
*** 2.0x
cDC1
Cluster 6
PBS (28)
FL (23)
n.s. 0.6x
cDC2
n.s. 1.6x
mye
Cluster 7
PBS (74)
FL (100)
n.s. 1.6x
pDC
** 3.2x
mye
Cluster 8
PBS (52)
FL (144)
**** 4.0x
cDC1
n.s. 0.7x
cDC2
Cluster 9
PBS (110)
FL (144)
**** 8.5x
cDC1
*** 3.5x
cDC2
n.s. 2.3x
pDC
n.s. 1.4x
mye
Cluster 10
PBS (102)
FL (48)
** 6.5x
cDC2
n.s. 2.6x
pDC
n.s. 0.9x
mye
FL
PBS

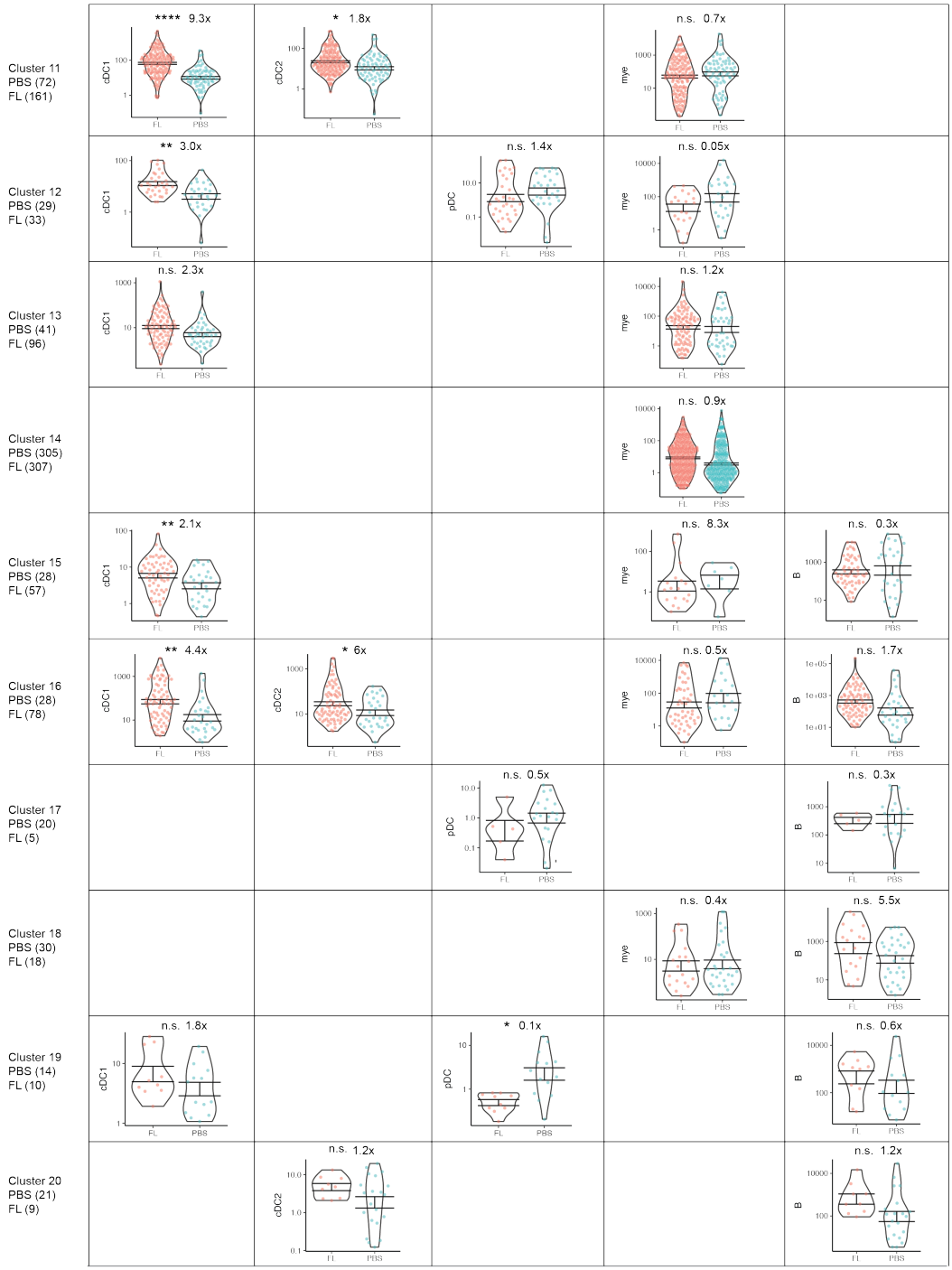
Cluster 11
PBS (72)
FL (161)
**** 9.3x
cDC1
* 1.8x
cDC2
n.s. 0.7x
mye
Cluster 12
PBS (29)
FL (33)
** 3.0x
cDC1
n.s. 1.4x
pDC
n.s. 0.05x
mye
Cluster 13
PBS (41)
FL (96)
n.s. 2.3x
cDC1
n.s. 1.2x
mye
Cluster 14
PBS (305)
FL (307)
n.s. 0.9x
mye
Cluster 15
PBS (28)
FL (57)
** 2.1x
cDC1
n.s. 8.3x
mye
n.s. 0.3x
B
Cluster 16
PBS (28)
FL (78)
** 4.4x
cDC1
* 6x
cDC2
n.s. 0.5x
mye
n.s. 1.7x
B
Cluster 17
PBS (20)
FL (5)
n.s. 0.5x
pDC
n.s. 0.3x
B
Cluster 18
PBS (30)
FL (18)
n.s. 0.4x
mye
n.s. 5.5x
B
Cluster 19
PBS (14)
FL (10)
n.s. 1.8x
cDC1
* 0.1x
pDC
n.s. 0.6x
B
Cluster 20
PBS (21)
FL (9)
n.s. 1.2x
cDC2
n.s. 1.2x
B
FL
PBS

Supplementary Figure 4. Comparison of clone size between PBS- and FL-treated clones per cluster.

Violin plots showing number of cells to each cell type generated per clone (clone size) in either PBS or FL condition within each cluster. Each dot represents a barcoded clone. Numbers of PBS- and FL-treated barcodes in each cluster are shown on left panel. P-values in are calculated by unpaired t test. ns: no significant differences, *P < 0.01, **P < 0.001, ***P < 0.0001, ****P < 0.00001. Fold change in average clone size comparing FL-treated clones to PBS-treated clones are shown. Summary of P-values and fold changes is shown in **Fig. 4j**.

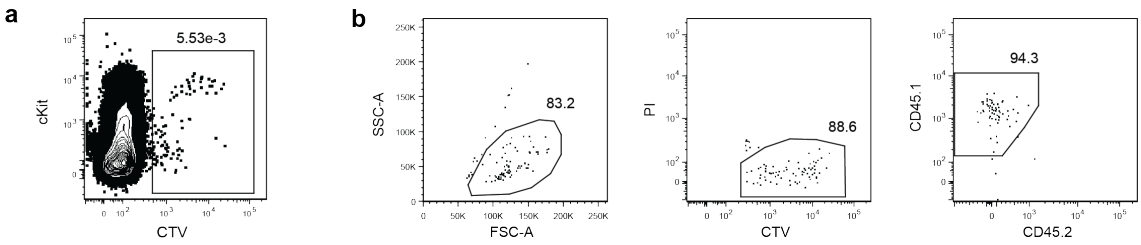

Supplementary Figure 5. Isolation and filtering of donor-derived cells.

a, gating strategy used during index sorting of single donor-derived cells as shown in **Fig. 5**. As donor cells were CTV-labelled prior to transplantation, CTV^{+} cells were sorted. **b,** gating strategy used to remove potential dead (based on FSC, SSC and PI) and contaminated endogenous cells ($CD45.1^{low}CD45.2^{+}$) after sorting.

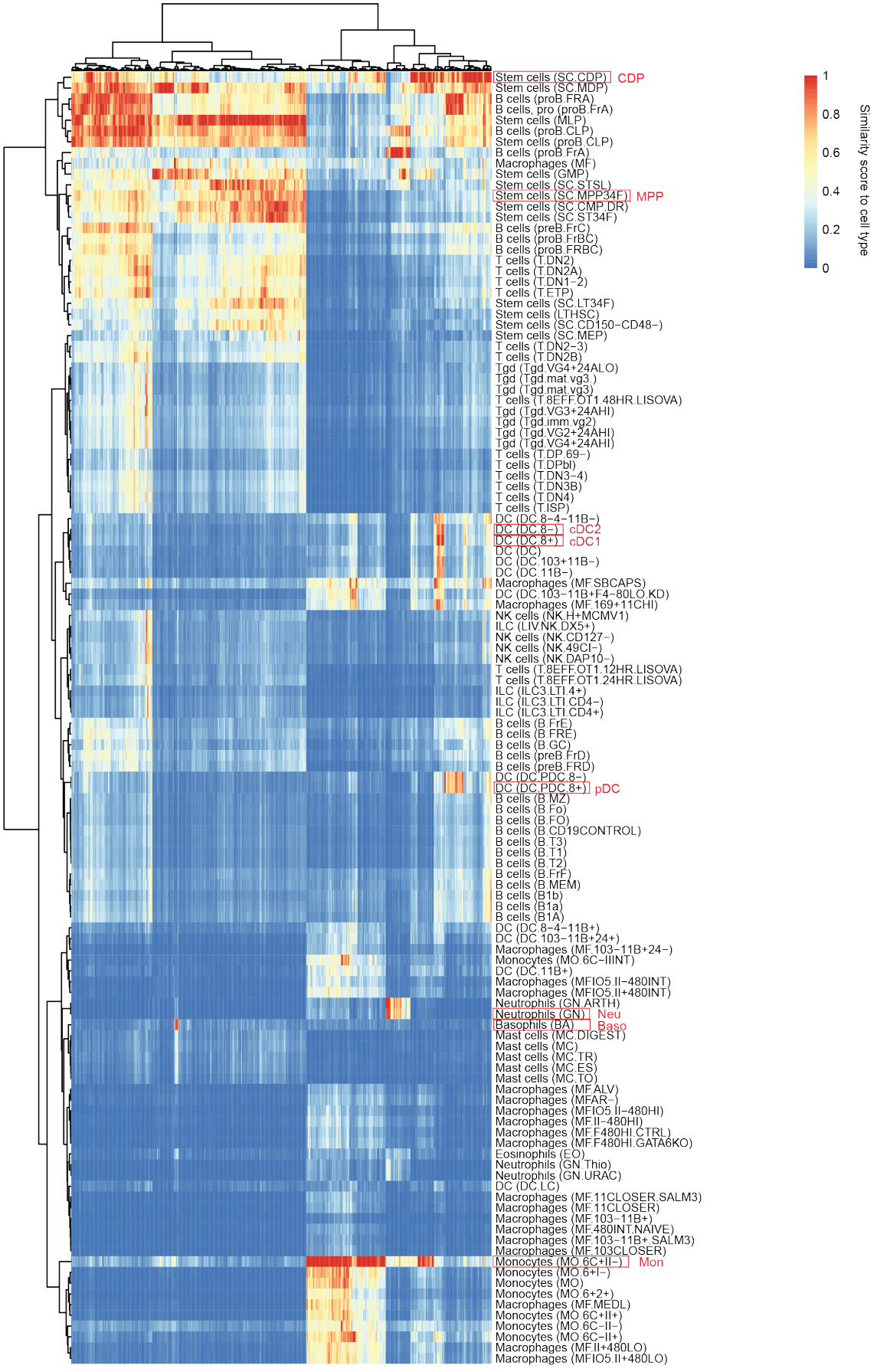
Stem cells (SC.CDP) CDP
Stem cells (SC.MDP)
B cells (proB.FRA)
B cells, pro (proB.FrA)
Stem cells (MLP)
B cells (proB.CLP)
Stem cells (proB.CLP)
B cells (proB.FrA)
Macrophages (MF)
Stem cells (GMP)
Stem cells (SC.STSL)
Stem cells (SC.MPP34F) MPP
Stem cells (SC.CMP.DR)
Stem cells (SC.ST34F)
B cells (preB.FrC)
B cells (proB.FrBC)
B cells (proB.FRBC)
T cells (T.DN2)
T cells (T.DN2A)
T cells (T.DN1-2)
T cells (T.ETP)
Stem cells (SC.LT34F)
Stem cells (LTHSC)
Stem cells (SC.CD150-CD48-)
Stem cells (SC.MEP)
T cells (T.DN2-3)
T cells (T.DN2B)
Tgd (Tgd.VG4+24ALO)
Tgd (Tgd.mat.vg3-)
Tgd (Tgd.mat.vg3+)
T cells (T.8EFF.OT1.48HR.LISOVA)
Tgd (Tgd.VG3+24AHI)
Tgd (Tgd.imm.vg2+)
Tgd (Tgd.VG2+24AHI)
Tgd (Tgd.VG4+24AHI)
T cells (T.DP.69-)
T cells (T.DPbl)
T cells (T.DN3-4)
T cells (T.DN3B)
T cells (T.DN4)
T cells (T.ISP)
DC (DC.8-4-11B-)
DC (DC.8-) cDC2
DC (DC.8+) cDC1
DC (DC)
DC (DC.103+11B-)
DC (DC.11B-)
Macrophages (MF.SBCAPS)
DC (DC.103-11B+F4-80LO.KD)
Macrophages (MF.169+11CHI)
NK cells (NK.H+MCMV1)
ILC (LIV.NK.DX5+)
NK cells (NK.CD127-)
NK cells (NK.49CI-)
NK cells (NK.DAP10-)
T cells (T.8EFF.OT1.12HR.LISOVA)
T cells (T.8EFF.OT1.24HR.LISOVA)
ILC (ILC3.LTI.4+)
ILC (ILC3.LTI.CD4-)
ILC (ILC3.LTI.CD4+)
B cells (B.FrE)
B cells (B.FRE)
B cells (B.GC)
B cells (preB.FrD)
B cells (preB.FRD)
DC (DC.PDC.8-)
DC (DC.PDC.8+) pDC
B cells (B.MZ)
B cells (B.Fo)
B cells (B.FO)
B cells (B.CD19CONTROL)
B cells (B.T3)
B cells (B.T1)
B cells (B.T2)
B cells (B.FrF)
B cells (B.MEM)
B cells (B1b)
B cells (B1a)
B cells (B1A)
DC (DC.8-4-11B+)
DC (DC.103-11B+24+)
Macrophages (MF.103-11B+24-)
Monocytes (MO.6C-IIINT)
DC (DC.11B+)
Macrophages (MFIO5.II-480INT)
Macrophages (MFIO5.II+480INT)
Neutrophils (GN.ARTH)
Neutrophils (GN) Neu
Basophils (BA) Baso
Mast cells (MC.DIGEST)
Mast cells (MC)
Mast cells (MC.TR)
Mast cells (MC.ES)
Mast cells (MC.TO)
Macrophages (MF.ALV)
Macrophages (MFAR-)
Macrophages (MFIO5.II-480HI)
Macrophages (MF.II-480HI)
Macrophages (MF.F480HI.CTRL)
Macrophages (MF.F480HI.GATA6KO)
Eosinophils (EO)
Neutrophils (GN.Thio)
Neutrophils (GN.URAC)
DC (DC.LC)
Macrophages (MF.11CLOSER.SALM3)
Macrophages (MF.11CLOSER)
Macrophages (MF.103-11B+)
Macrophages (MF.480INT.NAIVE)
Macrophages (MF.103-11B+.SALM3)
Macrophages (MF.103CLOSER)
Monocytes (MO.6C+II-) Mon
Monocytes (MO.6+I-)
Monocytes (MO)
Monocytes (MO.6+2+)
Macrophages (MF.MEDL)
Monocytes (MO.6C+II+)
Monocytes (MO.6C-II-)
Monocytes (MO.6C-II+)
Macrophages (MF.II+480LO)
Macrophages (MFIO5.II+480LO)
1
0.8
0.6
0.4
0.2
0
Similarity score to cell type

Supplementary Figure 6. Similarity scores to cell types.

Similarity scores to cell types were computed using SingleR. The top 120 cell types (out of 253) are shown. Cell types highlighted in red boxes were chosen for comparison in **Fig. 6**.

Chapter 5. Final Discussion

The overarching aim of this thesis was to understand the development of DCs at a single cell level. The current models of DC development are largely constructed based on observations and interpretation from population-based studies. Despite decades of research, controversies and confusions regarding several key questions remain, including the fundamental discrepancy between myeloid and lymphoid pathways of DC development and the existence of several intermediate developmental stages such as MDPs, amongst others (**Figure 1.3**). Therefore, a complete model of DC development is still lacking. These issues form part of a greater challenge in the creation of accurate models of haematopoiesis, with increasing evidence demonstrating substantial functional and transcriptional heterogeneity of HSPCs, as well as remarkable complexity of developmental trajectories. Collectively, these highlight the need to better evaluate the clonal output of HSPCs towards all haematopoietic lineages, including DCs, to help construct comprehensive models of haematopoiesis.

In **Chapter 3**, I developed a novel experimental and computational framework that utilised cellular barcoding to tag single HSPCs and follow their DC output longitudinally. This was performed in a well-established *in vitro* FL culture that mimics steady-state DC development (Naik et al., 2005). This framework, for the first time, allowed high-throughput and systematic characterization of clonal developmental dynamics of early HSPCs during DC development. In addition to the experimental setup, two novel computational approach were developed or adapted to analyse this barcoding data. First, 'DiSNE movies' were conceived to visualize this complex and dynamic process in an intuitive way. Second, a density-based algorithm was applied to classify the spectrum of HSPC clonal fate and allowed for systematic categorisation and measurement of reproducibility. As a result, **Chapter 3** helped define the key features of single HSPC clonal contribution during DC development, including features of which DCs (clone fate), how many DCs (clone size), and when DCs (clone timing) are generated. Collectively, these distinct properties contribute to what I defined as a clone's 'cellular trajectory'.

Although individual clones follow distinct clonal trajectories, major patterns can be revealed when large numbers of clones are tracked. After profiling cellular trajectories of

thousands of HSPC clones, three main classes were identified in **Chapter 3**. These included clones that can generate both cDCs and pDCs, and clones with biased output towards either cDCs or pDCs (**Chapter 3; Figure 4**). These findings indicate that a proportion of HSPCs have already committed to cDC and pDC development, while others are still uncommitted. This potentially helps reconcile conflicting models of DC development that stipulate either early (Dress et al., 2019; Helft et al., 2017; Lee et al., 2017; Rodrigues et al., 2018), or late separation of DC subtype fate (Naik et al., 2007; Onai et al., 2007). Future works can employ the framework described here to systematically compare the DC developmental trajectories from the different early and late DC progenitor populations described in the literature. Importantly, within each of the three major classes, HSPC clones can be further separated by their timing of DC contribution (**Chapter 3; Figure 4**). Collectively, the results presented in **Chapter 3** are consistent with the most recently proposed revised models of haematopoiesis, which imply the organization of HSPCs on a continuous developmental landscape (Guilliams et al., 2018; Haas et al., 2018; Laurenti and Göttgens, 2018; Velten et al., 2017b).

Most importantly, when cellular trajectories of sister sub-clones derived from the same founder clone were compared using a clone-splitting approach, I observed significant conservation of all features of clonal fate, size and timing (**Chapter 3; Figure 5**). This supports the notion that the properties of clonal cellular trajectories are largely intrinsic within individual HSPC clones. This key finding opens the possibility of probing several fundamental questions regarding clonal DC development in the future. One example is to combine clone-splitting and single cell RNA-sequencing to examine the molecular determinants of each aspect (clonal fate, size and timing) of cellular trajectories, similar to SIS-seq (Tian et al., 2018). Another example could be to investigate the changes in DC trajectories between steady-state and perturbed conditions on sister sub-clones. For example stimuli known to differentially affect DC subtype generation at a population level, such as M-CSF and TPO (Onai et al., 2013), could be added to one arm of the clone-splitting experiment while normal culture condition is maintained in the other arm.

The results from **Chapter 3**, together with evidence presented from other single cell studies regarding the development of DCs (Helft et al., 2017; Lee et al., 2017; Naik et al., 2013) or other haematopoietic lineages (Dykstra et al., 2007; Notta et al., 2016b; Velten et al., 2017b; Yamamoto et al., 2013), strongly support the notion that the majority of

single early HSPCs in the steady-state are already primed for distinct lineage fates. This raises a key question – how stable is such priming? For example, how do single HSPCs change in response to environmental cues such as elevated cytokines during infection or clinical intervention ('emergency haematopoiesis')? Such conditions are known to skew lineage production with, for example, increased numbers of cell type A and decreased numbers of cell type B. Theoretically, this could be due to an instructive role of the emergency cues, leading to lineage conversion of HSPC clones primed for cell type B to develop into cell type A, indicative of fate plasticity of these HSPCs. Alternatively, lineage priming is stably established in single HSPCs and cannot be easily diverged by emergency cues. Instead, these cues could enhance clonal expansion of pre-existing HSPCs primed for cell type A, leading to skewing in lineage production. To test the clonal parameters that change in order to account for these observations, we examined an *in vivo* model of emergency DC development induced by supra-physiological levels of FL stimulation in **Chapter 4**.

This model was chosen based on a few important considerations. First, unlike other haematopoietic cytokines, the receptor for FL (Flt3) is already expressed on the majority of early HSPCs. In particular, LMPPs are defined by their high levels of Flt3 (Adolfsson et al., 2005; Naik et al., 2013). In addition, most haematopoietic populations, including both myeloid and lymphoid lineages, develop through a Flt3-expressing stage (Boyer et al., 2011; Buza-Vidas et al., 2011). Therefore, early HSPCs are capable of responding to exogenous administration of FL. Second, despite the potential to influence the development of most haematopoietic lineages, supra-physiological levels of FL are known to preferentially expand DCs, particularly cDC1s, but not other lineages (Maraskovsky, 1996; O'Keeffe et al., 2002). Third, while FL is known to be an essential regulator of DC development, its role during early stages of DC development is controversial (Sitnicka et al., 2007; Tsapogas et al., 2014; Waskow et al., 2008). Fourth, increased cDC1 production via exogenous administration of FL is beneficial in controlling pathogenic infections and cancers (Guermonprez et al., 2013; Salmon et al., 2016), and has been shown to be safe and well tolerated in humans (Anandasabapathy et al., 2015). Therefore, a better understanding of the clonal aetiology of this process would not only provide insights into fundamental questions regarding 'fate plasticity' and the regulation of DC development, but also has implications regarding the potential utility and optimization of FL therapy.

Herein, I provided evidence of an active and possibly predominant contribution from early HSPCs to emergency DC generation in response to supra-physiological levels of FL (**Chapter 4; Figure 1 & 2**). My findings do not exclude a role for FL in expanding CDPs and mature DCs (Waskow et al., 2008) – indeed this may be a contributing factor in such progenitors derived from early HSPCs at a later stage in the 14-day cytokine exposure protocol. However, my results do clearly demonstrate that FL plays a role in expanding DCs from the earliest HSPCs.

Based on this finding, cellular barcoding was then used to tag individual early HSPCs and trace their lineage output *in vivo*, with or without exogeneous FL stimulation. Barcoded HSPCs were classified based on their distinct fate bias, followed by systematic comparison of barcode distribution and contribution to DC generation. I first examined the possibility of recruitment of HSPCs upon exogenous FL stimulation that were primed for lineages other than DCs, and found little evidence for this. Instead, there was a global increase in the expansion of pre-existing DC-primed HSPCs, particularly those HSPC clones with multi-lineage potentials (**Chapter 4; Figure 3 & 4**). Consistently, most early HSPCs were found to divide faster during the early phase of FL-mediated emergency haematopoiesis (**Chapter 4; Figure 5**), leading to enrichment of two groups of DC-primed progenitors. The first group represents a relatively mature cDC precursor population, while the second group contains early progenitors that are highly proliferative and exhibit molecular programs consistent with priming towards DC generation (**Chapter 4; Figure 6 & 7**). Collectively, these results demonstrate that FL-mediated emergency DC generation is predominantly driven by enhanced clonal expansion of a branch within individual HSPCs that already exhibit DC potential.

How extrinsic signals such as cytokine stimulation influence lineage commitment has been a central debate in haematopoiesis. Haematopoietic cytokines can provide survival, proliferation and differentiation signals to progenitors. Two non-mutually exclusive models have been proposed (Endele et al., 2014). In a 'permissive' model, cytokines mainly act as survival and/or proliferation factors that allow selective expansion of HSPCs that are already lineage committed. Conversely, an 'instructive' model implies an active role of cytokines in dictating lineage choices within single multi-potential HSPCs

by inducing lineage-specific transcriptional programs with/without inhibition of alternative fate programs.

Importantly, while some studies (Grover et al., 2014; Tsapogas et al., 2014) observe skewing in lineage production at the population level with different cytokine stimulation, this observation alone does not demonstrate an instructive role of cytokines in lineage determination. This is because changes in total cell numbers might not reflect changes at the clonal level; i.e. proliferation of some progenitors and simultaneous death of others can also result in skewing of lineage production. Therefore, it is crucial to follow the development of individual clones with or without stimulation to confirm an instructive role of extrinsic signals.

One landmark study utilized long-term live cell imaging to continuously track the output of individual GMPs after exposure to either M-CSF or G-CSF *in vitro* and demonstrated almost exclusive generation of monocytes or granulocytes, respectively (Rieger et al., 2009). Similarly, cytokines including M-CSF and TNF were demonstrated to directly induce up-regulation of transcription factor PU.1 and initiate myeloid fate in single HSCs using continuous live cell imaging (Etzrodt et al., 2019; Mossadegh-Keller et al., 2013). Together, these findings support the notion that cytokines can instruct lineage choice in single HSPCs. However, whether cytokine instruction represents the major source of fate determination in a more physiological relevant context remains to be determined.

Based on the results presented in **Chapter 4**, a permissive role of FL seems to account for the majority of emergency DC generation. Unlike the primitive HSCs used in the aforementioned studies (Etzrodt et al., 2019; Mossadegh-Keller et al., 2013), the majority of HSPCs examined in this thesis already exhibit some degree of lineage priming (Adolfsson et al., 2005; Naik et al., 2013). When examining this HSPC compartment ($CD11b^{-}cKit^{+}Sca1^{+}$), supra-physiological levels of FL do not seem to instruct DC development from HSPCs that are not DC-primed, but only affects those that already have pre-established DC potential. However, it is important to note that the majority of DCs are produced by HSPCs that have multi-lineage potential, rather than those with DC-restricted output. Furthermore, although FL stimulation fails to initiate a DC fate program in other HSPCs, it can preferentially guide DC generation from multipotent HSPCs, without inhibiting the development of myeloid or lymphoid lineages from the same

clones. Therefore, one could argue that although FL stimulation does not 'instruct' DC fate establishment in these settings, it can 'instruct' preferential DC production in these multipotent HSPC clones. Together, these results suggest that once HSPCs establish a lineage program, it is relatively stable and cannot be easily switched by cytokine stimulation.

Importantly, the results presented in this thesis do not exclude the possibility that FL can play an instructive role in DC fate determination within the most primitive HSCs that have not yet established any lineage bias. This question can potentially be addressed using long-term live cell imaging to follow DC development from primitive HSCs, once key technical challenges are overcome. One such challenge is the limitation regarding how long continuous imaging can be performed in DC cultures. One recent study attempted to image DC development from CDPs, and was able to follow individual clones for five days (Dursun et al., 2016). Importantly, most clones did not become fully differentiated during this period (Dursun et al., 2016). Therefore, it is currently not feasible to track DC development from an earlier HSC stage using continuous live cell imaging, as the time required for DC differentiation exceeds the maximal limit of the current technology.

Although the study conducted in this thesis does not allow a definitive assessment of how DC fate establishment occur within single HSPCs, a few potential novel regulators and/or markers of emergency DC development may have been identified. These are genes that were up-regulated in the unique group of DC-primed early progenitors, which were enriched after FL stimulation (**Chapter 4; Cluster 9 in Figure 6 & 7**). Some interesting candidates include surface markers such as CD93 and transcription factors such as Irf8 and Foxp1. Of those, Irf8 is a well-known regulator of DC development and its expression is recently shown to correlate with early DC fate priming in the LMPP population (Kurotaki et al., 2019b).

In contrast, little has been reported regarding the potential relationships between DC development and CD93 or Foxp1. CD93 is primarily known as a marker for early B cell development (Chevrier et al., 2009), but is also widely expressed in a variety of other cell types such as monocytes and neutrophils (Bohlson et al., 2005). Interestingly, an early study has reported positive expression of CD93 on DC progenitors that are $Flt3^{+}CD11b^{+}$ (Hieronymus et al., 2005). However, whether CD93 expression on early HSPCs

demarcates progenitors with DC-biased fate, and whether this applies in steady-state and/or emergency situations, remains to be determined.

On the other hand, the transcription factor Foxp1 is best known for its critical role in regulating brain development (Rocca et al., 2017). In the context of haematopoiesis, Foxp1 is shown to be essential in regulating the development of B cells (Hu et al., 2006), and it also appears to promote the expansion of early HSPCs (Naudin et al., 2017). Importantly, a recent study reports a potential role of Foxp1 in regulating DC maturation and function (Guo et al., 2019). However, whether Foxp1 differentially regulates DC development from early HSPCs is unknown. Together, future studies should determine whether CD93 or Foxp1 represents a novel regulator of DC development.

Cells in this unique group of DC-primed early progenitors (cluster 9) are shown to originate from the most responsive HSPC clones to FL stimulation (**Chapter 4; Figure 6**), and up-regulation of large numbers of cell cycle-related genes is observed (**Chapter 4; Figure 7**). Of those, *Ccnd1* is specifically expressed by DCs compared to other haematopoietic lineages (The Immunological Genome Project Consortium et al., 2008). Importantly, *Ccnd1* encodes for the protein cyclin D1, which forms a complex with cyclin-dependent kinases CDK4 and CDK6 and regulates their functions (Musgrove et al., 2011). Interestingly, CDK6 is also highly expressed by these DC-primed early progenitors in cluster 9 (**Chapter 4; Figure 7**). While CDK6 is commonly known as a cell cycle kinase, it also plays a potential role in regulating transcription of genes including Flt3 (Uras et al., 2016). Therefore, taken together, this might suggest the existence of a potential feedback loop between Flt3, CDK6 and cyclin D1, which might play a critical role in regulating DC development. Furthermore, it is important to understand the interplay between these factors, because both Flt3 and CDK6 are clinical targets in the treatment of a variety of cancers. In particular, a CDK4/6 inhibitor called palbociclib is an approved anti-cancer agent (Finn et al., 2009). Therefore, future experiments should address the fundamental and clinical relevance of any potential interaction between Flt3, cyclin D1 and CDK6.

In conclusion, this thesis examines clonal DC development during both the steady-state and emergency conditions. The findings presented here, together with other clonal studies, help to construct an alternative model of DC development (**Figure 5.1**). During

the steady-state, early HSPCs are not organized in a hierarchy as implied by traditional models of haematopoiesis, but are represented as a cloud of cells with different degrees of lineage priming. In particular, each HSPC clone may largely be programmed for their cellular trajectories, which include their lineage fate, clone size, and timing of contribution. During emergency conditions, such as in the case of FL-mediated emergency DC development, not all HSPCs are responsive despite harbouring the cytokine receptor for FL. Rather, only those with pre-established DC potential were amenable to expansion. These include clones that have multi-lineage potential as well as those with DC-restricted fate. Upon FL exposure, these clones become highly proliferative and selectively expand a DC-producing branch, leading to preferential generation of DCs. The findings presented in this thesis enhance our understanding of the clonal level control of HSPC fate, with implications for the maintenance or manipulation of DC numbers in health and disease.

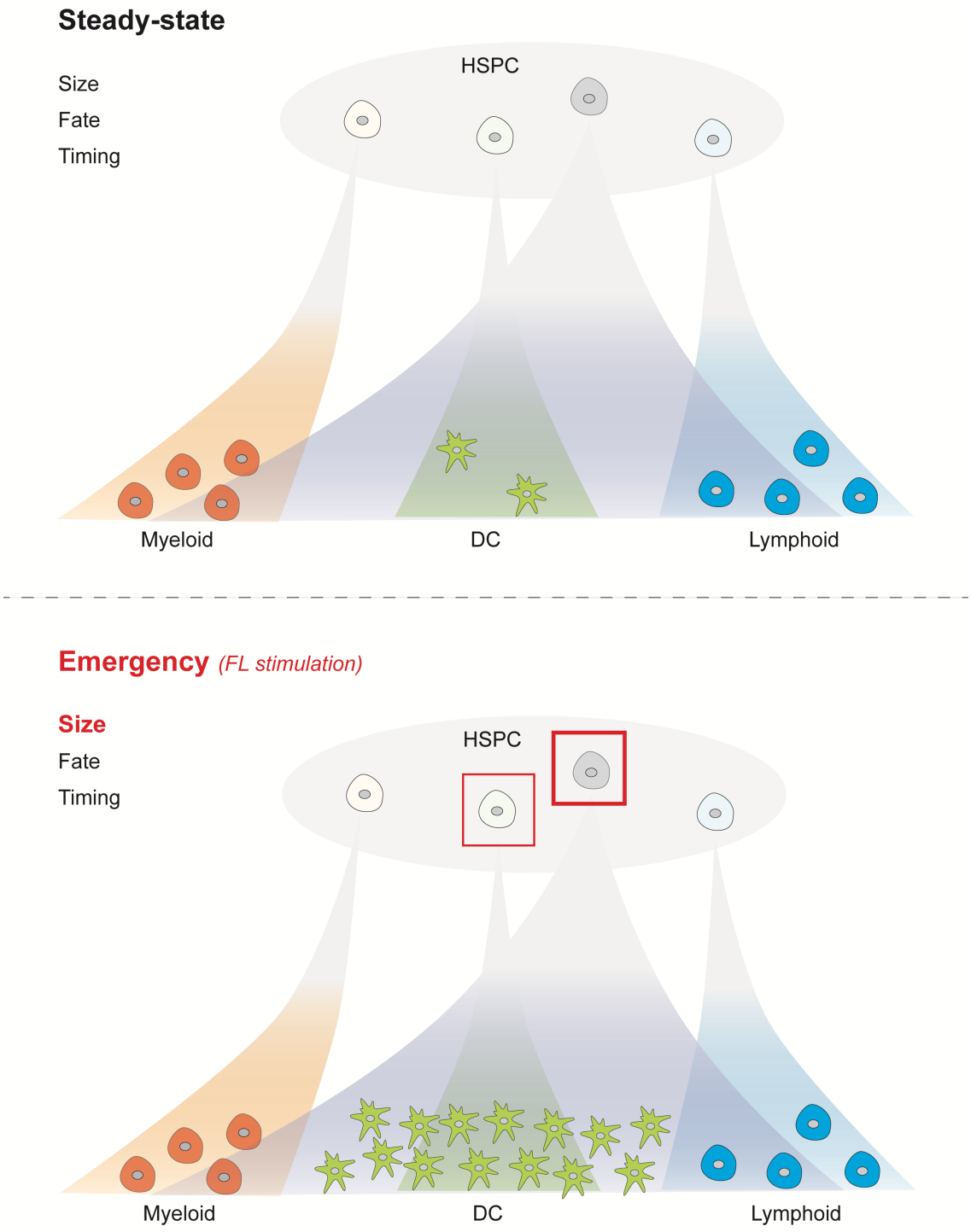

Figure 5.1 A revised model of DC development during steady-state and FL-mediated emergency condition.

In the steady-state, the cellular trajectories (clone size, fate and timing) of individual HSPCs are largely programmed. Upon exposure to supra-physiological levels of FL stimulation, enhanced expansion occurs in HSPC clones that are primed with DC potential (red boxes), including those that are DC-restricted and those with multi-lineage potential. This leads to preferential emergency DC generation.

References

Adolfsson, J., Borge, O.J., Bryder, D., Theilgaard-Monch, K., Astrand-Grundstrom, I., Sitnicka, E., Sasaki, Y., and Jacobsen, S.E. (2001). Upregulation of Flt3 expression within the bone marrow Lin(-)Sca1(+)c-kit(+) stem cell compartment is accompanied by loss of self-renewal capacity. Immunity *15*, 659–669.

Adolfsson, J., Månsson, R., Buza-Vidas, N., Hultquist, A., Liuba, K., Jensen, C.T., Bryder, D., Yang, L., Borge, O.-J., Thoren, L.A.M., et al. (2005). Identification of Flt3+ lympho-myeloid stem cells lacking erythro-megakaryocytic potential a revised road map for adult blood lineage commitment. Cell *121*, 295–306.

Akashi, K., Traver, D., Miyamoto, T., and Weissman, I.L. (2000). A clonogenic common myeloid progenitor that gives rise to all myeloid lineages. Nature *404*, 193–197.

Alcántara-Hernández, M., Leylek, R., Wagar, L.E., Engleman, E.G., Keler, T., Marinkovich, M.P., Davis, M.M., Nolan, G.P., and Idoyaga, J. (2017). High-Dimensional Phenotypic Mapping of Human Dendritic Cells Reveals Interindividual Variation and Tissue Specialization. Immunity *0*.

Alexandre, Y.O., Ghilas, S., Sanchez, C., Le Bon, A., Crozat, K., and Dalod, M. (2016). XCR1+ dendritic cells promote memory CD8+ T cell recall upon secondary infections with Listeria monocytogenes or certain viruses. Journal of Experimental Medicine *213*, 75–92.

Aliberti, J., Schulz, O., Pennington, D.J., Tsujimura, H., Reis e Sousa, C., Ozato, K., and Sher, A. (2003). Essential role for ICSBP in the in vivo development of murine CD8alpha + dendritic cells. Blood *101*, 305–310.

Alloatti, A., Rookhuizen, D.C., Joannas, L., Carpier, J.-M., Iborra, S., Magalhaes, J.G., Yatim, N., Kozik, P., Sancho, D., Albert, M.L., et al. (2017). Critical role for Sec22b-dependent antigen cross-presentation in antitumor immunity. The Journal of Experimental Medicine *214*, 2231–2241.

Anandasabapathy, N., Breton, G., Hurley, A., Caskey, M., Trumpfheller, C., Sarma, P., Pring, J., Pack, M., Buckley, N., Matei, I., et al. (2015). Efficacy and safety of CDX-301, recombinant human Flt3L, at expanding dendritic cells and hematopoietic stem cells in healthy human volunteers. Bone Marrow Transplantation 2015 50:7 *50*, 924–930.

Angelov, G.S., Tomkowiak, M., Marçais, A., Leverrier, Y., and Marvel, J. (2005). Flt3 ligand-generated murine plasmacytoid and conventional dendritic cells differ in their capacity to prime naive CD8 T cells and to generate memory cells in vivo. Journal of Immunology *175*, 189–195.

Annacker, O., Coombes, J.L., Malmstrom, V., Uhlig, H.H., Bourne, T., Johansson-Lindbom, B., Agace, W.W., Parker, C.M., and Powrie, F. (2005). Essential role for CD103 in the T cell-mediated regulation of experimental colitis. Journal of Experimental Medicine *202*, 1051–1061.

Annunziato, F., Romagnani, C., and Romagnani, S. (2015). The 3 major types of innate and adaptive cell-mediated effector immunity. Journal of Allergy and Clinical Immunology *135*, 626–635.

Ardavin, C., Wu, L., Li, C.L., and Shortman, K. (1993). Thymic dendritic cells and T cells develop simultaneously in the thymus from a common precursor population. Nature *362*, 761–763.

Asselin-Paturel, C., Boonstra, A., Dalod, M., Durand, I., Yessaad, N., Dezutter-Dambuyant, C., Vicari, A., O'Garra, A., Biron, C., Brière, F., et al. (2001). Mouse type I IFN-producing cells are immature APCs with plasmacytoid morphology. Nature Immunology *2*, 1144–1150.

Auffray, C., Fogg, D.K., Narni-Mancinelli, E., Senechal, B., Trouillet, C., Saederup, N., Leemput, J., Bigot, K., Campisi, L., Abitbol, M., et al. (2009). CX3CR1+ CD115+ CD135+ common macrophage/DC precursors and the role of CX3CR1 in their response to inflammation. The Journal of Experimental Medicine *206*, 595–606.

Bajaña, S., Roach, K., Turner, S., Paul, J., and Kovats, S. (2012). IRF4 promotes cutaneous dendritic cell migration to lymph nodes during homeostasis and inflammation. Journal of Immunology *189*, 3368–3377.

Bajaña, S., Turner, S., Paul, J., Ainsua-Enrich, E., and Kovats, S. (2016). IRF4 and IRF8 Act in CD11c+ Cells To Regulate Terminal Differentiation of Lung Tissue Dendritic Cells. Journal of Immunology *196*, 1666–1677.

Banchereau, J., and Steinman, R.M. (1998). Dendritic cells and the control of immunity. Nature *392*, 245–252.

Banu, N., Deng, B., Lyman, S.D., and Avraham, H. (1999). Modulation of haematopoietic progenitor development by FLT-3 ligand. Cytokine *11*, 679–688.

Barrat, F.J., Meeker, T., Gregorio, J., Chan, J.H., Uematsu, S., Akira, S., Chang, B., Duramad, O., and Coffman, R.L. (2005). Nucleic acids of mammalian origin can act as endogenous ligands for Toll-like receptors and may promote systemic lupus erythematosus. Journal of Experimental Medicine *202*, 1131–1139.

Barry, K.C., Hsu, J., Broz, M.L., Cueto, F.J., Binnewies, M., Combes, A.J., Nelson, A.E., Loo, K., Kumar, R., Rosenblum, M.D., et al. (2018). A natural killer-dendritic cell axis defines checkpoint therapy-responsive tumor microenvironments. Nature Medicine *24*, 1178–1191.

Båve, U., Magnusson, M., Eloranta, M.-L., Perers, A., Alm, G.V., and Rönnblom, L. (2003). Fc gamma RIIa is expressed on natural IFN-alpha-producing cells (plasmacytoid dendritic cells) and is required for the IFN-alpha production induced by apoptotic cells combined with lupus IgG. Journal of Immunology *171*, 3296–3302.

Becker, A.M., Michael, D.G., Satpathy, A.T., Sciammas, R., Singh, H., and Bhattacharya, D. (2012). IRF-8 extinguishes neutrophil production and promotes dendritic cell lineage commitment in both myeloid and lymphoid mouse progenitors. Blood *119*, 2003–2012.

Bedoui, S., Whitney, P.G., Waithman, J., Eidsmo, L., Wakim, L., Caminschi, I., Allan, R.S., Wojtasiak, M., Shortman, K., Carbone, F.R., et al. (2009). Cross-presentation of viral and self antigens by skin-derived CD103+ dendritic cells. Nature Immunology *10*, 488–495.

Belluschi, S., Calderbank, E.F., Ciaurro, V., Pijuan Sala, B., Santoro, A., Mende, N., Diamanti, E., Sham, K.Y.C., Wang, X., Lau, W.W.Y., et al. (2018). Myelo-lymphoid lineage restriction occurs in the human haematopoietic stem cell compartment before lymphoid-primed multipotent progenitors. Nat Commun *9*, 4100.

Belz, G.T., Shortman, K., Bevan, M.J., and Heath, W.R. (2005). CD8α+ Dendritic Cells Selectively Present MHC Class I-Restricted Noncytolytic Viral and Intracellular Bacterial Antigens In Vivo. The Journal of Immunology *175*, 196–200.

Benz, C., Copley, M.R., Kent, D.G., Wohrer, S., Cortes, A., Aghaeepour, N., Ma, E., Mader, H., Rowe, K., Day, C., et al. (2012). Hematopoietic stem cell subtypes expand differentially during development and display distinct lymphopoietic programs. Cell Stem Cell *10*, 273–283.

Berhanu, A., Huang, J., Alber, S.M., Watkins, S.C., and Storkus, W.J. (2006). Combinational FLt3 Ligand and Granulocyte Macrophage Colony-Stimulating Factor Treatment Promotes Enhanced Tumor Infiltration by Dendritic Cells and Antitumor CD8 +T-Cell Cross-priming but Is Ineffective as a Therapy. Cancer Res. *66*, 4895–4903.

Bevan, M.J. (1976). Cross-priming for a secondary cytotoxic response to minor H antigens with H-2 congenic cells which do not cross-react in the cytotoxic assay. Journal of Experimental Medicine *143*, 1283–1288.

Bevan, M.J. (1987). Class discrimination in the world of immunology. Nature *325*, 192–193.

Binnewies, M., Mujal, A.M., Pollack, J.L., Combes, A.J., Hardison, E.A., Barry, K.C., Tsui, J., Ruhland, M.K., Kersten, K., Abushawish, M.A., et al. (2019). Unleashing Type-2 Dendritic Cells to Drive Protective Antitumor CD4(+) T Cell Immunity. Cell *177*, 556–571.e16.

Birnberg, T., Bar-On, L., Sapoznikov, A., Caton, M.L., Cervantes-Barragan, L., Makia, D., Krauthgamer, R., Brenner, O., Ludewig, B., Brockschnieder, D., et al. (2008). Lack of conventional dendritic cells is compatible with normal development and T cell homeostasis, but causes myeloid proliferative syndrome. Immunity *29*, 986–997.

Björck, P. (2001). Isolation and characterization of plasmacytoid dendritic cells from Flt3 ligand and granulocyte-macrophage colony-stimulating factor-treated mice. Blood *98*, 3520–3526.

Blasius, A.L., Giurisato, E., Cella, M., Schreiber, R.D., Shaw, A.S., and Colonna, M. (2006). Bone marrow stromal cell antigen 2 is a specific marker of type I IFN-producing cells in the naive mouse, but a promiscuous cell surface antigen following IFN stimulation. Journal of Immunology *177*, 3260–3265.

Bogunovic, M., Ginhoux, F., Helft, J., Shang, L., Hashimoto, D., Greter, M., Liu, K., Jakubzick, C., Ingersoll, M.A., Leboeuf, M., et al. (2009). Origin of the lamina propria dendritic cell network. Immunity *31*, 513–525.

Bohlson, S.S., Silva, R., Fonseca, M.I., and Tenner, A.J. (2005). CD93 is rapidly shed from the surface of human myeloid cells and the soluble form is detected in human plasma. The Journal of Immunology *175*, 1239–1247.

Boyer, S.W., Schroeder, A.V., Smith-Berdan, S., and Forsberg, E.C. (2011). All hematopoietic cells develop from hematopoietic stem cells through Flk2/Flt3-positive progenitor cells. Cell Stem Cell *9*, 64–73.

Böttcher, J.P., Bonavita, E., Chakravarty, P., Blees, H., Cabeza-Cabrerizo, M., Sammicheli, S., Rogers, N.C., Sahai, E., Zelenay, S., and Reis e Sousa, C. (2018). NK Cells Stimulate Recruitment of cDC1 into the Tumor Microenvironment Promoting Cancer Immune Control. Cell *172*, 1022–1037.e14.

Brasel, K., De Smedt, T., Smith, J.L., and Maliszewski, C.R. (2000). Generation of murine dendritic cells from flt3-ligand-supplemented bone marrow cultures. Blood *96*, 3029–3039.

Brasel, K., McKenna, H.J., Charrier, K., Morrissey, P.J., Williams, D.E., and Lyman, S.D. (1997). Flt3 ligand synergizes with granulocyte-macrophage colony-stimulating factor or granulocyte colony-stimulating factor to mobilize hematopoietic progenitor cells into the peripheral blood of mice. Blood *90*, 3781–3788.

Brasel, K., McKenna, H.J., Morrissey, P.J., Charrier, K., Morris, A.E., Lee, C.C., Williams, D.E., and Lyman, S.D. (1996). Hematologic effects of flt3 ligand in vivo in mice. Blood *88*, 2004–2012.

Brashem-Stein, C., Flowers, D.A., and Bernstein, I.D. (1996). Regulation of colony forming cell generation by flt-3 ligand. Br J Haematol *94*, 17–22.

Braun, S.E., Chen, K., Blazar, B.R., Orchard, P.J., Sledge, G., Robertson, M.J., Broxmeyer, H.E., and Cornetta, K. (1999). Flt3 ligand antitumor activity in a murine breast cancer model: a comparison with granulocyte-macrophage colony-stimulating factor and a potential mechanism of action. Hum. Gene Ther. *10*, 2141–2151.

Brawand, P., Fitzpatrick, D.R., Greenfield, B.W., Brasel, K., Maliszewski, C.R., and De Smedt, T. (2002). Murine plasmacytoid pre-dendritic cells generated from Flt3 ligand-supplemented bone marrow cultures are immature APCs. Journal of Immunology *169*, 6711–6719.

Broxmeyer, H.E., Lu, L., Cooper, S., Ruggieri, L., Li, Z.H., and Lyman, S.D. (1995). Flt3 ligand stimulates/costimulates the growth of myeloid stem/progenitor cells. Experimental Hematology *23*, 1121–1129.

Broz, M.L., Binnewies, M., Boldajipour, B., Nelson, A.E., Pollack, J.L., Erle, D.J., Barczak, A., Rosenblum, M.D., Daud, A., Barber, D.L., et al. (2014). Dissecting the tumor myeloid compartment reveals rare activating antigen-presenting cells critical for T cell immunity. Cancer Cell *26*, 638–652.

Bryant, C., Fromm, P.D., Kupresanin, F., Clark, G., Lee, K., Clarke, C., Silveira, P.A., Suen, H., Brown, R., Newman, E., et al. (2016). A CD2 high-expressing stress-resistant human plasmacytoid dendritic-cell subset. Immunology and Cell Biology *94*, 447–457.

Buza-Vidas, N., Woll, P., Hultquist, A., Duarte, S., Lutteropp, M., Bouriez-Jones, T., Ferry, H., Luc, S., and Jacobsen, S.E.W. (2011). FLT3 expression initiates in fully multipotent mouse hematopoietic progenitor cells. Blood *118*, 1544–1548.

Cabeza-Cabrerizo, M., van Blijswijk, J., Wienert, S., Heim, D., Jenkins, R.P., Chakravarty, P., Rogers, N., Frederico, B., Acton, S., Beerling, E., et al. (2019). Tissue clonality of dendritic cell subsets and emergency DCpoiesis revealed by multicolor fate mapping of DC progenitors. Science Immunology *4*, eaaw1941.

Caminschi, I., Proietto, A.I., Ahmet, F., Kitsoulis, S., Shin Teh, J., Lo, J.C.Y., Rizzitelli, A., Wu, L., Vremec, D., van Dommelen, S.L.H., et al. (2008). The dendritic cell subtype-restricted C-type lectin Clec9A is a target for vaccine enhancement. Blood *112*, 3264–3273.

Carrelha, J., Meng, Y., Kettyle, L.M., Luis, T.C., Norfo, R., Alcolea, V., Boukarabila, H., Grasso, F., Gambardella, A., Grover, A., et al. (2018). Hierarchically related lineage-restricted fates of multipotent haematopoietic stem cells. Nature *554*, 106–111.

Ceribelli, M., Hou, Z.E., Kelly, P.N., Huang, D.W., Wright, G., Ganapathi, K., Evbuomwan, M.O., Pittaluga, S., Shaffer, A.L., Marcucci, G., et al. (2016). A Druggable TCF4- and BRD4-Dependent Transcriptional Network Sustains Malignancy in Blastic Plasmacytoid Dendritic Cell Neoplasm. Cancer Cell *30*, 764–778.

Cervantes-Barragan, L., Lewis, K.L., Firner, S., Thiel, V., Hugues, S., Reith, W., Ludewig, B., and Reizis, B. (2012). Plasmacytoid dendritic cells control T-cell response to chronic viral infection. Proceedings of the National Academy of Sciences of the United States of America *109*, 3012–3017.

Chakravarty, P.K., Alfieri, A., Thomas, E.K., Beri, V., Tanaka, K.E., Vikram, B., and Guha, C. (1999). Flt3-ligand administration after radiation therapy prolongs survival in a murine model of metastatic lung cancer. Cancer Res. *59*, 6028–6032.

Chaperot, L., Bendriss, N., Manches, O., Gressin, R., Maynadie, M., Trimoreau, F., Orfeuvre, H., Corront, B., Feuillard, J., Sotto, J.J., et al. (2001). Identification of a leukemic counterpart of the plasmacytoid dendritic cells. Blood *97*, 3210–3217.

Chen, K., Braun, S., Lyman, S., Fan, Y., Traycoff, C.M., Wiebke, E.A., Gaddy, J., Sledge, G., Broxmeyer, H.E., and Cornetta, K. (1997). Antitumor activity and immunotherapeutic properties of Flt3-ligand in a murine breast cancer model. Cancer Res. *57*, 3511–3516.

Chevrier, S., Genton, C., Kallies, A., Karnowski, A., Otten, L.A., Malissen, B., Malissen, M., Botto, M., Corcoran, L.M., Nutt, S.L., et al. (2009). CD93 is required for maintenance of antibody secretion and persistence of plasma cells in the bone marrow niche. Proceedings of the National Academy of Sciences *106*, 3895–3900.

Chicha, L., Jarrossay, D., and Manz, M.G. (2004). Clonal type I interferon-producing and dendritic cell precursors are contained in both human lymphoid and myeloid progenitor populations. The Journal of Experimental Medicine *200*, 1519–1524.

Christensen, J.L., and Weissman, I.L. (2001). Flk-2 is a marker in hematopoietic stem cell differentiation: a simple method to isolate long-term stem cells. Proceedings of the National Academy of Sciences of the United States of America *98*, 14541–14546.

Ciavarra, R.P., Somers, K.D., Brown, R.R., Glass, W.F., Consolvo, P.J., Wright, G.L., and Schellhammer, P.F. (2000). Flt3-ligand induces transient tumor regression in an ectopic treatment model of major histocompatibility complex-negative prostate cancer. Cancer Res. *60*, 2081–2084.

Cisse, B., Caton, M.L., Lehner, M., Maeda, T., Scheu, S., Locksley, R., Holmberg, D., Zweier, C., Hollander, den, N.S., Kant, S.G., et al. (2008). Transcription factor E2-2 is an essential and specific regulator of plasmacytoid dendritic cell development. Cell *135*, 37–48.

Coffman, R.L., and Weissman, I.L. (1981). B220: a B cell-specific member of th T200 glycoprotein family. Nature *289*, 681–683.

Corcoran, L., Ferrero, I., Vremec, D., Lucas, K., Waithman, J., O'Keeffe, M., Wu, L., Wilson, A., and Shortman, K. (2003). The lymphoid past of mouse plasmacytoid cells and thymic dendritic cells. Journal of Immunology *170*, 4926–4932.

Cresswell, P. (2005). Antigen processing and presentation. Immunol. Rev. *207*, 5–7.

Crozat, K., Guiton, R., Contreras, V., Feuillet, V., Dutertre, C.-A., Ventre, E., Vu Manh, T.-P., Baranek, T., Storset, A.K., Marvel, J., et al. (2010). The XC chemokine receptor 1 is a conserved selective marker of mammalian cells homologous to mouse CD8alpha+ dendritic cells. The Journal of Experimental Medicine *207*, 1283–1292.

Crozat, K., Tamoutounour, S., Vu Manh, T.-P., Fossum, E., Luche, H., Ardouin, L., Guilliams, M., Azukizawa, H., Bogen, B., Malissen, B., et al. (2011). Cutting edge: expression of XCR1 defines mouse lymphoid-tissue resident and migratory dendritic cells of the CD8α+ type. Journal of Immunology *187*, 4411–4415.

Curran, M.A., and Allison, J.P. (2009). Tumor vaccines expressing flt3 ligand synergize with ctla-4 blockade to reject preimplanted tumors. Cancer Res. *69*, 7747–7755.

D'Amico, A., and Wu, L. (2003). The early progenitors of mouse dendritic cells and plasmacytoid predendritic cells are within the bone marrow hemopoietic precursors expressing Flt3. The Journal of Experimental Medicine *198*, 293–303.

de Kruijf, E.-J.F.M., Hagoort, H., Velders, G.A., Fibbe, W.E., and van Pel, M. (2010). Hematopoietic stem and progenitor cells are differentially mobilized depending on the duration of Flt3-ligand administration. Haematologica *95*, 1061–1067.

Del Fresno, C., Saz-Leal, P., Enamorado, M., Wculek, S.K., Martinez-Cano, S., Blanco-Menendez, N., Schulz, O., Gallizioli, M., Miro-Mur, F., Cano, E., et al. (2018). DNGR-1 in dendritic cells limits tissue damage by dampening neutrophil recruitment. Science *362*, 351–356.

del Rio, M.-L., Bernhardt, G., Rodriguez-Barbosa, J.-I., and Förster, R. (2010). Development and functional specialization of CD103+ dendritic cells. Immunol. Rev. *234*, 268–281.

Desch, A.N., Randolph, G.J., Murphy, K., Gautier, E.L., Kedl, R.M., Lahoud, M.H., Caminschi, I., Shortman, K., Henson, P.M., and Jakubzick, C.V. (2011). CD103+ pulmonary dendritic cells preferentially acquire and present apoptotic cell–associated antigen. Journal of Experimental Medicine *208*, 1789–1797.

Diamond, M.S., Kinder, M., Matsushita, H., Mashayekhi, M., Dunn, G.P., Archambault, J.M., Lee, H., Arthur, C.D., White, J.M., Kalinke, U., et al. (2011). Type I interferon is selectively required by dendritic cells for immune rejection of tumors. Journal of Experimental Medicine *208*, 1989–2003.

Disis, M.L., Rinn, K., Knutson, K.L., Davis, D., Caron, D., Rosa, dela, C., and Schiffman, K. (2002). Flt3 ligand as a vaccine adjuvant in association with HER-2/neu peptide-based vaccines in patients with HER-2/neu-overexpressing cancers. Blood *99*, 2845–2850.

Dong, J., McPherson, C.M., and Stambrook, P.J. (2002). Flt-3 Ligand: A Potent Dendritic Cell Stimulator and Novel Antitumor. Cancer Biology & Therapy *1*, 486–489.

Dress, R.J., Dutertre, C.-A., Giladi, A., Schlitzer, A., Low, I., Shadan, N.B., Tay, A., Lum, J., Kairi, M.F.B.M., Hwang, Y.Y., et al. (2019). Plasmacytoid dendritic cells develop from Ly6D(+) lymphoid progenitors distinct from the myeloid lineage. Nature Immunology *20*, 852–864.

Dress, R.J., Wong, A.Y., and Ginhoux, F. (2018). Homeostatic control of dendritic cell numbers and differentiation. Immunology and Cell Biology *96*, 463–476.

Dudziak, D., Kamphorst, A.O., Heidkamp, G.F., Buchholz, V.R., Trumpfheller, C., Yamazaki, S., Cheong, C., Liu, K., Lee, H.-W., Park, C.G., et al. (2007). Differential antigen processing by dendritic cell subsets in vivo. Science *315*, 107–111.

Dupont, C.D., Harms Pritchard, G., Hidano, S., Christian, D.A., Wagage, S., Muallem, G., Tait Wojno, E.D., and Hunter, C.A. (2015). Flt3 Ligand Is Essential for Survival and Protective Immune Responses during Toxoplasmosis. Journal of Immunology.

Durai, V., and Murphy, K.M. (2016). Functions of Murine Dendritic Cells. Immunity *45*, 719–736.

Durai, V., Bagadia, P., Briseño, C.G., Theisen, D.J., Iwata, A., Davidson, J.T.4., Gargaro, M., Fremont, D.H., Murphy, T.L., and Murphy, K.M. (2018). Altered compensatory cytokine signaling underlies the discrepancy between Flt3(-/-) and Flt3l(-/-) mice. Journal of Experimental Medicine *215*, 1417–1435.

Dursun, E., Endele, M., Musumeci, A., Failmezger, H., Wang, S.-H., Tresch, A., Schroeder, T., and Krug, A.B. (2016). Continuous single cell imaging reveals sequential steps of plasmacytoid dendritic cell development from common dendritic cell progenitors. Sci Rep *6*, 37462.

Dykstra, B., Kent, D., Bowie, M., McCaffrey, L., Hamilton, M., Lyons, K., Lee, S.-J., Brinkman, R., and Eaves, C. (2007). Long-term propagation of distinct hematopoietic differentiation programs in vivo. Cell Stem Cell *1*, 218–229.

Edelson, B.T., Bradstreet, T.R., Hildner, K., Carrero, J.A., Frederick, K.E., Kc, W., Belizaire, R., Aoshi, T., Schreiber, R.D., Miller, M.J., et al. (2011). CD8α(+) dendritic

cells are an obligate cellular entry point for productive infection by Listeria monocytogenes. Immunity *35*, 236–248.

Edelson, B.T., Kc, W., Juang, R., Kohyama, M., Benoit, L.A., Klekotka, P.A., Moon, C., Albring, J.C., Ise, W., Michael, D.G., et al. (2010). Peripheral CD103+ dendritic cells form a unified subset developmentally related to CD8α+ conventional dendritic cells. Journal of Experimental Medicine *207*, 823–836.

Ema, H., Morita, Y., and Suda, T. (2014). Heterogeneity and hierarchy of hematopoietic stem cells. Experimental Hematology *42*, 74–82e2.

Endele, M., Etzrodt, M., and Schroeder, T. (2014). Instruction of hematopoietic lineage choice by cytokine signaling. Experimental Cell Research *329*, 207–213.

Esche, C., Subbotin, V.M., Maliszewski, C., Lotze, M.T., and Shurin, M.R. (1998). FLT3 ligand administration inhibits tumor growth in murine melanoma and lymphoma. Cancer Res. *58*, 380–383.

Etzrodt, M., Ahmed, N., Hoppe, P.S., Loeffler, D., Skylaki, S., Hilsenbeck, O., Kokkaliaris, K.D., Kaltenbach, H.-M., Stelling, J., Nerlov, C., et al. (2019). Inflammatory signals directly instruct PU.1 in HSCs via TNF. Blood *133*, 816–819.

Evans, T.G., Hasan, M., Galibert, L., and Caron, D. (2002). The use of Flt3 ligand as an adjuvant for hepatitis B vaccination of healthy adults. Vaccine *21*, 322–329.

Fallarino, F., Asselin-Paturel, C., Vacca, C., Bianchi, R., Gizzi, S., Fioretti, M.C., Trinchieri, G., Grohmann, U., and Puccetti, P. (2004). Murine plasmacytoid dendritic cells initiate the immunosuppressive pathway of tryptophan catabolism in response to CD200 receptor engagement. Journal of Immunology *173*, 3748–3754.

Favre-Felix, N., Martin, M., Maraskovsky, E., Fromentin, A., Moutet, M., Solary, E., Martin, F., and Bonnotte, B. (2000). Flt3 ligand lessens the growth of tumors obtained after colon cancer cell injection in rats but does not restore tumor-suppressed dendritic cell function. Int. J. Cancer *86*, 827–834.

Finn, R.S., Dering, J., Conklin, D., Kalous, O., Cohen, D.J., Desai, A.J., Ginther, C., Atefi, M., Chen, I., Fowst, C., et al. (2009). PD 0332991, a selective cyclin D kinase 4/6 inhibitor, preferentially inhibits proliferation of luminal estrogen receptor-positive human breast cancer cell lines in vitro. Breast Cancer Res *11*, R77.

Fogg, D.K., Sibon, C., Miled, C., Jung, S., Aucouturier, P., Littman, D.R., Cumano, A., and Geissmann, F. (2006). A clonogenic bone marrow progenitor specific for macrophages and dendritic cells. Science *311*, 83–87.

Fong, L., Hou, Y., Rivas, A., Benike, C., Yuen, A., Fisher, G.A., Davis, M.M., and Engleman, E.G. (2001). Altered peptide ligand vaccination with Flt3 ligand expanded dendritic cells for tumor immunotherapy. Proceedings of the National Academy of Sciences *98*, 8809–8814.

Forsberg, E.C., Serwold, T., Kogan, S., Weissman, I.L., and Passegué, E. (2006). New evidence supporting megakaryocyte-erythrocyte potential of flk2/flt3+ multipotent hematopoietic progenitors. Cell *126*, 415–426.

Fuertes, M.B., Kacha, A.K., Kline, J., Woo, S.-R., Kranz, D.M., Murphy, K.M., and Gajewski, T.F. (2011). Host type I IFN signals are required for antitumor CD8+ T cell responses through CD8{alpha}+ dendritic cells. The Journal of Experimental Medicine *208*, 2005–2016.

Fukuda, S., Broxmeyer, H.E., and Pelus, L.M. (2005). Flt3 ligand and the Flt3 receptor regulate hematopoietic cell migration by modulating the SDF-1alpha(CXCL12)/CXCR4 axis. Blood *105*, 3117–3126.

Ganguly, D., Haak, S., Sisirak, V., and Reizis, B. (2013). The role of dendritic cells in autoimmunity. Nature Reviews. Immunology *13*, 566–577.

Garris, C.S., Arlauckas, S.P., Kohler, R.H., Trefny, M.P., Garren, S., Piot, C., Engblom, C., Pfirschke, C., Siwicki, M., Gungabeesoon, J., et al. (2018). Successful Anti-PD-1 Cancer Immunotherapy Requires T Cell-Dendritic Cell Crosstalk Involving the Cytokines IFN-γ and IL-12. Immunity *49*, 1148–1161.e7.

Gasparetto, C., Gasparetto, M., Morse, M., Rooney, B., Vredenburgh, J.J., Long, G.D., Rizzieri, D.A., Loftis, J., Chao, N.J., and Smith, C. (2002). MOBILIZATION OF DENDRITIC CELLS FROM PATIENTS WITH BREAST CANCER INTO PERIPHERAL BLOOD STEM CELL LEUKAPHERESIS SAMPLES USING Flt-3-LIGAND AND G-CSF OR GM-CSF. Cytokine *18*, 8–19.

Gerrits, A., Dykstra, B., Kalmykowa, O.J., Klauke, K., Verovskaya, E., Broekhuis, M.J., de Haan, G., and Bystrykh, L.V. (2010). Cellular barcoding tool for clonal analysis in the hematopoietic system. Blood *115*, 2610–2618.

Ghosh, H.S., Cisse, B., Bunin, A., Lewis, K.L., and Reizis, B. (2010). Continuous expression of the transcription factor e2-2 maintains the cell fate of mature plasmacytoid dendritic cells. Immunity *33*, 905–916.

Giladi, A., Paul, F., Herzog, Y., Lubling, Y., Weiner, A., Yofe, I., Jaitin, D., Cabezas-Wallscheid, N., Dress, R., Ginhoux, F., et al. (2018). Single-cell characterization of haematopoietic progenitors and their trajectories in homeostasis and perturbed haematopoiesis. Nature Cell Biology *20*, 836–846.

Ginhoux, F., Liu, K., Helft, J., Bogunovic, M., Greter, M., Hashimoto, D., Price, J., Yin, N., Bromberg, J., Lira, S.A., et al. (2009). The origin and development of nonlymphoid tissue CD103+ DCs. The Journal of Experimental Medicine *206*, 3115–3130.

Grajales-Reyes, G.E., Iwata, A., Albring, J., Wu, X., Tussiwand, R., Kc, W., Kretzer, N.M., Briseño, C.G., Durai, V., Bagadia, P., et al. (2015). Batf3 maintains autoactivation of Irf8 for commitment of a CD8α(+) conventional DC clonogenic progenitor. Nature Immunology *16*, 708–717.

Gregory, S.H., Sagnimeni, A.J., Zurowski, N.B., and Thomson, A.W. (2001). Flt3 ligand pretreatment promotes protective immunity to Listeria monocytogenes. Cytokine *13*, 202–208.

Grover, A., Mancini, E., Moore, S., Mead, A.J., Atkinson, D., Rasmussen, K.D., O'Carroll, D., Jacobsen, S.E., and Nerlov, C. (2014). Erythropoietin guides multipotent

hematopoietic progenitor cells toward an erythroid fate. The Journal of Experimental Medicine *211*, 181–188.

Grover, A., Sanjuan-Pla, A., Thongjuea, S., Carrelha, J., Giustacchini, A., Gambardella, A., Macaulay, I., Mancini, E., Luis, T.C., Mead, A., et al. (2016). Single-cell RNA sequencing reveals molecular and functional platelet bias of aged haematopoietic stem cells. Nat Commun *7*, 11075.

Guermonprez, P., Helft, J., Claser, C., Deroubaix, S., Karanje, H., Gazumyan, A., Darasse-Jèze, G., Telerman, S.B., Breton, G., Schreiber, H.A., et al. (2013). Inflammatory Flt3l is essential to mobilize dendritic cells and for T cell responses during Plasmodium infection. Nature Medicine *19*, 730–738.

Guilliams, M., Dutertre, C.-A., Scott, C.L., McGovern, N., Sichien, D., Chakarov, S., Van Gassen, S., Chen, J., Poidinger, M., De Prijck, S., et al. (2016). Unsupervised High-Dimensional Analysis Aligns Dendritic Cells across Tissues and Species. Immunity *45*, 669–684.

Guilliams, M., Ginhoux, F., Jakubzick, C., Naik, S.H., Onai, N., Schraml, B.U., Segura, E., Tussiwand, R., and Yona, S. (2014). Dendritic cells, monocytes and macrophages: a unified nomenclature based on ontogeny. Nature Reviews. Immunology *14*, 571–578.

Guilliams, M., Mildner, A., and Yona, S. (2018). Developmental and Functional Heterogeneity of Monocytes. Immunity *49*, 595–613.

Guo, G., Luc, S., Marco, E., Lin, T.-W., Peng, C., Kerenyi, M.A., Beyaz, S., Kim, W., Xu, J., Das, P.P., et al. (2013). Mapping cellular hierarchy by single-cell analysis of the cell surface repertoire. Cell Stem Cell *13*, 492–505.

Guo, Z., Tao, Y., Yin, S., Song, Y., Lu, X., Li, X., Fan, Y., Fan, X., Xu, S., Yang, J., et al. (2019). The transcription factor Foxp1 regulates the differentiation and function of dendritic cells. Mech Dev.

Gurka, S., Hartung, E., Becker, M., and Kroczek, R.A. (2015). Mouse Conventional Dendritic Cells Can be Universally Classified Based on the Mutually Exclusive Expression of XCR1 and SIRPα. Front. Immunol. *6*, 1142.

Haan, den, J.M., Lehar, S.M., and Bevan, M.J. (2000). CD8(+) but not CD8(-) dendritic cells cross-prime cytotoxic T cells in vivo. Journal of Experimental Medicine *192*, 1685–1696.

Haas, S., Hansson, J., Klimmeck, D., Loeffler, D., Velten, L., Uckelmann, H., Wurzer, S., Prendergast, Á.M., Schnell, A., Hexel, K., et al. (2015). Inflammation-Induced Emergency Megakaryopoiesis Driven by Hematopoietic Stem Cell-like Megakaryocyte Progenitors. Cell Stem Cell *17*, 422–434.

Haas, S., Trumpp, A., and Milsom, M.D. (2018). Causes and Consequences of Hematopoietic Stem Cell Heterogeneity. Cell Stem Cell *22*, 627–638.

Hacker, C., Kirsch, R.D., Ju, X.-S., Hieronymus, T., Gust, T.C., Kuhl, C., Jorgas, T., Kurz, S.M., Rose-John, S., Yokota, Y., et al. (2003). Transcriptional profiling identifies Id2 function in dendritic cell development. Nature Immunology *4*, 380–386.

Hannum, C., Culpepper, J., Campbell, D., McClanahan, T., Zurawski, S., Bazan, J.F., Kastelein, R., Hudak, S., Wagner, J., and Mattson, J. (1994). Ligand for FLT3/FLK2 receptor tyrosine kinase regulates growth of haematopoietic stem cells and is encoded by variant RNAs. Nature *368*, 643–648.

Harman, B.C., Miller, J.P., Nikbakht, N., Gerstein, R., and Allman, D. (2006). Mouse plasmacytoid dendritic cells derive exclusively from estrogen-resistant myeloid progenitors. Blood *108*, 878–885.

Hartung, E., Becker, M., Bachem, A., Reeg, N., Jäkel, A., Hutloff, A., Weber, H., Weise, C., Giesecke, C., Henn, V., et al. (2015). Induction of Potent CD8 T Cell Cytotoxicity by Specific Targeting of Antigen to Cross-Presenting Dendritic Cells In Vivo via Murine or Human XCR1. The Journal of Immunology *194*, 1069–1079.

Hashimshony, T., Senderovich, N., Avital, G., Klochendler, A., de Leeuw, Y., Anavy, L., Gennert, D., Li, S., Livak, K.J., Rozenblatt-Rosen, O., et al. (2016). CEL-Seq2: sensitive highly-multiplexed single-cell RNA-Seq. Genome Biology *17*, 77.

He, S., Chu, J., Vasu, S., Deng, Y., Yuan, S., Zhang, J., Fan, Z., Hofmeister, C.C., He, X., Marsh, H.C., et al. (2014). FLT3L and plerixafor combination increases hematopoietic stem cell mobilization and leads to improved transplantation outcome. Biol. Blood Marrow Transplant. *20*, 309–313.

Heath, W.R., Belz, G.T., Behrens, G.M.N., Smith, C.M., Forehan, S.P., Parish, I.A., Davey, G.M., Wilson, N.S., Carbone, F.R., and Villadangos, J.A. (2004). Cross-presentation, dendritic cell subsets, and the generation of immunity to cellular antigens. Immunol. Rev. *199*, 9–26.

Helft, J., Anjos-Afonso, F., van der Veen, A.G., Chakravarty, P., Bonnet, D., and Reis e Sousa, C. (2017). Dendritic Cell Lineage Potential in Human Early Hematopoietic Progenitors. Cell Reports *20*, 529–537.

Helft, J., Ginhoux, F., Bogunovic, M., and Merad, M. (2010). Origin and functional heterogeneity of non-lymphoid tissue dendritic cells in mice. Immunol. Rev. *234*, 55–75.

Hieronymus, T., Gust, T.C., Kirsch, R.D., Jorgas, T., Blendinger, G., Goncharenko, M., Supplitt, K., Rose-John, S., Muller, A.M., and Zenke, M. (2005). Progressive and controlled development of mouse dendritic cells from Flt3+CD11b+ progenitors in vitro. The Journal of Immunology *174*, 2552–2562.

Higano, C.S., Vogelzang, N.J., Sosman, J.A., Feng, A., Caron, D., and Small, E.J. (2004). Safety and biological activity of repeated doses of recombinant human Flt3 ligand in patients with bone scan-negative hormone-refractory prostate cancer. Clinical Cancer Research *10*, 1219–1225.

Hildner, K., Edelson, B.T., Purtha, W.E., Diamond, M., Matsushita, H., Kohyama, M., Calderon, B., Schraml, B.U., Unanue, E.R., Diamond, M.S., et al. (2008). Batf3 deficiency reveals a critical role for CD8alpha+ dendritic cells in cytotoxic T cell immunity. Science *322*, 1097–1100.

Hirayama, F., Lyman, S.D., Clark, S.C., and Ogawa, M. (1995). The flt3 ligand supports proliferation of lymphohematopoietic progenitors and early B-lymphoid progenitors. Blood *85*, 1762–1768.

Hochrein, H., Shortman, K., Vremec, D., Scott, B., Hertzog, P., and O'Keeffe, M. (2001). Differential production of IL-12, IFN-alpha, and IFN-gamma by mouse dendritic cell subsets. The Journal of Immunology *166*, 5448–5455.

Honda, K., Yanai, H., Negishi, H., Asagiri, M., Sato, M., Mizutani, T., Shimada, N., Ohba, Y., Takaoka, A., Yoshida, N., et al. (2005). IRF-7 is the master regulator of type-I interferon-dependent immune responses. Nature *434*, 772–777.

Hu, H., Wang, B., Borde, M., Nardone, J., Maika, S., Allred, L., Tucker, P.W., and Rao, A. (2006). Foxp1 is an essential transcriptional regulator of B cell development. Nature Immunology *7*, 819–826.

Huang, A.Y., Golumbek, P., Ahmadzadeh, M., Jaffee, E., Pardoll, D., and Levitsky, H. (1994). Role of bone marrow-derived cells in presenting MHC class I-restricted tumor antigens. Science *264*, 961–965.

Hudak, S., Hunte, B., Culpepper, J., Menon, S., Hannum, C., Thompson-Snipes, L., and Rennick, D. (1995). FLT3/FLK2 ligand promotes the growth of murine stem cells and the expansion of colony-forming cells and spleen colony-forming units. Blood *85*, 2747–2755.

Inaba, K., Inaba, M., Deguchi, M., Hagi, K., Yasumizu, R., Ikehara, S., Muramatsu, S., and Steinman, R.M. (1993). Granulocytes, macrophages, and dendritic cells arise from a common major histocompatibility complex class II-negative progenitor in mouse bone marrow. Proceedings of the National Academy of Sciences of the United States of America *90*, 3038–3042.

Jackson, J.T., Hu, Y., Liu, R., Masson, F., D'Amico, A., Carotta, S., Xin, A., Camilleri, M.J., Mount, A.M., Kallies, A., et al. (2011). Id2 expression delineates differential checkpoints in the genetic program of CD8α+ and CD103+ dendritic cell lineages. The EMBO Journal *30*, 2690–2704.

Jacobsen, S.E., Okkenhaug, C., Myklebust, J., Veiby, O.P., and Lyman, S.D. (1995). The FLT3 ligand potently and directly stimulates the growth and expansion of primitive murine bone marrow progenitor cells in vitro: synergistic interactions with interleukin (IL) 11, IL-12, and other hematopoietic growth factors. The Journal of Experimental Medicine *181*, 1357–1363.

Janela, B., Patel, A.A., Lau, M.C., Goh, C.C., Msallam, R., Kong, W.T., Fehlings, M., Hubert, S., Lum, J., Simoni, Y., et al. (2019). A Subset of Type I Conventional Dendritic Cells Controls Cutaneous Bacterial Infections through VEGFalpha-Mediated Recruitment of Neutrophils. Immunity *50*, 1069–1083.e8.

Jiang, W., Swiggard, W.J., Heufler, C., Peng, M., Mirza, A., Steinman, R.M., and Nussenzweig, M.C. (1995). The receptor DEC-205 expressed by dendritic cells and thymic epithelial cells is involved in antigen processing. Nature *375*, 151–155.

Jirmo, A.C., Nagel, C.-H., Bohnen, C., Sodeik, B., and Behrens, G.M.N. (2009). Contribution of Direct and Cross-Presentation to CTL Immunity against Herpes Simplex Virus 1. The Journal of Immunology *182*, 283–292.

Kamogawa-Schifter, Y., Ohkawa, J., Namiki, S., Arai, N., Arai, K.-I., and Liu, Y. (2005). Ly49Q defines 2 pDC subsets in mice. Blood *105*, 2787–2792.

Karamitros, D., Stoilova, B., Aboukhalil, Z., Hamey, F., Reinisch, A., Samitsch, M., Quek, L., Otto, G., Repapi, E., Doondeea, J., et al. (2018). Single-cell analysis reveals the continuum of human lympho-myeloid progenitor cells. Nature Immunology *19*, 85–97.

Karsunky, H., Merad, M., Cozzio, A., Weissman, I.L., and Manz, M.G. (2003). Flt3 ligand regulates dendritic cell development from Flt3+ lymphoid and myeloid-committed progenitors to Flt3+ dendritic cells in vivo. The Journal of Experimental Medicine *198*, 305–313.

Kasahara, S., and Clark, E.A. (2011). Dendritic cell-associated lectin 2 (DCAL2) defines a distinct CD8α −dendritic cell subset. Journal of Leukocyte Biology *91*, 437–448.

Kashiwada, M., Pham, N.-L.L., Pewe, L.L., Harty, J.T., and Rothman, P.B. (2011). NFIL3/E4BP4 is a key transcription factor for CD8α+ dendritic cell development. Blood *117*, 6193–6197.

Kingston, D., Schmid, M.A., Onai, N., Obata-Onai, A., Baumjohann, D., and Manz, M.G. (2009). The concerted action of GM-CSF and Flt3-ligand on in vivo dendritic cell homeostasis. Blood *114*, 835–843.

Kinnebrew, M.A., Buffie, C.G., Diehl, G.E., Zenewicz, L.A., Leiner, I., Hohl, T.M., Flavell, R.A., Littman, D.R., and Pamer, E.G. (2012). Interleukin 23 Production by Intestinal CD103+CD11b+ Dendritic Cells in Response to Bacterial Flagellin Enhances Mucosal Innate Immune Defense. Immunity *36*, 276–287.

Kondo, M., Weissman, I.L., and Akashi, K. (1997). Identification of clonogenic common lymphoid progenitors in mouse bone marrow. Cell *91*, 661–672.

Kreiter, S., Diken, M., Selmi, A., Diekmann, J., Attig, S., Hüsemann, Y., Koslowski, M., Huber, C., Türeci, Ö., and Sahin, U. (2011). FLT3 ligand enhances the cancer therapeutic potency of naked RNA vaccines. Cancer Res. *71*, 6132–6142.

Kurotaki, D., Kawase, W., Sasaki, H., Nakabayashi, J., Nishiyama, A., Morse, H.C.3., Ozato, K., Suzuki, Y., and Tamura, T. (2019a). Epigenetic control of early dendritic cell lineage specification by the transcription factor IRF8 in mice. Blood *133*, 1803–1813.

Kurotaki, D., Kawase, W., Sasaki, H., Nakabayashi, J., Nishiyama, A., Morse, H.C.3., Ozato, K., Suzuki, Y., and Tamura, T. (2019b). Epigenetic control of early dendritic cell lineage specification by the transcription factor IRF8 in mice. Blood *133*, 1803–1813.

Kurotaki, D., Yamamoto, M., Nishiyama, A., Uno, K., Ban, T., Ichino, M., Sasaki, H., Matsunaga, S., Yoshinari, M., Ryo, A., et al. (2014). IRF8 inhibits C/EBPα activity to restrain mononuclear phagocyte progenitors from differentiating into neutrophils. Nat Commun *5*, 4978.

Kwissa, M., Amara, R.R., Robinson, H.L., Moss, B., Alkan, S., Jabbar, A., Villinger, F., and Pulendran, B. (2007). Adjuvanting a DNA vaccine with a TLR9 ligand plus Flt3 ligand results in enhanced cellular immunity against the simian immunodeficiency virus. The Journal of Experimental Medicine *204*, 2733–2746.

Lahoud, M.H., Proietto, A.I., Gartlan, K.H., Kitsoulis, S., Curtis, J., Wettenhall, J., Sofi, M., Daunt, C., O'Keeffe, M., Caminschi, I., et al. (2006). Signal regulatory protein molecules are differentially expressed by CD8- dendritic cells. The Journal of Immunology *177*, 372–382.

Laurenti, E., and Göttgens, B. (2018). From haematopoietic stem cells to complex differentiation landscapes. Nature *553*, 418–426.

Lee, J., Zhou, Y.J., Ma, W., Zhang, W., Aljoufi, A., Luh, T., Lucero, K., Liang, D., Thomsen, M., Bhagat, G., et al. (2017). Lineage specification of human dendritic cells is marked by IRF8 expression in hematopoietic stem cells and multipotent progenitors. Nature Immunology *15*, 3221.

LENNERT, K., and REMMELE, W. (1958). [Karyometric research on lymph node cells in man. I. Germinoblasts, lymphoblasts & lymphocytes]. Acta Haematol. *19*, 99–113.

Lewis, K.L., Caton, M.L., Bogunovic, M., Greter, M., Grajkowska, L.T., Ng, D., Klinakis, A., Charo, I.F., Jung, S., Gommerman, J.L., et al. (2011). Notch2 Receptor Signaling Controls Functional Differentiation of Dendritic Cells in the Spleen and Intestine. Immunity *35*, 780–791.

Lin, D.S., Kan, A., Gao, J., Crampin, E.J., Hodgkin, P.D., and Naik, S.H. (2018). DiSNE Movie Visualization and Assessment of Clonal Kinetics Reveal Multiple Trajectories of Dendritic Cell Development. Cell Reports *22*, 2557–2566.

Liu, K., Victora, G.D., Schwickert, T.A., Guermonprez, P., Meredith, M.M., Yao, K., Chu, F.-F., Randolph, G.J., Rudensky, A.Y., and Nussenzweig, M. (2009). In vivo analysis of dendritic cell development and homeostasis. Science *324*, 392–397.

Lu, R., Neff, N.F., Quake, S.R., and Weissman, I.L. (2011). Tracking single hematopoietic stem cells in vivo using high-throughput sequencing in conjunction with viral genetic barcoding. Nature Biotechnology *29*, 928–933.

Lundie, R.J., de Koning-Ward, T.F., Davey, G.M., Nie, C.Q., Hansen, D.S., Lau, L.S., Mintern, J.D., Belz, G.T., Schofield, L., Carbone, F.R., et al. (2008). Blood-stage Plasmodium infection induces CD8+ T lymphocytes to parasite-expressed antigens, largely regulated by CD8α+ dendritic cells. Proceedings of the National Academy of Sciences *105*, 14509–14514.

Lyman, S.D., James, L., Johnson, L., Brasel, K., de Vries, P., Escobar, S.S., Downey, H., Splett, R.R., Beckmann, M.P., and McKenna, H.J. (1994). Cloning of the human homologue of the murine flt3 ligand: a growth factor for early hematopoietic progenitor cells. Blood *83*, 2795–2801.

Lyman, S.D., James, L., Vanden Bos, T., de Vries, P., Brasel, K., Gliniak, B., Hollingsworth, L.T., Picha, K.S., McKenna, H.J., and Splett, R.R. (1993). Molecular

cloning of a ligand for the flt3/flk-2 tyrosine kinase receptor: a proliferative factor for primitive hematopoietic cells. Cell *75*, 1157–1167.

Lynch, D.H., Andreasen, A., Maraskovsky, E., Whitmore, J., Miller, R.E., and Schuh, J.C. (1997). Flt3 ligand induces tumor regression and antitumor immune responses in vivo. Nature Medicine *3*, 625–631.

Mackarehtschian, K., Hardin, J.D., Moore, K.A., Boast, S., Goff, S.P., and Lemischka, I.R. (1995). Targeted disruption of the flk2/flt3 gene leads to deficiencies in primitive hematopoietic progenitors. Immunity *3*, 147–161.

Manz, M.G., and Boettcher, S. (2014). Emergency granulopoiesis. Nature Reviews. Immunology *14*, 302–314.

Manz, M.G., Traver, D., Miyamoto, T., Weissman, I.L., and Akashi, K. (2001). Dendritic cell potentials of early lymphoid and myeloid progenitors. Blood *97*, 3333–3341.

Maraskovsky, E. (1996). Dramatic increase in the numbers of functionally mature dendritic cells in Flt3 ligand-treated mice: multiple dendritic cell subpopulations identified. The Journal of Experimental Medicine *184*, 1953–1962.

Marroquin, C.E., Westwood, J.A., Lapointe, R., Mixon, A., Wunderlich, J.R., Caron, D., Rosenberg, S.A., and Hwu, P. (2002). Mobilization of Dendritic Cell Precursors in Patients With Cancer by Flt3 Ligand Allows the Generation of Higher Yields of Cultured Dendritic Cells. Journal of Immunotherapy *25*, 278–288.

Mashayekhi, M., Sandau, M.M., Dunay, I.R., Frickel, E.M., Khan, A., Goldszmid, R.S., Sher, A., Ploegh, H.L., Murphy, T.L., Sibley, L.D., et al. (2011). CD8α(+) dendritic cells are the critical source of interleukin-12 that controls acute infection by Toxoplasma gondii tachyzoites. Immunity *35*, 249–259.

Matsui, T., Connolly, J.E., Michnevitz, M., Chaussabel, D., Yu, C.-I., Glaser, C., Tindle, S., Pypaert, M., Freitas, H., Piqueras, B., et al. (2009). CD2 distinguishes two subsets of human plasmacytoid dendritic cells with distinct phenotype and functions. Journal of Immunology *182*, 6815–6823.

Matthews, W., Jordan, C.T., Wiegand, G.W., Pardoll, D., and Lemischka, I.R. (1991). A receptor tyrosine kinase specific to hematopoietic stem and progenitor cell-enriched populations. Cell *65*, 1143–1152.

McKenna, H.J., Stocking, K.L., Miller, R.E., Brasel, K., De Smedt, T., Maraskovsky, E., Maliszewski, C.R., Lynch, D.H., Smith, J., Pulendran, B., et al. (2000). Mice lacking flt3 ligand have deficient hematopoiesis affecting hematopoietic progenitor cells, dendritic cells, and natural killer cells. Blood *95*, 3489–3497.

McKenna, H.J. (2000). FLT3 ligand. In New Cytokines as Potential Drugs, (Basel: Birkhäuser, Basel), pp. 81–100.

Means, T.K., Latz, E., Hayashi, F., Murali, M.R., Golenbock, D.T., and Luster, A.D. (2005). Human lupus autoantibody-DNA complexes activate DCs through cooperation of CD32 and TLR9. The Journal of Clinical Investigation *115*, 407–417.

Merad, M., Sathe, P., Helft, J., Miller, J., and Mortha, A. (2013). The dendritic cell lineage: ontogeny and function of dendritic cells and their subsets in the steady state and the inflamed setting. Annual Review of Immunology *31*, 563–604.

Merad, M., Sugie, T., Engleman, E.G., and Fong, L. (2002). In vivo manipulation of dendritic cells to induce therapeutic immunity. Blood *99*, 1676–1682.

Meredith, M.M., Liu, K., Darrasse-Jeze, G., Kamphorst, A.O., Schreiber, H.A., Guermonprez, P., Idoyaga, J., Cheong, C., Yao, K.-H., Niec, R.E., et al. (2012). Expression of the zinc finger transcription factor zDC (Zbtb46, Btbd4) defines the classical dendritic cell lineage. The Journal of Experimental Medicine *209*, 1153–1165.

Mesnil, C., Sabatel, C.M., Marichal, T., Toussaint, M., Cataldo, D., Drion, P.-V., Lekeux, P., Bureau, F., and Desmet, C.J. (2012). Resident CD11b+Ly6C− Lung Dendritic Cells Are Responsible for Allergic Airway Sensitization to House Dust Mite in Mice. PloS One *7*, e53242.

Miller, J.C., Brown, B.D., Shay, T., Gautier, E.L., Jojic, V., Cohain, A., Pandey, G., Leboeuf, M., Elpek, K.G., Helft, J., et al. (2012). Deciphering the transcriptional network of the dendritic cell lineage. Nature Immunology *13*, 888–899.

Molineux, G., McCrea, C., Yan, X.Q., Kerzic, P., and McNiece, I. (1997). Flt-3 ligand synergizes with granulocyte colony-stimulating factor to increase neutrophil numbers and to mobilize peripheral blood stem cells with long-term repopulating potential. Blood *89*, 3998–4004.

Mooney, C.J., Cunningham, A., Tsapogas, P., Toellner, K.-M., and Brown, G. (2017). Selective Expression of Flt3 within the Mouse Hematopoietic Stem Cell Compartment. International Journal of Molecular Sciences *18*, 1037.

Morita, Y., Ema, H., and Nakauchi, H. (2010). Heterogeneity and hierarchy within the most primitive hematopoietic stem cell compartment. Journal of Experimental Medicine *207*, 1173–1182.

Morse, M.A., Nair, S., Fernandez-Casal, M., Deng, Y., St Peter, M., Williams, R., Hobeika, A., Mosca, P., Clay, T., Cumming, R.I., et al. (2000). Preoperative mobilization of circulating dendritic cells by Flt3 ligand administration to patients with metastatic colon cancer. J. Clin. Oncol. *18*, 3883–3893.

Mossadegh-Keller, N., Sarrazin, S., Kandalla, P.K., Espinosa, L., Stanley, E.R., Nutt, S.L., Moore, J., and Sieweke, M.H. (2013). M-CSF instructs myeloid lineage fate in single haematopoietic stem cells. Nature *497*, 239–243.

Muller-Sieburg, C.E., Cho, R.H., Karlsson, L., Huang, J.F., and Sieburg, H.B. (2004). Myeloid-biased hematopoietic stem cells have extensive self-renewal capacity but generate diminished lymphoid progeny with impaired IL-7 responsiveness. Blood *103*, 4111–4118.

Muller-Sieburg, C.E., Cho, R.H., Thoman, M., Adkins, B., and Sieburg, H.B. (2002). Deterministic regulation of hematopoietic stem cell self-renewal and differentiation. Blood *100*, 1302–1309.

Muller-Sieburg, C.E., Sieburg, H.B., Bernitz, J.M., and Cattarossi, G. (2012). Stem cell heterogeneity: implications for aging and regenerative medicine. Blood *119*, 3900–3907.

Murphy, T.L., Grajales-Reyes, G.E., Wu, X., Tussiwand, R., Briseño, C.G., Iwata, A., Kretzer, N.M., Durai, V., and Murphy, K.M. (2015). Transcriptional Control of Dendritic Cell Development. Annual Review of Immunology *34*, 93–119.

Musgrove, E.A., Caldon, C.E., Barraclough, J., Stone, A., and Sutherland, R.L. (2011). Cyclin D as a therapeutic target in cancer. Nat. Rev. Cancer *11*, 558–572.

Nagasawa, M., Schmidlin, H., Hazekamp, M.G., Schotte, R., and Blom, B. (2008). Development of human plasmacytoid dendritic cells depends on the combined action of the basic helix-loop-helix factor E2-2 and the Ets factor Spi-B. European Journal of Immunology *38*, 2389–2400.

Naik, S.H., Proietto, A.I., Wilson, N.S., Dakic, A., Schnorrer, P., Fuchsberger, M., Lahoud, M.H., O'Keeffe, M., Shao, Q.X., Chen, W.F., et al. (2005). Cutting edge: generation of splenic CD8+ and CD8- dendritic cell equivalents in Fms-like tyrosine kinase 3 ligand bone marrow cultures. Journal of Immunology *174*, 6592–6597.

Naik, S.H., Sathe, P., Park, H.Y., Metcalf, D., Proietto, A.I., Dakic, A., Carotta, S., O'Keeffe, M., Bahlo, M., Papenfuss, A., et al. (2007). Development of plasmacytoid and conventional dendritic cell subtypes from single precursor cells derived in vitro and in vivo. Nature Immunology *8*, 1217–1226.

Naik, S.H., Metcalf, D., van Nieuwenhuijze, A., Wicks, I., Wu, L., O'Keeffe, M., and Shortman, K. (2006). Intrasplenic steady-state dendritic cell precursors that are distinct from monocytes. Nature Immunology *7*, 663–671.

Naik, S.H., Perié, L., Swart, E., Gerlach, C., van Rooij, N., de Boer, R.J., and Schumacher, T.N. (2013). Diverse and heritable lineage imprinting of early haematopoietic progenitors. Nature *496*, 229–232.

Naik, S.H., Schumacher, T.N., and Perié, L. (2014). Cellular barcoding: a technical appraisal. Experimental Hematology *42*, 598–608.

Nakano, H., Yanagita, M., and Gunn, M.D. (2001). CD11c(+)B220(+)Gr-1(+) cells in mouse lymph nodes and spleen display characteristics of plasmacytoid dendritic cells. Journal of Experimental Medicine *194*, 1171–1178.

Namikawa, R., Muench, M.O., de Vries, J.E., and Roncarolo, M.G. (1996). The FLK2/FLT3 ligand synergizes with interleukin-7 in promoting stromal-cell-independent expansion and differentiation of human fetal pro-B cells in vitro. Blood *87*, 1881–1890.

Naudin, C., Hattabi, A., Michelet, F., Miri-Nezhad, A., Benyoucef, A., Pflumio, F., Guillonneau, F., Fichelson, S., Vigon, I., Dusanter-Fourt, I., et al. (2017). PUMILIO/FOXP1 signaling drives expansion of hematopoietic stem/progenitor and leukemia cells. Blood *129*, 2493–2506.

Nayak, B.P., Sailaja, G., and Jabbar, A.M. (2006). Augmenting the immunogenicity of DNA vaccines: role of plasmid-encoded Flt-3 ligand, as a molecular adjuvant in genetic vaccination. Virology *348*, 277–288.

Neipp, M., Zorina, T., Domenick, M.A., Exner, B.G., and Ildstad, S.T. (1998). Effect of FLT3 ligand and granulocyte colony-stimulating factor on expansion and mobilization of facilitating cells and hematopoietic stem cells in mice: kinetics and repopulating potential. Blood *92*, 3177–3188.

Nestorowa, S., Hamey, F.K., Pijuan Sala, B., Diamanti, E., Shepherd, M., Laurenti, E., Wilson, N.K., Kent, D.G., and Göttgens, B. (2016). A single-cell resolution map of mouse hematopoietic stem and progenitor cell differentiation. Blood *128*, e20–e31.

Niederquell, M., Kurig, S., Fischer, J.A.A., Tomiuk, S., Swiecki, M., Colonna, M., Johnston, I.C.D., and Dzionek, A. (2013). Sca-1 expression defines developmental stages of mouse pDCs that show functional heterogeneity in the endosomal but not lysosomal TLR9 response. European Journal of Immunology *43*, 2993–3005.

Nopora, K., Bernhard, C.A., Ried, C., Castello, A.A., Murphy, K.M., Marconi, P., Koszinowski, U.H., and Brocker, T. (2012). MHC Class I Cross-Presentation by Dendritic Cells Counteracts Viral Immune Evasion. Front. Immunol. *3*.

Notta, F., Zandi, S., Takayama, N., Dobson, S., Gan, O.I., Wilson, G., Kaufmann, K.B., McLeod, J., Laurenti, E., Dunant, C.F., et al. (2016a). Distinct routes of lineage development reshape the human blood hierarchy across ontogeny. Science *351*, aab2116–aab2116.

Notta, F., Zandi, S., Takayama, N., Dobson, S., Gan, O.I., Wilson, G., Kaufmann, K.B., McLeod, J., Laurenti, E., Dunant, C.F., et al. (2016b). Distinct routes of lineage development reshape the human blood hierarchy across ontogeny. Science *351*, aab2116.

O'Keeffe, M., Hochrein, H., Vremec, D., Pooley, J., Evans, R., Woulfe, S., and Shortman, K. (2002). Effects of administration of progenipoietin 1, Flt-3 ligand, granulocyte colony-stimulating factor, and pegylated granulocyte-macrophage colony-stimulating factor on dendritic cell subsets in mice. Blood *99*, 2122–2130.

Omatsu, Y., Iyoda, T., Kimura, Y., Maki, A., Ishimori, M., Toyama-Sorimachi, N., and Inaba, K. (2005). Development of murine plasmacytoid dendritic cells defined by increased expression of an inhibitory NK receptor, Ly49Q. Journal of Immunology *174*, 6657–6662.

Onai, N., Kurabayashi, K., Hosoi-Amaike, M., Toyama-Sorimachi, N., Matsushima, K., Inaba, K., and Ohteki, T. (2013). A clonogenic progenitor with prominent plasmacytoid dendritic cell developmental potential. Immunity *38*, 943–957.

Onai, N., Obata-Onai, A., Schmid, M.A., Ohteki, T., Jarrossay, D., and Manz, M.G. (2007). Identification of clonogenic common Flt3+M-CSFR+ plasmacytoid and conventional dendritic cell progenitors in mouse bone marrow. Nature Immunology *8*, 1207–1216.

Onai, N., Obata-Onai, A., Tussiwand, R., Lanzavecchia, A., and Manz, M.G. (2006). Activation of the Flt3 signal transduction cascade rescues and enhances type I interferon-producing and dendritic cell development. The Journal of Experimental Medicine *203*, 227–238.

Papayannopoulou, T., Nakamoto, B., Andrews, R.G., Lyman, S.D., and Lee, M.Y. (1997). In vivo effects of Flt3/Flk2 ligand on mobilization of hematopoietic progenitors in primates and potent synergistic enhancement with granulocyte colony-stimulating factor. Blood *90*, 620–629.

Parajuli, P., Pisarev, V., Sublet, J., Steffel, A., Varney, M., Singh, R., LaFace, D., and Talmadge, J.E. (2001). Immunization with wild-type p53 gene sequences coadministered with Flt3 ligand induces an antigen-specific type 1 T-cell response. Cancer Res. *61*, 8227–8234.

Pardoll, D.M. (2012). The blockade of immune checkpoints in cancer immunotherapy. Nat. Rev. Cancer *12*, 252–264.

Paul, F., Arkin, Y., Giladi, A., Jaitin, D.A., Kenigsberg, E., Keren-Shaul, H., Winter, D., Lara-Astiaso, D., Gury, M., Weiner, A., et al. (2015). Transcriptional Heterogeneity and Lineage Commitment in Myeloid Progenitors. Cell *163*, 1663–1677.

Pelayo, R., Hirose, J., Huang, J., Garrett, K.P., Delogu, A., Busslinger, M., and Kincade, P.W. (2005). Derivation of 2 categories of plasmacytoid dendritic cells in murine bone marrow. Blood *105*, 4407–4415.

Perié, L., and Naik, S.H. (2015). Toward defining a “lineage” – The case for dendritic cells. Seminars in Cell & Developmental Biology *41*, 3–8.

Perié, L., Duffy, K.R., Kok, L., de Boer, R.J., and Schumacher, T.N. (2015). The Branching Point in Erythro-Myeloid Differentiation. Cell *163*, 1655–1662.

Persson, E.K., Uronen-Hansson, H., Semmrich, M., Rivollier, A., Hägerbrand, K., Marsal, J., Gudjonsson, S., Håkansson, U., Reizis, B., Kotarsky, K., et al. (2013). IRF4 Transcription-Factor-Dependent CD103+CD11b+ Dendritic Cells Drive Mucosal T Helper 17 Cell Differentiation. Immunity *38*, 958–969.

Pina, C., Fugazza, C., Tipping, A.J., Brown, J., Soneji, S., Teles, J., Peterson, C., and Enver, T. (2012). Inferring rules of lineage commitment in haematopoiesis. Nature Cell Biology *14*, 287–294.

Pina, C., Teles, J., Fugazza, C., May, G., Wang, D., Guo, Y., Soneji, S., Brown, J., Eden, P., Ohlsson, M., et al. (2015). Single-Cell Network Analysis Identifies DDIT3 as a Nodal Lineage Regulator in Hematopoiesis. Cell Reports *11*, 1503–1510.

Ploegh, H.L. (1998). Viral Strategies of Immune Evasion. Science *280*, 248–253.

Pooley, J.L., Heath, W.R., and Shortman, K. (2001). Cutting Edge: Intravenous Soluble Antigen Is Presented to CD4 T Cells by CD8− Dendritic Cells, but Cross-Presented to CD8 T Cells by CD8+ Dendritic Cells. The Journal of Immunology *166*, 5327–5330.

Poulin, L.F., Salio, M., Griessinger, E., Anjos-Afonso, F., Craciun, L., Chen, J.-L., Keller, A.M., Joffre, O., Zelenay, S., Nye, E., et al. (2010). Characterization of human DNGR-1 +BDCA3 +leukocytes as putative equivalents of mouse CD8α +dendritic cells. The Journal of Experimental Medicine *207*, 1261–1271.

Ray, R.J., Paige, C.J., Furlonger, C., Lyman, S.D., and Rottapel, R. (1996). Flt3 ligand supports the differentiation of early B cell progenitors in the presence of interleukin-11 and interleukin-7. European Journal of Immunology *26*, 1504–1510.

Reeves, R.K., Wei, Q., Stallworth, J., and Fultz, P.N. (2009). Systemic dendritic cell mobilization associated with administration of FLT3 ligand to SIV- and SHIV-infected macaques. AIDS Res. Hum. Retroviruses *25*, 1313–1328.

Reizis, B. (2019). Plasmacytoid Dendritic Cells: Development, Regulation, and Function. Immunity *50*, 37–50.

Rieger, M.A., Hoppe, P.S., Smejkal, B.M., Eitelhuber, A.C., and Schroeder, T. (2009). Hematopoietic cytokines can instruct lineage choice. Science *325*, 217–218.

Roberts, E.W., Broz, M.L., Binnewies, M., Headley, M.B., Nelson, A.E., Wolf, D.M., Kaisho, T., Bogunovic, D., Bhardwaj, N., and Krummel, M.F. (2016). Critical Role for CD103(+)/CD141(+) Dendritic Cells Bearing CCR7 for Tumor Antigen Trafficking and Priming of T Cell Immunity in Melanoma. Cancer Cell *30*, 324–336.

Rocca, D.L., Wilkinson, K.A., and Henley, J.M. (2017). SUMOylation of FOXP1 regulates transcriptional repression via CtBP1 to drive dendritic morphogenesis. Sci Rep *7*, 877.

Rodrigues, P.F., Alberti-Servera, L., Eremin, A., Grajales-Reyes, G.E., Ivanek, R., and Tussiwand, R. (2018). Distinct progenitor lineages contribute to the heterogeneity of plasmacytoid dendritic cells. Nature Immunology 1.

Rodriguez-Fraticelli, A.E., Wolock, S.L., Weinreb, C.S., Panero, R., Patel, S.H., Jankovic, M., Sun, J., Calogero, R.A., Klein, A.M., and Camargo, F.D. (2018). Clonal analysis of lineage fate in native haematopoiesis. Nature *553*, 212–216.

Rosnet, O., Matteï, M.-G., Marchetto, S., and Birnbaum, D. (1991). Isolation and chromosomal localization of a novel FMS-like tyrosine kinase gene. Genomics *9*, 380–385.

Salmon, H., Idoyaga, J., Rahman, A., Leboeuf, M., Remark, R., Jordan, S., Casanova-Acebes, M., Khudoynazarova, M., Agudo, J., Tung, N., et al. (2016). Expansion and Activation of CD103+ Dendritic Cell Progenitors at the Tumor Site Enhances Tumor Responses to Therapeutic PD-L1 and BRAF Inhibition. Immunity *44*, 924–938.

Salvermoser, J., van Blijswijk, J., Papaioannou, N.E., Rambichler, S., Pasztoi, M., Pakalniskyte, D., Rogers, N.C., Keppler, S.J., Straub, T., Reis e Sousa, C., et al. (2018). Clec9a-Mediated Ablation of Conventional Dendritic Cells Suggests a Lymphoid Path to Generating Dendritic Cells In Vivo. Front. Immunol. *9*, 699.

Sancho, D., Mourão-Sá, D., Joffre, O.P., Schulz, O., Rogers, N.C., Pennington, D.J., Carlyle, J.R., and Reis e Sousa, C. (2008). Tumor therapy in mice via antigen targeting to a novel, DC-restricted C-type lectin. The Journal of Clinical Investigation *118*, 2098–2110.

Sanjuan-Pla, A., Macaulay, I.C., Jensen, C.T., Woll, P.S., Luis, T.C., Mead, A., Moore, S., Carella, C., Matsuoka, S., Jones, T.B., et al. (2013). Platelet-biased stem cells reside at the apex of the haematopoietic stem-cell hierarchy. Nature *502*, 232–236.

Sathe, P., Metcalf, D., Vremec, D., Naik, S.H., Langdon, W.Y., Huntington, N.D., Wu, L., and Shortman, K. (2014). Lymphoid tissue and plasmacytoid dendritic cells and macrophages do not share a common macrophage-dendritic cell-restricted progenitor. Immunity *41*, 104–115.

Sathe, P., Vremec, D., Wu, L., Corcoran, L., and Shortman, K. (2013). Convergent differentiation: myeloid and lymphoid pathways to murine plasmacytoid dendritic cells. Blood *121*, 11–19.

Satpathy, A.T., Briseño, C.G., Cai, X., Michael, D.G., Chou, C., Hsiung, S., Bhattacharya, D., Speck, N.A., and Egawa, T. (2014). Runx1 and Cbfβ regulate the development of Flt3+ dendritic cell progenitors and restrict myeloproliferative disorder. Blood *123*, 2968–2977.

Satpathy, A.T., Briseño, C.G., Lee, J.S., Ng, D., Manieri, N.A., Kc, W., Wu, X., Thomas, S.R., Lee, W.-L., Turkoz, M., et al. (2013). Notch2-dependent classical dendritic cells orchestrate intestinal immunity to attaching-and-effacing bacterial pathogens. Nature Immunology *14*, 937–948.

Satpathy, A.T., Kc, W., Albring, J.C., Edelson, B.T., Kretzer, N.M., Bhattacharya, D., Murphy, T.L., and Murphy, K.M. (2012). Zbtb46 expression distinguishes classical dendritic cells and their committed progenitors from other immune lineages. The Journal of Experimental Medicine *209*, 1135–1152.

Sánchez-Paulete, A.R., Cueto, F.J., Martínez-López, M., Labiano, S., Morales-Kastresana, A., Rodríguez-Ruiz, M.E., Jure-Kunkel, M., Azpilikueta, A., Aznar, M.A., Quetglas, J.I., et al. (2016). Cancer Immunotherapy with Immunomodulatory Anti-CD137 and Anti-PD-1 Monoclonal Antibodies Requires BATF3-Dependent Dendritic Cells. Cancer Discov *6*, 71–79.

Schiavoni, G., Mattei, F., Sestili, P., Borghi, P., Venditti, M., Morse, H.C., Belardelli, F., and Gabriele, L. (2002). ICSBP is essential for the development of mouse type I interferon-producing cells and for the generation and activation of CD8alpha(+) dendritic cells. Journal of Experimental Medicine *196*, 1415–1425.

Schlitzer, A., Heiseke, A.F., Einwächter, H., Reindl, W., Schiemann, M., Manta, C.-P., See, P., Niess, J.-H., Suter, T., Ginhoux, F., et al. (2012). Tissue-specific differentiation of a circulating CCR9- pDC-like common dendritic cell precursor. Blood *119*, 6063–6071.

Schlitzer, A., Loschko, J., Mair, K., Vogelmann, R., Henkel, L., Einwächter, H., Schiemann, M., Niess, J.-H., Reindl, W., and Krug, A. (2011). Identification of CCR9- murine plasmacytoid DC precursors with plasticity to differentiate into conventional DCs. Blood *117*, 6562–6570.

Schlitzer, A., McGovern, N., Teo, P., Zelante, T., Atarashi, K., Low, D., Ho, A.W.S., See, P., Shin, A., Wasan, P.S., et al. (2013). IRF4 transcription factor-dependent CD11b+

dendritic cells in human and mouse control mucosal IL-17 cytokine responses. Immunity *38*, 970–983.

Schlitzer, A., Sivakamasundari, V., Chen, J., Sumatoh, H.R.B., Schreuder, J., Lum, J., Malleret, B., Zhang, S., Larbi, A., Zolezzi, F., et al. (2015). Identification of cDC1- and cDC2-committed DC progenitors reveals early lineage priming at the common DC progenitor stage in the bone marrow. Nature Immunology *16*, 718–728.

Schnorrer, P., Behrens, G.M.N., Wilson, N.S., Pooley, J.L., Smith, C.M., El-Sukkari, D., Davey, G., Kupresanin, F., Li, M., Maraskovsky, E., et al. (2006). The dominant role of CD8+ dendritic cells in cross-presentation is not dictated by antigen capture. Proceedings of the National Academy of Sciences *103*, 10729–10734.

Schotte, R., Nagasawa, M., Weijer, K., Spits, H., and Blom, B. (2004). The ETS transcription factor Spi-B is required for human plasmacytoid dendritic cell development. Journal of Experimental Medicine *200*, 1503–1509.

Schraml, B.U., and Reis e Sousa, C. (2015). Defining dendritic cells. Curr. Opin. Immunol. *32*, 13–20.

Schraml, B.U., van Blijswijk, J., Zelenay, S., Whitney, P.G., Filby, A., Acton, S.E., Rogers, N.C., Moncaut, N., Carvajal, J.J., and Reis e Sousa, C. (2013). Genetic Tracing via DNGR-1 Expression History Defines Dendritic Cells as a Hematopoietic Lineage. Cell *154*, 843–858.

Schroeder, T. (2010). Hematopoietic stem cell heterogeneity: subtypes, not unpredictable behavior. Cell Stem Cell *6*, 203–207.

Schulz, O., Edwards, A.D., Schito, M., Aliberti, J., Manickasingham, S., Sher, A., and Reis e Sousa, C. (2000). CD40 Triggering of Heterodimeric IL-12 p70 Production by Dendritic Cells In Vivo Requires a Microbial Priming Signal. Immunity *13*, 453–462.

See, P., Dutertre, C.-A., Chen, J., Günther, P., McGovern, N., Irac, S.E., Gunawan, M., Beyer, M., Händler, K., Duan, K., et al. (2017). Mapping the human DC lineage through the integration of high-dimensional techniques. Science *66*, eaag3009.

Segura, E., Wong, J., and Villadangos, J.A. (2009). Cutting edge: B220+CCR9- dendritic cells are not plasmacytoid dendritic cells but are precursors of conventional dendritic cells. Journal of Immunology *183*, 1514–1517.

Sharma, P., and Allison, J.P. (2015). The future of immune checkpoint therapy. Science *348*, 56–61.

Shigematsu, H., Reizis, B., Iwasaki, H., Mizuno, S.-I., Hu, D., Traver, D., Leder, P., Sakaguchi, N., and Akashi, K. (2004). Plasmacytoid dendritic cells activate lymphoid-specific genetic programs irrespective of their cellular origin. Immunity *21*, 43–53.

Shortman, K., and Heath, W.R. (2010). The CD8+ dendritic cell subset. Immunol. Rev. *234*, 18–31.

Shortman, K., and Naik, S.H. (2007). Steady-state and inflammatory dendritic-cell development. Nature Reviews. Immunology *7*, 19–30.

Shortman, K., Sathe, P., Vremec, D., Naik, S., and O'Keeffe, M. (2013). Plasmacytoid dendritic cell development. Adv. Immunol. *120*, 105–126.

Sieburg, H.B., Cho, R.H., Dykstra, B., Uchida, N., Eaves, C.J., and Muller-Sieburg, C.E. (2006). The hematopoietic stem compartment consists of a limited number of discrete stem cell subsets. Blood *107*, 2311–2316.

Siegal, F.P., Kadowaki, N., Shodell, M., Fitzgerald-Bocarsly, P.A., Shah, K., Ho, S., Antonenko, S., and Liu, Y.J. (1999). The nature of the principal type 1 interferon-producing cells in human blood. Science *284*, 1835–1837.

Silver, D.F., Hempling, R.E., Piver, M.S., and Repasky, E.A. (2000). Flt-3 Ligand Inhibits Growth of Human Ovarian Tumors Engrafted in Severe Combined Immunodeficient Mice. Gynecologic Oncology *77*, 377–382.

Sisirak, V., Faget, J., Gobert, M., Goutagny, N., Vey, N., Treilleux, I., Renaudineau, S., Poyet, G., Labidi-Galy, S.I., Goddard-Leon, S., et al. (2012). Impaired IFN-α production by plasmacytoid dendritic cells favors regulatory T-cell expansion that may contribute to breast cancer progression. Cancer Res. *72*, 5188–5197.

Sitnicka, E., Buza-Vidas, N., Ahlenius, H., Cilio, C.M., Gekas, C., Nygren, J.M., Månsson, R., Cheng, M., Jensen, C.T., Svensson, M., et al. (2007). Critical role of FLT3 ligand in IL-7 receptor independent T lymphopoiesis and regulation of lymphoid-primed multipotent progenitors. Blood *110*, 2955–2964.

Sitnicka, E., Buza-Vidas, N., Larsson, S., Nygren, J.M., Liuba, K., and Jacobsen, S.E.W. (2003). Human CD34+ hematopoietic stem cells capable of multilineage engrafting NOD/SCID mice express flt3: distinct flt3 and c-kit expression and response patterns on mouse and candidate human hematopoietic stem cells. Blood *102*, 881–886.

Sonnenberg, G.F., and Artis, D. (2015). Innate lymphoid cells in the initiation, regulation and resolution of inflammation. Nature Medicine *21*, 698–708.

Sousa, C.R.E., Hieny, S., Scharton-Kersten, T., Jankovic, D., Charest, H., Germain, R.N., and Sher, A. (1997). In Vivo Microbial Stimulation Induces Rapid CD40 Ligand–independent Production of Interleukin 12 by Dendritic Cells and their Redistribution to T Cell Areas. Journal of Experimental Medicine *186*, 1819–1829.

Spranger, S., Bao, R., and Gajewski, T.F. (2015). Melanoma-intrinsic β-catenin signalling prevents anti-tumour immunity. Nature *523*, 231–235.

Spranger, S., Dai, D., Horton, B., and Gajewski, T.F. (2017). Tumor-Residing Batf3 Dendritic Cells Are Required for Effector T Cell Trafficking and Adoptive T Cell Therapy. Cancer Cell *31*, 711–723.e714.

Steinman, R.M., and Cohn, Z.A. (1973). Identification of a novel cell type in peripheral lymphoid organs of mice. I. Morphology, quantitation, tissue distribution. The Journal of Experimental Medicine *137*, 1142–1162.

Steinman, R.M., and Cohn, Z.A. (1974). Identification of a novel cell type in peripheral lymphoid organs of mice. II. Functional properties in vitro. The Journal of Experimental Medicine *139*, 380–397.

Steinman, R.M., Adams, J.C., and Cohn, Z.A. (1975). Identification of a novel cell type in peripheral lymphoid organs of mice. IV. Identification and distribution in mouse spleen. The Journal of Experimental Medicine *141*, 804–820.

Steinman, R.M., Lustig, D.S., and Cohn, Z.A. (1974). Identification of a novel cell type in peripheral lymphoid organs of mice. 3. Functional properties in vivo. The Journal of Experimental Medicine *139*, 1431–1445.

Sudo, Y., Shimazaki, C., Ashihara, E., Kikuta, T., Hirai, H., Sumikuma, T., Yamagata, N., Goto, H., Inaba, T., Fujita, N., et al. (1997). Synergistic effect of FLT-3 ligand on the granulocyte colony-stimulating factor-induced mobilization of hematopoietic stem cells and progenitor cells into blood in mice. Blood *89*, 3186–3191.

Sumida, S.M., McKay, P.F., Truitt, D.M., Kishko, M.G., Arthur, J.C., Seaman, M.S., Jackson, S.S., Gorgone, D.A., Lifton, M.A., Letvin, N.L., et al. (2004). Recruitment and expansion of dendritic cells in vivo potentiate the immunogenicity of plasmid DNA vaccines. The Journal of Clinical Investigation *114*, 1334–1342.

Sun, T., Rojas, O.L., Li, C., Ward, L.A., Philpott, D.J., and Gommerman, J.L. (2017). Intestinal Batf3-dependent dendritic cells are required for optimal antiviral T-cell responses in adult and neonatal mice. Mucosal Immunology 2016 10:3 *10*, 775–788.

Suzuki, S., Honma, K., Matsuyama, T., Suzuki, K., Toriyama, K., Akitoyo, I., Yamamoto, K., Suematsu, T., Nakamura, M., Yui, K., et al. (2004). Critical roles of interferon regulatory factor 4 in CD11bhighCD8alpha- dendritic cell development. Proceedings of the National Academy of Sciences *101*, 8981–8986.

Swiecki, M., and Colonna, M. (2015). The multifaceted biology of plasmacytoid dendritic cells. Nature Reviews. Immunology *15*, 471–485.

Swiecki, M., Gilfillan, S., Vermi, W., Wang, Y., and Colonna, M. (2010). Plasmacytoid dendritic cell ablation impacts early interferon responses and antiviral NK and CD8(+) T cell accrual. Immunity *33*, 955–966.

Swiecki, M., Wang, Y., Riboldi, E., Kim, A.H.J., Dzutsev, A., Gilfillan, S., Vermi, W., Ruedl, C., Trinchieri, G., and Colonna, M. (2014). Cell depletion in mice that express diphtheria toxin receptor under the control of SiglecH encompasses more than plasmacytoid dendritic cells. Journal of Immunology *192*, 4409–4416.

Takizawa, H., Boettcher, S., and Manz, M.G. (2012). Demand-adapted regulation of early hematopoiesis in infection and inflammation. Blood *119*, 2991–3002.

The Immunological Genome Project Consortium, Heng, T.S.P., Painter, M.W., Elpek, K., Lukacs-Kornek, V., Mauermann, N., Turley, S.J., Koller, D., Kim, F.S., Wagers, A.J., et al. (2008). The Immunological Genome Project: networks of gene expression in immune cells. Nature Immunology *9*, 1091–1094.

Tian, L., Schreuder, J., Zalcenstein, D., Tran, J., Kocovski, N., Su, S., Diakumis, P., Bahlo, M., Sargeant, T., Hodgkin, P.D., et al. (2018). SIS-seq, a molecular “time machine,” connects single cell fate with gene programs. bioRxiv 403113.

Torti, N., Walton, S.M., Murphy, K.M., and Oxenius, A. (2011). Batf3 transcription factor-dependent DC subsets in murine CMV infection: Differential impact on T-cell priming and memory inflation. European Journal of Immunology *41*, 2612–2618.

Traver, D., Akashi, K., Manz, M., Merad, M., Miyamoto, T., Engleman, E.G., and Weissman, I.L. (2000). Development of CD8alpha-positive dendritic cells from a common myeloid progenitor. Science *290*, 2152–2154.

Tsapogas, P., Swee, L.K., Nusser, A., Nuber, N., Kreuzaler, M., Capoferri, G., Rolink, H., Ceredig, R., and Rolink, A. (2014). In vivo evidence for an instructive role of fms-like tyrosine kinase-3 (FLT3) ligand in hematopoietic development. Haematologica *99*, 638–646.

Tusi, B.K., Wolock, S.L., Weinreb, C., Hwang, Y., Hidalgo, D., Zilionis, R., Waisman, A., Huh, J.R., Klein, A.M., and Socolovsky, M. (2018). Population snapshots predict early haematopoietic and erythroid hierarchies. Nature *555*, 54–60.

Tussiwand, R., Everts, B., Grajales-Reyes, G.E., Kretzer, N.M., Iwata, A., Bagaitkar, J., Wu, X., Wong, R., Anderson, D.A., Murphy, T.L., et al. (2015). Klf4 expression in conventional dendritic cells is required for T helper 2 cell responses. Immunity *42*, 916–928.

Tussiwand, R., Onai, N., Mazzucchelli, L., and Manz, M.G. (2005). Inhibition of natural type I IFN-producing and dendritic cell development by a small molecule receptor tyrosine kinase inhibitor with Flt3 affinity. Journal of Immunology *175*, 3674–3680.

Uras, I.Z., Walter, G.J., Scheicher, R., Bellutti, F., Prchal-Murphy, M., Tigan, A.S., Valent, P., Heidel, F.H., Kubicek, S., Scholl, C., et al. (2016). Palbociclib treatment of FLT3-ITD+ AML cells uncovers a kinase-dependent transcriptional regulation of FLT3 and PIM1 by CDK6. Blood *127*, 2890–2902.

Vander Lugt, B., Khan, A.A., Hackney, J.A., Agrawal, S., Lesch, J., Zhou, M., Lee, W.P., Park, S., Xu, M., DeVoss, J., et al. (2014). Transcriptional programming of dendritic cells for enhanced MHC class II antigen presentation. Nature Immunology *15*, 161–167.

Varol, C., Vallon-Eberhard, A., Elinav, E., Aychek, T., Shapira, Y., Luche, H., Fehling, H.J., Hardt, W.-D., Shakhar, G., and Jung, S. (2009). Intestinal lamina propria dendritic cell subsets have different origin and functions. Immunity *31*, 502–512.

Veiby, O.P., Lyman, S.D., and Jacobsen, S.E. (1996). Combined signaling through interleukin-7 receptors and flt3 but not c-kit potently and selectively promotes B-cell commitment and differentiation from uncommitted murine bone marrow progenitor cells. Blood *88*, 1256–1265.

Velten, L., Haas, S.F., Raffel, S., Blaszkiewicz, S., Islam, S., Hennig, B.P., Hirche, C., Lutz, C., Buss, E.C., Nowak, D., et al. (2017a). Human haematopoietic stem cell lineage commitment is a continuous process. Nature Cell Biology *19*, 271–281.

Velten, L., Haas, S.F., Raffel, S., Blaszkiewicz, S., Islam, S., Hennig, B.P., Hirche, C., Lutz, C., Buss, E.C., Nowak, D., et al. (2017b). Human haematopoietic stem cell lineage commitment is a continuous process. Nature Cell Biology *19*, 271–281.

Villani, A.-C., Satija, R., Reynolds, G., Sarkizova, S., Shekhar, K., Fletcher, J., Griesbeck, M., Butler, A., Zheng, S., Lazo, S., et al. (2017). Single-cell RNA-seq reveals new types of human blood dendritic cells, monocytes, and progenitors. Science *356*, eaah4573.

Vremec, D., Lieschke, G.J., Dunn, A.R., Robb, L., Metcalf, D., and Shortman, K. (1997). The influence of granulocyte/macrophage colony-stimulating factor on dendritic cell levels in mouse lymphoid organs. European Journal of Immunology *27*, 40–44.

Waskow, C., Liu, K., Darrasse-Jeze, G., Guermonprez, P., Ginhoux, F., Merad, M., Shengelia, T., Yao, K., and Nussenzweig, M. (2008). The receptor tyrosine kinase Flt3 is required for dendritic cell development in peripheral lymphoid tissues. Nature Immunology *9*, 676–683.

Williams, J.W., Tjota, M.Y., Clay, B.S., Vander Lugt, B., Bandukwala, H.S., Hrusch, C.L., Decker, D.C., Blaine, K.M., Fixsen, B.R., Singh, H., et al. (2013). Transcription factor IRF4 drives dendritic cells to promote Th2 differentiation. Nat Commun *4*, 4345.

Wilson, N.K., Kent, D.G., Buettner, F., Shehata, M., Macaulay, I.C., Calero-Nieto, F.J., Sanchez Castillo, M., Oedekoven, C.A., Diamanti, E., Schulte, R., et al. (2015). Combined Single-Cell Functional and Gene Expression Analysis Resolves Heterogeneity within Stem Cell Populations. Cell Stem Cell *16*, 712–724.

Wu, L., D'Amico, A., Hochrein, H., O'Keeffe, M., Shortman, K., and Lucas, K. (2001). Development of thymic and splenic dendritic cell populations from different hemopoietic precursors. Blood *98*, 3376–3382.

Wu, L., D'Amico, A., Winkel, K.D., Suter, M., Lo, D., and Shortman, K. (1998). RelB is essential for the development of myeloid-related CD8alpha- dendritic cells but not of lymphoid-related CD8alpha+ dendritic cells. Immunity *9*, 839–847.

Wu, L., Vremec, D., Ardavin, C., Winkel, K., Süss, G., Georgiou, H., Maraskovsky, E., Cook, W., and Shortman, K. (1995). Mouse thymus dendritic cells: kinetics of development and changes in surface markers during maturation. European Journal of Immunology *25*, 418–425.

Yamamoto, R., Morita, Y., Ooehara, J., Hamanaka, S., Onodera, M., Rudolph, K.L., Ema, H., and Nakauchi, H. (2013). Clonal analysis unveils self-renewing lineage-restricted progenitors generated directly from hematopoietic stem cells. Cell *154*, 1112–1126.

Yang, G.-X., Lian, Z.-X., Kikuchi, K., Liu, Y.-J., Ansari, A.A., Ikehara, S., and Gershwin, M.E. (2005). CD4- plasmacytoid dendritic cells (pDCs) migrate in lymph nodes by CpG inoculation and represent a potent functional subset of pDCs. Journal of Immunology *174*, 3197–3203.

Zelenay, S., Keller, A.M., Whitney, P.G., Schraml, B.U., Deddouche, S., Rogers, N.C., Schulz, O., Sancho, D., and Reis e Sousa, C. (2012). The dendritic cell receptor DNGR-1 controls endocytic handling of necrotic cell antigens to favor cross-priming of CTLs in virus-infected mice. The Journal of Clinical Investigation *122*, 1615–1627.

Zhang, H., Gregorio, J.D., Iwahori, T., Zhang, X., Choi, O., Tolentino, L.L., Prestwood, T., Carmi, Y., and Engleman, E.G. (2017). A distinct subset of plasmacytoid dendritic

cells induces activation and differentiation of B and T lymphocytes. Proceedings of the National Academy of Sciences of the United States of America *114*, 1988–1993.

Zhang, J., Raper, A., Sugita, N., Hingorani, R., Salio, M., Palmowski, M.J., Cerundolo, V., and Crocker, P.R. (2006). Characterization of Siglec-H as a novel endocytic receptor expressed on murine plasmacytoid dendritic cell precursors. Blood *107*, 3600–3608.